Title

THE TRANSPORT PROPERTIES OF SODIUM POLYSULFIDE MELTS AND A THEORETICAL COMPARISON OF FLOW-THROUGH AND FLOW-BY POROUS ELECTRODES AT THE LIMITING CURRENT

Author

Risch, T.

Publication Date

1983-12-01

Lawrence Berkeley Laboratory
UNIVERSITY OF CALIFORNIA

Materials & Molecular Research Division

THE TRANSPORT PROPERTIES OF SODIUM POLYSULFIDE MELTS AND A THEORETICAL COMPARISON OF FLOW-THROUGH AND FLOW-BY POROUS ELECTRODES AT THE LIMITING CURRENT

T. Risch
(M.S. Thesis)

December 1983

Prepared for the U.S. Department of Energy under Contract DE-AC03-76SF00098

DISCLAIMER

The Transport Properties of Sodium Polysulfide Melts

and

A Theoretical Comparison of Flow–Through and Flow–By Porous Electrodes at the Limiting Current

Tim Risch

Master's Thesis

Materials and Molecular Research Division

Lawrence Berkeley Laboratory

and

Department of Chemical Engineering

University of California

Berkeley, California 94720

December 15, 1983

The Transport Properties of Sodium Polysulfide Melts and A Theoretical Comparison of Flow–Through and Flow–By Porous Electrodes at the Limiting Current

Timothy Kent Risch

Abstract

Two current problems of electrochemical interest are addressed. In the first section, the transport properties of sodium polysulfide melts are investigated using two models. A macroscopic model is first proposed which considers the melt to be composed of sodium cations and sulfide anions in a neutral sulfur solvent. A rigorous set of governing equations is derived for this pseudo–binary melt model which accounts for binary ionic–ionic and ionic–solvent interactions. Fundamental transport parameters are defined which quantify the interactions within the melt. These are then related to measurable transport properties and calculated from experimental data. The resulting values for the transport parameters are shown to exhibit unpredictable behavior.

A more sophisticated model is then developed which considers sodium cations and seven different polysulfide anions as the sole melt components. A consistent set of transport equations is then derived for this assumed melt composition. Transport parameters appearing in these equations are related to bulk transport melt properties. Predictions of the melt diffusion coefficient are made from this model using available transference number and conductivity data. The predictions are shown to lie within the ranges of conflicting experimental data for diffusion coefficients in polysulfide melts.

In the second part, a limiting current model for the potential and concentration distribution for a flow-by porous electrode of infinite length to width ratio is developed and compared to previous models of Alkire and Ng and Fedkiw. For flow-by electrodes of practical interest, the maximum solution phase potential drop is shown to be dependent upon one relevant parameter: the product of the electrode width and the reciprocal of the penetration depth, αd. Criteria delineating the optimal electrode configuration are given using this potential difference as a basis for comparison. Design equations are also derived for the flow-through and flow-by electrode at the limiting current relating fixed and variable costs to electrode design and operating variables. The sum of fixed and variable costs is then optimized for the flow-through and flow-by configurations. The results of this optimization give the conditions under which each configuration is preferred.

To my parents

Acknowledgements

I would like to express my gratitude to Professor John Newman who has guided me throughout the preparation of the thesis. His patient approach toward his students has made learning a very valuable experience which is not easily forgotten. The helpful suggestions and discussions with committee members Elton Cairns and Lutgard De Jonghe were also much appreciated.

Many thanks are due to Stuart Naftel who assisted with the experimental portions of this thesis. I am also grateful to him and to Professor Cairns for the use of their equipment required in many of the experiments.

The assistance of Kathy Macbride and Pat Charley who have produced the figures in this thesis is also appreciated.

I would also like to acknowledge the contribution of Professor E. A. Grens who has made this Master's Thesis possible.

Finally, words cannot express the thanks I have to the many family members, friends, fellow students, and faculty who have helped me throughout my stay at Berkeley. The most important part of my education has been the relationships that I have developed and sustained throughout this time.

This work was supported by the Assistant Secretary of Conservation and Renewable Energy, Office of Energy Systems Research, Energy Storage Division of the U.S. Department of Energy under Contract DE-AC03-76SF00098.

Contents

Dedication i

Acknowledgements ii

Contents iii

Chapter 1 Overview. 1

Chapter 2 The Transport Properties of Sodium Polysulfide Melts; Introduction . . . 3

Chapter 3 Transport Properties for a Binary Melt 33

Chapter 4 Transport Properties for a Multicomponent Melt. 63

Chapter 5 Experimental Determination of Diffusion Coefficients . . . 120

Chapter 6 Conclusions 151

List of Symbols for Chapters One through Six 154

Chapter 7 A Theoretical Comparison of Flow-Through and Flow-By Porous Electrodes at the Limiting Current; Introduction . 158

Chapter 8 Potential Distribution 169

Chapter 9 Comparison of Flow-Through and Flow-By Porous Electrodes; Maximum Potential Drop . 183

Chapter 10 Electrode Design 191

Chapter 11 Electrode Cost Optimization 202

Chapter 12 Summary. 227

Chapter 13 Conclusions 231

List of Symbols for Chapters Seven through Thirteen 233

References 236

Appendix A Binary Composition Conventions 245

Appendix B Calculation of Transference Numbers for Sodium Polysulfide Melts . 248

Appendix C Entropy Production 252

Appendix D Multicomponent Melt Phase Compositions. 254

Appendix E Multi–Anion Transport Equations and Properties 257

Appendix F Computer Programs for Sodium Polysulfide Melts 265

Appendix G Derivation of Potential Distribution for a Semi–Infinite Flow–By Electrode at the Limiting Current . 299

Appendix H Computer Programs for Porous Electrodes. 304

Chapter 1

Overview

This thesis deals with two separate problems of current electrochemical interest. In the first section comprising Chapters Two, through Six, the transport properties of sodium polysulfide melts are investigated. The second part, Chapters Seven through Thirteen, deals with the optimization of flow porous electrodes.

Sodium–sulfur cells, which are undergoing intensive development, utilize a melt composed of varying amounts of sodium and sulfur. For accurate design and scale up of this system, it is important to understand the transport processes of the melt. The combined effects of diffusion, migration, and convection are studied in this work. A consistent set of transport equations which completely describe these processes is formulated in terms of two viewpoints regarding the composition of the melt. A macroscopic melt model is first developed with the principal constituents of the melt assumed to be sodium cations, sulfur anions, and neutral sulfur solvent. This macroscopic model is used to define and correlate measurable thermodynamic and transport properties. A second model considers the melt to include only sodium cations and polysulfide anions without neutral sulfur. Using this microscopic model, the transport properties of sodium polysulfide melts are predicted and compared with some recent experimental data. Reasonable agreement between the model and the data is obtained.

The second portion of the thesis studies porous flow electrodes. The use of these electrodes has been suggested for many industrially important

processes. Currently, opinion within the literature is divided over the optimum configuration of porous electrodes. The flow–through design, where current flows parallel to fluid flow has been the long–established configuration for flow porous electrodes. More recently, the flow–by design, with perpendicular fluid and current flow, has been suggested by many to be superior to the flow–through design. A economic optimization is performed here to determine the conditions favoring the application of each configuration. It is shown that the flow–by design is more economical for processes with high feed concentrations and low maximum allowable solution potential drops. The flow–by configuration is preferred for low feed concentrations and high maximum solution potential drops.

Chapter 2

The Transport Properties of Sodium Polysulfide Melts;

Introduction

Molten sodium sulfide and sodium polysulfides are involved in a number of practical engineering applications. The regeneration of caustic in the Kraft process for pulp production requires a slag of molten salts containing high concentrations of sulfides.[1] Sodium polysulfides have also been used as a source for the growth of high purity metal sulfide crystals.[2] By far the most promising application for sodium sulfides is as the positive electrode in a sodium-sulfur secondary cell. Sodium–sulfur batteries are expected to possess a high specific energy, greater than 150 W-hr/kg, and a cycle life greater than 1000 cycles.[3] These characteristics, combined with the abundant availability and the low price of sulfur, make the sulfur electrode and the sodium-sulfur battery attractive for both vehicle propulsion and utility load leveling applications.

The sodium-sulfur cell is perhaps the most advanced of the current molten–salt high temperature systems, and the closest to commercial viability. Many corporations through private research and development programs along with the cooperation of government laboratories are developing the sodium-sulfur cell. Some recent reviews can be useful in supplementing the information which follows.[3-6]

2.1. Fundamental Reactions and Phase Diagram

The fundamental reaction in the sodium–sulfur cell is the combination of metallic sodium with sulfur to form sodium polysulfides

$$2Na + yS \rightarrow Na_2S_y \quad (2-1)$$

The formula Na_2S_y designates the non-stoichiometric sodium polysulfide. The value of y can lie between the value of 2 and approximately 5. This behavior can best be explained by referring to a phase diagram for sodium and sulfur shown in Figure 2-1.[7] In this figure, the existence of different phases is plotted for different temperatures and varying overall melt compositions. The melt composition has been designated by the mole percent of sulfur or by the variable y. The most important part of this diagram is for atom percents of sulfur from about 60 to 100 percent. This is the composition range where the sodium-sulfur battery operates.

Figure 2-1 shows the existence of five regions between the temperatures of 573 to 673 K spanning the compositions of 33 to 100 mole percent sulfur. For a melt composed of nearly pure sulfur, located at the far right of this figure, the first region of the phase diagram is encountered. For clarity, the width of this region has been exaggerated. The actual size of this region is very much smaller, and if drawn accurately, the actual width of this region would be no wider than the lines used to separate the regions. In this region, sodium and sulfur combine to form a single phase of polysulfides. The composition of this phase at any point in this region is so nearly that of pure sulfur, that the actual composition of this phase is frequently ignored, and its composition is considered to be that of pure sulfur.

At slightly lower sulfur compositions, from 72 to 100 mole percent sulfur and temperatures above 415 K, sodium and sulfur combine to form two liquid phases in equilibrium. One phase is composed of the essentially pure sulfur defined by the limit of the first single phase region, while the second phase contains sodium polysulfides with a composition of about

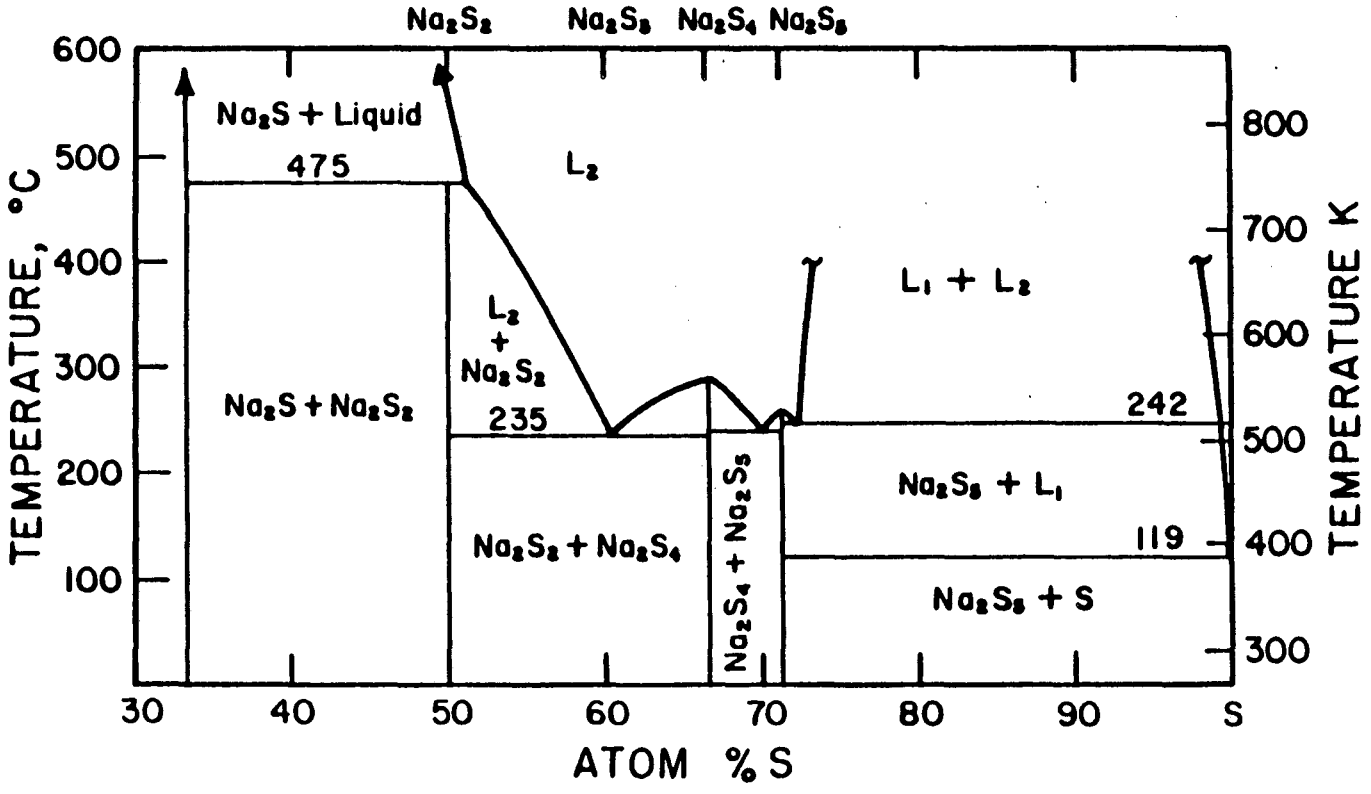

Figure 2–1 Sodium–sulfur phase diagram according to Gupta and Tischer.[7]

$Na_2S_{5.2}$. The compositions of both of the phases are nearly independent of temperature, since the lines defining these compositions are nearly vertical. The amount of each of these phases varies for different overall sulfur compositions. The amounts can be determined from application of the inverse lever rule. To apply this rule one first draws a line parallel to the abscissa, intersecting the two vertical lines defining the composition of the two phases. The distance between these compositions is recorded. The amount for one phase is then given by the distance from the overall composition to the composition of the other phase divided by the recorded distance.

For sulfur compositions below $Na_2S_{5.2}$, a second one–phase region of liquid polysulfides becomes present. Like the first one–phase region, the composition of this phase varies directly with the overall melt composition.

The phase diagram illustrates that for melts composed of less than about sixty mole percent sulfur, a fourth region of the phase diagram will define the composition. Here, at a composition highly dependent upon temperature, a second two–phase region is present. This region is not of practical interest, since sodium–sulfur cells are not designed to operate in this region of the phase diagram. Solid sodium disulfide is present along with a liquid polysulfide. The approximate composition for this liquid near 523 K is Na_2S_3. Here again, the inverse lever rule can be applied to determine the amounts of each of these phases present.

The fifth region of the phase diagram is for overall sulfur compositions less than a one to one mole ratio of sulfur to sodium. This region contains no liquid phase, but is a region of two solid phases. Sodium polysulfides less than 50 mole percent overall sulfur are produced by combining sodium

monosulfide with sodium disulfide. Sodium disulfide melts at 748 K while sodium monosulfide melts at over 1473 K; hence no liquid is formed unless the temperature is increased above the melting point of the disulfide.

2.2. Equilibrium Cell Discharge

The progress of a cell through an equilibrium discharge can be followed by examining the cell potential versus the overall sulfur composition while referring to the phase diagram. Figure 2–2 is a plot of cell potential versus sulfur melt composition.[3] From an initial state of pure sulfur, the sulfur composition decreases as sodium ions are added to the melt. As the discharge proceeds and sodium is added to the melt, the overall sulfur composition of the melt decreases steadily. The discharge begins at time zero with an initial state of pure sulfur on the left of Figure 2–2 and on the right of Figure 2–1. In Figure 2–2, the potential versus sulfur composition shows four distinct regions. At the start of the discharge, the potential drops rapidly corresponding to the depletion of sulfur in the first single phase region. Upon formation of two phases, at an overall sodium composition of less than one percent, the potential becomes constant with state of charge. For this mixture of two components with two equilibrium phases and at a fixed temperature, the phase rule requires a fixed potential. This value is dependent upon temperature, but it is around 2.1 V. Throughout the discharge in this two phase region, the potential remains constant at this value.

When the overall melt composition reaches the approximate formula $Na_2S_{5.2}$, all of the sulfur rich phase has been depleted. Only a single phase remains, and as discharge continues, the concentration of sulfur in this phase decreases. The potential decreases nearly linearly with the mole

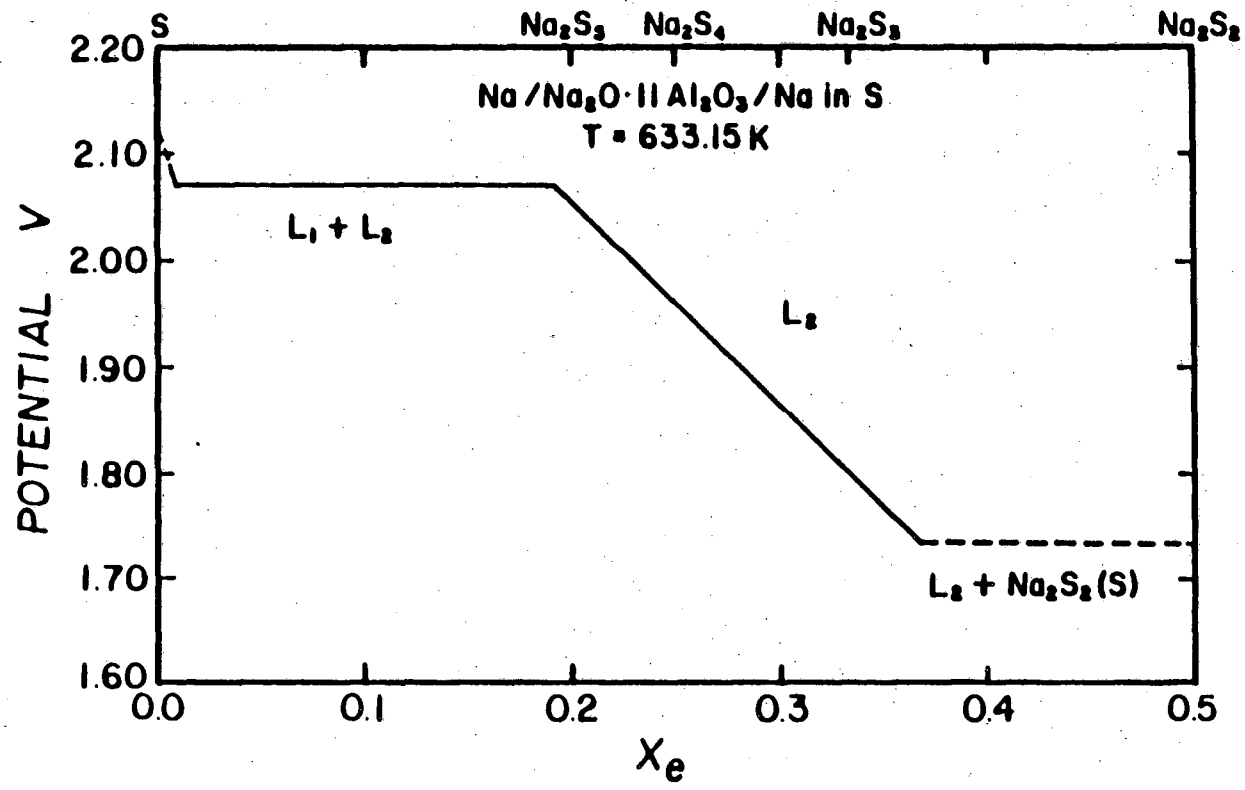

Figure 2–2 Cell potential versus sulfur electrode melt composition for an equilibrium cell discharge. Melt composition is defined by the mole fraction of sodium sulfide x_e. Graph is modified from Cairns.[3]

fraction of sulfur. Finally, if the discharge is continued far enough, the second two phase region is encountered. Again, the presence of two phases requires that the potential remain constant in this region. The potential of the cell in this region would be about 1.75 V but, sodium sulfur cells are not designed to operate in this region of the phase diagram. Cell discharge should be terminated before this composition is reached.

2.3. Practical Cell Designs

The origin of the sodium sulfur cell is generally credited to Kummer and Weber[8,9] at Ford who discovered the ionic conductive properties of β–aluminas. It's development was not a conscious design effort to produce a viable secondary battery, but instead the result of work designed to produce ionically conducting glasses. Since that time, many other companies have followed the pattern laid out by Ford and added their own innovations to this cell's design. One company, however, has broken from this path and developed this same property of ionic conduction in glasses. Like the other companies, their goal is an economical sodium–sulfur cell; however, their approach to achieving this has been quite different.

Two designs of the sodium–sulfur battery are currently being developed: cells incorporating hollow glass fibers as electrolytes and cells with the original type of ceramic electrolyte. These are distinguishable mainly by the material composing the electrolyte and by the configuration of the cell.

The two types of sodium sulfur cells are most easily described in terms of their similarities, however, rather than their differences. All sodium–sulfur cells have three basic features: a liquid sodium negative electrode, a sulfur positive electrode, and a glass or ceramic electrolyte.

These cells operate at relatively high temperatures, between 573 and 633 K. The inclusion of liquid sodium and molten polysulfides in these cells requires a moisture–free environment. Therefore, the cells must be well sealed and isolated from the ambient air.

The sulfur electrode consists of liquid sulfur and contains, depending upon the state of charge, varying amounts of sodium in the form of sodium polysulfides. The sulfur electrode, while under many conditions possesses a respectable ionic conductivity, has a very poor electronic conductivity. Consequently, the sulfur electrode requires a current collector. Common materials are graphite felt, coated steel, semiconducting ceramics or in some designs, coated aluminum foils. To reduce ohmic drop within the melt and to provide a high surface area to the reaction, the current–collecting material is interspersed within the sulfur–polysulfide mixture. This gives a porous, macroscopically, homogeneous phase. These components are contained within a metal can made from stainless steel or other metals. The can may be protected from the highly corrosive sulfur by plating it with resistant metals such as chromium or molybdenum.

Sodium anodes are quite simply, molten sodium metal. The electronic conductivity of molten sodium is very high and requires no other current collector. The sodium metal itself, acts as its own current collector. The liquid sodium is contained in a metal reservoir and must be relatively free of impurities. Other alkali metals, besides sodium, are especially harmful and degrade the performance of the cell. These metals enter the surface structure of the electrolyte and can block the passage of ions. When this happens, the resistance of the electrolyte increases dramatically, causing loss of performance during cycling.

The electrolyte in these cells has but one function– to prevent the physical mixing of molten sodium metal and molten sulfur, while at the same time allowing sodium ions free passage. The electrolyte must possess a small, if not negligible, electronic conductivity to prevent self discharge of the cell. The material constraint on the electrolyte is quite severe. It must be stable in the extremely reducing environment of sodium metal while at the same it must remain unaffected by the oxidizing properties of sulfur. In addition, it must not crack or mechanically rupture from thermal stresses while under variations of temperature during freeze thaw cycles. Even more demanding, the electrolyte must not allow sodium metal to deposit within the crystal lattice structure. Even the strongest electrolytes can fracture if this process occurs. It is no wonder why the electrolyte has been the source of the major problems in the development of this system.

2.3.1. Glass Fiber Cells*

One type of cell is the glass fiber cell. These cells, developed by the Dow Chemical Company, use borate glasses as the electrolye. These fiber cells consist of several hundred to several thousand small hollow glass fibers immersed in a sulfur reservoir. These fibers typically have an outside diameter of 70 μm and an inside diameter of 50 μm, with 10 μm as a wall thickness. Because these fibers are sensitive to moisture, all processes involving the fibers are conducted in low humidity rooms. To produce a glass fiber cell requires a number of detailed processes. First, glass fibers are produced by a proprietary process which yields an extremely uniform, hollow cylindrical fiber. These fibers are then cut to size, sealed at one end, and then placed on a long strip of coated aluminum foil. The purpose of the

*This section is written, in part, from observations made on a visit to the Dow Chemical Research Center, Walnut Creek, CA, March 18, 1982.

coated aluminum foil is to serve as the current collector. Graphite has been used as a coating, although molybdenum seems to the most common material used today. On a special machine, the foil and tubes are then spirally wound around a circular mandrill. This completed assembly, or "jelly–roll," then contains alternating layers of foil and the cylindrical fibers. The tube and current collector assembly are then immersed with the closed end of the tubes down in a sulfur–polysulfide reservoir. Sodium metal fills the tubes from above through the open end of the tubes. The glass tubes thus contain molten sodium metal on the inside and the sulfur–polysulfide melt on the outside. In some designs, however, the polysulfide melt can be placed on the inside, with the molten sodium surrounding the tubes on the outside. Separating the two reservoirs and holding the glass tubes together is a glass "tube sheet" which resembles the ends of a shell and tube heat exchanger. The tube sheet forms a leak–proof seal around the tubes and isolates the positive electrode from the negative electrode.

During discharge of the cell, sodium ions are transferred through the electrolyte and into the sulfur reservoir. The high surface area of the fibers requires only a low flux of ions through the glass, but this is necessary because the glass has a very high resistance. Over 90 percent of the cell resistance is associated with the glass. As sodium ions pass through the glass, sulfur reacts electrochemically at the current collector to produce sodium polysulfides. Because of the large number of glass tubes and the arrangement of the current collector, the sodium ions need not travel far, and concentration variations through the cell are small.

Glass fiber cells have been experimentally tested in 0.5, 6, and 40 A–hr sizes. The sodium glass cell has not been perfected to the point where failure–free operation for acceptable lengths of time is possible. This trouble is especially severe when the cell is thermally cycled or cooled and then reheated. Ideally, cells should provide at least 1500 to 2000 continuous cycles and allow for a large number of thermal cycles. At this time, the 0.5 A–hr cells have achieved no more than 1000 continuous cycles, and 6 A–hr cells have achieved only 400 to 500 cycles. These cycles are for 80 to 90 percent of rated capacity. Very few 40 A–hr cells have been tested. Current specific energies for these cells are not available.

None of these cells have been successfully thermally cycled. The major weak point of the cell is at the tube sheet connection where fracture of the glass fibers commonly occurs. Contrary to intuition, fracture of the fibers may not be critically damaging to the cell. Many times when a fiber fractures, it seals itself, leaving however one less fiber in the cell. If enough fibers are damaged, unacceptable cell performance results. In a number of cases, though, if enough fibers fracture simultaneously, the sodium and sulfur can mix, leading to an uncontrollable thermal runaway of the cell.

Current research is aimed at reducing the fracture of the tube sheet. Thermal cycling is a definite requirement if this design is to be used successfully for electric vehicle applications. Correction of this fracture problem is therefore a must. Corrosion of the anode container is also another significant problem which must be overcome if the cells are to last many years. Other work is being directed toward reducing the cost of each cell. While the sodium–sulfur system is probably the most economically promising high temperature battery, the cost is still too high for realistic

consumer acceptance. Costs for experimental cells are very high at the present time, greater than 1000 $/kW–hr. Estimated production costs for a bare 0.8 A–hr cell are 32 $/kW–hr (May, 1979 dollars) with projections of 35 $/kW–hr (1980 dollars) for complete 400 A–hr cells by 1984. These estimates seem rather optimistic though, given the current state of technology.

2.3.2. Ceramic Cells

The second type of sodium–sulfur cell, which has had better success, is the ceramic sodium–sulfur cell. The progress of this cell has benefited from a greater amount of research and development as well as a larger number of developers, including several foreign companies. Ceramic electrolyte cells are being developed by the American companies Ford and General Electric. Current foreign companies involved with sodium–sulfur cells include Brown–Boveri, Chloride Silent Power, CGE Marcoussis, and the Yuasa Battery Company.

Ceramic sodium–sulfur cells differ from the glass fiber cells in the type of electrolyte which is used. The electrolyte in these cells is a ceramic composed of Al_2O_3 and Na_2O. The ceramic β–alumina contains these two compounds in the molal ratio of 9 to 11. A more suitable ceramic because of higher conductivity is β''–alumina. This contains Al_2O_3 and Na_2O in the molal ratio of approximately 6 to 1. Both β–alumina and β''–alumina are degraded by moisture and β'' is believed to be unstable at high temperatures. Like the glass electrolyte, the reactivity with respect to moisture requires that a dry environment be available for the electrolytes during cell construction and operation.

Unlike the sodium glass cells, ceramic sodium cells contain only a single tube of electrolyte, sealed at one end, with a diameter of 1 to 5 cm. Because the conductivity of the ceramic is much higher than that of the glass in the glass cells, a thin walled, high surface area electrolyte is not needed. The sulfur electrode can be placed within the electrolyte in so called sulfur–core cells or externally with sodium contained in the electrolyte. Sulfur–core cells are generally designed for traction applications where specific power as opposed to specific energy is required. An advantage of sulfur–core cells is the reduction in corrosion of the container. A corrosion resistant current collector is still necessary, however. Even with this advantage, most cell designs, however, are sodium core cells.

The current collectors for cathodes can be constructed from fine carbon mats. As described before, these are distributed throughout the sulfur electrode compartment. The melt of polysulfide and sulfur permeates the current collector mat which results in intimate contact of the melt and mat. The high surface area encourages the interfacial reactions to occur with a minimum of polarization losses. During cycling into the two phase region of the melt, sulfur can be formed near to the mat interface. The sulfur tends to increase the cell resistance by forming insulating layers, preferentially wetting the graphite current collector. For this reason, some sulfur cell designs incorporate alumina fibers into the mat, which are not preferentially wetted by sulfur. Cells with very high specific energies can then be constructed, since operation deep into the upper two phase region is possible.

Ceramic sulfur cells have had greater success than their glass–fiber counterparts. At the present time, these cells exhibit cycle lives of 500 to

1200. Some companies have demonstrated cells lasting 1400 cycles. Ceramic cells are also capable of multiple freeze–thaw cycles, although the total number of charge–discharge cycles is reduced for each thermal cycle.

The testing of ceramic cells has been more extensive than the glass fiber cells. Cells of 2 to 50 A–hr are common for experimental testing although, cells with capacities as high as 160 A–hr have been built. Current single ceramic cells exhibit specific energies between 90 to 200 Whr/kg with specific powers about 170 W/kg.[10] As with all experimental battery systems, costs for the ceramic cell are too high. Like their glass counterparts, current experimental ceramic cells cost in excess of 1000 $/kW–hr. Future development work seeks to reduce this cost to less than 50 $/kW–hr.

Current problems which must be solved include corrosion of the sulfur chamber, degradation and cracking of the electrolyte, and reduction of the electrolyte resistance. Corrosion of the sulfur chamber may be solved by using highly resistant metals which are unaffected by the corrosive properties of sulfur and polysulfides. These materials are quite expensive and thus do not represent the ultimate solution to this problem.

A mechanism for electrolye degradation has recently been proposed by De Jonghe.[11] In this work he has identified the most important factors responsible for degradation and failure of the electrolyte. Improper fabrication, poor thermal management, and improper charging procedures have been identified as the most common causes. Future work is aimed at finding improvements in these areas.

The increased resistance of the electrolyte has also been found as a significant cause of cell failures. One cause for a high electrolyte resistivity has been the buildup of low conducting reaction products very near the

electrolyte–melt interface. The low conductivity of the melt compared to the current collector matrix has been identified as the source of this problem. The low melt conductivity causes much of the cell reaction to occur in a region very near the electrolyte melt interface. One solution to this problem has been the introduction of a "gradated resistivity" current collector or a current collector with a spatially varying resistivity. This type of current collector has a high resistance near the electrolyte melt interface which decreases away from the electrolyte. The resistance of the current collector can be modified by combining material of differing conductivities in varying proportions through the current collector to produce a gradual change in its resistance. Another design is more straightforward. It is to sandwich two current collectors of different resistivities next to each other to produce and abrupt variation in the resistivity. In either design, the result is the same. Because of the higher ohmic drop in the current collector, more current is carried within the melt near the electrolyte, and the reaction is spread more uniformly through the sulfur electrode.

2.4. Previous Work and Literature Review

While numerous cell development programs have been undertaken, the availability of fundamental thermodynamic and transport data is still not as sufficient as one would expect for a system so close to production. Fundamental understanding of the transport processes occurring within the polysulfide melt also have not received sufficient attention. Even though the polysulfide is a highly nonideal, concentrated molten salt, the analysis of experimental data has been performed using equations applicable for ideal, dilute systems. The errors incurred by such an analysis are unknown. One

of the aims of this study is to identify deficiencies in the available transport data and to formulate a consistent set of transport equations. These can then be used to accurately interpret past experimental data and, eventually, as a basis for cell design and scale–up.

To characterize the transport processes in any system of three distinct species requires the determination of three independent transport properties. For a single electrolyte in a solvent, the three transport properties most commonly used are the diffusion coefficient of the salt, the transference number of either ion relative to the solvent, and the conductivity of the electrolyte–solvent mixture. However, many electrolytes can be formed from constituents where no discernible solvent exists. A eutectic mixture of the salts LiCl–KCl is an example. Three transport properties are still required to describe fully such a system. In this example, the transport properties are defined differently from the simpler electrolyte–solvent mixture. However, three independent transport properties defining this system are still a diffusion coefficient, a transference number, and a conductivity.

In addition to the three transport properties described above, accurate thermodynamic data are also needed. While the transport properties characterize the irreversible process, thermodynamic data define the driving forces for these processes. It is necessary to have activity data for all components of the mixture.

2.4.1. Preparation

The preparation of sodium polysulfides is covered in many of the articles appearing in this literature review. Preparation methods of polysulfides can roughly be divided into two types, chemical methods and

electrochemical methods. Chemical methods of preparing sodium polysulfides generally first require producing moisture–free sodium sulfide. This can be done in three general ways. First, relatively pure hydrated sodium sulfide, which is readily obtainable, can be dried and purified directly. This method is the most common. It is also possible to react pure sodium and sulfur, in the molten state, directly, but this synthesis is considered too dangerous and is generally not used. Last, sodium and sulfur can be combined in organic solvents which reduce the speed and consequently the risk of too rapid a reaction. Because methods requiring organic solvents are not able to produce a sufficiently pure product for experimental work, these procedures are less desirable. Traces of the organic solvent always remain after synthesis. Anhydrous sodium sulfide is most commonly produced today by the direct drying of the hydrated salt. Sodium polysulfides can also be prepared directly by electrochemical means, which yield very pure polysulfides. The product purity by this method is limited by the purity of the starting materials, sodium and sulfur; but these elements can generally be obtained in forms that are purer than sodium sulfide. In recent years ceramic electrolytes have become generally available, and this technique may become the favored method of synthesizing polysulfides in the future.

A single reference source covering many methods of preparation is Brauer.[12] Here, the preparation of sodium polysulfides of various compositions is discussed. Rosén and Tegman[13] describe, in very good detail, a method yielding very pure polysulfides from hydrated sodium sulfide and sulfur. Procedures for preparation of polysulfides from ceramic electrolytes are given by Cleaver and Davies.[14]

2.4.2. Physical and Transport Properties

The properties of sodium polysulfide melts have been studied and determined by a number of investigators. The most comprehensive sources of data for molten sodium polysulfides are the papers by Cleaver, Davies, and Hames[14] and Cleaver and Davies.[15,16] In these, the authors tabulate the following physical properties: densities, surface tensions, and viscosities for polysulfide melts at several temperatures and melt compositions. Values for the melt conductivity are also given. These authors also report measurements on the open–circuit potentials for cells composed of sodium and sulfur electrodes and cells with transference composed of two sulfur electrodes. Activities of polysulfide melts obtained from transpiration experiments of polysulfide melts are also included. Polysulfide activities calculated from vapor pressures compare favorably with those determined from equilibrium cell potentials.

Thermodynamic studies of open–circuit potentials for sodium–sulfur cells have also been performed by Gupta and Tischer.[7] They measured the open–circuit potential of sodium–sulfur cells at six temperatures and several different melt compositions. From these experiments, they calculated the chemical potential of sodium polysulfide and sulfur in the melt. They were also able to determine sulfur solubility in the upper two–phase region. Tegman[17] has also determined the activities for polysulfide melts from vapor transpiration experiments. This study is an extensive source of thermodynamic information. Many data are collected in this study over the range of temperatures from 523 K to 1273 K and sulfur compositions from 30 to 100 mole percent sulfur. Tegman empirically fits his thermodynamic data to a microscopic model for the actual composition

of polysulfide melts. He postulates the ions $S^{=}$ to $S_6^{=}$ and $S_8^{=}$ to exist in the melt. Very good agreement between the model and the thermodynamic data is obtained.

Determinations of the sulfur–polysulfide equilibria have been performed by Rule and Thomas,[18] Pearson and Robinson,[19] Oei,[20] and Rosén and Tegman.[21] The first sodium–sulfur phase diagram was published by Freidlich[22] in 1914. He assumed that sodium polysulfides existed as tetrasodium sulfides with a general formula Na_4S_y. Subsequently, Rule and Thomas[18] disproved Freidlich showing instead that sodium sulfides exist as disodium compounds. Rule and Thomas also established the first accurate phase diagram for the sodium–sulfur system. Following Rule and Thomas, Pearson and Robinson[19] determined a more accurate phase diagram for the sodium–sulfur system, which was the definitive standard for over 40 years. More recently, Oei[20] has redetermined the phase diagram for this system and redefined many of the phase boundaries. Rosén and Tegman[21] have repeated the determination of the phase diagram using more accurate and precise experimental techniques. The phase diagram of Tegman is probably the most accurate one available today.

Relatively little work has been performed on characterizing the transport of polysulfide melts. Transference numbers have received an especially scant treatment in the literature. The work of Cleaver and Davies[18] concludes with these authors attributing unity to the transference number of sodium ions relative to sulfur solvent. Such a conclusion, while appealing, leads to very ambiguous conclusions regarding the interactions of ions in the melt. Yoshida and Nakajima[23] present erroneous values of transference numbers for the ions with respect to laboratory fixed

reference frames. They obtained these values from experiments, but did not consider the variations of concentration through their apparatus when they performed their calculations.

Conductivities have fared only slightly better. Good values for conductivities have been tabulated in only one reference. Cleaver and Davies[14] present conductivities for a wide range of temperature and melt compositions. These were measured by an AC conductance bridge technique.

There have been a number of investigators in the past which have attempted to determine the diffusion coefficient in pure polysulfide melts. A review of several experiments and calculations is given in the comprehensive review by Tischer and Ludwig.[24] Tischer and Ludwig have combined limiting current rotating disk data obtained by Armstrong, Dickenson, and Reid[25] and the chronopotentiometric data of South and Sudworth[26] to obtain diffusion coefficients for a single polysulfide composition at one temperature. These authors have also obtained fair agreement between these results and diffusion coefficients estimated from conductivity and viscosity data. The values for D estimated by these methods are 6 to 9 $\times 10^{-7}$ cm^2/s at 623 K for Na_2S_3. Both Armstrong, Dickenson, and Reid[25] and South and Sudworth in their respective papers report the formation of an insoluble film on the surface of the electrode at high cathodic potentials. Independently, they both determine that the formation of such a film affects quantitative interpretation of their experimental results. Tischer and Ludwig, however, argue from subsequent unpublished experiments that the formation of a film occurs only in the "vicinity" of the electrode and not directly on the surface. Hence, Tischer and Ludwig argue that quantitative

interpretation of these experiments is not altered by this effect. Diffusion coefficients obtained from these experiments are thus stated to be representative of the melt.

Under anodic polarization, both groups have observed the formation of a second phase near the electrode surface. Unlike the sodium polysulfide film which was observed on the electrode, this second phase forms within the melt and is thought to be a sulfur rich phase in the two phase region. Armstrong, Dickenson, and Reid[25] postulate, however, that this second phase might also cover the electrode surface. They therefore, give no quantitative values for diffusion coefficients obtained from either anodic or cathodic limiting currents.

Recently, Divesek *et al.*[27] have determined the diffusion coefficient in sodium polysulfide melts using a rotating disk. To inhibit the effects of film formation, these investigators utilize a transient pulsing technique described by Nanis and Klein.[28] No film formation or second phase is observed when this technique is used. These authors report that no insoluble polysulfide film forms on the rotating disk when it is cathodically polarized to the limiting current. This, however, directly conflicts with the observations of Armstrong Dickenson, and Reid,[25] who observed the formation of such a film. The authors also observe the formation of a second distinct phase when the electrode is anodically polarized to the limiting current. Using the results of the transient rotating disk experiments combined with the cathodic limiting current results these investigators calculate values of diffusion coefficients and the concentration of electroactive species in the melt. Their results for the diffusion coefficient are near those determined by Tischer and Ludwig.[24] A

representative value of the diffusion coefficient for a concentration driving force is 2.0 × 10^{-6} cm^2/s for Na_2S_4 at 623 K. Divesek *et al.* also have measured the self diffusion coefficients for sulfur in melts of sulfur and sodium polysulfides. A stirred capillary diffusion apparatus was used with radioactive sulfur–35 as a tracer. Measured self diffusion coefficients are 2 × 10^{-5} cm^2/s for Na_2S_4 at 573 K.

Armstrong, Dickenson, and Reid[29] have performed AC impedance studies on the sodium polysulfide system using inert carbon electrodes at 623 K. They assume a thermodynamically ideal binary model for the melt and a single electron transfer reaction with equal diffusion coefficients for the oxidized and reduced species. From this, they calculate a diffusion coefficient for a concentration driving force of 1.4 × 10^{-5} cm^2/s for Na_2S_5. This value is quite a bit higher than any published before. The assumptions used in the analysis have been questioned by Divesek *et al.*,[27] and this determination is open to speculation.

Other investigations of pertinent interest are those performed by Rosén and Tegman,[13] Oei,[30] and Janz *et al.*.[31] Rosén and Tegman[13] have conducted x–ray diffraction on solid sodium polysulfides and determined the crystal symmetry and lattice parameters. Oei,[30] using x–ray diffraction techniques, seems to prove that $S_3^=$ is not stable in the solid phase above 373 K. Some density and surface tension data are also reported although this is not as extensive as the data of Cleaver and Davies.[15] Janz *et al.*[31] have conducted laser raman studies of solid polysulfides to determine the actual species in these solids. These investigators claim this technique supports the existence of the polysulfide ions $S_2^=$, $S_4^=$, and $S_5^=$. The existence of the polysulfide ion $S_3^=$ is not supported in these studies, nor is it disproven.

The work characterizing the behavior of sulfide ions in other nonaqueous solvents also deserves mentioning. Other articles of general interest are those of Boedewig and Plambeck,[32] Cleaver, Davies, and Schiffrin,[33] and Cleaver and Davies.[34] Boedewig and Plambeck have observed polysulfide ions in molten melts of LiCl–KCl eutectics. Polysulfide ions have also been studied in molten potassium thiocynate melts by Cleaver, Davies, and Schiffrin. Cleaver and Davies[34] have conducted freezing point depression experiments on polysulfides in fused potassium thiocynates. Tischer and Ludwig[24] review these and other investigations and discuss their implications to sodium polysulfide melts.

This literature review, while not exhaustive, gives most of the recent articles pertinent to the study of the thermodynamic and transport properties. From this, one can see that the availability of such data is quite limited. No doubt, there are countless other sources of proprietary data which are not available openly. Much work is still needed before an adequate data base is available sufficient for accurate battery design.

2.4.3. Mathematical Models

Several researches have proposed a number of models to predict the behavior of the sulfur electrode. The first of these were generally relatively straightforward and calculated the steady state spatial reaction distribution for a uniform composition melt. Gibson[35] was the first to propose such a model. His was a specific application of the more general model presented by Euler and Nonnenmacher.[36] The assumptions in these two models are linear kinetics, constant conductivities in the solid and melt phases, and a one–dimensional planar geometry. These restrictions, however, allow the governing equations to solved in closed–form, analytic expressions.

Brennan[37] and Breiter and Dunn[38] improved upon Gibson's model by allowing for a spatially varying resistivity in the current collector. The restriction to a melt of uniform composition was retained, but the planar geometry was replaced by a one–dimensional cylindrical geometry which is more representative of practical sodium–sulfur cells. These models were aimed at predicting the performance of cells containing "gradated resistivity" current collectors. Brennan formulated a model applicable for a current collector containing any number of concentric current collector "rings" with different conductivities. The governing equations were formulated in terms of an equivalent circuit model and solved by a computer using an equivalent resistance formula. Breiter and Dunn's model was similar to Brennan's although the approach was quite different. This model allows for a current collector of two materials with two different resistivities in the direction of current flow. Breiter and Dunn solved the resulting governing ordinary differential equations analytically, and were able to obtain a closed form solution for the variation of the reaction rate. They compared their results to some actual cell data and concluded that a "gradated resistivity" current collector has merit for improving the performance of these cells.

Kao and Wayner[39,40] have proposed a model based on a more thorough treatment of the actual processes involved in the sulfur electrode. Unlike the other models, which are restricted to melts of uniform composition, Kao and Wayner accounted for the effects of the non–uniform concentration variations upon the reaction distribution. They also present results for the transient behavior of the sulfur electrode during constant current discharges. The bulk convective velocities accompanying changes in the melt composition as well as the effect of migration were included. Solutions

to the governing equations were obtained by a computer using a ten–point collocation technique. Unfortunately, these authors over–simplify the transport equations neglecting the effects of diffusion on the concentration profiles. While their results are useful for the high rate discharges they present, these models will not be accurate in predicting the behavior of transient current discharges.

As one can see, a model encompassing all of the important features of sodium–sulfur cells has not yet been published. All of the models above treat only the behavior of the sulfur electrode and to varying degrees of complexity. A more accurate model would incorporate all of the considerations mentioned above, and would include the behavior of the sodium anode and electrolyte as well. The effect of diffusion has also not been considered. Proper formulation of the governing equations to account for this would be required for proper modeling of cycled cells. Also, thermal management of these cells has not received much treatment. The thermal response of the cell, especially the variation of electrolye conductivity with temperature would be quite useful. This too could be included in a future model.

2.5. Microscopic versus Macroscopic Model

Molten polysulfides are commonly formed by dissolving sodium monosulfide in a melt of molten sulfur. One might consider such a mixture to be composed of sodium cations and sulfur anions in a neutral sulfur solvent. While this assumption sounds simplistic, such an assumption about the melt composition can be very useful in cataloging both the transport and especially the thermodynamic properties.

A more sophisticated model for the electrolyte can be conceived by considering that neutral sulfur probably does not exist in melts of sodium polysulfides. Moreover, the actual composition of these melts is thought to involve various polysulfide anions and sodium cations. The polysulfide anions have a general formula given by $S_n^=$, where n varies from one to eight.

These two assumptions regarding the composition of the melt are not necessarily in conflict with each other. Each is defined from separate observations on the melt composition. From an external view, since sodium sulfide and sulfur were the original components, it is the simplest to expect that these components remain when combined to form the melt. Macroscopically, or from this outward view, sodium sulfide and sulfur then compose the melt. Upon detailed examination from perhaps spectroscopic or other techniques, one sees that polysulfide ions really are the actual species present. This microscopic view point leads to proposals about the detailed interaction and mechanisms between these melt species.

It is appropriate, at this point, to distinguish further the concept of models based on the macroscopic composition or the microscopic composition. In the late 1800's, Gibbs defined by example the usefulness of such a distinction. The dimerization of acetic acid was chosen to illustrate this concept. In this work, Gibbs shows how the vapor–liquid equilibria for acetic acid–water mixtures can be measured and correlated assuming that the vapor phase consists solely of a mixture of single acetic acid molecules and single water molecules. The choice of chemical constituents and their compositions in this model follow logically from observations on the individual items composing the mixture. The term "macroscopic" is given to denote this type of model. Thermodynamic data can be correlated assuming

this macroscopic view to apply with single acetic acid molecules and single water molecules actually composing the mixture. Gibbs shows, however, that ideal behavior for individual water and acetic acid molecules cannot be ascribed to this system even at low pressures.

To reconcile this discrepancy between theory and experiment, Gibbs postulates the concept of dimerized acetic acid molecules. This "microscopic" assumption regarding the composition of the system resolves the non–ideal behavior at low pressures. Theoretically, ideal behavior at low pressures assuming dimerized acetic acid molecules can now be calculated which differs from the behavior obtained when single acetic acid molecules were assumed. When the same data are correlated using this model, ideal behavior of the acetic acid–water vapor system is obtained. Thus, while the existence of acetic acid dimer did not impair Gibb's ability to obtain data on the system and correlate them, it did prevent agreement with calculated results derived from assumptions regarding the actual components present in the mixture.

Modern scientists and engineers would recognize the two fields which have grown from the concepts presented by Gibbs. The first is classical thermodynamics while the second is molecular thermodynamics or statistical mechanics. Classical thermodynamics is the macroscopic science. It provides a framework allowing the correlation and interpretation of data to be performed for any assumed state of aggregation, regardless of the true or actual configuration of species present. Statistical mechanics, on the other hand, deals with the individual particles which actually compose the mixture. The individual forces and particle interactions are predicted in this science.

As in the example presented above, thermodynamics and statistical mechanics meet at an intermediate point. Here, the results of statistical mechanics are combined with the observations and correlations of thermodynamics. If each separate field predicts the same result, credence to the assumed microscopic model can be inferred. If the unfortunate case occurs where the two sciences disagree, then one may revise the thinking about the actual state of aggregation. When the thermodynamic data did not match the limiting behavior with the assumption of a single acetic molecule, Gibbs revised his microscopic model by postulating the existence of the dimer.

The field of transport phenomena is analogous to thermodynamics. Transport properties describing the irreversible processes occurring can be defined and correlated for any assumed macroscopic model. Again, however, the properties must be predicted from a microscopic model which nearly represents the true state of the system.

This simpler example considered by Gibbs allows us to draw an analogy to the sodium–sulfur system. The transport properties and thermodynamic data of sodium polysulfide melts have been most commonly correlated using a macroscopic model consisting of sodium cations, sulfide anions, and neutral sulfur solvent. The transport and thermodynamic properties when correlated in this manner vary in very unpredictable ways. For the thermodynamic properties, the unpredictable behavior is lumped into activity coefficients which absorb this undesirable effect.

Again, the actual molecules composing polysulfide melts are definitely not these cations, anions, and solvent. A microscopic model can be formulated to predict the thermodynamic and transport properties without

resorting to the use of activity coefficients or other empirical relationships. The ultimate result of such a model would be a complete set of thermodynamic and transport properties spanning the range of temperatures and compositions found in the sodium–sulfur cell.

2.6. Purpose

This thesis does not deal with the optimization or design of any sodium–sulfur cells directly. The results of this study will be useful, however, for the designer of these cells. The long term objective is to predict the behavior of this system so that the costly and time consuming experiments can be minimized. The mathematical model of Pollard and Newman[41,42] would be an ideal tool for the prediction of the sodium–sulfur cell behavior. Many "numerical" experiments can be performed in much less time and at a considerably reduced cost than if these were actually performed in the laboratory. One can also include all of the improvements for a model suggested earlier, since all of these capabilities are presently available. To do so, however, requires accurate knowledge of thermodynamic and transport properties for sodium polysulfides. A proper theoretical framework providing a consistent set of transport equations is also needed.

This thesis has three purposes. They are: first, to predict the properties of sodium–polysulfide melts using a microscopic model and compare them to data obtained and correlated from information given for the macroscopic system; second, to identify shortcomings in the available experimental data and suggest ways in which required information can be obtained; and finally, to define rigorously the governing equations useful for battery design and determine how experimental data can be transformed

into quantities appearing in these equations. All of these will be covered here.

Chapter 3

Transport Properties For a Binary Melt

3.1. Introduction

In this chapter we will explore the description of transport processes based on the macroscopic melt composition. We develop transport equations for a melt of sodium polysulfides considering the melt to be composed of sodium cations, monosulfide anions, and a neutral sulfur solvent. While we choose to consider only these species, this in no way will affect the final outcome of our work. It will however, determine the path which we follow to the final result. Chapter Four will present a more sophisticated approach toward describing the transport processes within the melt.

In this chapter, we will not consider the effects of kinetically–limited homogeneous reactions. For now, we will require that local equilibrium prevail throughout the melt. By this, we mean that at every point through the melt each species is in an equilibrated state with the other species at the same location. We will not consider the possibility of "slow" homogeneous reactions occurring within the melt. The term slow refers to the time frame appropriate to the bulk movement of species through the melt. The rate of influx of species into any location must be much less than the rate of production of these species through homogeneous reactions. In effect, we require that as species diffuse through the melt, any homogeneous reactions must occur virtually instantaneously.

This model presented here is based on concentrated solution theory developed by Newman, Bennion, and Tobias[43] which has found widespread use for describing transport in aqueous systems. The more recent work by Newman[44] reviews this work in more detail and gives some additional information.

The transport of ions in sodium polysulfide melts is affected by the physical and chemical properties of the ions and their mutual interactions within the melt. The development of transport equations capable of accounting for these processes in a general way has so far not been developed. We will develop here a consistent set of transport equations which will be general enough to describe the transport processes under many situations. Fundamental transport parameters and measurable transport properties will be defined. Some recent experimental work then will be examined and related to the measurable transport properties. Finally, these data will be used to determine fundamental transport parameters and the implications with regard to fundamental solution interactions will be addressed.

3.2. Development of Transport Equations

The fundamental transport equation for an electrolyte relates the driving force per unit volume on species i with the frictional forces which oppose these driving forces. For a system at constant temperature and pressure, this is

$$c_i \nabla \mu_i = \sum_j K_{ij}(\mathbf{v}_j - \mathbf{v}_i) \qquad (3-1)$$

The left side of Equation (3–1) expresses the driving force for movement of species i in terms of the concentration of species i times the gradient of the electrochemical potential of species i. The opposing frictional forces are

written in terms of the summation of the differences in velocities of two general species $\mathbf{v}_j - \mathbf{v}_i$ multiplied by an appropriate friction coefficient K_{ij}. The friction coefficients K_{ij} can be replaced by binary interaction coefficients $\mathscr{D}_{ij}$ which are defined by

$$K_{ij} = RT \frac{c_i c_j}{c_T \mathscr{D}_{ij}} . \tag{3-2}$$

The K_{ij} and the corresponding $\mathscr{D}_{ij}$ parameters are dependent upon temperature, pressure, and composition; but independent of the magnitude of the driving forces. For a system composed of N species, Equation 3–2 defines $N(N-1)/2$ independent $\mathscr{D}_{ij}$ parameters. Newton's third law requires that

$$K_{ij} = K_{ji} , \tag{3-3}$$

or

$$\mathscr{D}_{ij} = \mathscr{D}_{ji} . \tag{3-4}$$

The parameters $\mathscr{D}_{ii}$ are not defined. One also finds that for N species, only $N-1$ independent transport equations are defined. Summation of equation (3–1) over subscript i yields

$$\sum_i c_i \nabla \mu_i = \sum_i \sum_j K_{ij} (\mathbf{v}_j - \mathbf{v}_i) . \tag{3-5}$$

The left side is zero by virtue of the Gibbs–Duhem Equation, and the right side is zero since $K_{ij} = K_{ji}$.

For solutions of varying temperature, the driving force in Equation (3–1) must be modified to include contributions from thermal diffusion (Soret Fluxes) and transport arising from body force interactions. The generalized driving forces accounting for these processes can be obtained from Hirschfelder, Curtis, and Bird[45] but will not be explored further here.

3.2.1. Binary Electrolye

For a binary electrolyte, Equation (3–1) can be expanded into two independent equations. Consider a single cation denoted by the subscript +, a single anion denoted by the subscript − and a neutral solvent denoted by o. The flux equations are then

$$c_+\nabla\mu_+ = K_{o+}(\mathbf{v}_o - \mathbf{v}_+) + K_{+-}(\mathbf{v}_- - \mathbf{v}_+) , \tag{3-6}$$

$$c_-\nabla\mu_- = K_{o-}(\mathbf{v}_o - \mathbf{v}_-) + K_{+-}(\mathbf{v}_+ - \mathbf{v}_-) . \tag{3-7}$$

These express the driving forces in terms of two differences in velocities and contain three independent transport parameters.

Normally one knows the driving forces, and the velocities of the species must be found. Equations (3–6) and (3–7) express the driving forces as linear combinations of the unknown velocities. One can mathematically invert these equations using the definition for the current density

$$\mathbf{i} = \sum_i c_i z_i \mathbf{v}_i , \tag{3-8}$$

to obtain expressions for the fluxes

$$\mathbf{N}_+ = c_+\mathbf{v}_+ = -\frac{\nu_+ \mathscr{D}}{\nu RT}\frac{c_T}{c_o} c\,\nabla\mu_o + \frac{\mathbf{i}t_+^o}{z_+F} + c_+\mathbf{v}_o , \tag{3-9}$$

$$\mathbf{N}_- = c_-\mathbf{v}_- = -\frac{\nu_- \mathscr{D}}{\nu RT}\frac{c_T}{c_o} c\,\nabla\mu_o + \frac{\mathbf{i}t_-^o}{z_-F} + c_-\mathbf{v}_o , \tag{3-10}$$

and

$$\mathbf{N}_o = c_o\mathbf{v}_o . \tag{3-11}$$

In the above equations $\nu = \nu_+ + \nu_-$ and $\mu_o = \nu_+\mu_+ + \nu_-\mu_-$. The total solution concentration or the sum of the anion concentration, the cation concentration, and the solvent concentration has been denoted by c_T. One has combined two of the independent K_{ij} parameters in Equations (3–6) and (3–7) into two transport properties appearing in Equations (3–9) and (3–10). The parameter $\mathscr{D}$ is the diffusion coefficient for the electrolyte

based on a thermodynamic driving force. In terms of the $\mathscr{D}_{ij}$ parameters it is

$$\mathscr{D} = \frac{\mathscr{D}_{0+}\,\mathscr{D}_{0-}(z_+ - z_-)}{z_+\,\mathscr{D}_{0+} - z_-\,\mathscr{D}_{0-}} . \tag{3-12}$$

This describes the movement of the neutral electrolyte due to variations in its chemical potential through the solution. The transference numbers with respect to the solvent velocity are defined

$$t_+^0 = 1 - t_-^0 = \frac{z_+\,\mathscr{D}_{0+}}{z_+\,\mathscr{D}_{0+} - z_-\,\mathscr{D}_{0-}} . \tag{3-13}$$

These represent the proportionality between the flux of ions and the current which flows in the solution. In a solution of uniform composition where the gradient of chemical potential is zero, the transference numbers with respect to a neutral solvent can be related to the fraction of current carried by the individual ions.

The driving force for diffusion used in Equations (3–9) and (3–10) is the gradient of the chemical potential of the electrolyte $\nabla\mu_e$. However, one most often encounters diffusion coefficients D based on concentration driving forces. One can relate these two through the following expression

$$D = \mathscr{D}\,\frac{c_T}{c_0}\left[1 + \frac{d\,\ln\gamma_{+-}}{d\,\ln m}\right], \tag{3-14}$$

where γ_{+-} is the molal activity coefficient and m is the molality of the electrolye. The relationship

$$\nabla\mu_e = \nu RT\,\nabla\ln(m\gamma_{+-}) . \tag{3-15}$$

has been used in obtaining Equation 3–14 which is the definition for the gradient of the electrochemical potential. Using these definitions, the diffusive fluxes in Equation (3–9) and (3–10) can be written equivalently as

$$\frac{\mathscr{D}}{\nu RT}\frac{c_T}{c_0}\, c\, \nabla\mu_e = D\left[1 - \frac{d\ \ln c_0}{d\ \ln c}\right]\nabla c\ . \tag{3-16}$$

The transport equations defined in Equations (3–9) and (3–10) define the fluxes in terms of the gradient of electrochemical potential and the current as driving forces. Many times, however, it is convenient to describe the transport in solutions using the potential as a driving force. To do so, one must first develop the concept of a potential within the solution. Newman[44] has shown that the potential can be measured at any point in the cell using a suitable reference electrode. An arbitrary half cell–reaction

$$s_- M_-^{z-} + s_+ M_+^{z+} + s_0 M_0 = ne^- \tag{3-17}$$

involving the anions, cations, and solvent can be considered. Application of thermodynamic principles to the reaction in Equation (3–17) gives

$$s_-\nabla\mu_- + s_+\nabla\mu_+ + s_0\nabla\mu_0 = -nF\nabla\Phi\ . \tag{3-18}$$

Using this definition of the potential, one may eliminate the electrochemical potential of one of the ionic species appearing in Equation (3–6) and (3–7) and in its place substitute the potential. One can then eliminate the electrochemical potential of the remaining ion in favor of the chemical potential of the electrolyte. When these manipulations are performed, the definition of the current density becomes

$$\mathbf{i} = -\kappa\nabla\Phi - \frac{\kappa}{F}\left[\frac{s_+}{n\nu_+} + \frac{t_+^0}{z_+\nu_+} - \frac{s_0 c}{nc_0}\right]\nabla\mu_e\ . \tag{3-19}$$

Equation (3–19) includes a new transport property, the conductivity κ. In terms of the $\mathscr{D}_{ij}$ parameters it is

$$\frac{1}{\kappa} = -\frac{RT}{c_T z_+ z_- F^2}\left[\frac{1}{\mathscr{D}_{+-}} + \frac{c_0 t_-^0}{c_+\ \mathscr{D}_{0-}}\right]. \tag{3-20}$$

The physical meaning of the conductivity can be described by considering a solution of uniform composition. Under this condition,

Equation (3–19) reduces to

$$\mathbf{i} = -\kappa \nabla \Phi, \tag{3-21}$$

which is Ohm's Law. Thus the conductivity is the proportionality constant between the gradient of potential and the resulting current density for a solution of uniform composition. The additional terms in Equation (3–19) account for the variations in potential due a nonuniform composition profile.

Unlike the transference number and the diffusion coefficient, the conductivity contains all three of the independent $\mathscr{D}_{ij}$ parameters. From the initial three independent K_{ij} which were defined in Equations (3–6) and (3–7), the inverted transport equations have been expressed in terms of three new independent transport properties. These are the conductivity κ, the transference number t_+^0, and the diffusion coefficient $\mathscr{D}$ all of which are functions of temperature, pressure, and composition. Each of these is a well defined solution property which can be obtained from experiments. In contrast, the three $\mathscr{D}_{ij}$ parameters are not accessible by direct experimentation but are an equivalent means of specifying the transport processes.

At this point, the development of the flux equations is completed. The final equations are Equations (3–9), (3–10), (3–11), (3–15), and (3–19). Equations (3–9), (3–10), and (3–11) give the fluxes in terms of the gradient of chemical potential of the electrolyte, the current density, and the solvent velocity. The definition of the current density is given in Equation (3–8). Equation (3–19) relates the current density to the gradient of the solution potential and to the gradient of the chemical potential of the electrolyte. The gradient of the chemical potential of the electrolyte can be related to

the concentration through the thermodynamic relationship given in Equation (3–15). If the electrolyte concentration and the solvent velocity are known, then any of the other quantities can be calculated from these equations. The solvent concentration, which is unknown, may also be needed. To obtain the two concentrations and the solvent velocity, one needs additional equations specifying these quantities.

For the electrolyte concentration and solvent concentration, the additional required equations can come from a material balance. For N species one may write N independent material balances, thus for a binary electrolyte, there are three independent material balances. The material balance for any species i can be expressed as

$$\frac{\partial c_i}{\partial t} = \nabla \cdot \mathbf{N}_i + R_i \,. \tag{3-22}$$

This states that the rate of change of any amount of material in a differential volume is given by the sum of the net external inflow plus the net internal generation. One may need additional equations to relate the internal generation process to the other known quantities.

The three material balance equations can be arranged to provide an equal number of independent expressions for conservation of other quantities. For example, the continuity equation, which expresses conservation of total mass, can be obtained by summing the individual species conservation equations. The electroneutrality condition

$$\sum_i z_i c_i = 0 \,,$$

can be obtained by considering the conservation of charge which requires

$$\nabla \cdot \mathbf{i} = 0 \,.$$

One must also specify the velocity of the reference species, which in this case has be designated as the solvent velocity. If this is not known, it must be determined. The equations of fluid mechanics provide the basis for obtaining this quantity. The equation of continuity and the Navier–Stokes Equations are two generalizations of fluid mechanics which are often used if the flow field is determined from external forces acting upon the system. The continuity equation is not a separate independent conservation equation, but it can be obtained by summing the material balance equations derived above over all individual species. It is also possible for chemical or electrochemical reactions to generate fluid motion within the electrolyte. The generation of reaction products which have volumes significantly different from the constituent reactants can cause a bulk movement of fluid. In this case, one must relate the fluid velocity to the reaction process to obtain the velocity throughout the solution.

3.2.2. Reference Velocities

It is possible, and sometimes very desirable, to choose a reference velocity other than the solvent velocity. Analogous forms of Equation (3–9) through (3–11) can be obtained which define new properties appropriate to the chosen convention. One may pick the velocity of a species as the reference velocity or one may choose to use linear combinations of the velocities of all species. The mass average or molar average velocity are examples of these conventions. The mass average velocity is advantageous if the flow is determined from the equations of motion since these are formulated most conveniently in terms of the mass average velocity. When the flow is determined by the rate of the reaction, the molar average velocity can prove to be more useful.

For the sodium–sulfur system, an alternate approach might involve choosing the velocity of the cation as the reference velocity. This convention has been used by Kao and Wayner[39,40] in a previous investigation to describe the transport processes. They have used the velocity of the sodium cation as their reference species instead of the neutral sulfur solvent. One can obtain the equations for this reference frame by algebraic manipulation of Equations (3–9) through (3–11). If one solves Equation (3–9) for the solvent velocity in terms of the cation velocity and then replaces the solvent velocity appearing in Equations (3–10) and (3–11) with this expression, the following set of equations is obtained:

$$\mathbf{N}_+ = c_+ \mathbf{v}_+ . \tag{3-23}$$

$$\mathbf{N}_- = \frac{\mathbf{i}}{z_- F} + c_- \mathbf{v}_+ . \tag{3-24}$$

$$\mathbf{N}_s = -\frac{\mathscr{D}}{\nu RT}\frac{c_s c_s}{c_T}\nabla\mu_s - \frac{c_s}{c_+}\frac{\mathbf{i}t_+^s}{z_+ F} + c_s \mathbf{v}_+ . \tag{3-25}$$

These are nearly identical to the Equations obtained by Kao and Wayner† except for the additional diffusive term appearing in Equation (3–25). Later, we will discuss why Kao and Wayner have neglected this term and what the consequences of this approximation are.

The equations developed here provide a consistent framework for the description of transport in a system containing a solvent and binary electrolyte. For these three components, two independent flux equations have been defined containing three independent transport properties. We have shown that the structure of the equations depends upon the chosen reference velocity; however the number of transport properties is the same regardless of this choice. The next section will focus on the experimental determination of these properties.

†See Equations (2), (3), and (4) of reference [40]

3.3. Experimentally Determined Transport Properties

The three transport properties defined above have been well documented for a number of binary aqueous electrolytes. Techniques for obtaining these properties have been well developed for these systems enabling the properties to be gathered accurately and with a high degree of precision. The high–temperature polysulfide melt, however, represents a new challenge for the experimentalist. Most of these techniques become unusable when one must deal with compounds as reactive and corrosive as the sodium polysulfides. Moreover, the high temperatures and the inability to work in an ambient atmosphere place limits on the types of experiments which can be performed. One is unable to gather an equivalent amount of data with the same precision as for an aqueous system. Given these considerations, the recent work on the transport properties is discussed next.

3.3.1. Transference Number

The transference number for many common aqueous electrolytes can be measured from either the Hittorf method or the moving boundary method. The Hittorf method involves measuring the concentration changes near two electrodes when current is passed between them. The more accurate moving boundary method determines transference numbers by monitoring the progress of the boundary between two electrolytes while current is flowing through the boundary. For sodium polysulfide melts, each of these methods is impractical due to the high temperatures and the opaque nature of the electrolyte. It is possible, however, to obtain transference number data from open circuit potential measurements on a

cell with transference. Such a cell is made by combining two sulfur electrodes of different compositions with a "transition region" or diffusion junction separating the two. Cleaver and Davies[18] were the first to suggest such a method but did not perform any calculations. Newman[46] has demonstrated the calculation of transference numbers from open circuit potential measurements using the same data of Cleaver and Davies.

A slightly modified analysis from that of Newman has been performed to determine the transference numbers within the melt. The highlights of the method are presented here while detailed derivations of the Equations are given in Appendix B.

Open–circuit–potential measurements have been performed on the following cell with transference

Cell 2

$$\begin{array}{ccccccc} \alpha & & \beta & & \gamma & \delta & \alpha' \\ C\,| & Na_2S_y\,| & & |\,Na_2S_y\,| & & S\,(l) & |\,C\,. \end{array}$$

The potential U_2 of this cell is shown to be given by

$$FU_2 = -\frac{1}{2}\int_{\gamma}^{\beta}\left[t_+^{\circ}\,\frac{1-x_e}{x_e}+1\right]d\mu_o\,. \qquad (3\text{–}26)$$

where x_e denotes the mole fraction of sodium sulfide in the transition region. A complete discussion of the various composition conventions in polysulfide melts is given in Appendix A. Differentiating this expression for the cell potential gives

$$dU_2 = -\frac{RT}{2F}\left[t_+^{\circ}\,\frac{1-x_e}{x_e}+1\right]d(ln\ a_o)\,. \qquad (3\text{–}27)$$

Provided the differential of the activity of sulfur and the differential of the cell potential are known, the transference number can be determined.

The differential of the activity of sulfur within the melt can be determined from the potential U_1 of the cell

Cell 1

α	β	γ	δ	α'
C |	Na (l) |	β–alumina |	Na_2S_y (l)	| C .

This is

$$d(ln\ a_e) = \frac{2F}{RT} x_e dU_1 . \tag{3-28}$$

Combining Equations (3–27) and (3–28), the transference number of sodium ions relative to neutral sulfur is

$$t_+^e = \frac{-\frac{dU_2}{dx_e}\cdot\frac{dx_e}{dU_1} - x_e}{1 - x_e} . \tag{3-29}$$

The important result of Equation (3–29) is that the transference number of sodium ions relative to neutral sulfur solvent can be related to the variation in the two cell potentials with the variation mole fraction of sodium sulfide.

Cleaver and Davies[16] present cell potential versus melt composition for the cells described above (see Figures 4–9 and 4–10). The potentials of the cells for two temperatures, 573.15 K and 633.15 K are given. The essential feature of these curves is that the cell potential is very nearly linear with the mole fraction of sodium sulfide. The potential of the cells can therefore be described by the following relationships

$$U_1 = \alpha_1 + \beta_1 x_e , \tag{3-30}$$

and

$$U_2 = \alpha_2 + \beta_2 x_e . \tag{3-31}$$

Thus,

$$\frac{dU_2}{dx_e}\,\frac{dx_e}{dU_1} = \frac{\beta_2}{\beta_1}, \tag{3-32}$$

and

$$t_+^o = \frac{-\frac{\beta_2}{\beta_1} - x_e}{1 - x_e}. \tag{3-33}$$

Values for the α's and β's at the two temperatures are given in Table 3–1 and 3–2. While Equation (3–29) gives the transference number for sodium ions relative to sulfur solvent, the value of this number is very close to one, and it is more convenient to consider the transference number of sulfide ions. The transference number of sulfide ions is given by

Table 3–1 Values for α_1 and β_1 describing the open circuit potential of cell 1 for the data of Cleaver and Davies.

Temperature, K	α_1, V	β_1, V	Rel. Std. Dev., %
573	+2.4681	-1.9812	0.0007
623	+2.4632	-2.0253	0.05

Table 3–2 Values for α_2 and β_2 describing the open circuit potential of cell 2.

Temperature, K	α_1, V	β_1, V	Rel. Std. Dev., %
573	-0.34955	1.8111	0.4
623	-0.39371	1.9958	0.2

$$t_-^o = 1 - t_+^o \quad . \tag{3-34}$$

Figure 3–1 plots the transference number for sulfide ion as a function of composition for the two temperatures. This shows, subject to the stated assumptions, the transference number is nearly constant over the range of compositions encountered.

3.3.2. Conductivity

The conductivity of electrolytic solutions can be determined by the measurement of current resulting from the application of a known potential. Most often, an alternating voltage source is used to eliminate the undesirable effects of concentration gradients. Cleaver and Davies[14] have utilized this technique to obtain conductivity data on several polysulfide melts at different temperatures. They have correlated the data for discrete melt compositions using an empirical function of temperature

$$\kappa = Ae^{-\frac{E_\kappa}{R(T - T_0)}} \quad . \tag{3-35}$$

The values of A, T_0, and E_κ depend upon the melt composition and are given in Table 3–3.

A plot of the melt conductivity at two different temperatures is given in Figure 3–2. The conductivity exhibits some rather unusual behavior at higher electrolyte compositions. Instead of increasing at a constant rate with the mole fraction of sodium sulfide, the values for the conductivity level out in this range.

3.3.3. Diffusion Coefficient

The determination of the diffusion coefficient in polysulfide melts has been attempted by a number of investigators. Most of these works are reviewed in Chapter Two. A more thorough discussion of the problems

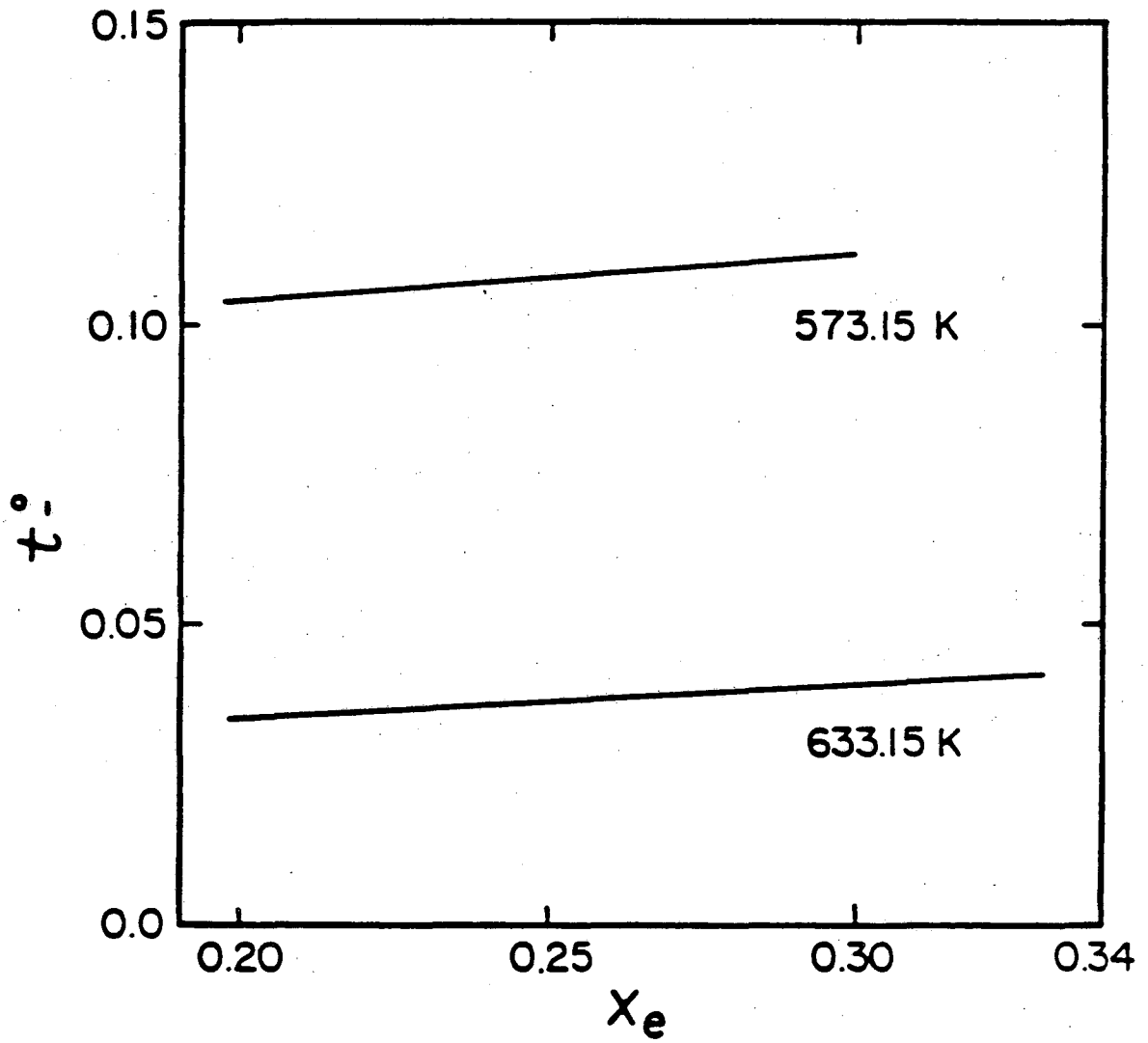

Figure 3–1 Calculated sulfide ion transference numbers relative to neutral sulfur solvent as a function of melt composition for sodium polysulfide melts. Numbers calculated from the data of Cleaver and Davies.[16]

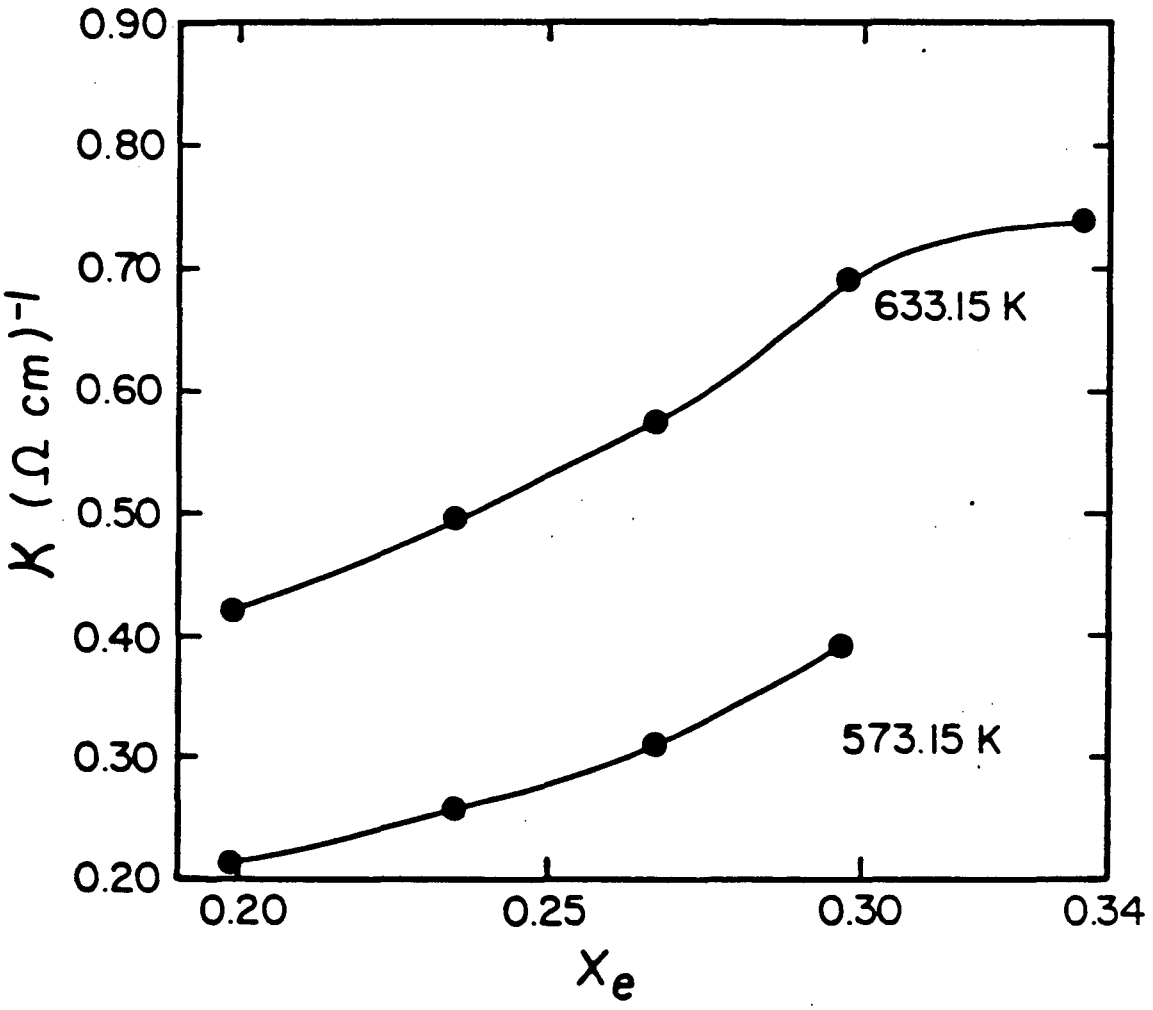

Figure 3–2 Experimental conductivity for sodium polysulfides as a function of melt composition. Figure reproduced from Cleaver and Davies.[14]

Table 3–3 Values of the parameters in Equation (3–35) describing the conductivity of polysulfide melts, from Cleaver and Davies.[14]

Melt	wt % S	Temp. range K	A $(\Omega\text{-cm})^{-1}$	E_κ kJ/mol	T_0 K
$Na_2S_{2.1}$	60.0	728-840	5.478	3079	499
$Na_2S_{2.9}$	66.1	642-698	3.863	2478	458
$Na_2S_{3.0}$	67.5	582-693	7.033	5693	329
$Na_2S_{3.2}$	70.1	458-694	7.048	5854	330
$Na_2S_{3.8}$	72.3	428-694	7.056	6436	325
$Na_2S_{4.2}$	74.8	456-671	6.279	6163	341
$Na_2S_{5.1}$	77.8	477-681	5.815	6329	344

encountered in measuring diffusion coefficients is given later in Chapter Five. At this time, no reliable experimental data for the diffusion coefficient exist.

3.3.4. Thermodynamic versus Concentration Driving Force

In the development of the flux equations, we have shown how one may express diffusive fluxes in terms of a driving forces based on gradients of chemical potential or ones based on gradients of concentration. The diffusion coefficient for a concentration driving force D has been related to the more fundamental diffusion coefficient $\mathscr{D}$ based on the thermodynamic driving force by Equation (3–14). Many investigators report diffusion coefficient data in terms of D rather than $\mathscr{D}$. It is therefore necessary to interconvert between these two properties. One needs an expression relating $1 + d \ln \gamma_{+-} / d \ln m$ to measurable quantities.

The definition of the chemical potential of sodium sulfide can be written in two ways

$$\mu_s = \mu_s^o + RT \ln a_s = \mu_s^o + \nu RT \ln(m_s \gamma_{+-}) . \qquad (3\text{-}36)$$

The far right side of Equation (3–36) is the convention preferred by Newman[44] while the middle expression is used by Cleaver and Davies.[16] By differentiating Equation (3–36) and dividing by the parameter ν we obtain

$$1 + \frac{d \ln \gamma_{+-}}{d \ln m} = \frac{1}{\nu} \frac{d \ln a_s}{d \ln m} , \qquad (3\text{-}37)$$

which relates the desired quantity to the variation of the activity of sodium sulfide in polysulfide melts with respect the molality of sodium sulfide. One may obtain the activity of sodium sulfide from the activity of sulfur by applying the Gibbs–Duhem Equation to the melt

$$x_s \, d(\ln a_s) + x_o \, d(\ln a_o) = 0 . \qquad (3\text{-}38)$$

The activity of sulfur in the melt can be obtained from the potential of Cell 1 in Equation (3–28). Combining Equations (3–28) and (3–38) along with the definition of the electrolyte molality

$$m = \frac{1}{M_o} \frac{x_s}{(1 - x_s)} , \qquad (3\text{-}39)$$

and using the chain rule we obtain

$$1 + \frac{d \ln \gamma_{+-}}{d \ln m} = - \frac{x_s (1 - x_s)^2}{\nu} \frac{2F}{RT} \frac{dU_1}{dx_s} . \qquad (3\text{-}40)$$

The potential of Cell 1 has been measured by Cleaver and Davies[16] at two temperatures but additionally, Gupta and Tischer[7] have also measured the potential of this cell. They have tabulated the cell potential for several melt compositions at six temperatures of interest. Like the data of Cleaver and Davies, the data of Gupta and Tischer are very nearly linear with the mole fraction of sodium sulfide. Table 3–4 gives the parameters defined in Equation (3–30) for the cell potential versus mole fraction of sodium sulfide.

Table 3–4 Values for α_1 and β_1 describing the open circuit potential of cell 1 for the data of Gupta and Tischer.

Temperature, K	α_1, V	β_1, V	Rel. Std. Dev., %
553.15	2.46	-1.984	0.02
573.15	2.47	-2.057	0.01
603.15	2.47	-2.088	0.03
633.15	2.48	-2.158	0.004
663.15	2.50	-2.232	0.01

The quantity $1 + d \ln \gamma_{+-} / d \ln m$ calculated from Equation (3–40) is plotted versus melt composition in Figure 3–3. We have shown this quantity calculated from the data of Cleaver and Davies and Gupta and Tischer for the several temperatures. One can see that there is slight disagreement between the two works, but since these curves have been obtained by differentiating data, some error is expected. The general trends between the two sets of data are not similar. The data of Gupta and Tischer predict that the quantity $1 + d \ln \gamma_{+-} / d \ln m$ generally decreases with temperature while the measurements of Cleaver and Davies show the opposite trend.

3.3.5. Concentrations

In addition to the three independent transport properties, the flux equations also require that the concentrations of the solvent and the electrolyte be known. Concentrations of the melt components can not be obtained directly from the literature. It is possible, however, to calculate the concentrations from density data if the overall melt composition is known. Our convention for describing the overall melt composition has been

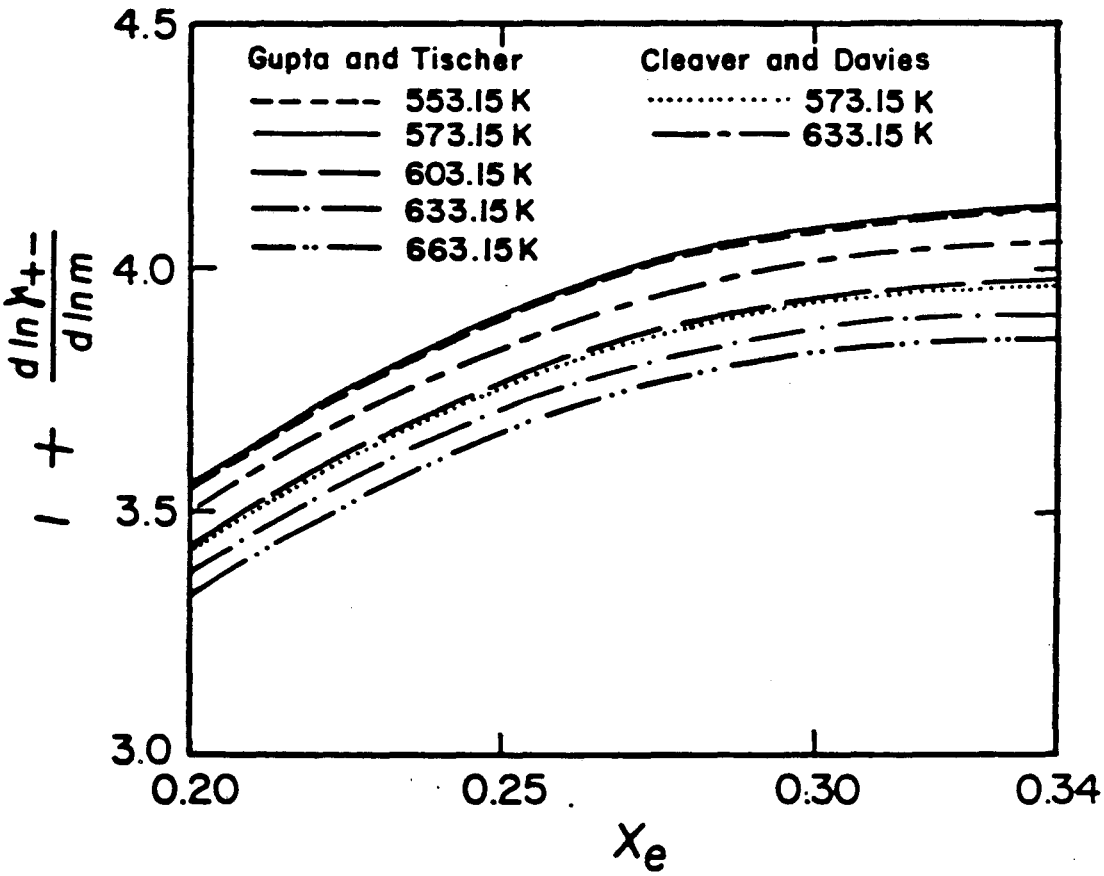

Figure 3–3 Calculated activity coefficient factor for sodium polysulfide melts using the data of Gupta and Tischer[7] and Cleaver and Davies.[16]

to use the mole fraction of the sodium sulfide electrolyte. Given this definition for the melt composition, the concentration of the electrolyte can be determined from

$$c = \frac{\rho}{M_{av}} x_e \,, \tag{3–41}$$

where M_{av} is the average molecular weight of the melt

$$M_{av} = x_e M_e + (1 - x_e) M_o \,. \tag{3–42}$$

The molecular weight of sodium sulfide has been designated by M_e while the molecular weight of sulfur is M_o. The concentrations of the anions and cations follow directly from Equation (3–41) and are

$$c_+ = \nu_+ c = \frac{\rho}{M_{av}} \nu_+ x_e \,, \tag{3–43}$$

and

$$c_- = \nu_- c = \frac{\rho}{M_{av}} \nu_- x_e \,. \tag{3–44}$$

The concentration of the solvent is

$$c_o = \frac{\rho}{M_{av}} (1 - x_e) \,, \tag{3–45}$$

and the total solution concentration is

$$c_T = \nu c + c_o = \left[1 + (\nu - 1) x_e\right] \frac{\rho}{M_{av}} \,. \tag{3–46}$$

3.3.6. Densities

The densities of polysulfide melts were taken from the experimental results of Cleaver and Davies.[15] They have correlated densities for several discrete melt compositions as linear functions of temperature

$$\rho = D + E(T - 600). \tag{3–47}$$

In Equation (3–47), D and E are constants dependent on melt composition, and T is the temperature in K. Values for D and E are given in Table 3–5. The uncertainity in these density measurements is estimated at 1%.

Table 3–5 Values of parameters in Equation (3–47) taken from Cleaver and Davies.[15]

Melt	Wt. % S	Temp. range K	D g/cm^3	E × 10^4 $g/cm^3/K$
Na_2S_3	67.6	590-683	1.887	-5.65
$Na_2S_{3.3}$	69.7	576-689	1.901	-7.96
$Na_2S_{3.7}$	72.0	563-669	1.926	-5.47
$Na_2S_{4.4}$	75.4	571-680	1.869	-6.66
$Na_2S_{4.8}$	77.0	573-683	1.876	-7.16

A graph of the densities for the discrete compositions as a function of temperature is given in Figure 3–4. Melt densities as a function of composition for several temperatures are given Figure 3–5. The somewhat unusual composition dependence of the experimental density values on temperature may be misleading. Much of the variation may be due to experimental uncertainities since the precision of the experimental measurements is only 1 %.

3.4. Calculation of Transport Parameters

If the conductivity, the transference number, and the diffusion coefficient are all known, then the binary $\mathscr{D}_{ij}$ transport parameters can be calculated. The $\mathscr{D}_{ij}$ can be calculated at different temperatures, pressures, and compositions provided the three measurable properties are also known as functions of these same variables. The objective of using the $\mathscr{D}_{ij}$'s is to reduce the complications involved with correlating the three transport properties which represent three very different processes. One

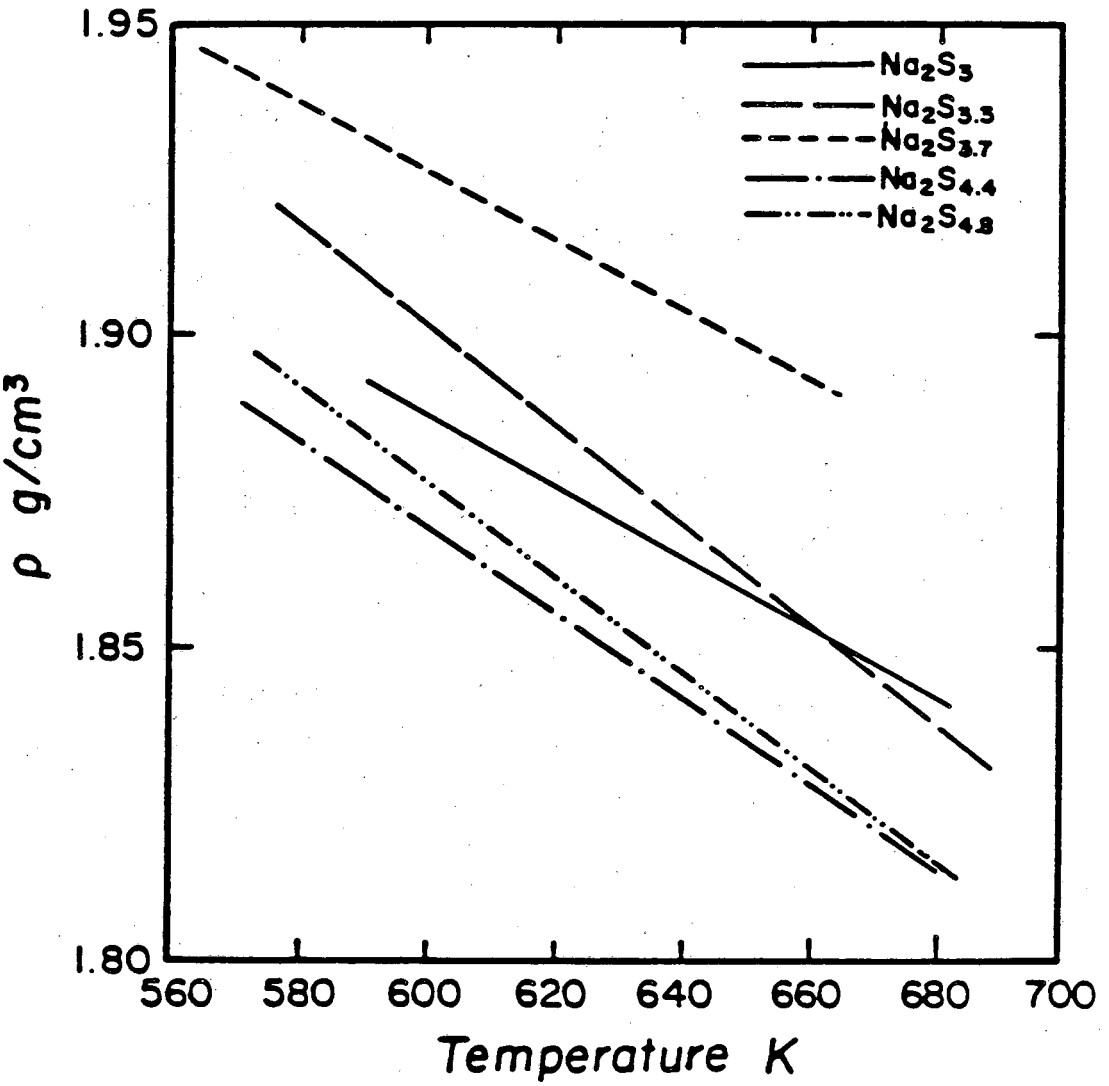

Figure 3–4 Sodium polysulfide density versus temperature for various melt compositions. Data obtained from Cleaver and Davies.[15]

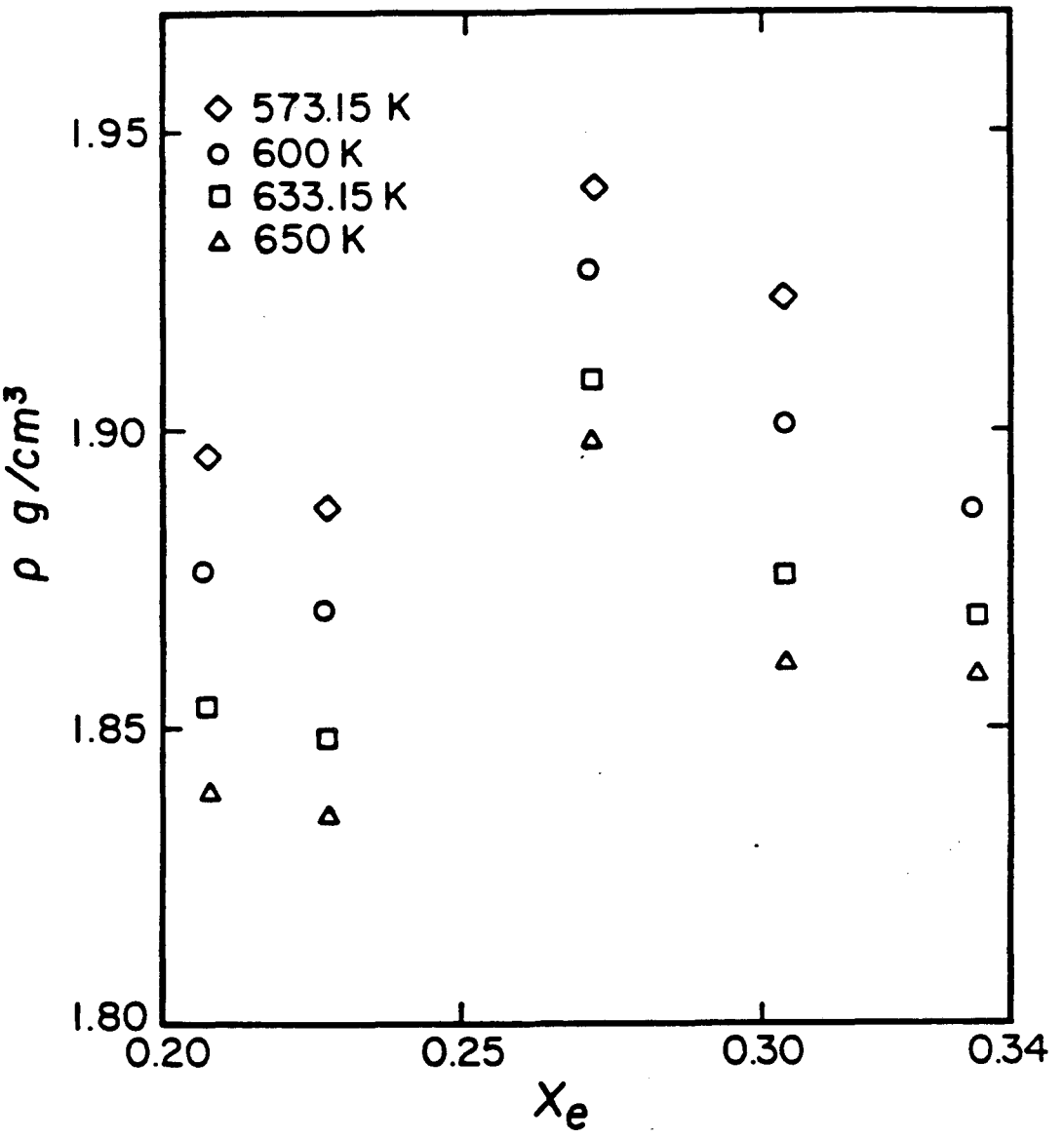

Figure 3–5 Sodium polysulfide density versus composition for several temperatures. Data obtained from Cleaver and Davies.[15]

would hope that the $\mathscr{D}_{ij}$'s would be much more fundamental parameters and one could correlate these much more successfully. If values of $\mathscr{D}$, κ, and t_+^0 are all known, then the transport parameters $\mathscr{D}_{0+}$, $\mathscr{D}_{0-}$, and $\mathscr{D}_{+-}$ are uniquely determined.

One can invert Equations (3–12), (3–13), and (3–20) for the transport properties into expressions explicit in the three $\mathscr{D}_{ij}$. From Newman[44] these equations are

$$\mathscr{D}_{0-} = \frac{z_+}{z_+ - z_-} \frac{\mathscr{D}}{t_+^0}, \tag{3-48}$$

$$\mathscr{D}_{0+} = \frac{-z_-}{z_+ - z_-} \frac{\mathscr{D}}{1 - t_+^0}, \tag{3-49}$$

and

$$\frac{1}{\mathscr{D}_{+-}} = -\frac{z_+ z_- c_T F^2}{RT\kappa} - \frac{z_+ - z_-}{z_+ \nu_+} \frac{c_0 t_+^0 t_-^0}{c\,\mathscr{D}}. \tag{3-50}$$

If one measures D instead of $\mathscr{D}$, it is necessary to correct D using Equation (3–14).

The values for the three transport parameters have been calculated for a polysulfide melt at 633.15 K over the range of compositions commonly encountered in the sodium sulfur cell. We have used the conductivity data of Cleaver and Davies[14] and transference numbers calculated from the equilibrium cell potentials of Cleaver and Davies.[16] Accurate diffusion coefficients, which are unavailable, were estimated. A constant value for D equal to 4.0×10^{-6} cm^2/s has been assumed.

Since not all of the required physical and transport properties were not available at the same melt composition, it was necessary to develop an interpolating procedure. The cubic spline technique was chosen to determine the needed properties at any composition. The principle of this

technique is to construct a set of cubic equations through each consecutive set of four data points. The curves are constructed such that the values of the functions at the given points are matched and so the slopes of the curves are continuous at the given points. The necessary calculations for the cubic spline are performed by the subroutine CUBSPL. The sodium–sulfur physical and transport property data are calculated by the subroutine PROPRT. The necessary data at intermediate compositions are calculated by the subroutine CURVE. These subroutines are all listed in Appendix F.

Figure 3–6 shows the variation of the $\mathscr{D}_{ij}$ parameters for the polysulfide melt at 633.15 K. The most important feature of this plot is the nearly constant values of the $\mathscr{D}_{0-}$ and the $\mathscr{D}_{0+}$ parameters. Unfortunately, the value of $\mathscr{D}_{+-}$ exhibits some rather unpredictable behavior. The very unusual variation in the conductivity causes this unusual trend. One can see that the $\mathscr{D}_{+-}$ behaves as unpredictably with respect to the melt composition as the conductivity does. There seems to be very little advantage in dealing with the $\mathscr{D}_{ij}$ parameters versus the three transport properties using this binary model. While it is useful to consider a binary melt composition, we see that the fundamental analysis does not lead to results which have an inherent advantage over the consideration of the transport properties alone.

3.5. Second Law Requirements

One might wonder whether the $\mathscr{D}_{ij}$ parameters calculated satisfy the second law. This requires that the total entropy change for any irreversible change must be greater than zero. In Appendix C, constraints on the $\mathscr{D}_{ij}$'s have been derived which lead to conditions which satisfy the second law.

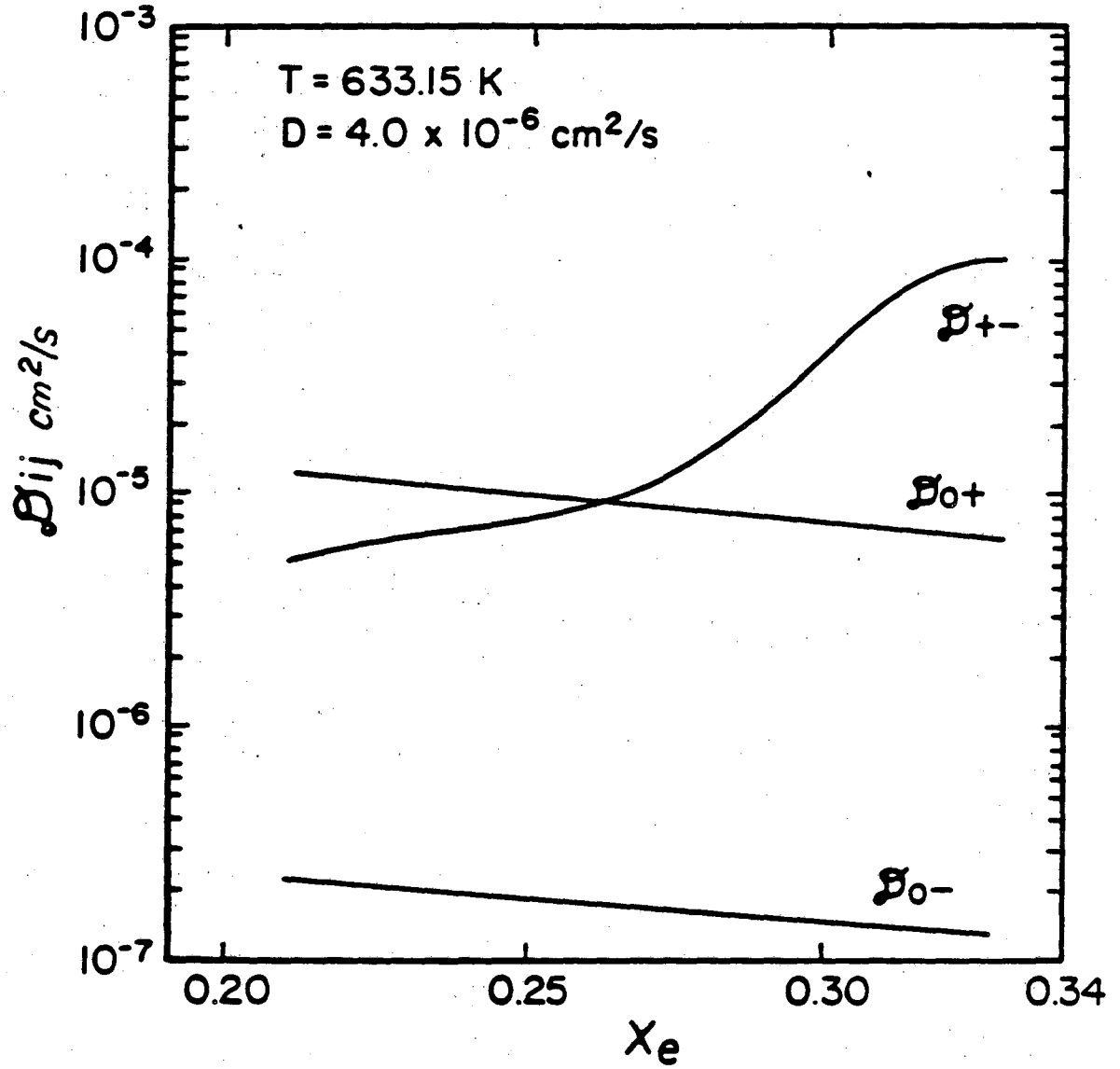

Figure 3–6 Binary interaction coefficients as a function of melt composition for sodium polysulfide melts at 633.15 K.

The results of Appendix C show that for the second law to be obeyed, the diffusion coefficient $\mathscr{D}$ and the conductivity κ must be greater than zero. Since the $\mathscr{D}_{ij}$'s in Figure 3–6 have been calculated from conductivities and diffusion coefficients which are greater than zero, they must satisfy the second law.

3.6. Applications to Previous Work We have discussed the work of Kao and Wayner in regard to the choice of reference velocities. Kao and Wayner have formulated a model for transport processes in the sodium polysulfide which is very similar to the work performed here. Their governing equations do not include the diffusive term contained in Equation (3–25). By observing the values of transference numbers which are very near one, they have assumed that K_{o-} is effectively infinity or $\mathscr{D}_{o-}$ is zero. From Figure 3–6 we see that while $\mathscr{D}_{o-}$ is small compared to $\mathscr{D}_{+-}$ or $\mathscr{D}_{o+}$ it is not zero. If $\mathscr{D}_{o-}$ is assumed to be equal to zero, then one is left with the unsatisfactory result that $\mathscr{D}$ must also be zero. One cannot then consider the process of diffusion within the melt if this assumption is invoked. Consequently, one must recognize that the transference number of sodium ions is not unity, and it is therefore important to have accurate data for all of the three transport properties.

3.7. Conclusions

A consistent set of transport equations has been developed for a melt of sodium polysulfides. We have used the concept of the binary melt where the constituents were defined as sodium cations, monosulfide anions, and neutral sulfur. The starting point for this derivation considered the interactions between these three species in the melt which could be expressed as two independent force balances. Appearing in these force

balances are three interaction parameters describing the forces acting upon these components as they move through the melt. From these, three independent, measurable transport properties were derived by inverting the transport equations. The conductivity, transference number, and diffusion coefficient were found to define uniquely the transport processes within the melt.

Experiments to determine the measurable transport properties were discussed. Conductivities were taken directly from literature data while transference numbers were calculated from cell potential data. Diffusion coefficients for polysulfide melts were estimated.

The fundamental binary interaction parameters for molten sodium polysulfides have been calculated from experimental data on the conductivity, transference number, and diffusion coefficient. These have been correlated with the melt composition based on the mole fraction of sodium sulfide. The resulting interaction parameters have been shown to exhibit unpredictable behavior.

Chapter 4

Transport Properties for a Multicomponent Melt

4.1. Introduction

In Chapter Three, the transport properties for sodium polysulfide melts were defined considering a binary melt. Three species were considered: sodium cations, monosulfide anions, and neutral sulfur solvent. In this chapter, we will calculate transport properties from first principles considering a microscopic melt model.

4.2. Definitions of Melt Properties

4.2.1. Microscopic Melt Composition

Determination of the actual species present in polysulfide melts has been attempted in several past works. The early works of Rule and Thomas[18] and Pearson and Robinson[19] established the existence of the disodium sulfur compounds in polysulfide melts. The recent work of Oei[20] has confirmed these observations. He has used differential thermal analysis to assess the microscopic composition by examining the behavior of the polysulfide melting curves. From his work, Oei confirms that solid sodium polysulfides contain the stable compounds Na_2S, Na_2S_2, Na_2S_4, and Na_2S_5. The solid polysulfide with the nonstoichiometric formula Na_2S_3 was judged to be an equimolar mixture of Na_2S_4 and Na_2S_2.

New techniques for investigating the melt microcomposition have been used. Recent laser Raman studies of solid sodium polysulfides by Janz *et al.*[31] seem to be in accord with the predictions of Oei. The existence of the

polysulfide compounds Na_2S, Na_2S_2, Na_2S_4, and Na_2S_5 were confirmed. Their results could not support the existence of the polysulfide Na_2S_3; however, they could not conclusively disprove its presence either. In laser Raman work by these same authors,[47,48] the existence of the $S_3^=$ anion was confirmed in solid potassium and barium sulfides. The x-ray diffraction work of Tegman[13] also shows that the compounds Na_2S_2, Na_2S_4, and Na_2S_5 are formed into well-defined crystal structures in the solid phase. No x-ray data were obtained for solid Na_2S_3.

While these few investigations on solid polysulfides have been performed, no work has been performed which would directly indicate the actual species and their concentration in polysulfide melts, although several methods which indirectly suggest the makeup of the melt have been performed. Tischer and Ludwig[24] have interpreted linear sweep voltammograms and postulate that the ions $S_2^=$, $S_4^=$, $S_5^=$, and $S_6^=$ are present. They also conclude that the polysulfide anion $S_3^=$ exists only in small quantities as an unstable intermediate. Again, these results are left open to question regarding the simplifications used in their theoretical analysis. The errors introduced by application of dilute solution theory to polysulfide melts are unknown.

Tegman[17] has developed a very comprehensive model that can be used to calculate the microscopic melt composition. His is also the only work which quantitatively postulates the actual composition of polysulfide melts. Tegman has measured activities of sulfur vapor obtained from transpiration experiments on polysulfide melts, and he has empirically fit these data for an assumed microscopic melt composition. An ideal solution of sodium cations and polysulfide anions was assumed. Contrary to these other works,

Tegman's results indicate significant amounts of the polysulfide ion $S_3^=$ along with $S_2^=$, $S_4^=$, and $S_5^=$, is present in the melt. His model shows excellent agreement with his thermodynamic data, as well as agreeing very well with other independent thermodynamic experimental results.

The above review illustrates the uncertainities which exist with regard to the microscopic melt composition. The microscopic melt composition has not been conclusively determined by any investigator. Suitable qualitative and quantitative techniques which would directly confirm the presence of the microscopic species have not been developed. While we recognize the differences between the works, we have chosen to use the microscopic model of Tegman. His model is the most comprehensive, having been tested over a wide range of temperatures and compositions. As we will show, his model also predicts the results of other independent works very well. The disadvantage of the work is in its empirical foundation. The melt species are only postulated, and their relative amounts are determined from the macroscopic thermodynamic sulfur activity. No direct confirmation of the composition is possible. We have adopted his model for this work, but we acknowledge the underlying uncertainity which exists.

4.2.1.1. **Microscopic Melt Model**

The model of Tegman predicts the equilibrium composition of polysulfide melts considering the equilibria among seven polysulfide ions. The formulation and a detailed derivation of the requisite equations are given in Appendix D. Here we will present the essential results. For the melt, the reactions between polysulfide ions and ideal sulfur diatomic vapor are considered. The melt will be assumed to contain N total different ions, or N-1 polysulfide ions. The definition for the subscript conventions on

variables for ions is shown in Table 4–1.

For the arbitrary reaction

$$\frac{i-1}{2} S_2(g) + S^{=} \rightarrow S_i^{=}, \qquad (4-1)$$

at equilibrium,

$$c_i = K_i \, c_1 \, p_{S_2}^{\frac{i-1}{2}} . \qquad (4-2)$$

Here K_i is the equilibrium constant for the reaction, c_i is the concentration of the polysulfide ion $S_i^{=}$, and p_{S_2} is the vapor pressure of ideal diatomic sulfur vapor. Equation (4–2) implies that the polysulfide anions form an ideal solution, since the equilibrium constant is defined in terms of the species concentration. The equilibrium constants K_i can be expressed in terms of a free energy change for the reaction

Table (4-1) Ions in Multicomponent Model.

Ions	Species Number
$S^{=}$	1
$S_2^{=}$	2
$S_3^{=}$	3
⋮	⋮
$S_j^{=}$	j
⋮	⋮
$S_{N-1}^{=}$	N-1
Na^{+}	N

$$\Delta G_i^o = - RT \ln K_i \ . \qquad (4-3)$$

The dependence of ΔG_i^o is defined to be composed of an enthalpy and entropy term .

$$\Delta G_i^o = \Delta H_i^o - T \Delta S_i^o \ , \qquad (4-4)$$

where ΔH_i^o and ΔS_i^o are assumed to be independent of temperature. For the melt composed of N-1 polysulfide ions, $N-2$ values for ΔH_i^o and $N-2$ values of ΔS_i^o are required. To fit accurately thermodynamic data, Tegman included the polysulfide anions $S^{=}$, $S_2^{=}$, $S_3^{=}$, $S_4^{=}$, $S_5^{=}$, $S_6^{=}$, and $S_8^{=}$. The polysulfide anion $S_7^{=}$ was required only in such small amounts, that it was not included in the model.

The quantitative melt composition can be determined by considering an overall material balance and a material balance on sulfur. This gives an equation relating the overall melt composition to the equilibrium vapor pressure of sulfur

$$x_s = \frac{1 + \sum_{i=2}^{N-1} K_i \, p_{S_2}^{\frac{(i-1)}{2}}}{1 + \sum_{i=2}^{N-1} i \, K_i \, p_{S_2}^{\frac{(i-1)}{2}}} \ . \qquad (4-5)$$

If the overall melt composition is known, then one can solve Equation (4–5) by trial and error for the partial pressure of sulfur vapor. Once the vapor pressure of sulfur is known, the individual concentrations of the ions can be determined. Considering the distribution of ions in terms particle fractions gives the fraction of polysulfide ion $S_i^{=}$ as

$$n_i = \frac{K_i \, p_{S_2}^{\frac{(i-1)}{2}}}{1 + \sum_{i=2}^{N-1} K_i \, p_{S_2}^{\frac{(i-1)}{2}}} \ . \qquad (4-6)$$

The particle fraction of sulfide ions is defined as

$$n_i = \frac{c_i}{\sum_{j=1}^{N-1} c_i} . \qquad (4-7)$$

The required calculations are performed by the program COMPOS, which will calculate the particle fractions of the various polysulfide ions for any overall melt composition.

Once the particle fractions are known, the individual ionic concentrations may also be calculated. The equations derived in Chapter Three can be used here. The sodium cation concentration is independent of the two models, and consequently

$$c_N = c_+ = \nu_+ c . \qquad (4-8)$$

The concentration of the individual anions can be determined from

$$c_i = n_i c_- = n_i \nu_- c . \qquad (4-9)$$

These relationships also account for conservation of charge within the melt.

Figure 4–1 and 4–2 show the calculated distribution of polysulfide ions in the melt as a function of the overall sulfur melt composition. These curves are for the two temperatures 573 and 633 K. It is apparent from these curves that the ions $S_2^=$, $S_4^=$, $S_5^=$, and $S_6^=$ are present in large quantities. Smaller amounts of the ions $S^=$ and $S_8^=$ exist, while the ion $S_7^=$ was not included.

Although not very obvious by an initial inspection, these curves show that the distribution of ions in the melt is nearly independent of temperature. The two curves at different temperatures are nearly superimposable.

4.2.2. Application to Open Circuit Potentials

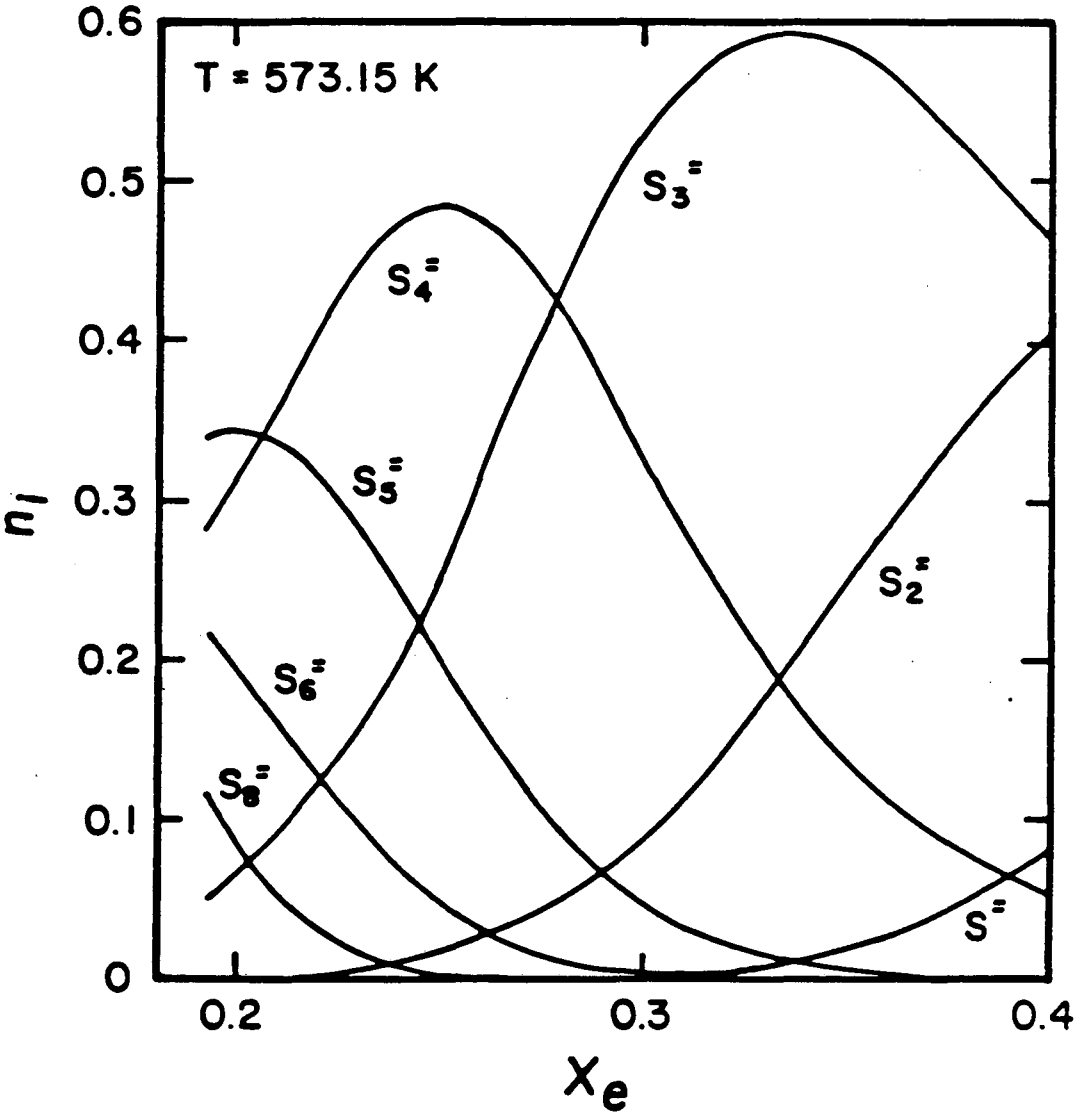

Figure 4–1 Distribution of polysulfide ions in sodium polysulfide melts at 573.15 K calculated from the model of Tegman.[17]

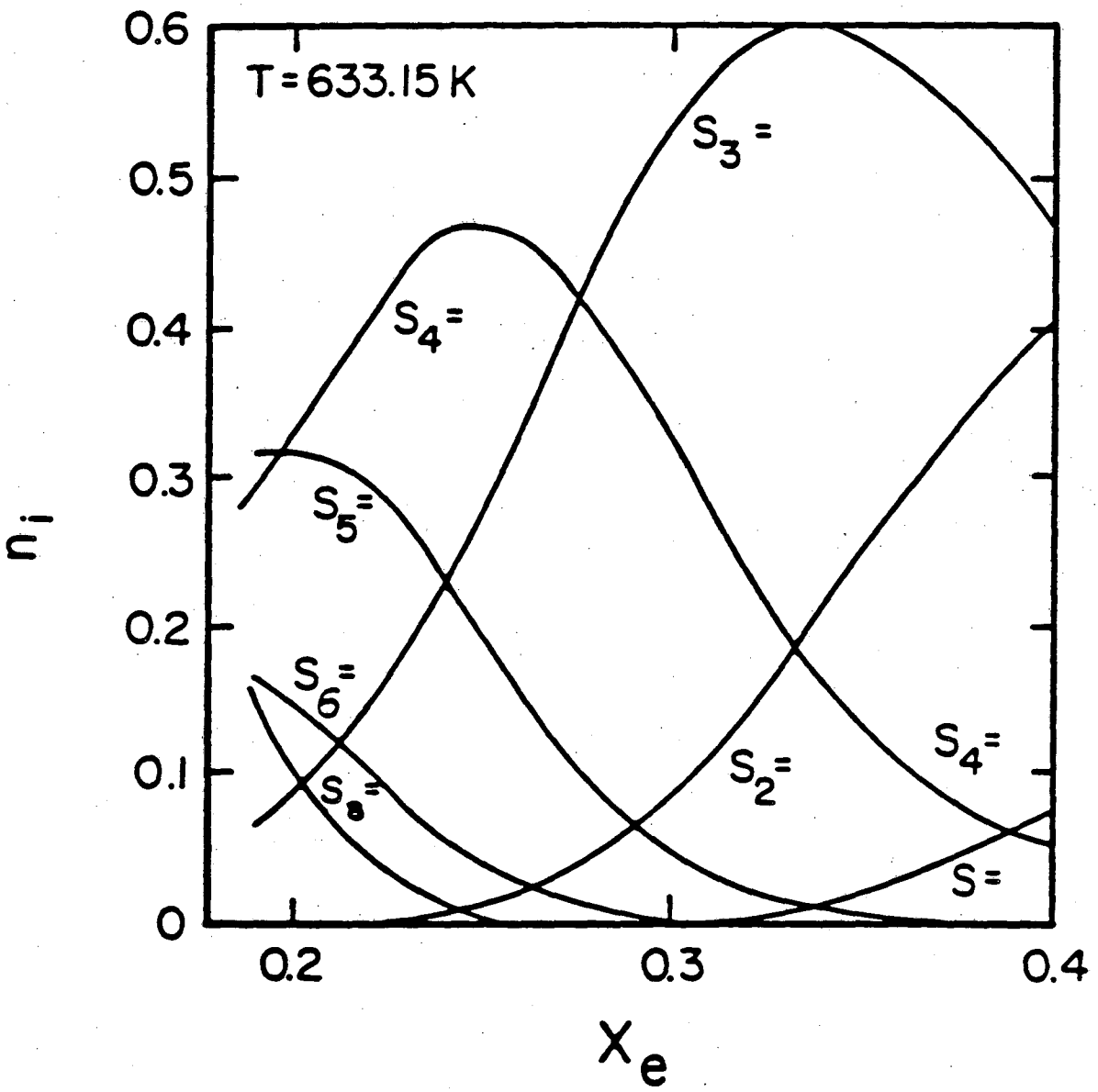

Figure 4–2 Distribution of polysulfide ions in sodium polysulfide melts at 633.15 K calculated from the model of Tegman.[17]

4.2.2.1. Single Phase Region

The microscopic model of Tegman can be used to determine the open circuit potential of sodium–sulfur cells. A shorthand notation for this cell is

$$\begin{array}{ccccc} \alpha & \beta & \gamma & \delta & \alpha' \\ \mathrm{C}\,| & \mathrm{Na(l)} & |\ \beta\text{–}alumina\ | & \mathrm{Na_2S} + (y-1)\,S(l) & |\,\mathrm{C} \end{array}$$

The potential of this cell in terms of chemical potentials of reactants and products is derived in detail in Appendix B. The result is

$$FU_1 = \mu^{\alpha}_{\mathrm{Na}} + \frac{1}{2}\,\mu^{\delta}_{\mathrm{S}} - \frac{1}{2}\,\mu^{\delta}_{\mathrm{Na_2S}}\,. \qquad (4\text{–}10)$$

One now needs to express the chemical potential of sodium sulfide and sulfur in the polysulfide phase in terms of neutral sulfide compounds consistent with the microscopic model. If the arbitrary polysulfide compounds $\mathrm{Na_2S_a}$ and $\mathrm{Na_2S_b}$ are chosen, then the potential of the cell can be written equivalently as

$$FU_1 = \mu^{\alpha}_{\mathrm{Na}} + \frac{1}{2}\,\frac{a}{(b-a)}\,\mu^{\delta}_{\mathrm{Na_2S_b}} - \frac{1}{2}\,\frac{b}{(b-a)}\,\mu^{\delta}_{\mathrm{Na_2S_a}}\,, \qquad (4\text{–}11)$$

if one relates the chemical potential of sulfur in the melt to these compounds by

$$\mu_{\mathrm{Na_2S_i}} = \mu_{\mathrm{Na_2S}} + \frac{(i-1)}{2}\,\mu_{\mathrm{S}}\,. \qquad (4\text{–}12)$$

The chemical potentials of the sulfide compounds are given by

$$\mu_{\mathrm{Na_2S_i}} = \mu^{\delta}_{\mathrm{Na_2S_i}} + RT\,\ln x_{\mathrm{Na_2S_i}}\,, \qquad (4\text{–}13)$$

since they are assumed to be ideal components in the melt. The mole fraction of the compound $\mathrm{Na_2S_i}$ is the same as the particle fraction of the corresponding $\mathrm{S_i^=}$ polysulfide ion

$$x_{\mathrm{Na_2S_i}} = n_i\,. \qquad (4\text{–}14)$$

Finally, the standard chemical potentials for the polysulfide compounds can

be expressed in terms of the chemical potential of sodium monosulfide by

$$\Delta G_i^o = \mu^o_{Na_2S_i} - \frac{(i-1)}{2}\mu^*_{S_2} - \mu^o_{Na_2S} \qquad (4-15)$$

If one combines Equation (4–11) and Equation (4–13) through (4–15) with some algebraic manipulation one obtains

$$FU_1 = \mu^o_{Na} - \frac{1}{2}\frac{b}{(b-a)}\Delta G^o_a + \frac{1}{2}\frac{a}{(b-a)}\Delta G^o_b + \frac{1}{4}\mu^*_{S_2} - \frac{1}{2}\mu^o_{Na_2S} + \frac{1}{2}\frac{a}{(b-a)}RT\ln n_b - \frac{1}{2}\frac{b}{(b-a)}RT\ln n_a \qquad (4-16)$$

for the potential of the cell. The choice of the species Na_2S_a and Na_2S_b can be arbitrary. If the individual particle fractions of any two polysulfide anions and the standard chemical potentials for molten sodium metal, solid sodium monosulfide, and ideal sulfur diatomic vapor are known, then the cell potential can be calculated.

4.2.2.2. Standard Chemical Potentials

The standard chemical potential of the compounds required in Equation (4–16) can be obtained from thermodynamic data compiled in any of several sources. A comprehensive source used here is the JANAF tables.[49] Values for standard chemical potentials are not directly available but must be calculated from tabulated differences of free energies of formation. The required differences of chemical potentials in the standard states can be related to the free energies of formation by

$$\mu^o_{Na} + \frac{1}{4}\mu^*_{S_2} - \frac{1}{2}\mu^o_{Na_2S} = \Delta G^o_{f,Na} + \frac{1}{4}\Delta G^o_{f,S_2} - \frac{1}{2}\Delta G^o_{f,Na_2S} = \Delta G^o \qquad (4-17)$$

Values for the free energies of formation of liquid sodium, solid sodium sulfide, and ideal diatomic sulfur vapor are all available for the temperatures of interest in the sodium–sulfur cell. The values appearing these tables for liquid sodium are given in Table 4–2 while values for solid

Table 4–2 Selected JANAF thermodynamic quantities for liquid sodium.

T	C_p°	ΔH_f°	ΔG_f°
K	cal/mol–K	kcal/mol	kcal/mol
500	7.302	0.000	0.000
600	7.124	0.000	0.000
700	6.996	0.000	0.000

sodium sulfide are given in Table 4–3. Thermodynamic values for diatomic sulfur vapor are tabulated in Table 4–4. For temperatures other than those given in the table, one can determine the required combination of standard chemical potentials from

$$\frac{d(\Delta G^\circ / T)}{dT} = -\frac{\Delta H^\circ}{T^2}, \qquad (4\text{–}18)$$

where ΔH° is a function of temperature and is given by

Table 4–3 Selected JANAF thermodynamic quantities for solid sodium sulfide.

T	C_p°	ΔH_f°	ΔG_f°
K	cal/mol–K	kcal/mol	kcal/mol
500	19.600	-91.346	-83.903
600	19.900	-91.670	-82.381
700	20.200	-91.877	-80.793

Table 4–4 Selected JANAF thermodynamic quantities for diatomic sulfur in the ideal gas state.

T	C_p°	ΔH_f°	ΔG_f°
K	cal/mol–K	kcal/mol	kcal/mol
500	8.389	28.385	11.806
600	8.549	27.518	8.575
700	8.658	26.779	5.525

$$\Delta H^\circ = \Delta H^\circ_{T_o} + \int_{T_o}^{T} \Delta C_p^\circ \, dT \tag{4–19}$$

The quantity $\Delta H^\circ_{T_o}$ is the value of ΔH° at the reference temperature T_o. The individual heat capacities of the compounds can be assumed to have the following dependence on temperature

$$C_{p_i}^\circ = a_i + b_i T \, . \tag{4–20}$$

The variable ΔC_p° can then be defined by

$$\Delta C_p^\circ = \Delta a + \Delta b T \, , \tag{4–21}$$

where Δ has the same significance as it does in ΔG° and ΔH°. Substitution of Equation (4–21) into Equation (4–19) and integrating Equation (4–18) gives an expression for ΔG° and any arbitrary temperature T, in terms of thermodynamic properties at a temperature of T_o

$$\Delta G^\circ = \frac{T}{T_o} \Delta G^\circ_{T_o} + \Delta H_{T_o} \left[1 - \frac{T}{T_o}\right] - T \, \Delta a \, \ln \frac{T}{T_o} + \Delta a \, (T - T_o)$$

$$- \frac{\Delta b}{2} (T - T_o)^2 \, . \tag{4–22}$$

Values for ΔG° at the various temperatures are given in Table 4–5.

Table 4–5 Values for ΔG° at several temperatures.

Temperature, K	ΔG°, kcal/mol
500.00	44.903
553.15	44.068
573.15	43.754
600.00	43.334
603.15	43.285
633.15	42.817
663.15	42.350
700.00	41.778

4.2.2.3. Cell Potentials

The open circuit cell potential at any melt composition and temperature can now be computed using the equations derived above. The standard free energies of formation at the reference temperature are obtained and are used to determine the required differences in standard chemical potentials. They are corrected to the desired temperature using enthalpy of formation and heat capacity data. The melt composition is calculated at the desired temperature, and the values of the change in free energy for the polysulfide compounds are also determined. Finally, the potential is calculated by combining all of these quantities. Figure 4–3 presents the calculated potential versus the mole fraction of sodium sulfide in the melt. The melt temperature has been used as a parameter. The model predicts that the cell potential generally decreases with increasing temperature.

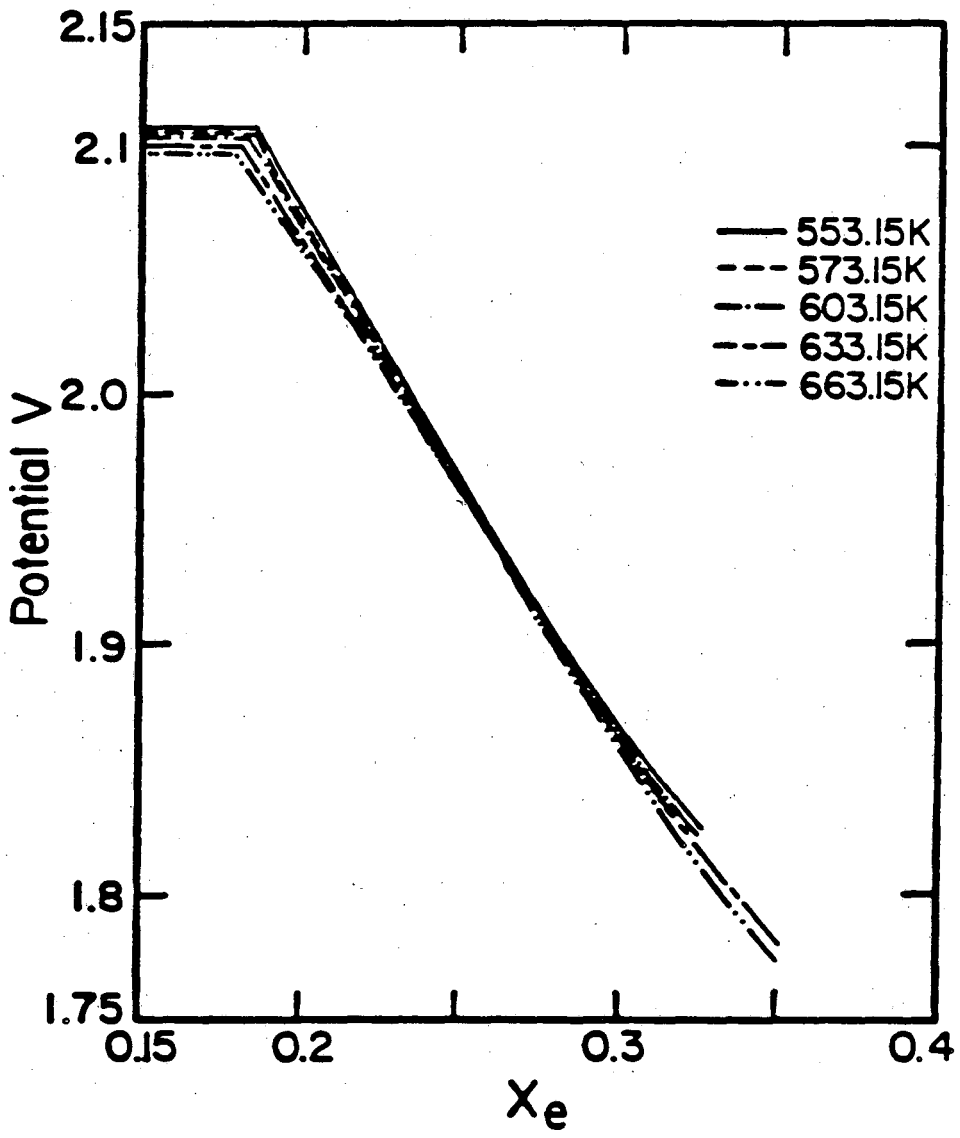

Figure 4–3 Calculated open circuit cell potentials as a function of melt composition for several temperatures.

The predicted open circuit potential can be compared to the available thermodynamic data for cell potentials obtained from Gupta and Tischer[7] and Cleaver and Davies.[16] Figures 4–4 through 4–8 compare the theory to the model with the data of Gupta and Tischer for a range of temperature from 553 K to 663 K. The comparison with the data of Cleaver and Davies at 573 and 633 K is shown in Figures 4–9 and 4–10. In general, good agreement with the experimental data is seen. There are some deviations with the data of Gupta and Tischer at the higher temperatures, but the model reproduces the data of Cleaver and Davies very well at both temperatures.

4.2.2.4. Two Phase Regions

The potential in the two phase regions and the overall melt composition at the juncture of these regions can also be ascertained from the previous analysis. First consider the two phase region at high sulfur compositions. At the upper solubility limit, polysulfides with the approximate formula $Na_2S_{5.2}$ are in equilibrium with a sulfur–rich phase which is very close to pure sulfur. Schematically, the equilibrium between phases can be shown as

$$\begin{array}{ccc} 1 & & 2 \\ Na_2S_y & | & Na_2S_{y'} \end{array}$$

where the variable y denoting the composition in phase 1 is near 5.2 and the variable y' in phase 2 is very large. The requirement of equilibrium between the two phases can be expressed as

$$\mu^1_{Na_2S_i} = \mu^2_{Na_2S_i} \qquad (4\text{–}23)$$

where the superscripts 1 and 2 denote the polysulfide and sulfur–rich phase respectively. Because the model of Tegman was fitted for a range of sulfur

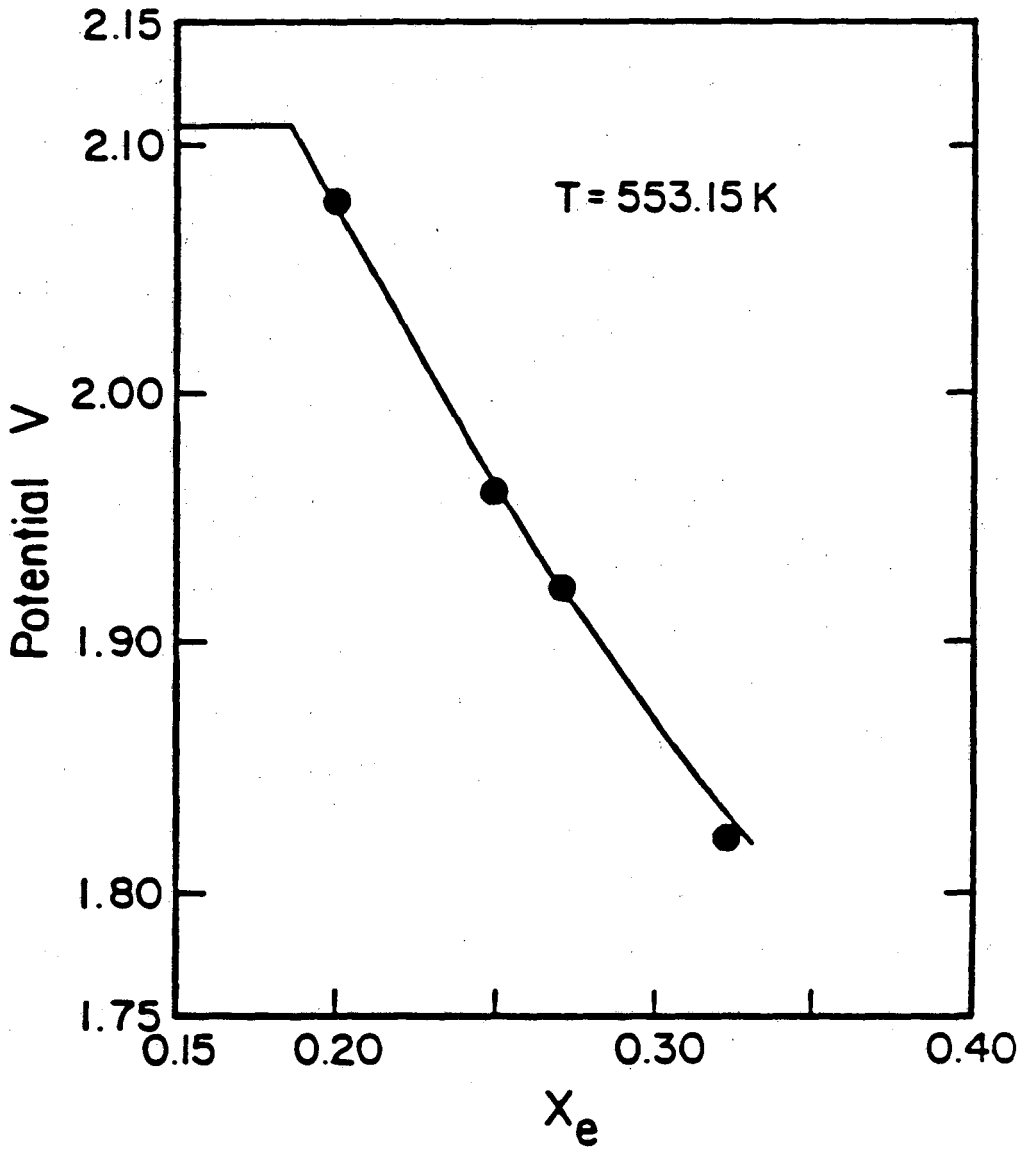

Figure 4–4 Comparison of calculated and experimental open circuit cell potential as a function of melt composition at a temperature of 553.15 K. Data is that of Gupta and Tischer.[7]

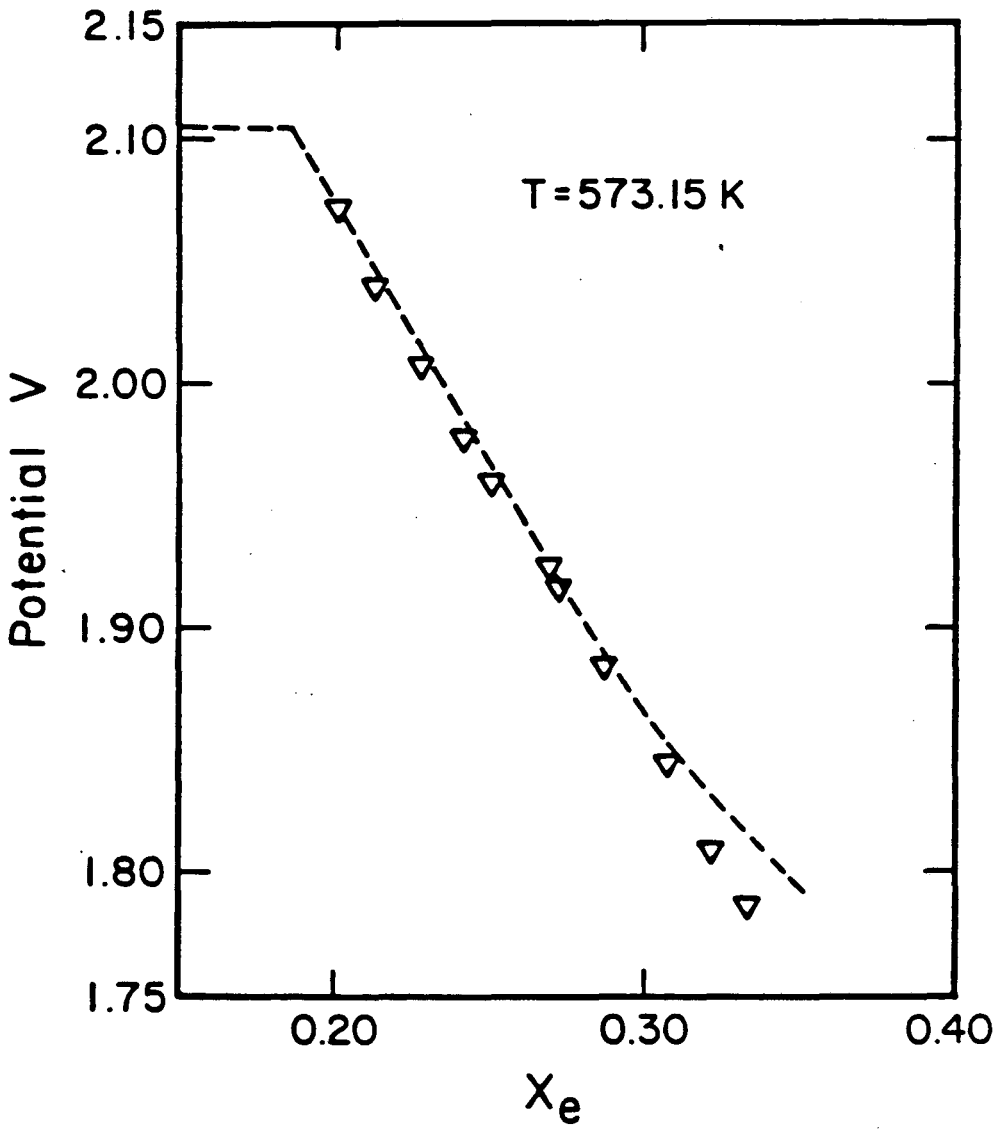

Figure 4–5 Comparison of calculated and experimental open circuit cell potential as a function of melt composition at a temperature of 573.15 K. Data is that of Gupta and Tischer.[7]

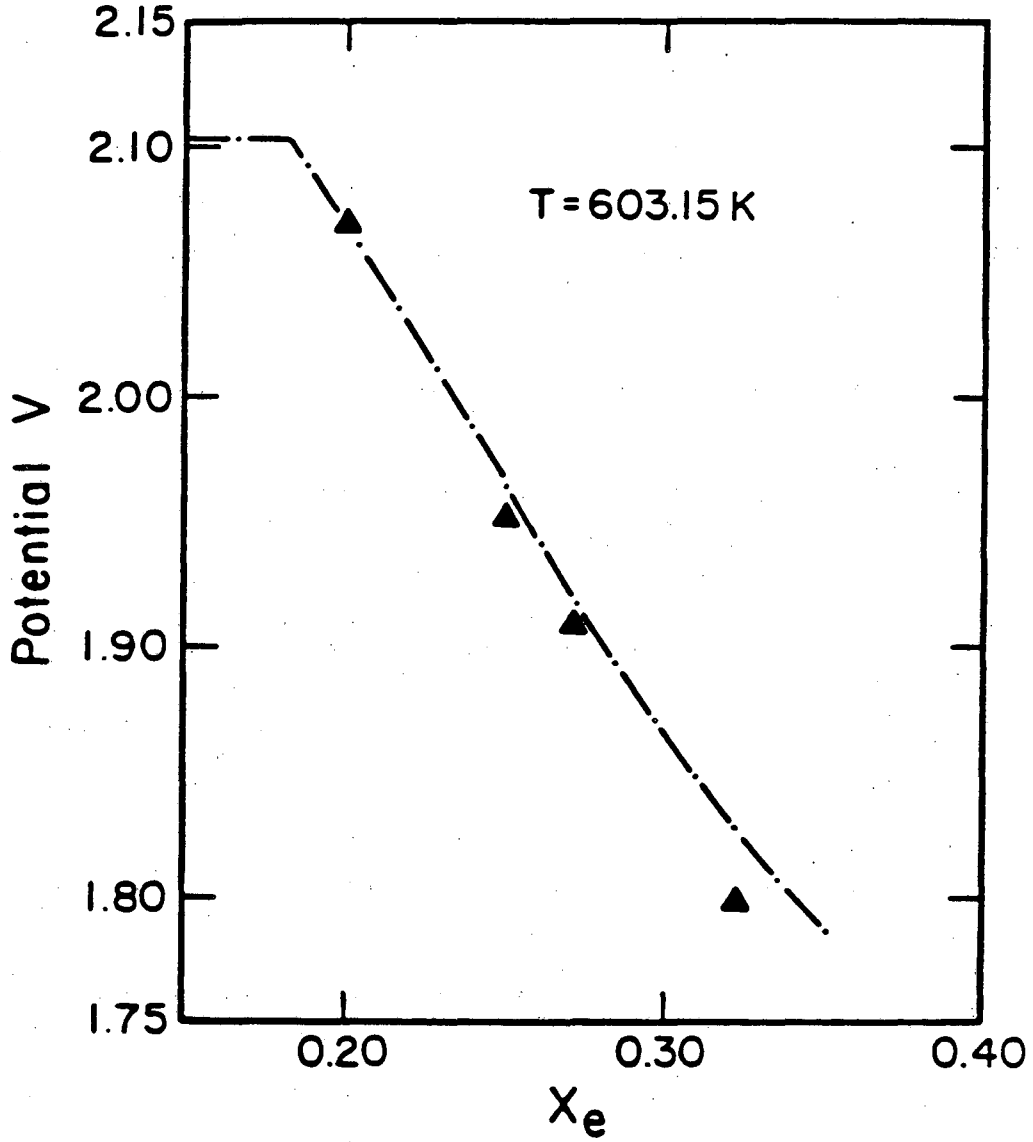

Figure 4–6 Comparison of calculated and experimental open circuit cell potential as a function of melt composition at a temperature of 603.15 K. Data is that of Gupta and Tischer.[7]

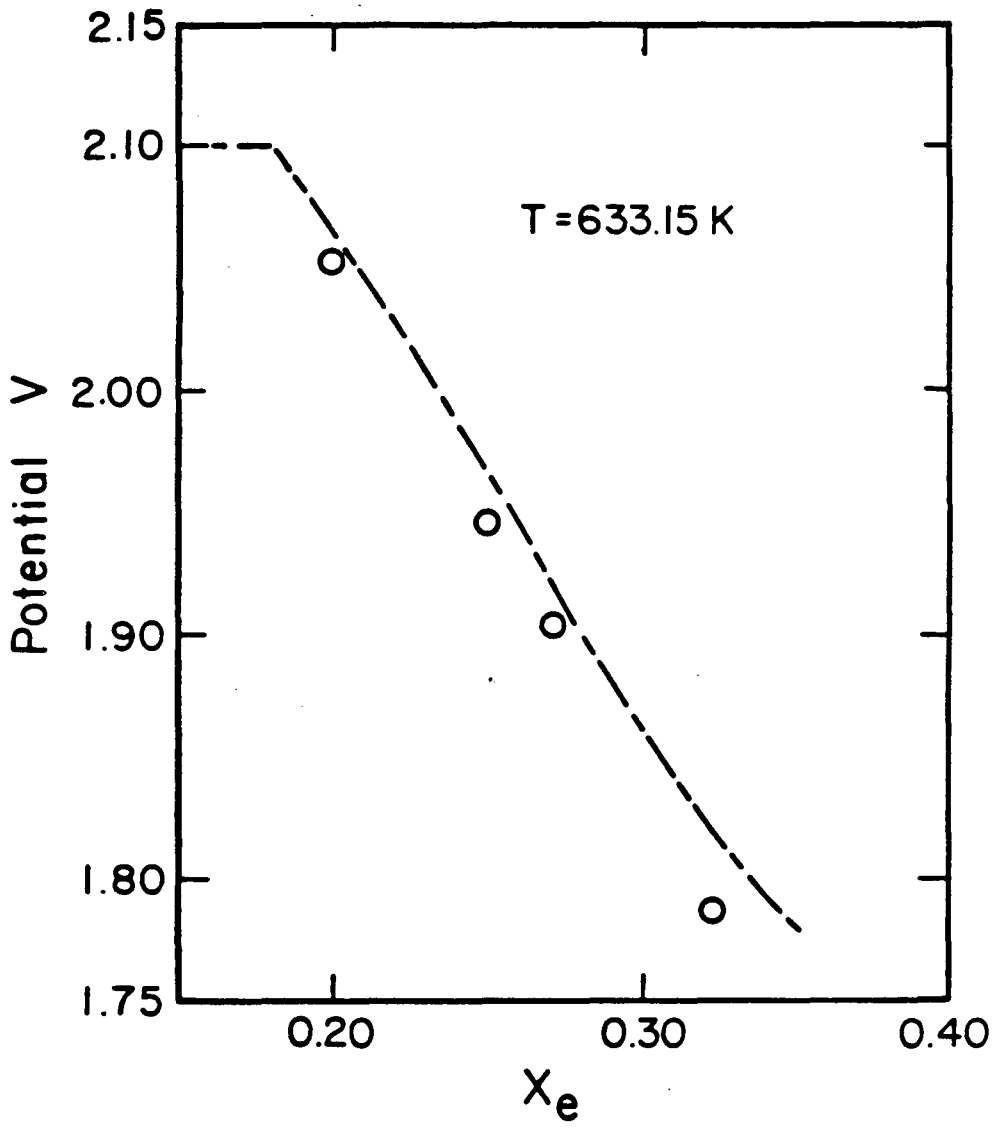

Figure 4–7 Comparison of calculated and experimental open circuit cell potential as a function of melt composition at a temperature of 633.15 K. Data is that of Gupta and Tischer.[7]

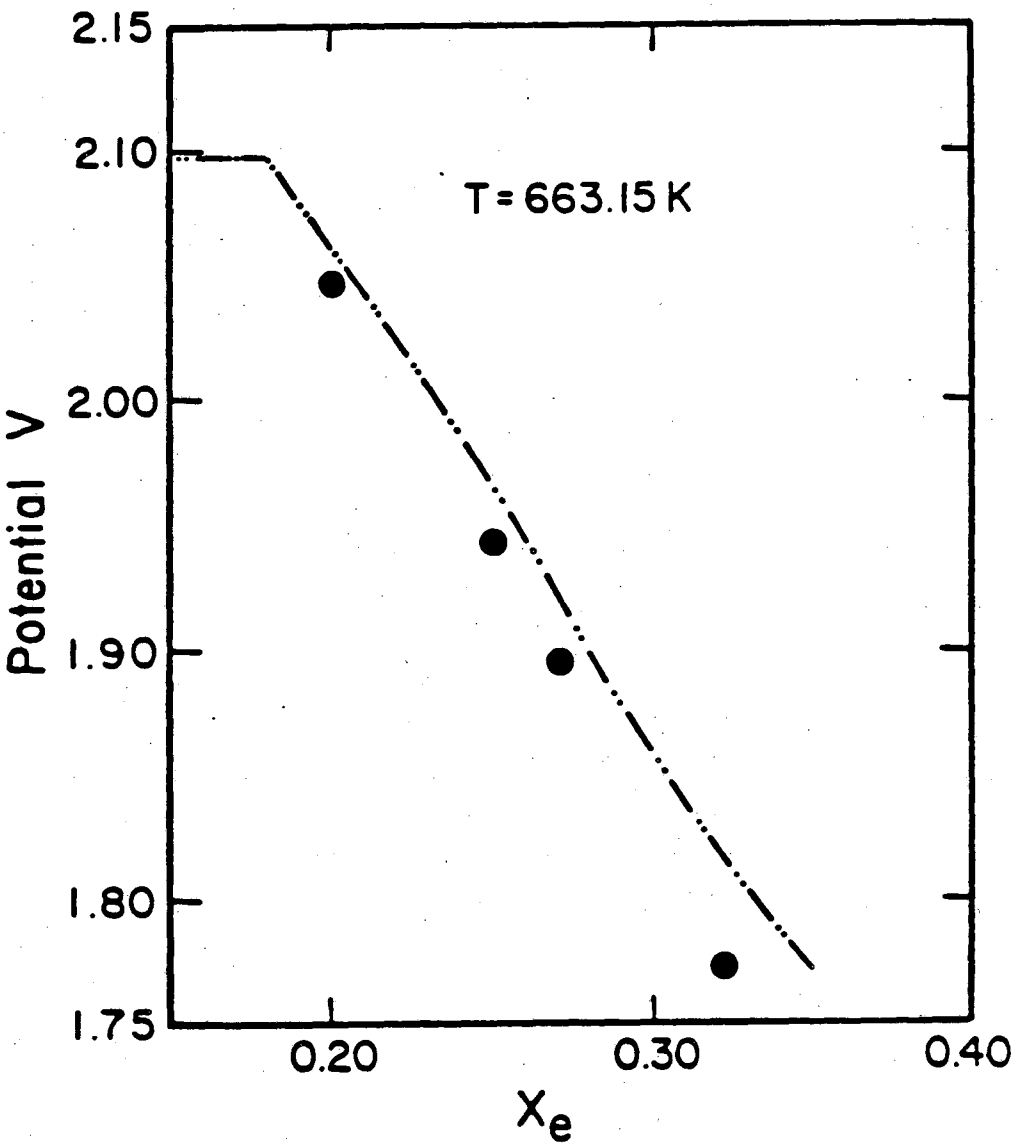

Figure 4–8 Comparison of calculated and experimental open circuit cell potential as a function of melt composition at a temperature of 663.15 K. Data is that of Gupta and Tischer.[7]

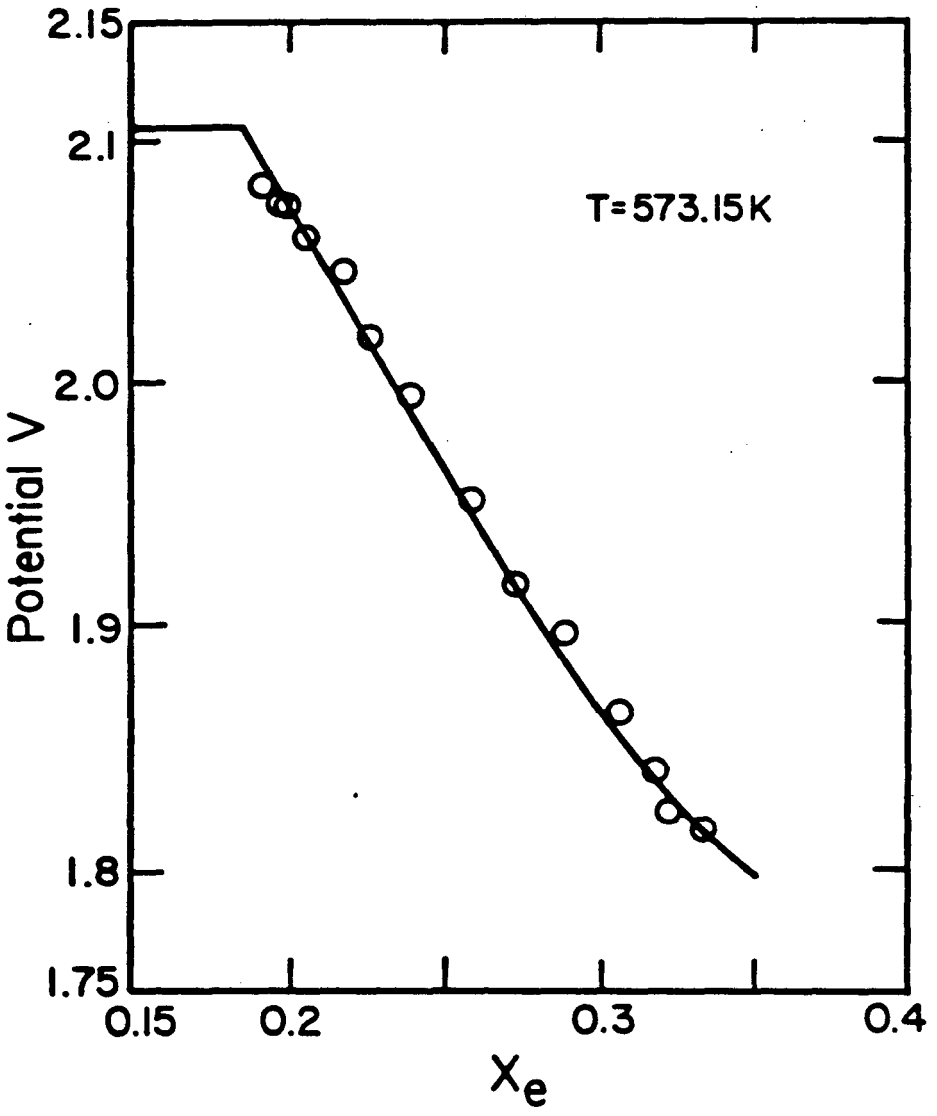

Figure 4–9 Comparison of calculated and experimental open circuit cell potential as a function of melt composition at a temperature of 573.15 K. Data is that of Cleaver and Davies.[16]

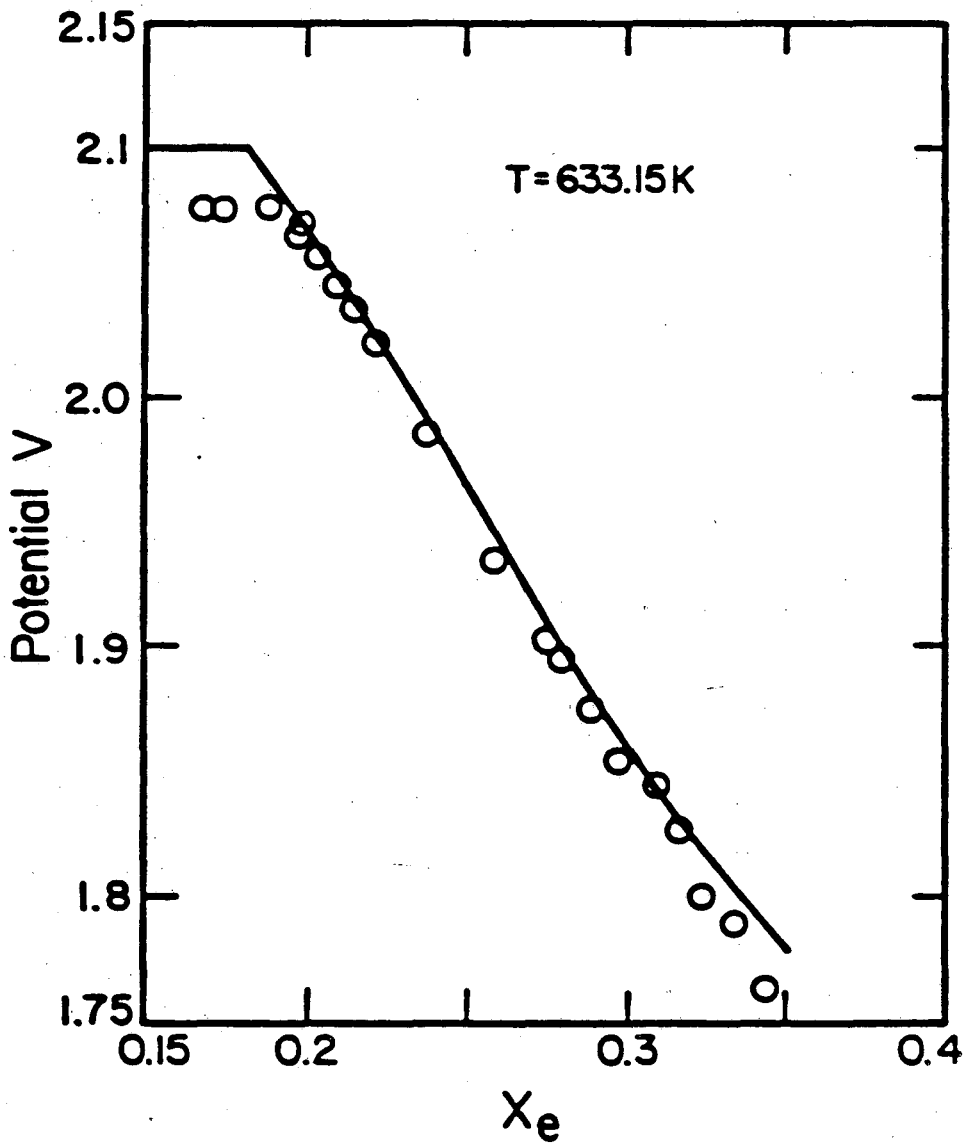

Figure 4–10 Comparison of calculated and experimental open circuit cell potential as a function of melt composition at a temperature of 633.15 K. Data is that of Cleaver and Davies.[16]

compositions much less than the composition of the nearly pure sulfur phase, it is not likely that the distribution of chemical constituents can be calculated with any accuracy in this phase. But as an approximation, we can assume that the sulfur–rich phase contains only pure sulfur. Under this condition, the requirement for equilibrium becomes

$$\mu_S^l = \mu_S^o \qquad (4-24)$$

where the macroscopic chemical potential of sulfur has been used. The chemical potential of sulfur in the polysulfide phase can be determined from Equation (4–10), which was derived earlier. Rearrangement of this equation gives

$$\mu_S^o = 2FU_1 - 2\mu_{Na}^o + \mu_{Na_2S} = 2FU_1 - 2\mu_{Na}^o + \mu_{Na_2S}^o + RT \ln n_1 . \qquad (4-25)$$

To obtain the composition of the polysulfide phase, one is required to solve this equation iteratively for the chemical potential in terms of the corresponding mole fraction of sulfide ion. The standard chemical potentials of liquid sulfur are also needed. Again, these have been obtained from the JANAF tables and are given in Table 4–6.

Table 4–6 Selected JANAF thermodynamic quantities for liquid sulfur.

T	C_p^o	ΔH_f^o	ΔG_f^o
K	cal/mol–K	kcal/mol	kcal/mol
500	9.081	0.000	0.000
600	8.200	0.000	0.000
700	7.799	0.000	0.000

Figure 4–11 presents the results of this calculation. The calculated saturation composition of the melt is given in terms of the mole fraction of Na_2S. The experimental values of Cleaver and Davies and Gupta and Tischer are also shown. One can see that the approximation of a pure sulfur rich phase does not exactly predict the actual measured composition. While, some of the discrepancy between the two curves is due to the slight solubility of polysulfides in the sulfur rich phase, the majority of the differences between the two curves is probably due to differences in the assumed standard state energies.

In the two phase region located at lower overall sulfur compositions, solid sodium disulfide is in equilibrium with a phase containing a mixture of polysulfides. A similar calculation for the melt composition at the junction of these two regions could be performed by considering the equilibrium for sodium disulfide. Accurate values for the chemical potential of sodium disulfide in the standard state do not seem to be available, although Gupta and Tischer present a single value which they indicate is of questionable accuracy. No heat capacities or heats of formation are available. This calculation must await further experimental determinations of these required quantities.

4.2.3. Thermodynamic versus Concentration Driving Force

The microscopic model of Tegman also allows the thermodynamic factor

$$1 + \frac{d \ln \gamma_{+-}}{d \ln m} \qquad (4\text{–}26)$$

to be calculated. This is needed to relate $\mathscr{D}$ to the more commonly reported, but less fundamental D.

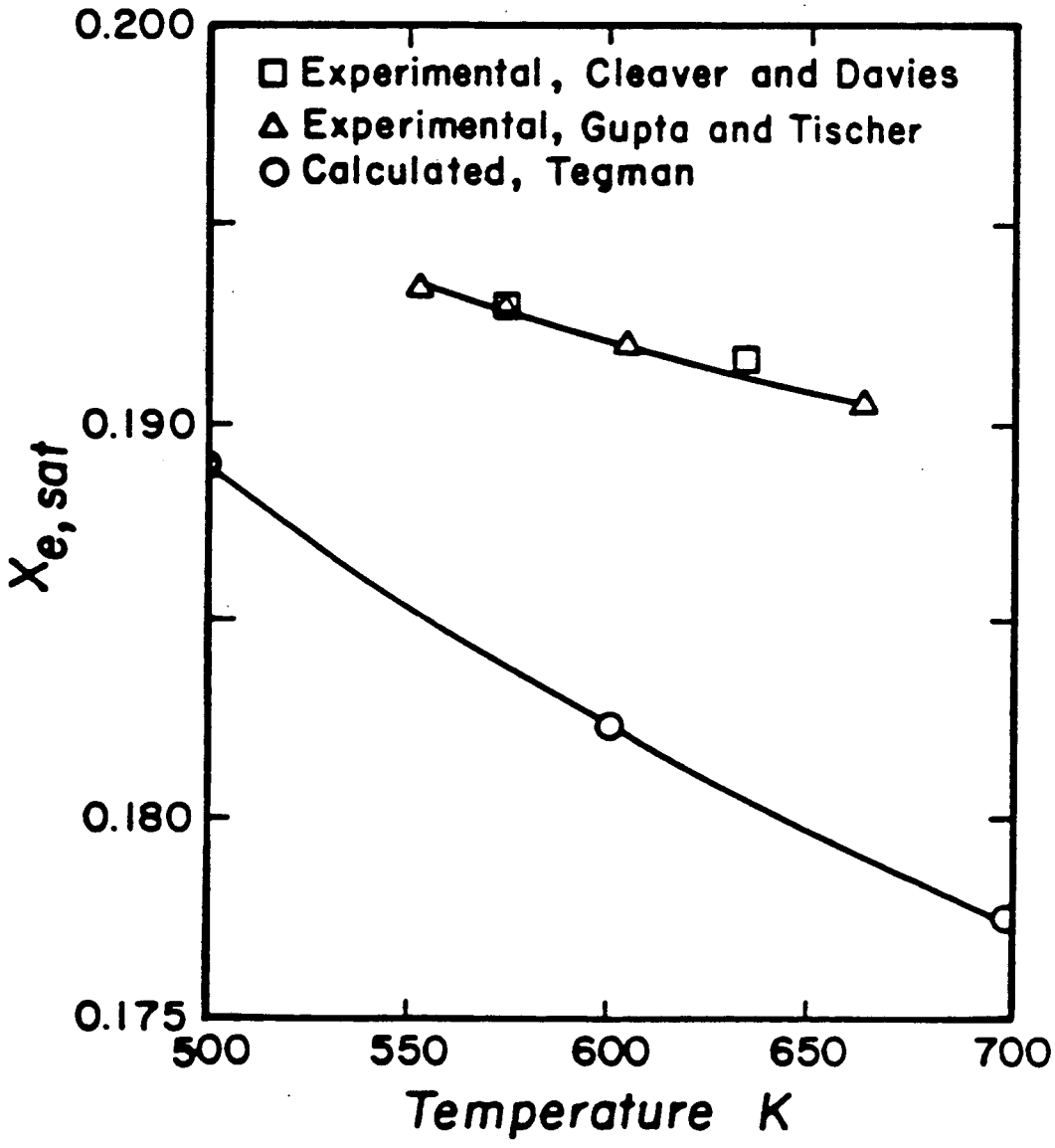

Figure 4–11 Calculated and experimental saturation composition of the polysulfide–rich phase in the upper two phase region. The calculated points are obtained using the model of Tegman[17] while experimental data of Cleaver and Davies[16] and Gupta and Tischer[7] are shown for comparison.

The required expression relating this desired quantity to polysulfide ion compositions can most easily be derived by considering the definitions for the chemical potential of sodium sulfide

$$\mu_e = \mu_e^o + \nu RT \ln (\gamma_{+-} m) = \mu^o_{Na_2S} + RT \ln n_1 . \qquad (4-27)$$

The definition for the chemical potential on the left has been taken from the macroscopic melt model derived in Chapter Three. The ideal microscopic melt model definition is on the right. Taking the differential of the two definitions and applying the definition of the molality in Equation (3–39) gives

$$1 + \frac{d \ln \gamma_{+-}}{d \ln m} = \frac{x_e(1 - x_e)}{\nu n_1} \frac{dn_1}{dx_e} . \qquad (4-28)$$

One can now obtain the derivative of the particle fraction of the single sulfide anion with respect to the electrolyte mole fraction using the chain rule

$$\frac{dn_1}{dx_e} = \frac{dn_1}{dp_{S_2}} \frac{dp_{S_2}}{dx_e} . \qquad (4-29)$$

Equations (4–5) and (4–6) give the electrolyte mole fraction and any polysulfide anion particle fraction in terms of the vapor pressure of diatomic sulfur vapor. If these expressions are differentiated and substituted into Equation (4–29), then the final expression is obtained

$$1 + \frac{d \ln \gamma_{+-}}{d \ln m} = \frac{(1 - x_e)}{\nu} \frac{1}{\dfrac{x_e \sum_{i=2}^{N-1} K_i i(i-1) p_{S_2}^{\frac{i-3}{2}}}{\sum_{i=2}^{N-1} K_i (i-1) p_{S_2}^{\frac{i-3}{2}}} - 1} \qquad (4-30)$$

This quantity is also calculated by the subroutine COMPOS when the microscopic composition is calculated.

4.3. Determination of Transport Properties

4.3.1. Inversion of the Transport Equations

The treatment of the binary melt in Chapter Three can be extended to the melt where the individual species are now considered to be totally ionic. Thus, sodium cations and polysulfide anions are the sole species present with neutral sulfur having been eliminated.

Again, the starting point for this analysis requires that one begin with fundamental equations. The equation

$$c_i \nabla \mu_i = \sum_{j=1}^{N} K_{ij}(\mathbf{v}_j - \mathbf{v}_i) = RT \sum_{j=1}^{N} \frac{c_i c_j}{c_T \mathscr{D}_{ij}}(\mathbf{v}_j - \mathbf{v}_i) \qquad (4\text{–}31)$$

describes isothermal transport in the melt composed of N species. If variations in temperature are encountered, the driving force on the left side of Equation (4–31) can be modified to include contributions from thermal diffusion.

Here, we have considered the individual species in the melt to consist of the individual anionic polysulfide species and the sodium cations. For the N total ions in the melt, the $N-1$ independent equations implied above define $N(N-1)/2$ independent transport parameters. Equation (4–31) is not explicit in the fluxes, but one may invert them in a similar but more involved manner as for the binary model. Since these are linear equations for the gradients of chemical potentials in terms of the driving forces, any technique for inverting linear equations can be applied in principle. Because of the large number of variables, the only practical method is numerical inversion. Algebraic inversion is too cumbersome and time consuming. A complete description of the inversion process is given in Appendix E.

The result of the inversion process is a set of equations for the fluxes in terms of the gradients of chemical potentials of the polysulfide anions or the neutral polysulfide compounds, the current density, and the reference velocity. If these equations were written out, the $N(N-1)/2$ independent transport parameters would be combined into the same number of independent transport properties. For the $N-1$ polysulfide anions with the single sodium cation, the independent transport parameters are described equivalently by $N-2$ independent transference numbers, 1 conductivity, and $(N-1)(N-2)/2$ independent diffusion coefficients. The transference numbers defined above must be defined relative to some given velocity. One of many such velocities we could choose would be the velocity of the sodium cation. Pollard and Newman[50] have demonstrated the advantages of this choice for describing the transport properties of a mixture of two binary molten salts with a common ion. For the reference ion, the transference number is by definition equal to zero, and the additional constraint of a unity sum for the remaining transference numbers leaves $N-2$ independent transference numbers.

It is not necessary to define a reference velocity for the conductivity or diffusion coefficients. These are invariant with respect to this choice. The $(N-1)(N-2)/2$ diffusion coefficients describe diffusion of any of $N-1$ neutral compounds under the influence of $N-2$ independent gradients of chemical potential.

While the $N(N-1)/2$ transport properties have been defined, it is impossible to compare any of these to any experimental data. Owing to the present inability to measure the movement of the individual ions, one must transform these into properties which can be measured. The work of

Chapter Three defined transport properties for the binary melt and established a firm foundation for the definition of binary transport properties. These properties were shown to posses physical meanings and all of these could be obtained from well–defined experiments.

The task now is to relate the fundamental $\mathscr{D}_{ij}$ parameters defined in the multicomponent model to the three independent binary transport properties. Independent of the details of the melt model, each set of equations must predict the same bulk movement of sodium and sulfur. In other words, the flux of sulfur transported by the polysulfide ions which is described by the multicomponent model must be equal to the flux of sulfur in neutral sulfur form and as monosulfide ion given in the binary model. The flux of sodium ions must also be identical. Mathematically, one equates the expressions for the flux of sodium ions and sulfur using expressions for each derived in the two models. The details of the manipulations are covered in Appendix E. The essential results can be summarized as

$$\kappa = F^2 \sum_{k=1}^{N-1}\sum_{j=1}^{N-1} z_k c_k z_j c_j L_{kj}^N , \tag{4–32}$$

$$t_+^o = \frac{\dfrac{1}{z_-} - \dfrac{\sum_{k=1}^{N-1} k c_k \sum_{j=1}^{N-1} L_{kj}^N c_j}{\sum_{k=1}^{N-1} z_k c_k \sum_{j=1}^{N-1} L_{kj}^N c_j}}{\dfrac{1}{z_-} + \dfrac{1}{z_+}\sum_{k=1}^{N-1} k \dfrac{c_k}{c_N}} , \tag{4–33}$$

and

$$\mathscr{D} = \frac{3RT}{c} \frac{\sum_{k=1}^{N-1} k c_k \sum_{j=1}^{N-1} L_{kj}^N c_j \left[\dfrac{B}{A} - (j-1)\right]}{(y+2)(y-1)} . \tag{4–34}$$

The constants A and B are defined by

$$A = \sum_{k=1}^{N-1} c_k \sum_{j=1}^{N-1} L_{kj}^{N} c_j \ . \qquad (4-35)$$

and

$$B = \sum_{k=1}^{N-1} c_k \sum_{j=1}^{N-1} L_{kj}^{N} c_j (j - 1) \ . \qquad (4-36)$$

The important feature of these equations is that the transport properties for the binary model can be expressed in terms of the inverted transport coefficients of the multicomponent model. The inverted transport parameters, L_{kj}^{N}, are related to the fundamental $\mathscr{D}_{ij}$ given in Equation (4–31) and defined completely in Appendix E. The velocity of the sodium ion has been designated as the reference velocity, and the inverted L_{ij}^{N}'s are dependent upon this choice. Hence the superscript designation N.

If seven polysulfide anions are assumed to be present in the melt, there are then 28 independent parameters. None of these is known. This is a large number, especially when these must be fit to only three observable quantities: the transference number, the conductivity, and the diffusion coefficient. One might attempt a multidimensional search assuming the parameters are all constant, looking for the optimum combination which would best fit the available data. This procedure has been utilized by Pintauro[31] in the study of electrolyte transport in membranes. His work involved only four species with 8 independent parameters. The larger number of parameters here makes this approach undesirable.

To reduce the number of parameters, one must resort to a method which relates the 28 independent $\mathscr{D}_{ij}$ parameters to each other. For a dilute gas, the value of $\mathscr{D}_{ij}$ can be obtained from statistical mechanics. From Bird, Stewart, and Lightfoot,[32] the relationship for the diffusion coefficient in a mixture of low pressure nonreactive gases is

$$\mathscr{D}_{AB} = \frac{2}{3}\left[\frac{k^3}{\pi^3}\right]^{\frac{1}{2}}\left[\frac{1}{2M_A} + \frac{1}{2M_B}\right]^{\frac{1}{2}} \frac{T^{\frac{3}{2}}}{p\left[r_a + r_b\right]^2} \qquad (4\text{–}37)$$

Equation (4–37) predicts that the diffusivity varies inversely as the square of the effective molecular diameters and directly with the square root of the sum of the reciprocal of the molecular weights. The molecular weight term arises from the velocity of the particles, which for a low pressure gas is proportional to the square root of the mass. The mean free path of the particles, or average distance between collisions is related to the inverse of the effective particle diameter.

For the dense liquid phase, the prediction of diffusivities is much more complex. No longer is the expression for the mass diffusivity in Equation (4–37) applicable. Other theories have been developed which attempt to predict the self diffusivity or the diffusivity of a dilute solute. The Eyring reaction rate theory[53] and the model of Li and Chang[54] suggest that the self diffusion coefficient is proportional to the inverse of the particle radii. The empirical relationship developed by Wilke and Chang[55] predicts that diffusivities for dilute solutes should vary inversely with very nearly the square of the diffusing species radii. The viscosity of the solution is also important in determining the magnitude of the diffusivity. The diffusivities are inversely proportional to the viscosity of the solution, decreasing with increasing solution viscosity. One therefore might relate the independent $\mathscr{D}_{ij}$ to some function of the inverse of the radii of each ion and melt viscosity. This is the approach we adopt here.

While the viscosity of the polysulfide melt has been measured experimentally, there are no known published techniques which will directly lead to predictions of effective collision radii of ions in polysulfide melts.

One must therefore adopt a strategy which attempts to predict these quantities indirectly. It has been common in many theories for diffusion in liquids to assume that the radii of the individual particles are related to their respective molar volumes. If the molar volumes of the individual ions can be ascertained, then the effective particle radii can be determined and an empirical relationship for the $\mathscr{D}_{ij}$ can be formulated.

4.3.2. Molar Volumes

The molar volumes of the ions from the melt can be related to density data which are available from the literature. The total melt density is related to the concentrations of the individual microscopic neutral compounds by

$$\rho = \sum_{i=1}^{N-1} c_{Na_2S_i} M_{Na_2S_i} . \qquad (4-38)$$

The definition for the molar volumes require

$$\sum_{i=1}^{N-1} c_{Na_2S_i} \bar{V}_{Na_2S_i} = 1 , \qquad (4-39)$$

while the concentrations of the individual compound are related to the particle fraction for the individual polysulfide anions by

$$c_{Na_2S_i} = n_i c . \qquad (4-40)$$

The molar volume for the neutral sodium polysulfide compound can be subdivided into the volume of the respective polysulfide anion and the two sodium cations

$$\bar{V}_{Na_2S_i} = \bar{V}_i + 2\bar{V}_N . \qquad (4-41)$$

When Equations (4–38) through (4–41) are combined, the reciprocal of the density can be expressed as a sum of terms all linear in the molar volumes of the individual ions

$$\frac{1}{\rho}\sum_{i=1}^{N-1} n_i M_i = 2\overline{V}_N + \sum_{i=1}^{N-1} n_i \overline{V}_i \,. \qquad (4-42)$$

In obtaining this equation we have assumed that the molar volumes of sodium ions are identical for any of the neutral polysulfide compounds. The polysulfide ion particle fractions must satisfy

$$\sum_{i=1}^{N-1} n_i = 1 \,. \qquad (4-43)$$

Equation (4–42) relates the molar volumes of the several ions in the melt to a directly measurable property, the density. For seven polysulfide anions, Equation (4–42) requires the determination of eight individual molar volumes. Again, in principle, one could perform a multidimensional search or utilize a fit of the experimental data to calculate all eight of the individual molar volumes. The presently available density data do not justify such a calculation. We must find a method to simplify this relationship to reduce the number of arbitrary constants.

The x–ray diffraction data of Tegman[13] can be used to identify possible simplifications which will relate the molar volumes. The x–ray diffraction data of solid sodium polysulfides were obtained at the ambient temperature of 297 K. Figure 4–12 shows the respective volumes of individual sodium polysulfide compounds obtained from this investigation. One would expect, that as the number of sulfur atoms in the polysulfide increases, so would the volume. Figure 4–12 shows that this indeed is the case for the three compounds shown. The data show that the volume is nearly, but not quite linear in the number of sulfur atoms. To fit the data better, the empirical relationship

$$\overline{V}_i = \overline{V}_1 \, i^p \qquad (4-44)$$

was introduced where p was an assumed constant. For different values of p, a least squares fit was performed so that the best values of $\overline{V}_n$ and $\overline{V}_1$ fitting

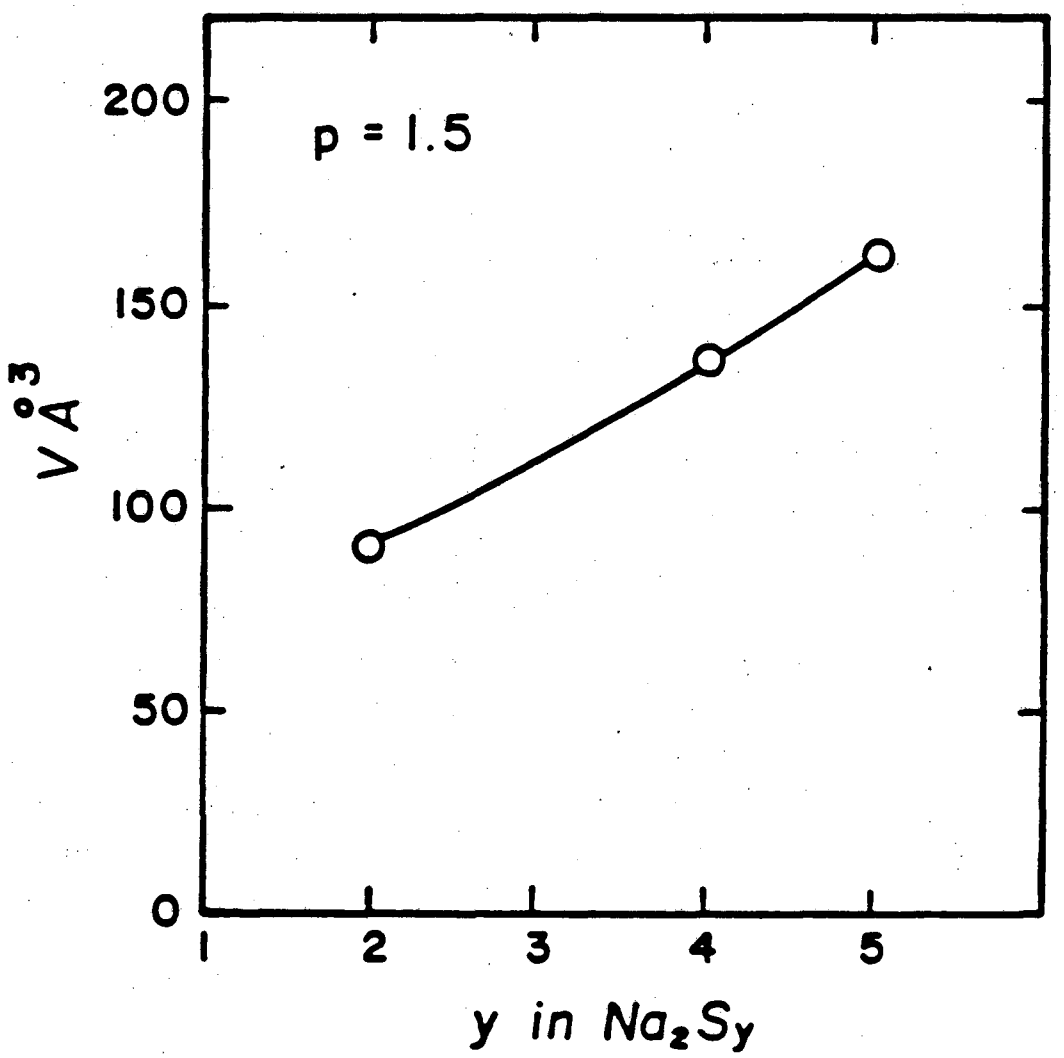

Figure 4–12 Volumes of sodium polysulfide compounds obtained from x–ray diffraction studies on solid sodium polysulfides at 297 K. Solid line is empirical fit using equation (4–44) with $p = 1.5$.

the experimental density data were obtained. The results of the fit indicated that the value of $p = 1.5$ fitted the data the best when the minimization of the standard deviation was used as a criterion. The x–ray diffraction data plotted in Figure 4–12 indicate that $p = 1.5$ indeed fits the three points very well.

The empirical relationship derived from the x–ray diffraction data was also compared with the density for molten polysulfides. Cleaver and Davies[15] present values for density at several compositions and temperatures. Their results show that the densities of polysulfide melts are well represented by linear functions of temperatures, but the dependence upon melt composition is very irregular and unpredictable. To confirm the predictions of the x–ray data, the empirical molar volume fit was compared to the density data of Cleaver and Davies. Again, a least square linear regression routine was used to find the best value of p which produced the best agreement between the calculated and experimental densities. It was found that the value of the exponent which best fit the data for all melt temperatures was again $p = 1.5$. The respective molar volumes calculated at the various temperatures are given in Table 4–7.

The variation of the melt density is shown in Figures 4–13 through 4–15. The predictions for the density using $p = 1.5$ fit the data rather well, very nearly within the experimental uncertainities for all of the points.

4.3.3. Calculation of Transport Properties

Now that we have determined the molar volumes of the individual ions, we can develop a relationship for the $\mathscr{D}_{ij}$ parameters. The previous work for estimation of liquid phase diffusion coefficients shows that the diffusion coefficient is related to the inverse of the diffusing species radii raised to an

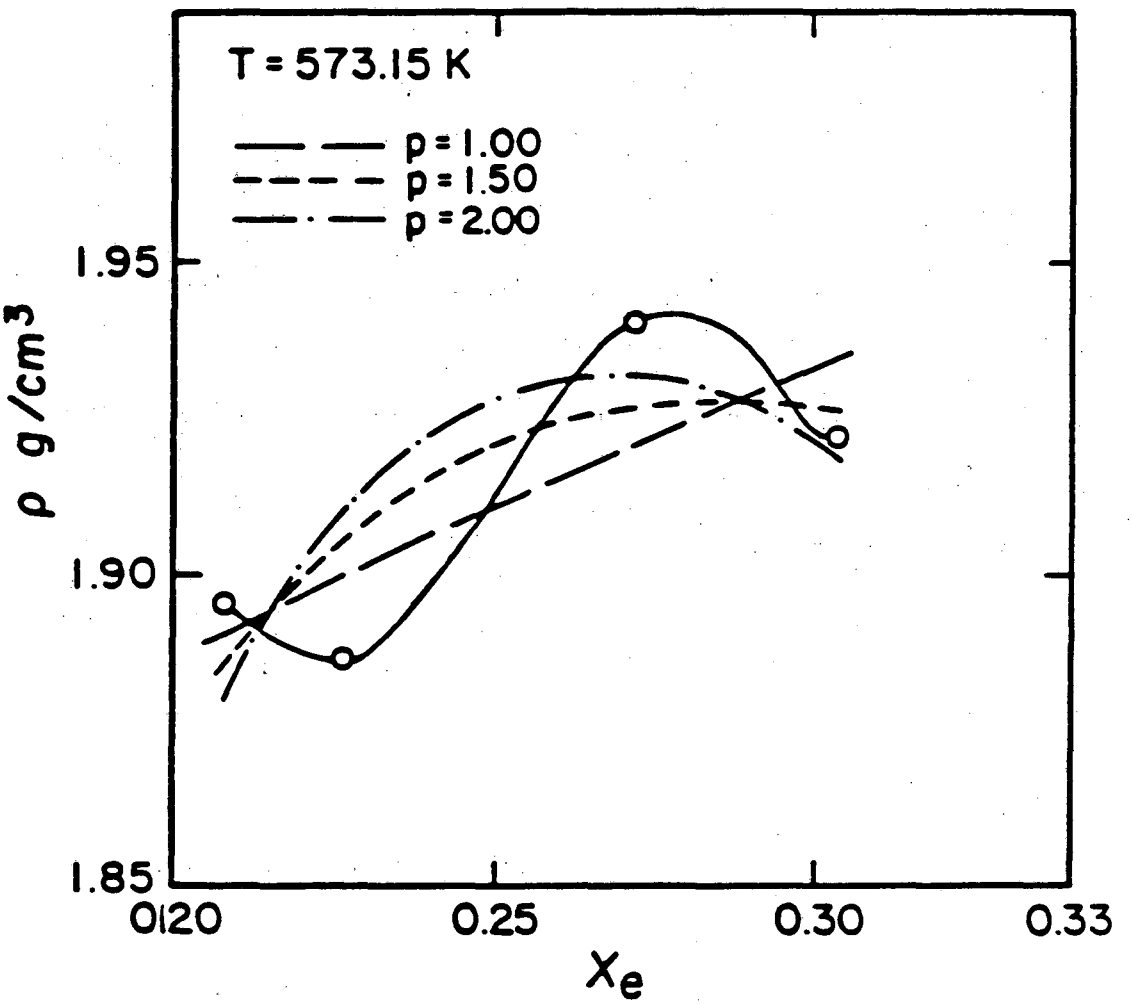

Figure 4–13 Experimental and calculated densities for sodium polysulfide melts versus melt composition at a temperature of 573.15 K. Curves for various values of the parameter p are shown.

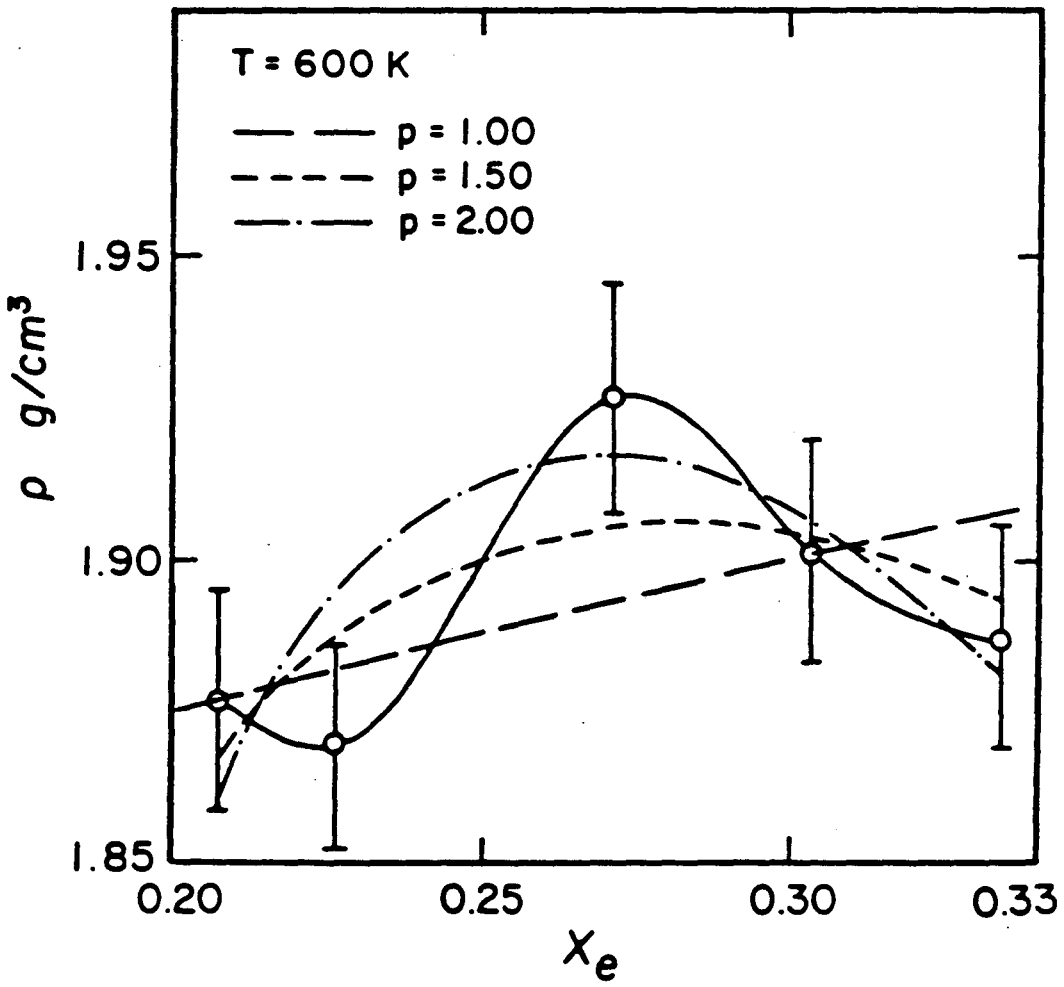

Figure 4–14 Experimental and calculated densities for sodium polysulfide melts versus melt composition at a temperature of 600 K. Curves for various values of the parameter p are shown.

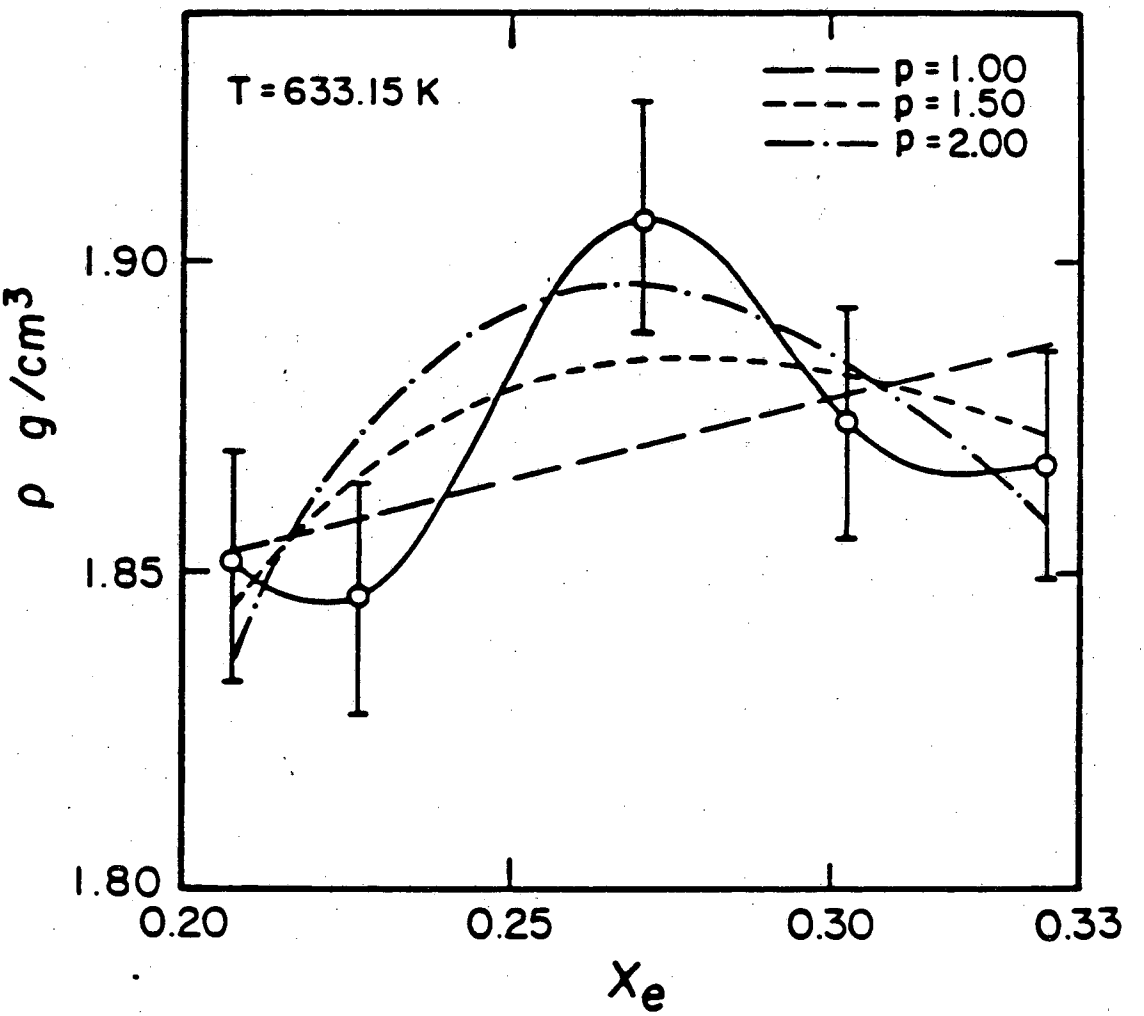

Figure 4–15 Experimental and calculated densities for sodium polysulfide melts versus melt composition at a temperature of 633.15 K. Curves for various values of the parameter p are shown.

Table 4–7 Values for $\overline{V}_N$ and $\overline{V}_1$ describing the molar volumes of sodium polysulfides for p = 1.5.

Temperature	$\overline{V}_N$	$\overline{V}_1$	Rel. Std. Dev.
K	cm^3/mol	cm^3/mol	%
	Density Data		
573.15	21.4581	5.8763	0.005
600.00	22.0298	5.8469	0.003
603.15	22.0547	5.8525	0.003
633.15	22.2949	5.9060	0.003
650.00	22.4316	5.9367	0.003
663.15	22.5387	5.9611	0.004
	X–Ray Data		
297	19.46	5.28	0.3

appropriate power. These works show that the power may be one, if the theoretical work of Eyring or Li and Chang is adopted, but is two if the empirical correlation of Wilke is accepted. These works estimate the self diffusivity or the diffusivity for a dilute solute in an excess solvent. The sodium polysulfide melt, however, is a concentrated solution of sodium cations and polysulfide anions. The diffusion of ions in the melt does not readily approach the dilute limits of these other methods. These methods suggest, however, that the $\mathscr{D}_{ij}$ parameters should be related to the inverse of the ionic radii to a given power. For species of two different radii, Equation (4–37) predicts that the sum of the individual radii are important. We therefore have adopted two relationships for all of the $\mathscr{D}_{ij}$ parameters

$$\mu \mathscr{D}_{ij} = \varepsilon_1 \frac{1}{(r_i + r_j)^q} \quad i,j \neq N, \tag{4-45}$$

$$\mu \mathscr{D}_{iN} = \varepsilon_2 \frac{1}{(r_i + r_N)^q} \quad i \neq N, \tag{4-46}$$

where

$$r_i = \left[\frac{V_i}{N_A} \frac{3}{4\pi} \right]^{1/3}. \tag{4-47}$$

The values of ε_1 and ε_2 should be independent of melt composition, but they can be functions of temperature and pressure. The ionic radii were assumed to be given as functions of the cube roots of the molar volumes as given above. If these two relationships were strictly valid, then the values for the three transport properties calculated should be identical to the experimental values at a given temperature when constant values of ε_1 and ε_2 are used.

To utilize Equations (4–45) and (4–46) above, it is necessary to have values for the viscosities of polysulfide melts as a function of composition. As we mentioned, these have been determined experimentally at a number of temperatures in the work of Cleaver and Davies.[15] Figure 4–16 plots the variation in the melt viscosity at a temperature of 633.15 K. The solid points are the experimental data, while the solid line is the best continuous interpretation. It is apparent, that no general trend is discernible from these data, and the viscosity exhibits very unpredictable behavior with respect the melt composition. The data of Cleaver and Davies suggest that these measurements should be precise to within one or two percent, hence random errors or statistical fluctuations should not be attributed to these variations.

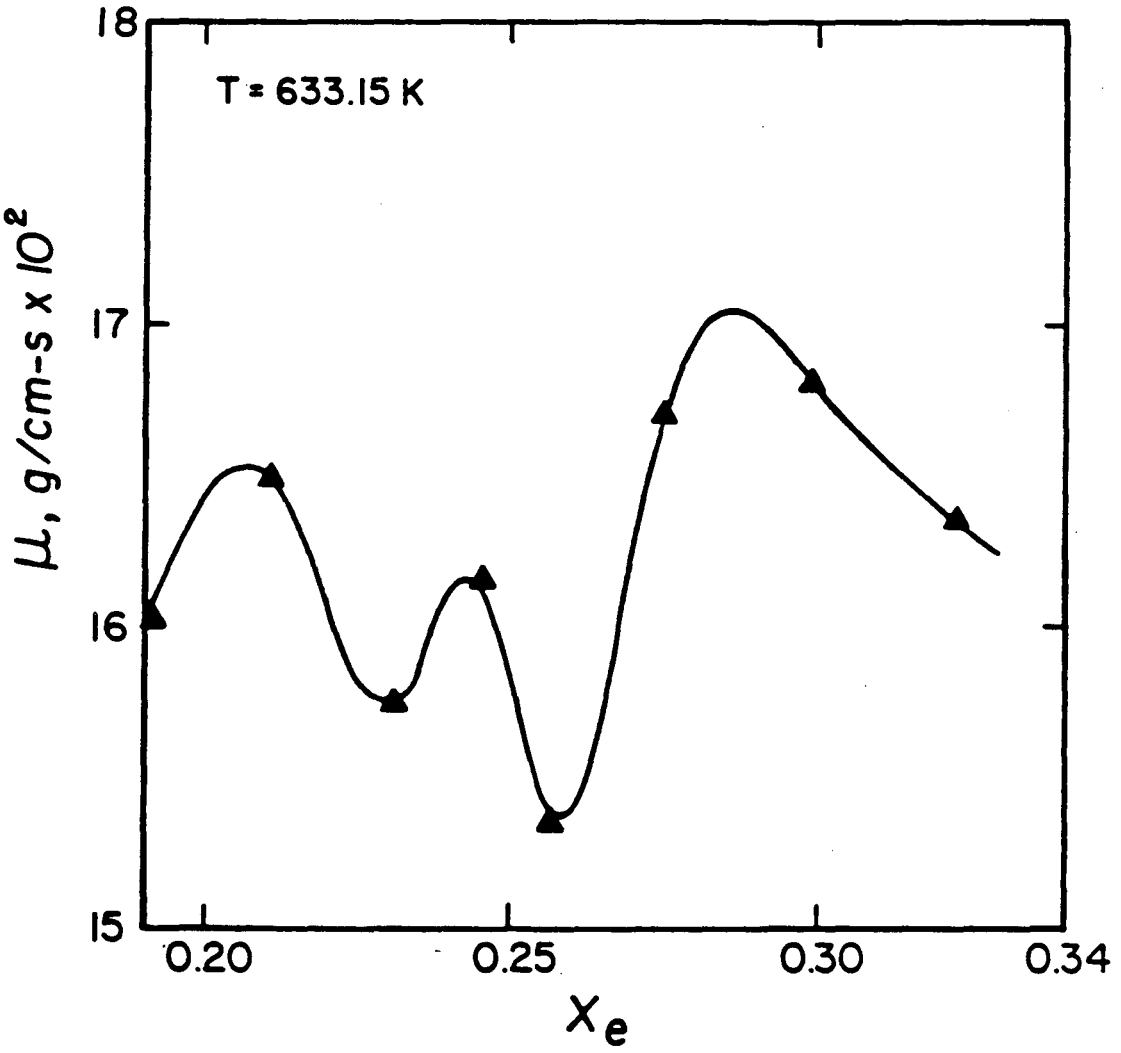

Figure 4–16 Experimental melt dynamic viscosity for several compositions from the data of Cleaver and Davies.[15]

To determine the best values of ε_1 and ε_2, we have fit these two values to the conductivity and transference number as a function of concentration. A two–dimensional Newton–Raphson method was used to find the values of these two variables which exactly fit the two measurable properties. The expressions for the $\mathscr{D}_{ij}$ parameters in Equations (4–45) and (4–46) have been used. The exponent q was assumed to be an integer. It was found that only for values of q greater than or equal to three could sets of ε_1 and ε_2 be calculated which matched the data over the entire composition range. Hence, a value of $q = 3$ was used for all of the calculations. The density, which was needed for the calculation of the ionic concentrations, was calculated from the molar volume correlations. Since the viscosity and the conductivity were needed at several compositions which possibly did not correspond to the measured compositions, a cubic spline technique was used to determine values of these properties at intermediate points. The solid curve in Figure 4–16 is an example of the use of this technique. While the predicted curve passes through each point, we do not imply that any physical meaning can be attached to it. This is simply a convenient way of generating properties at any composition. In fact, problems with the unpredictable variation in viscosity will be addressed in a moment.

Once the sets of ε_1 and ε_2 which gave an exact match with the experimental data were found, the transport properties were recalculated using constant values for these two parameters. The two values were chosen by averaging the variable values over the entire composition range. This produced nearly the best single set of ε_1 and ε_2 which reproduced the experimental data.

Figure 4–17 compares the experimental conductivity measured by Cleaver and Davies to the predictions of the model. The dashed curve is the calculated conductivity using constant values of the parameters ε_1 and ε_2 and with a composition varying viscosity. It is evident from this figure, that constant values of these two parameters do not predict the complicated variation of the conductivity with composition exactly. The rather unusual small variations in the curve are due to the very unpredictable trend in the viscosity as demonstrated in Figure 4–16. It is doubtful if variations as small as these posses any real meaning in a study as general as this. Therefore, the variation in the viscosity will not be considered any further. For all subsequent calculations, the viscosity will be assumed to be constant with composition. The general trends in the results will be unaffected by this choice. Figure 4–18 is the same prediction for the conductivity, but without the variation in viscosity. The general trend is still the same. The prediction for the conductivity at 573.15 K is shown in Figure 4–19.

Predicted transference numbers for a temperature of 633.15 K and 573.15 K are shown in Figures 4–20 and 4–21. The dashed curves are the predicted transference number assuming constant values of ε_1 and ε_2. It was not possible to fit the transference at the lower temperature of 573.15 K. No set of ε_1 and ε_2 could be found which would predict a sulfide anion transference number larger than about 0.05. The closest which could be approached to the experimental data is given Figure 4–21. There is a large difference here, but this is the best which could be calculated. One can also see from both figures that the model predicts a much larger variation in the transference number than is indicated from experiments. This is not serious, however, since the experimental transference numbers have been calculated by assuming constant values for slopes of potential versus

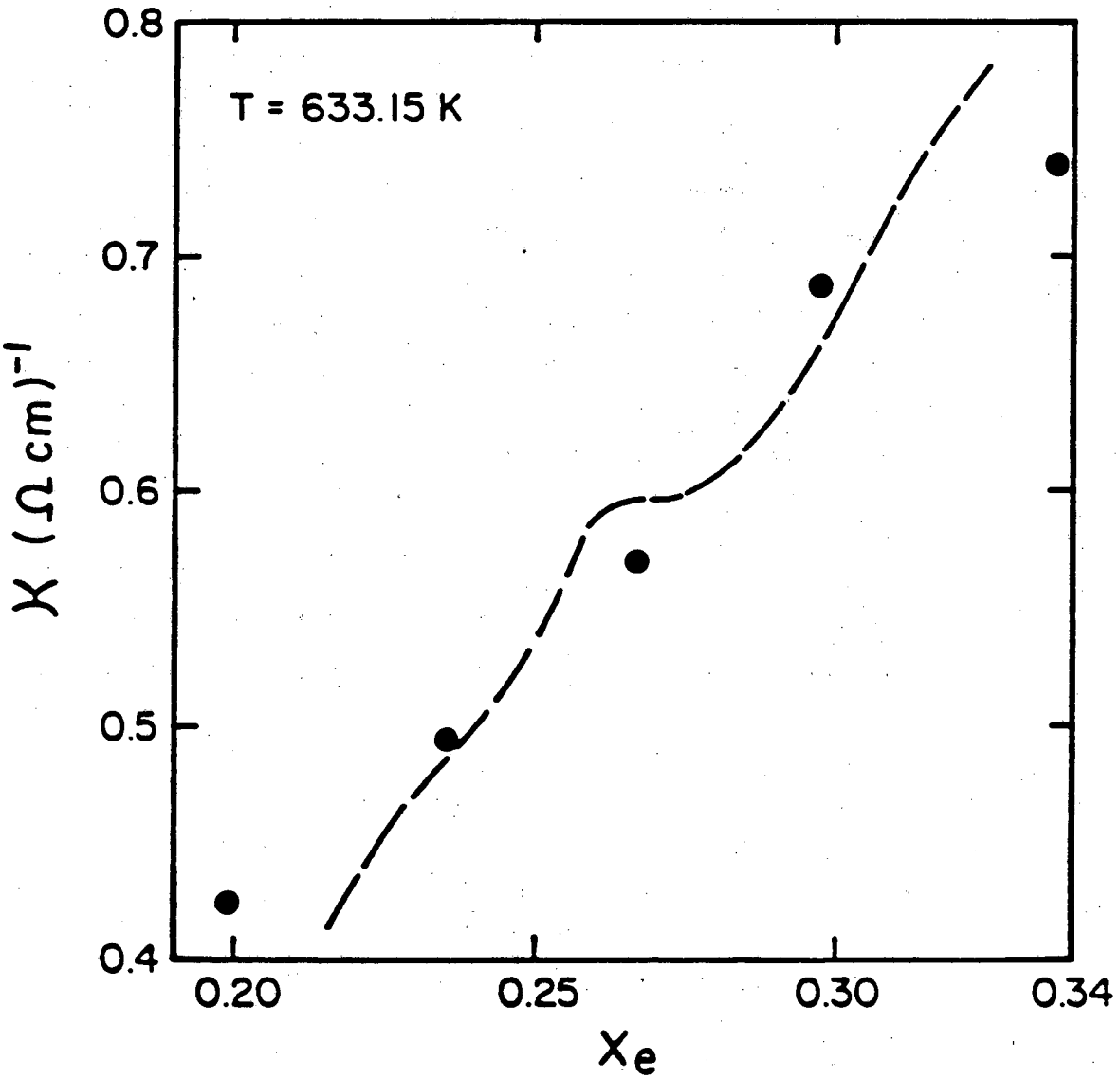

Figure 4–17 Experimental and calculated conductivities versus melt composition for a melt temperature of 633.15 K. Dashed curve is for constant $\varepsilon_1 = 1.03 \times 10^{-28}$ g cm^4/s and $\varepsilon_2 = 7.72 \times 10^{-29}$ g cm^4/s with variable viscosity.

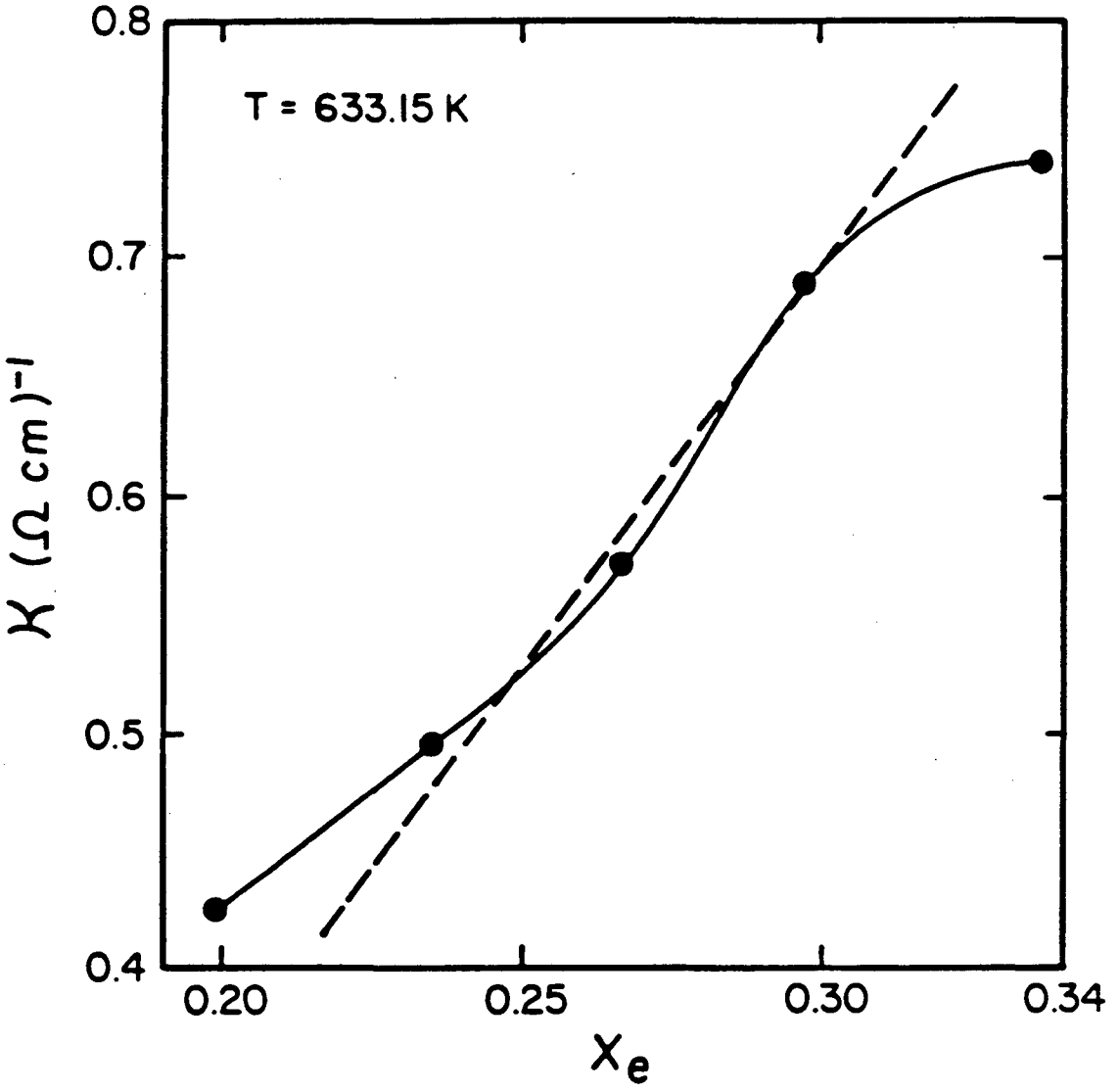

Figure 4–18 Experimental and calculated conductivities versus melt composition for a melt temperature of 633.15 K. Dashed curve is for constant $\varepsilon_1/\mu = 6.32 \times 10^{-28}$ cm^5/s and $\varepsilon_2/\mu = 4.68 \times 10^{-28}$ cm^5/s while solid line is best continuous interpretation.

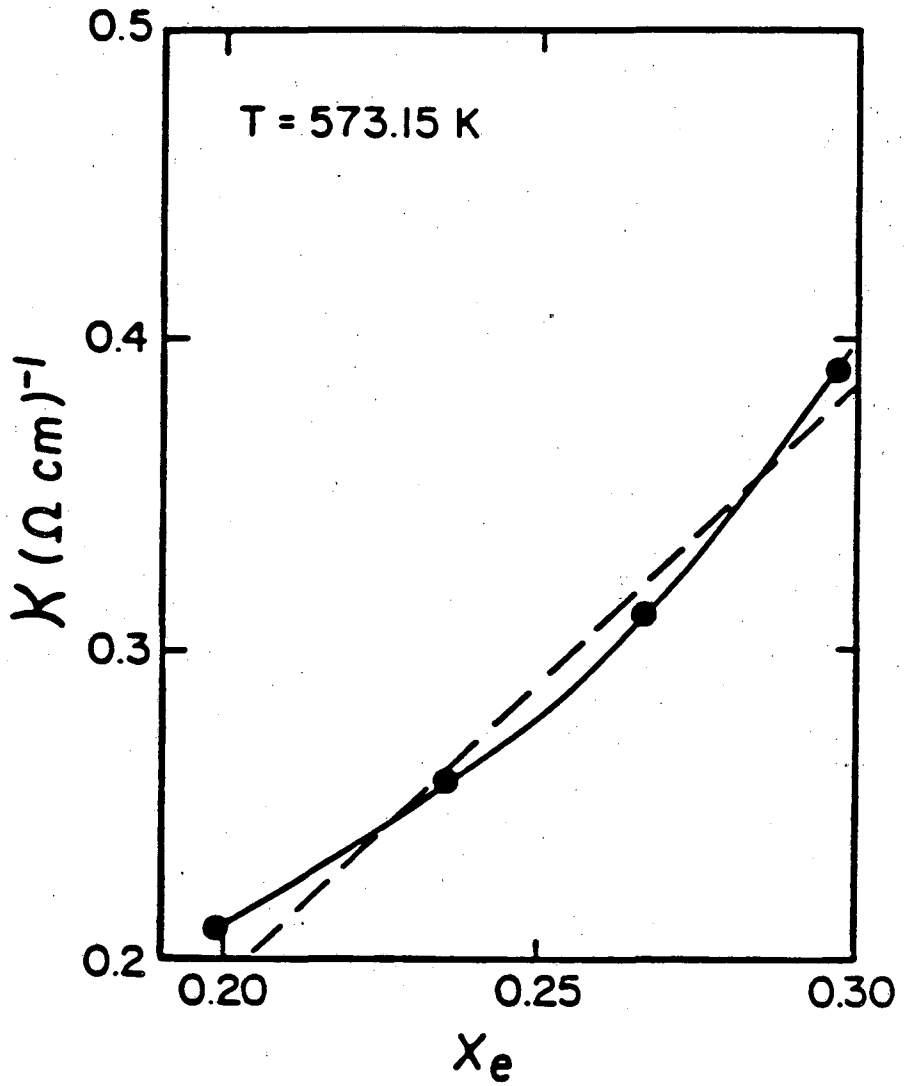

Figure 4–19 Experimental and calculated conductivities versus melt composition for a melt temperature of 573.15 K. Dashed curve is for constant $\varepsilon_1/\mu = 5.12 \times 10^{-28}$ cm^5/s and $\varepsilon_2/\mu = 2.21 \times 10^{-28}$ cm^5/s while solid line is best continuous interpretation.

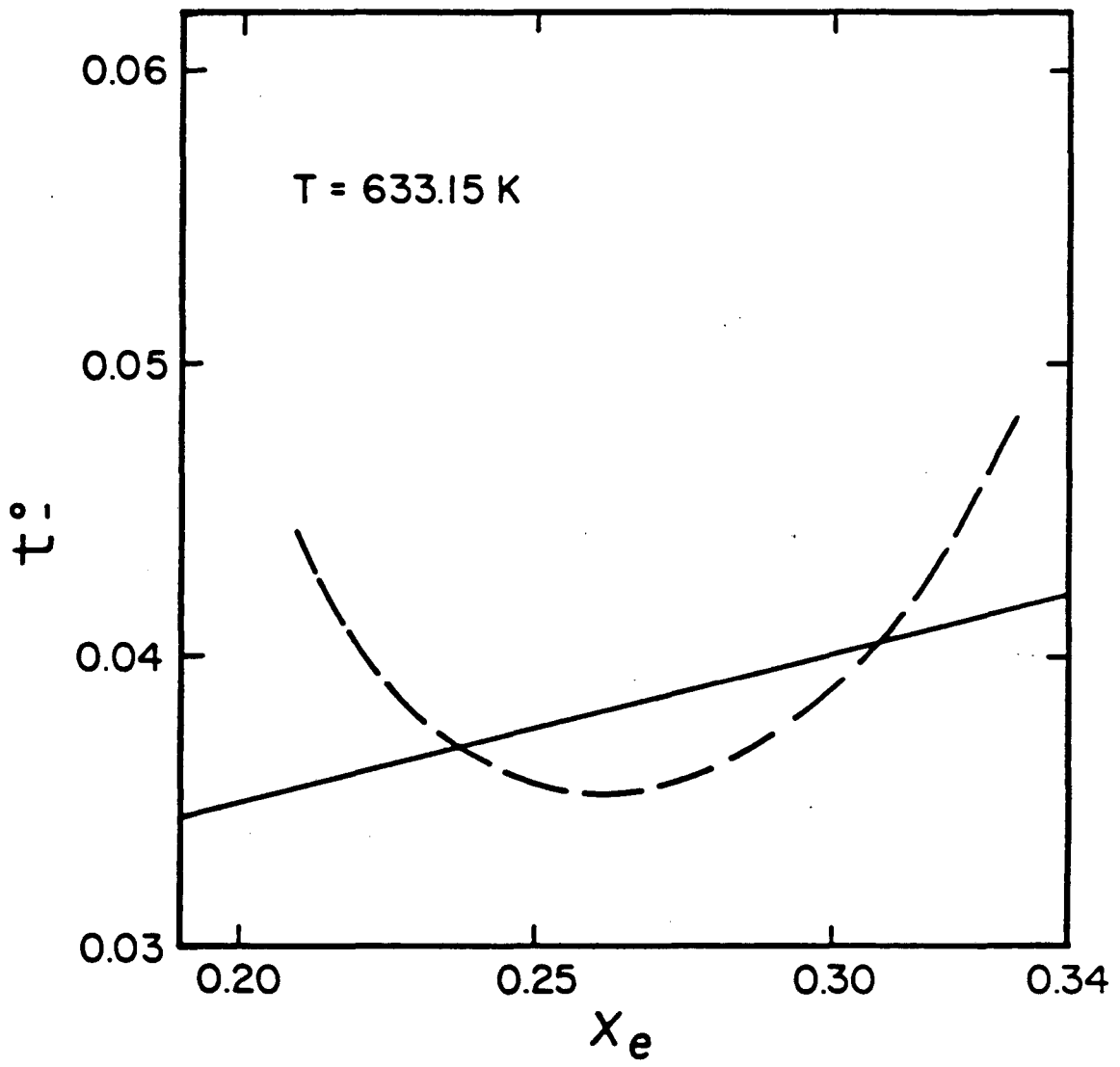

Figure 4–20 Experimental and calculated transference numbers versus melt composition for a melt temperature of 633.15 K. Dashed curve is for constant $\varepsilon_1/\mu = 6.32 \times 10^{-28}$ cm^5/s and $\varepsilon_2/\mu = 4.68 \times 10^{-28}$ cm^5/s while solid curve is calculated from experimental data.

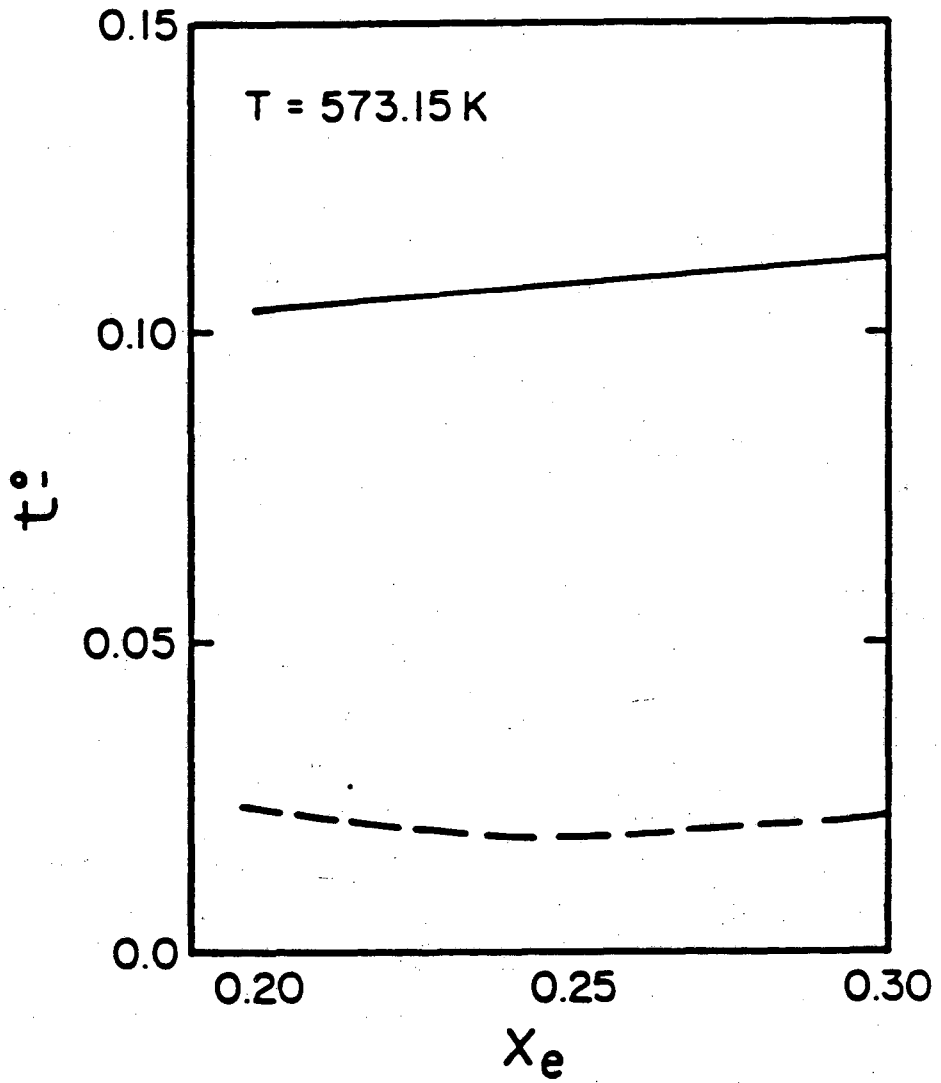

Figure 4–21 Experimental and calculated transference numbers versus melt composition for a melt temperature of 573.15 K. Dashed curve is for constant $\varepsilon_1/\mu = 5.12 \times 10^{-28}$ cm^5/s and $\varepsilon_2/\mu = 2.21 \times 10^{-28}$ cm^5/s while solid curve is calculated from experimental data.

composition curves. There is some uncertainity involved with this determination since differentiating this data is bound to introduce errors. In addition, the experimental curves are not truly straight lines. The actual variations of the experimental transference numbers are suppressed by the constant–slope approximation.

The main advantage of the model is that the diffusion coefficient for the melt can be predicted. The values of the diffusion coefficient for a thermodynamic driving force are given in Figure 4–22. The two temperatures of 573 and 633 K are shown. Two curves are shown, the solid curve is calculated from variable values of ε_1/μ and ε_2/μ, ones which exactly fit the transference number and conductivity data at all compositions. The dashed curves are for fixed values of the two parameters. There is some difference between the two curves, but this is not large, and the uncertainity is not too great.

Previous experimental work has determined D, or the diffusion coefficient for a concentration driving force rather than the more fundamental $\mathscr{D}$. The difference between these two quantities is the activity coefficient factor multiplied by the ratio of the solvent concentration to the electrolyte concentration and is expressed in Equation (3–14). The activity coefficient factor can be calculated from Equation (4–30). The predictions of the model for the thermodynamic correction factor are given in Figures 4–23 and 4–24 along with the curves calculated from the experimental data of Cleaver and Davies[18] and Gupta and Tischer.[7] Like the transference numbers, the activity coefficient factors calculated from the model exhibit much more variation with composition than the the experimental curves. Again, these curves are related to the slopes of the

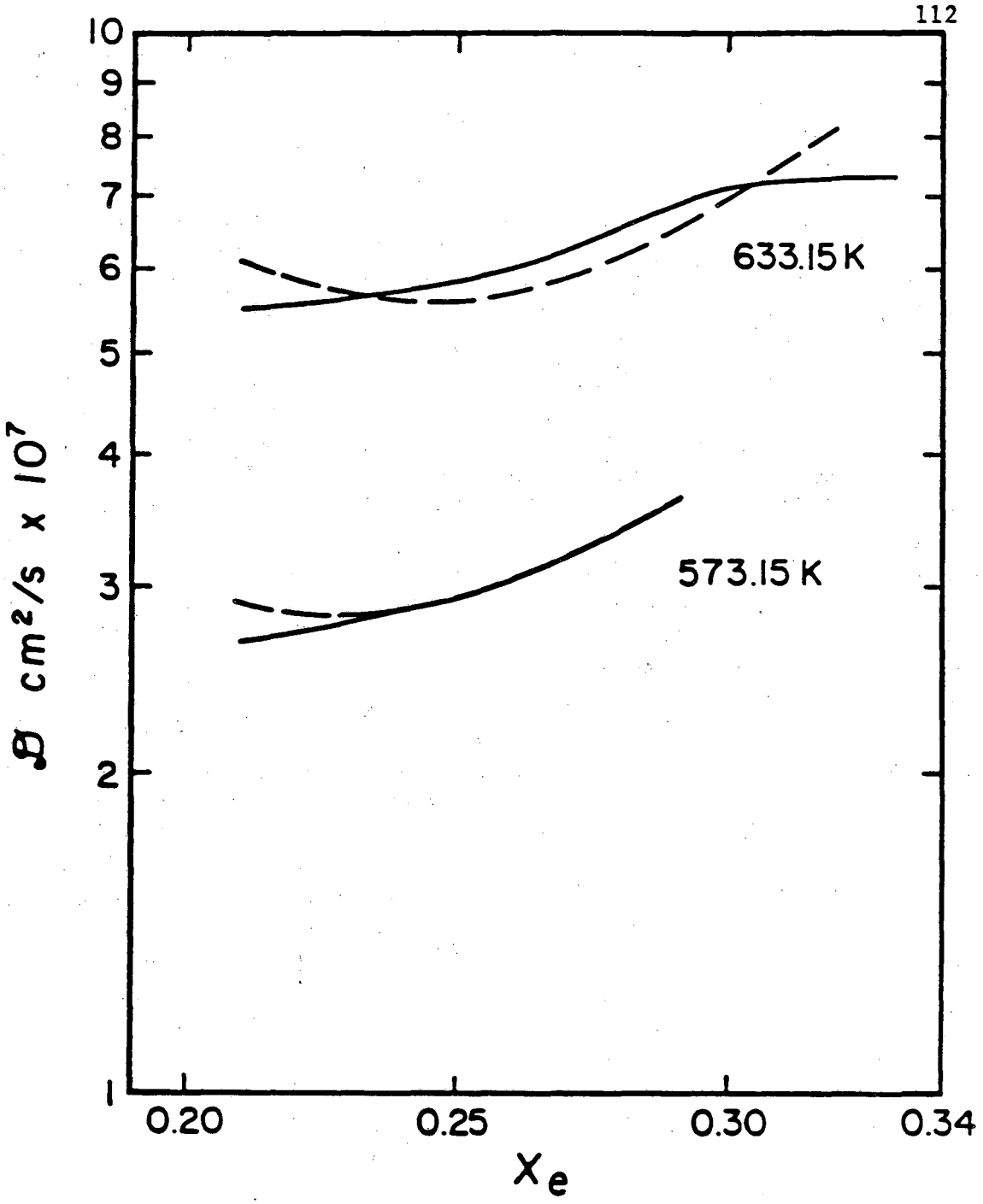

Figure 4–22 Predicted values of the diffusion coefficient for a thermodynamic driving force versus melt composition. Solid lines are for variable values ε_1 and ε_2 which fit the conductivity and transference data at all compositions. Dashed line is for constant values of ε_1/μ and ε_2/μ.

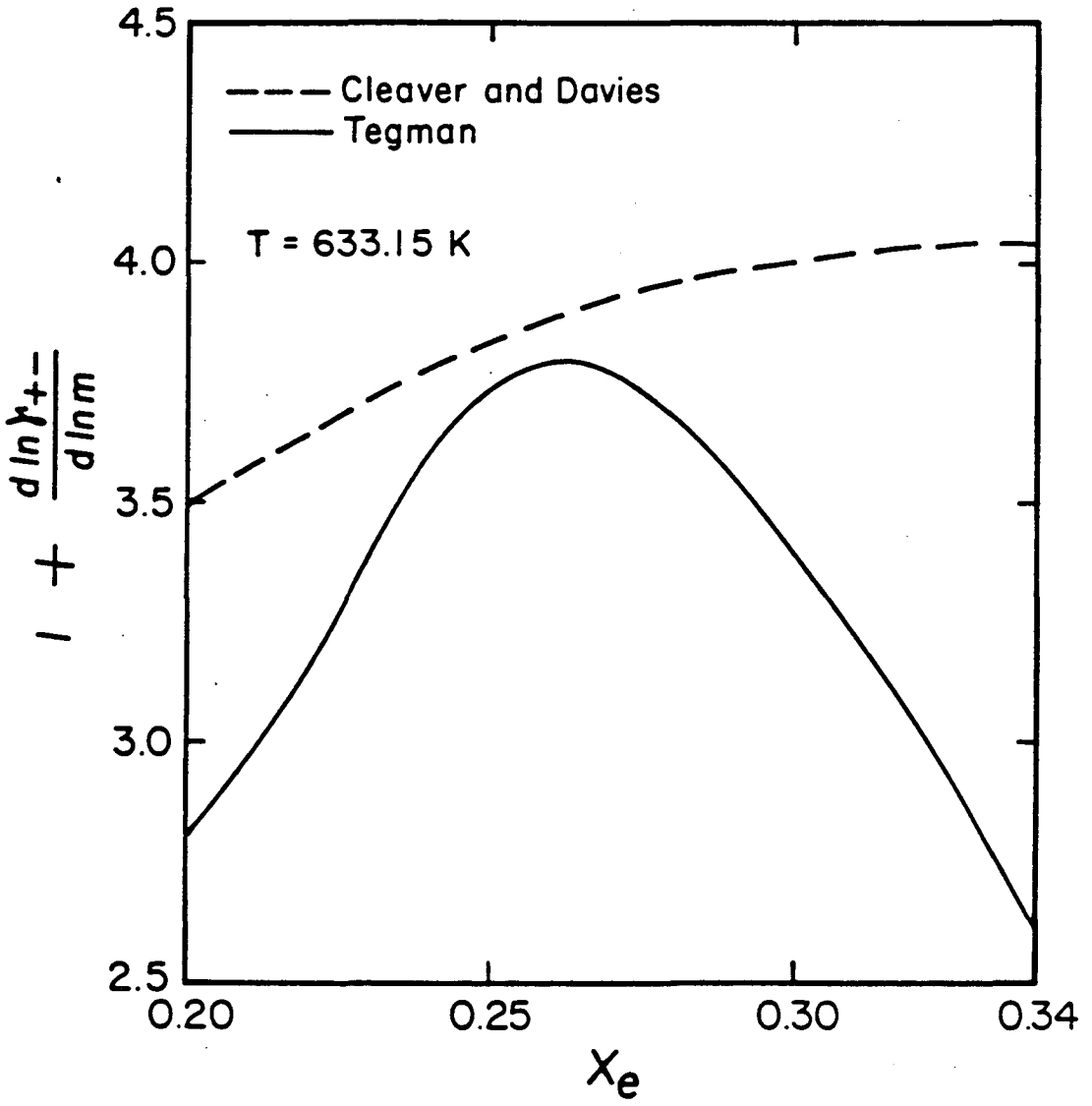

Figure 4–23 Predicted values of thermodynamic activity coefficient factor versus melt composition at 633.15 K. Solid line is calculated from the model. Dashed curve is obtained from experimental data.

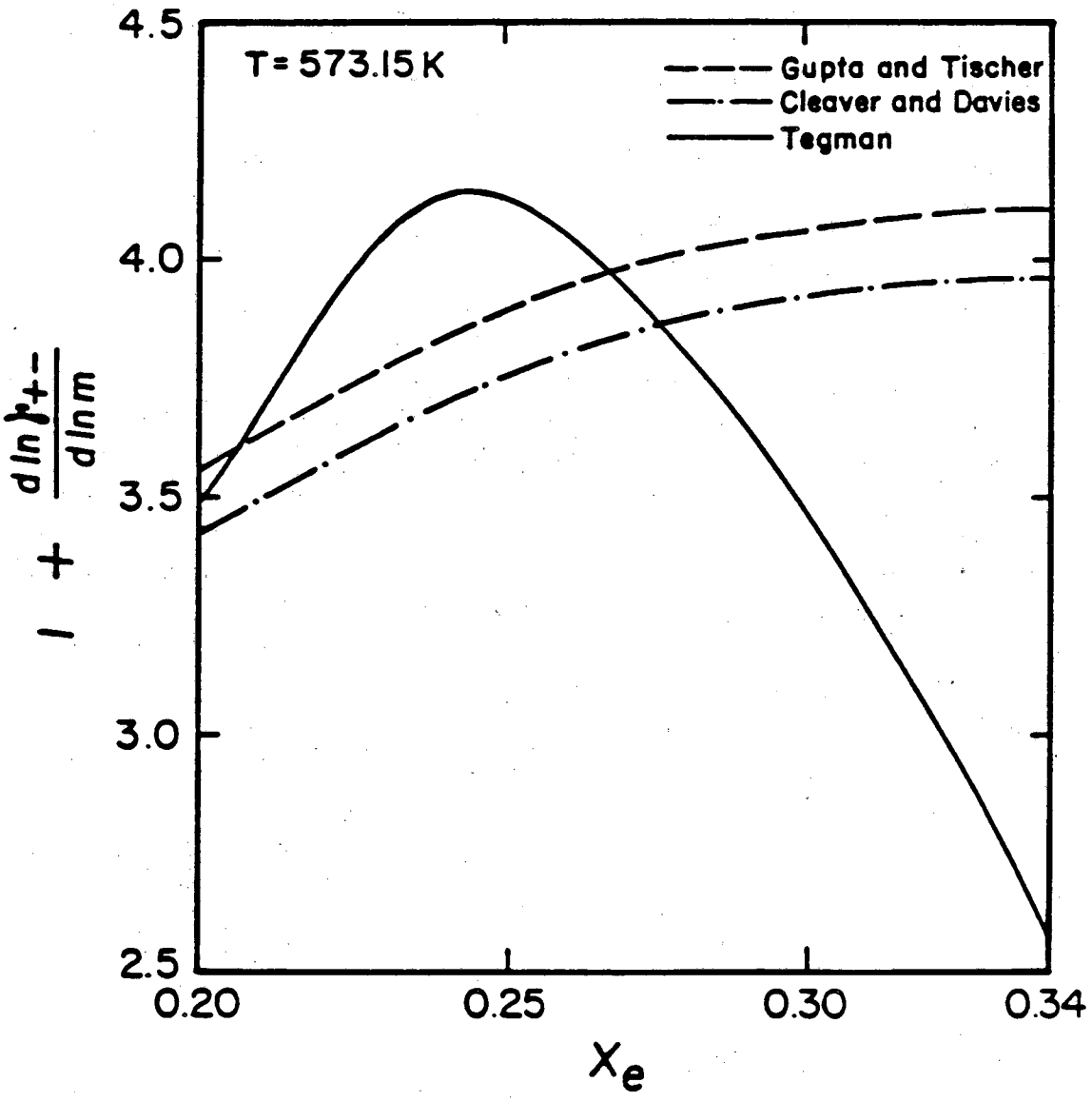

Figure 4–24 Predicted values of the thermodynamic activity coefficient factor versus melt composition at 573.15 K. Solid line is calculated from the model. Dashed curves are obtained from experimental data.

potential versus composition curve. The constant slope approximation used in reducing the experimental data tends to suppress any variations which might be present.

Figure 4–25 exhibits the prediction for the diffusion coefficient for a concentration driving force along with recent experimental data. The theoretical curve is calculated using constant values for ε_1 and ε_2 and applying the thermodynamic activity coefficient factor calculated from the microscopic model. The experimental results of three investigations are shown. The predictions for D fall in between those measured by Divisek *et al.*[27] and those of Armstrong, Dickenson, and Reid.[29] We have already discussed the uncertainities in each of these measurements.

The data point for Tischer and Ludwig was obtained by these two authors by combining the rotating disk data of South and Sudworth[26] and Armstrong, Dickenson, and Reid.[25] A value of 6.3×10^{-7} cm^2/s has been calculated for Na_2S_5 at 623.15 K. If the same data of South and Sudworth and Armstrong, Dickenson, and Reid are used to calculate the diffusion coefficient for Na_2S_3 at the same temperature, then a value for D of 2.9×10^{-8} cm^2/s is obtained. Similar calculations for the same data at 578.15 K yield values for diffusion coefficients of 2.5×10^{-7} cm^2/s for Na_2S_5 and 5×10^{-9} cm^2/s for Na_2S_3. These values for Na_2S_3 seem somewhat low with respect to the other measurements and the calculations presented here. We therefore suggest that this calculation is probably not accurate, and the result is open to question.

4.4. Effect of Slow Homogeneous Reactions

Throughout this discussion of the transport properties, we have not considered the possibility of slow homogeneous reactions between the melt

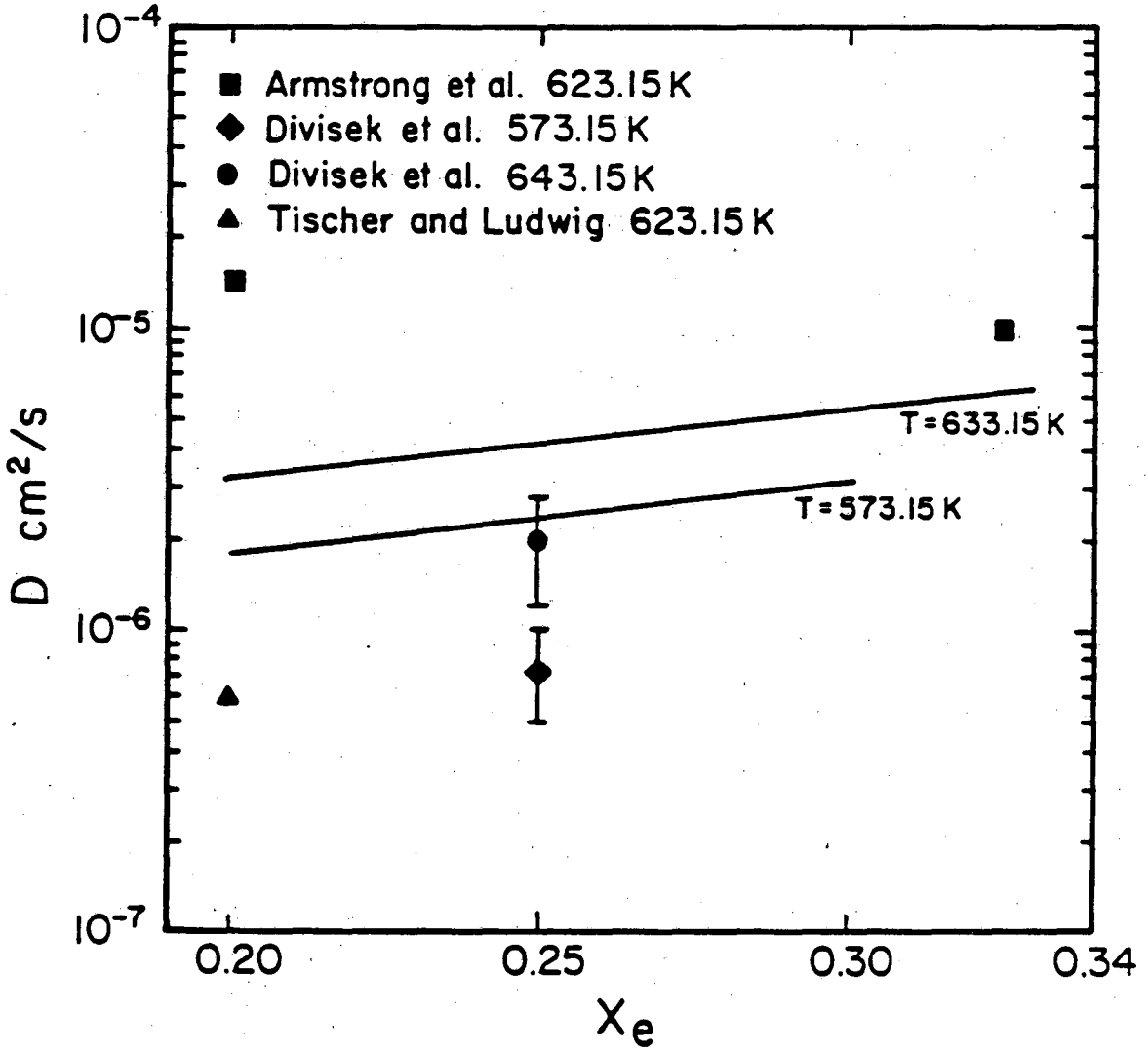

Figure 4–25 Comparison of predicted values of the measured diffusion coefficient with selected experimental data.

components. The assumption of infinitely fast kinetics for the reactions between melt species has been required, leading to the required condition of local equilibrium between melt components.

It is possible to modify the existing work to account for slow homogeneous reactions between melt constituents. To do this requires modification of the models developed here and reconsideration of experimental data. The general transport equations presented in this chapter remain applicable, but one must replace the concentrations of the individual species with actual composition at each position rather than using equilibrium concentrations. One must now use the conservation of species equations for each microscopic species to determine their concentrations at each point in time and space. The source term in these expressions must include the production or the consumption of each species by the slow homogeneous reactions.

The determination of the transport properties would also need to be modified. The transference number for the melt was calculated using the macroscopic model which assumed local equilibrium among all species. One would need to model the diffusion process occurring in the transition region accounting for the slow homogeneous reactions. One could not use the macroscopic transport equations, but instead the transport processes would have to be described using the microscopic equations.

If homogeneous reactions are to be accounted for, the limiting reactions must be identified, and the rate constants need to be determined. If all possible reactions between two species resulting were considered, then for the seven polysulfide ions assumed here this would require the determination of 9 independent rate constants. If tri–molecular reactions

are considered, then even more rate constants are required. Added to the 6 equilibrium constants and the 28 transport parameters, the number of parameters required to describe this system increases very rapidly. For seven polysulfide ions, there would be seven independent material balances, seven independent flux equations, and 9 reaction rate expressions. The possibility of modeling any system using such an approach seems too difficult and would require a large, expensive calculation. Perhaps if only one or two reactions were rate limiting, then it might be possible to include these, but the additional accuracy which would be obtained is probably not justified. For now, until more information is available, the approximation of a microscopic equilibrium melt is the most sophisticated approach which can reasonably be considered.

4.5. Summary

The transport properties for a binary melt have been predicted by considering the microscopic composition of a sodium polysulfide melt. The interactions within a melt composed of all ionic species has been considered. The macroscopic binary transport properties derived in Chapter Three were formulated in terms of fundamental interaction parameters for the individual sodium cations and polysulfide anions. It has been demonstrated that the equilibrium microscopic melt is equivalent to a binary melt with variable physical properties for describing the bulk transport of sodium and sulfur. Empirical relationships for the parameters defined in the microscopic model have been proposed which relate the 28 required parameters to two parameters dependent on the melt temperature but independent of melt composition. It has been demonstrated that the general trends of the transport properties can be predicted using this

approach. Furthermore, the diffusion coefficient for sodium polysulfide melts has been predicted and has shown general agreement with literature data.

Slow homogeneous reactions were not accounted for in this analysis, but the necessary modifications to account for these processes were outlined.

Chapter 5

Experimental Determination of Diffusion Coefficients

5.1. Introduction

Diffusion coefficients in electrochemical systems can be experimentally determined in a great number of ways. The rotating disk,[56] transient diffusion on a stationary electrode,[57] stagnant diffusion in a closed cell,[58] or a capillary[59] are all popular techniques. These have all have been utilized extensively. First we should distinguish these methods and the types of diffusion coefficients that are obtained.

Newman[60] presents a clear distinction between three types of diffusion coefficients: polarographic, integral, and differential. Polarographic diffusion coefficients are determined from transient experiments. Diffusion coefficients obtained from a falling mercury drop or by chronoamperometric means on a flat plate electrode constitute this type. Integral diffusion coefficients can be obtained from steady–state non–equilibrium flow systems such as a rotating disk or a flat plate. Since variations of transport properties are present across a diffusion layer, integral diffusion coefficients represent a weighted average of the behavior of the transport processes. Consequently, a measured integral diffusion coefficient cannot be assigned to a unique composition, or a correspondingly unique set of transport properties. While integral diffusion coefficients are useful for describing the transport properties in boundary layer flows, the inability to correlate the variation of these with specific solution compositions is a practical limit of their usefulness.

The most important type of diffusion coefficients with respect to this study is the differential diffusion coefficient. The salient feature of these diffusion coefficients is one's ability to relate these uniquely to a single solution composition, and a unique set of physical properties. Their determination requires a method which does not average over anything but an infinitesimally small concentration range. Because of the unique relationship to compositions, differential diffusion coefficients can be used with confidence in assessing the behavior of fundamental solution interactions Rigorously, integral and polarographic coefficients cannot be used for this purpose. The equations given in Chapter 3 provide the essential framework for the comparison of differential diffusion coefficients and solution interactions.

5.2. Application to Sodium Polysulfides

The literature review in Chapter Two shows that a number of investigations have been performed to determine diffusion coefficients of melts of sodium polysulfides. Integral diffusion coefficients have been obtained from the rotating disk and polarographic coefficients from chronoamperometry. Nearly all of these experiments have been plagued by a most difficult problem characteristic of the sodium–sulfur system, the inability to achieve a true limiting current. Consider an inert electrode in a single phase polysulfide melt. If one polarizes this electrode to high enough anodic potentials, a second, sulfur–rich liquid phase will be formed near the electrode. The depletion of sodium polysulfides near this electrode causes the solubility of sulfur to be reached. If instead, the same electrode is cathodically polarized, solid sodium disulfide will be produced instead of sulfur. The effects of two phases on the hydrodynamics and charge transfer

processes at the electrode surface cannot be predicted using any theories available today. One is therefore left with data which are very difficult to interpret.

The previous determinations for the diffusion coefficient have also relied on some very simplistic assumptions regarding transport processes in the melt. All of these have assumed that polysulfides are dilute solutions, with Fick's Law governing the diffusion process. However, the molten state of polysulfide melts where no nonionic species are present in excess makes this dilute solution assumption highly questionable. The thermodynamically ideal assumption of Fick's law is equally as bad. Sodium polysulfides exhibit significant deviations from ideality.

A more accurate technique for obtaining diffusion coefficient data would be one in which the presence of insolubles could be eliminated, and one in which the dilute-solution approximation could be abandoned. It has been suggested that a better method for obtaining diffusion data would be by the method of restricted diffusion.[61] This method is easily adapted to concentrated solutions with variable physical properties and requires that no high current densities be produced within the melt. Consequently, the formation of insoluble products is avoided.

5.3. Restricted Diffusion

5.3.1. Theoretical

The method of restricted diffusion was originally developed by Harned and French[62] for dilute solutions, but it has since been extended to concentrated solutions by Newman and Chapman.[58] The method can be described as follows. A concentration gradient of the species with an

unknown diffusivity, is imposed in a tall thin rectangular cell, the height of which is accurately known. The species within the cell are allowed to diffuse freely for long times, while the concentration difference between the top and the bottom of the cell is recorded. The diffusion coefficient can then be extracted from the measured difference in concentration. A good source for information on the origins of this experiment is given in Robinson and Stokes.[63] Although somewhat outdated, this reference also gives some useful insights into the measurement and correlation of transport properties.

In the original method described by Harned and French,[62] the concentrations are monitored by measuring the conductivity between two electrodes placed perpendicular to the direction of diffusion. If a unique relationship exists between the conductivity and the concentration, the change in conductivity will serve as an indicator of the change in the concentration. While useful as an indicator at at low concentrations, the conductivity loses accuracy in more concentrated solutions. The improved method, developed by Newman and Chapman, replaces the conductivity with the index of refraction as the indicator of concentration. Rayleigh interferometry is used to determine the change in refractive index with time, and this can be translated into corresponding changes in composition with time.

An analysis of this method has been demonstrated by Harned and French for dilute solutions and the rigorous analysis for concentrated solutions has been performed by Newman and Chapman. As an example, to highlight the important features of this method, let us consider the determination of the diffusion coefficient for a simple system. This system will involve a dilute solution where Fick's law is applicable, and the diffusion

coefficient is invariant with composition. Negligible changes of volume upon mixing will also be assumed. Mathematically, the solution for the composition distribution within the cell is identical to that for transient thermal diffusion within a finite slab if uniform physical properties are assumed. Consider a single diffusing species in a one dimensional planar medium. The conservation of species equation requires

$$\frac{\partial c}{\partial t} = D \nabla^2 c. \tag{5–1}$$

For the closed rectangle, the no–flux, impermeable boundaries at each end of the enclosure require the following boundary conditions:

$$at\ y = 0,\ \frac{\partial c}{\partial y} = 0, \tag{5–2}$$

and

$$at\ y = L,\ \frac{\partial c}{\partial y} = 0. \tag{5–3}$$

The assumed initial condition will be an arbitrary distribution of the diffusing species at time equal to zero,

$$at\ t = 0,\ c = f(y). \tag{5–4}$$

The solution to Equation (5–1), subject to the boundary conditions of Equations (5–2) and (5–3) and the initial condition of Equation (5–4), can be found in any good book on heat transfer or applied mathematics. One can also see Newman and Chapman.[58] The expression for the concentration at any position and time is

$$c = \sum_{n=0}^{\infty} A_n e^{-\frac{n^2\pi^2 Dt}{a^2}} \cos \frac{n\pi y}{a}, \tag{5–5}$$

where the constants, denoted by A_n, depend upon the initial concentration profile. At long times, the concentration profile reduces to an exponentially time decaying cosine profile along the vertical dimension of the cell.

If one monitors the difference in concentration between two fixed points at the end of the cell, say at the positions 1/6 and 5/6 of the length of the cell, then the following expression describes this difference in concentration,

$$\Delta c = c\left(\frac{a}{6}\right) - c\left(\frac{5a}{6}\right) = 2A_1 e^{-\frac{Dt\pi^2}{a^2}} \cos\frac{\pi}{6}$$

$$+ 2A_5 e^{-25\frac{Dt\pi^2}{a^2}} \cos\frac{5\pi}{6} + \cdots \qquad (5\text{–}6)$$

When one then plots the logarithm of this difference in concentration with time, it becomes linear as time tends toward infinity. Equation (5–6) for the concentration difference shows that the higher order terms in the expression rapidly become small compared to the leading term at long times. The diffusion coefficient can thus be determined from the slope of this straight line, which is $D\pi^2/a^2$.

The resulting diffusion coefficient obtained corresponds to a concentration given by a weighted average of the concentration profile present at the start of the experiment. This is the same as the well mixed composition of the solution, or the composition of the solution as time tends toward infinity. The resulting corresponding solution composition can thus be obtained after the diffusion process has occurred by measuring the composition of the final solution.

For concentrated solutions, the simplified analysis presented above may not be completely appropriate. Thermodynamic nonidealities may cause the driving force to differ significantly from the gradient in concentration. Fick's law may become quite inaccurate. The variation of solution properties, especially the diffusion coefficient itself, may also introduce uncertainities. Finally, the variation in the actual height of the

liquid column might respond to changes in the volume of components as they mix and might have to be considered.

Newman and Chapman have shown that all of these effects can be included in a more accurate analysis of restricted diffusion. Rigorous application of the concentrated flux equations presented in Chapter Three have been used as a basis for this analysis. The resulting equations can be solved in a more complicated way than in the dilute solution case. Using a perturbation expansion, an expression for the composition profile and the difference in concentration can be obtained. Again, though, the results show that the diffusion coefficient can be obtained in the same way as before. A logarithmic plot of concentration difference versus time recorded at long times will have a slope which can be related to the diffusion coefficient.

There are three very important advantages of the method of restricted diffusion. The first advantage is that the resulting diffusion coefficients are absolutely determined. The method requires no calibration with a standard solution of known diffusivity. Only the height of the liquid column must be known. Second, in either the dilute or concentrated solution case, the resulting diffusion coefficients do not depend on the initial concentration profile within the cell. Any initial profile can be used, yielding the same diffusion coefficient. Finally, it is also not necessary to know the exact relationship between the measured variable and the solution composition. As long as the measured property becomes linear at small differences in concentration, then it may be used as a relative reference for the difference in concentrations. The only restriction is that the measured property must not have a minimum or maximum near the composition where the

measurements are performed.

A schematic diagram of the experimental apparatus is shown in Figure 5–1. Here a cell is charged with a pure sample of sodium polysulfides and kept at the desired temperature by an external heater. Since sodium polysulfides are hygroscopic, the cell must be isolated from the ambient atmosphere. This can be achieved by sealing the cell or performing all experiments within an inert atmosphere. A glove box could be used for this purpose.

Located at the top and the bottom of the cell are two molybdenum electrodes. These serve two purposes. First, the concentration difference of the melt can be monitored using these as reference electrodes. Since sodium polysulfides form opaque liquids, the change in composition cannot be obtained from variations in index of refraction. Any electrode reaction could be be used for the reference reaction provided it is reversible to ions present in the melt. The equilibrium between sulfur and sulfide ions on molybdenum

$$S^{=} \rightarrow S + 2e^{-}, \qquad (5-7)$$

is a suitable reaction which would indicate the composition. The resulting potential difference between the two reference electrodes could be related to changes in concentration. The potential difference could be recorded using using a compensator circuit or high impedance electrometer, as shown. The electrodes could also be used to generate the initial concentration difference required. By polarizing the electrodes, an excess of polysulfide ions would be generated at one electrode and depleted at the other.

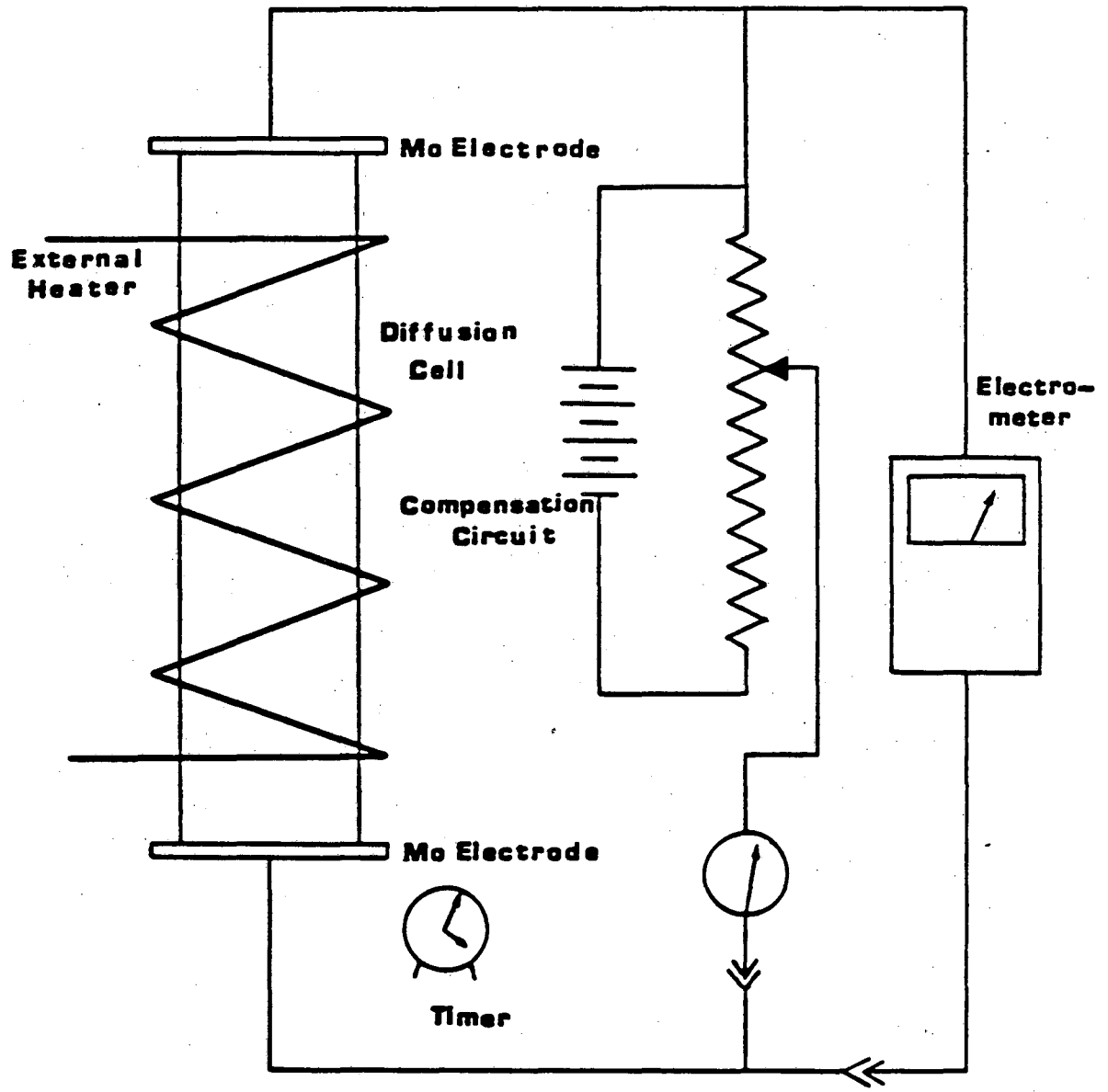

Figure 5—1 Schematic diagram of apparatus.

In the previous experiments of restricted diffusion, the concentration differences were measured at the points 1/6 and 5/6 of the length of the cell. Onsager suggested this method.[62] Careful examination of the governing equations shows that selected higher order terms can be eliminated, when this choice of positions is made. This makes the approach to infinite time shorter for a given cell height, allowing for a more accurate determination. For simplicity in cell construction, one may also monitor the concentrations at each end of the cell; however, a longer time will be required for a linear relationship to be achieved.

After the initial concentration profile has been generated, the melt would be allowed to diffuse freely. When sufficiently long times had passed, the potential between the two electrodes would be recorded at regular time intervals, and the diffusion coefficient will be obtained. The average melt composition must also be determined. This could be done chemically, but preferably electrochemically using open circuit potential measurements with respect to a sodium reference electrode as described by Gupta and Tischer[7] Using the method of restricted diffusion, the resulting diffusion coefficients should be several fold more accurate than those determined from any previous experiment. Accuracies of 0.2 to 0.3 percent have been obtained in aqueous solutions.

The procedure for determining the diffusion coefficients is shown symbolically in Figure 5–2. Four separate steps have been defined: assembly, filling, sliding, and running. The diffusion cell and the reference electrodes are first sandwiched together as shown in drawing (a). Next, the sodium polysulfide is placed into the cell using an external fill–tube and enough polysulfide is added to over fill the cell slightly. This is step (b). In

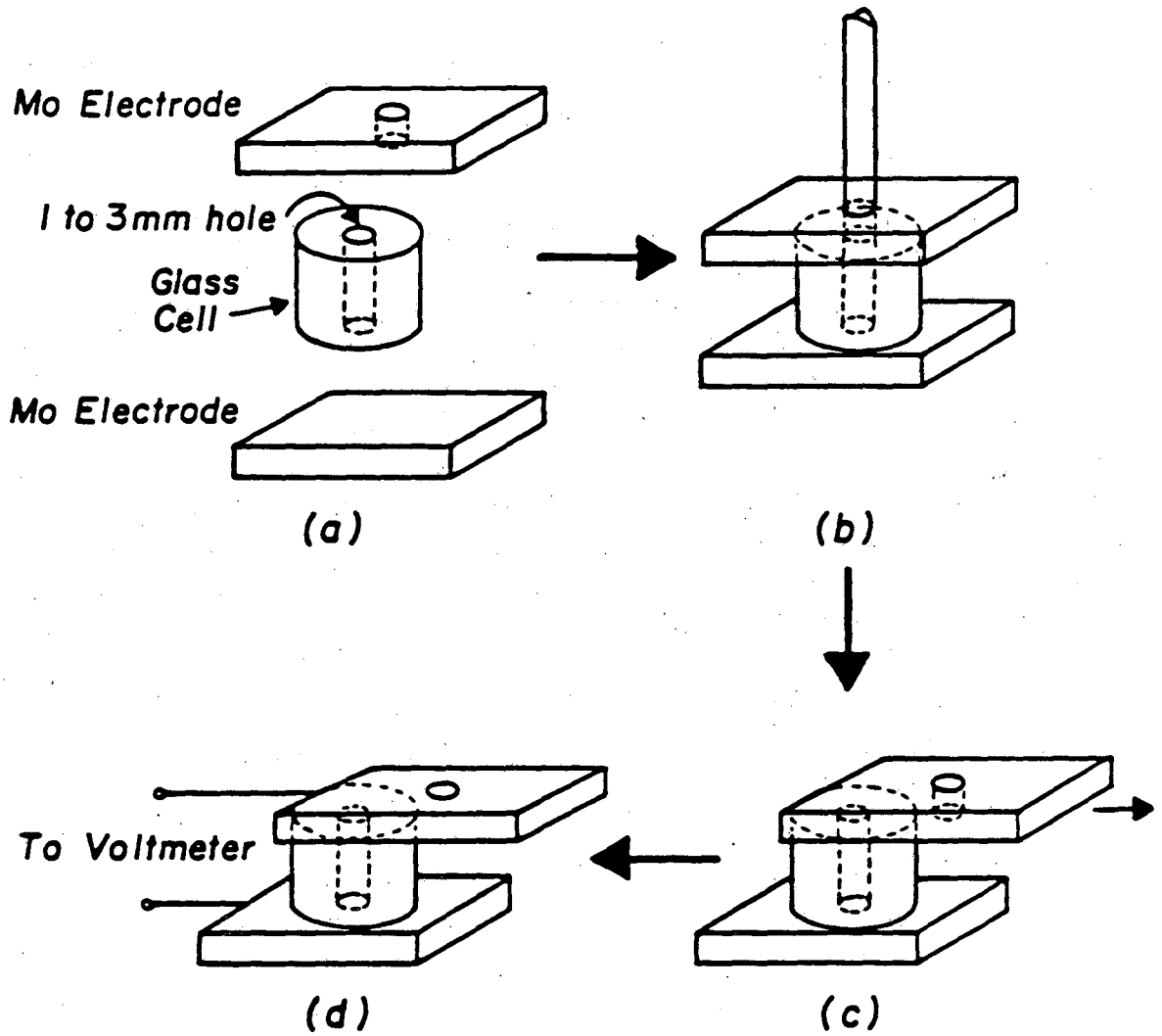

Figure 5–2 Symbolic representation of the method for obtaining diffusion coefficients; (a) assemble cell; (b) fill with polysulfide; (c) slide top electrode; (d) establish concentration gradient and measure potential with time.

step (c), the upper reference electrode is then moved sideways, covering the hole in the glass cell. The cell is therefore completely filled with the polysulfide, and a current path between the top and the bottom is formed. The voltmeter and power supply are then connected to the reference electrodes and once the concentration gradient is established, the potential between the two electrodes is recorded at regular intervals in step (d).

The selection of the height of the cell is not critical, so long as the time constant for diffusion in the cell is not too large or too small. Equation (5–6) shows that the concentration becomes linear at times on the order of $a^2/D\pi^2$. One therefore should select the height of the cell from this expression. For the aqueous electrolytes Newman and Chapman examined, the diffusion coefficient D was about 1×10^{-5} cm^2/s. They chose a time constant of about two days, which suggested a cell height of about 5 cm. For sodium polysulfides, the estimated diffusion coefficient is much smaller, probably around 5×10^{-7} to 5×10^{-6} cm^2/s. For the same time constant, the approximate cell height should then be about 0.5 to 2 cm.

5.3.2. Experimental Apparatus

The experimental apparatus consisted of a number of separate parts. The central piece of equipment in the experiment was the diffusion cell, which contained the melt and two molybdenum reference electrodes. The cell was located in an inert atmosphere glove box to protect the highly hygroscopic polysulfides from contact with moisture in the air. Potential measurements were made using a combination of equipment. Two high impedance amplifiers and a digital voltmeter were used. More detailed discussions of the diffusion cell, glove box, and electronic hardware follow in separate sections.

5.3.2.1. Diffusion Cell

A diagram of the diffusion cell is shown in Figure 5–3, and a photograph is shown in Figure 5–4. The main purpose of the diffusion cell is to provide a stable location for the determination of the diffusion measurement. The cell consists of four major parts: a base, the actual cell, a fill tube, and a sliding plate assembly. The diffusion cell was manufactured by the Chemistry Department fabrication shops of the University of California in Berkeley.

The base of the cell is a four inch diameter by one inch thick plate machined from aluminum. It provided a stable platform for the experiments. Connected to the base, by tapped holes, are four threaded steel drill rods which extend upwards. An insulating plate machined from transite, a high temperature electronic insulator, was located in the center of the base and fastened securely by four screws. Resting on this insulator was a one inch round plate of molybdenum machined from ¼ inch stock. This plate was used as the bottom reference electrode. The molybdenum plate was polished with abrasive paper on a Buehler Ecomet III rotating polisher to a fineness of 600 grit. This imparted a finely smooth, shiny finish to the molybdenum.

The diffusion cell is a one inch diameter Pyrex® glass rod cut to a length of approximately one centimeter. A 3 mm hole was drilled through the center of the rod, and the faces of the rod were polished with 600 grit polishing paste. This was placed on top of the molybdenum plate, and high temperature vacuum grease manufactured by VWR Scientific was used to form a seal between the glass and the plate. The sealing grease was rated to withstand temperatures up to 633 K.

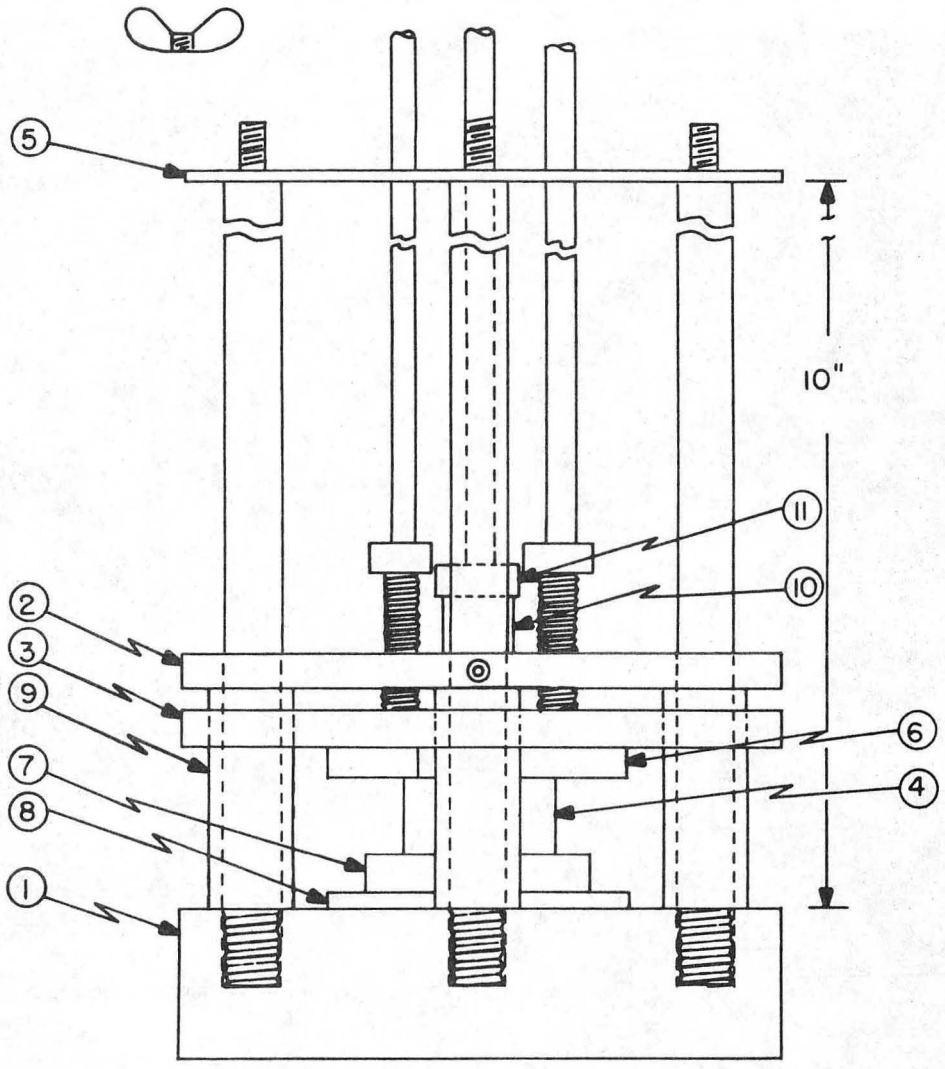

Figure 5–3 Diagram of diffusion cell showing: (1) cell base, (2) upper aluminum plate (3) lower aluminum plate (4) glass cell, (5) top plate, (6) upper molybdenum electrode, (7) lower molybdenum electrode, (8) transite insulator, (9) positioner sleeves, (10) stainless steel reservoir, and (11) stainless steel reservoir cap.

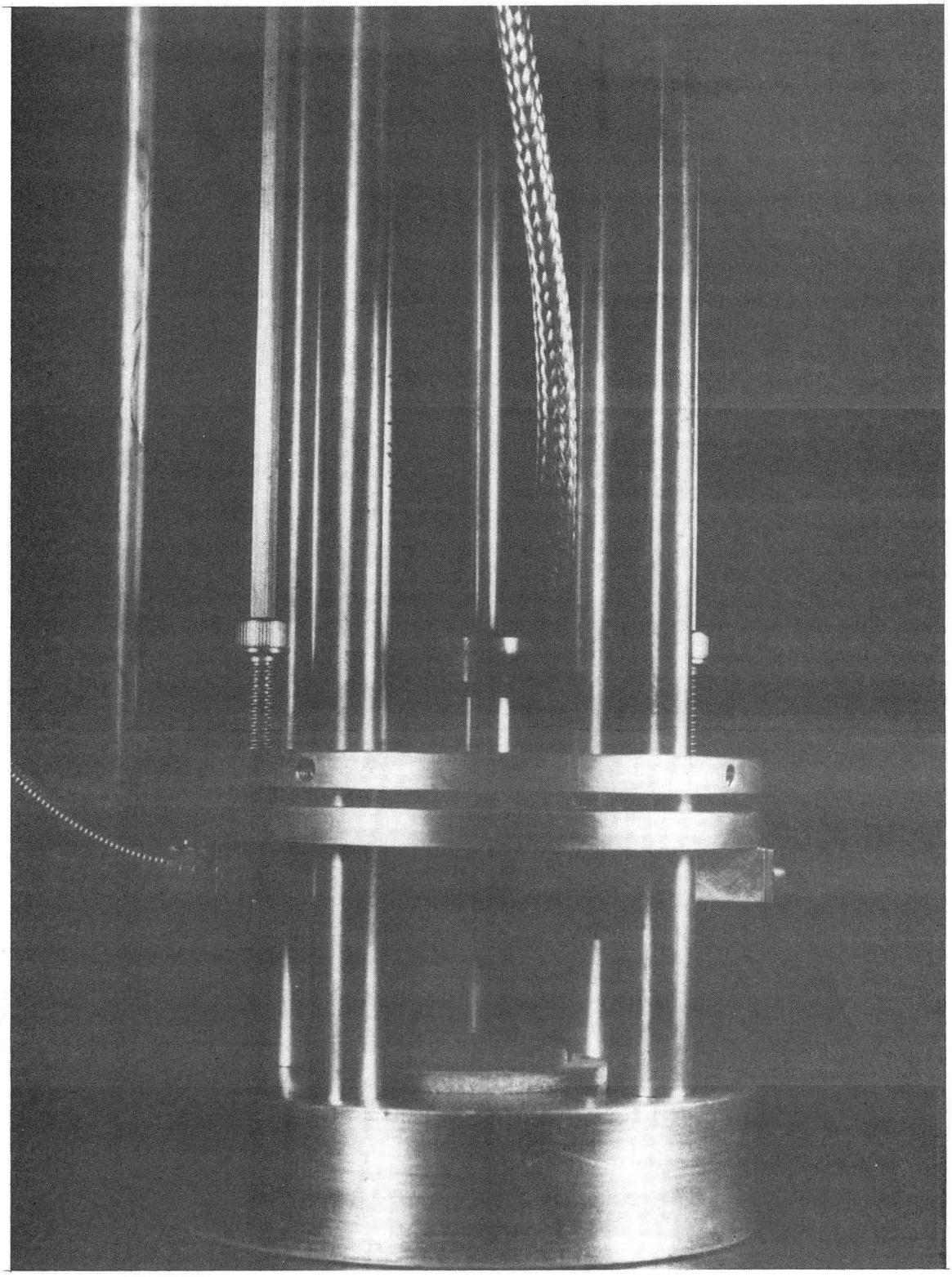

XBB 839-8334

Figure 5-4 Photograph of diffusion cell.

Located above the top of the cell is the sliding plate platform. This contains the upper molybdenum reference electrode. The upper molybdenum reference electrode was attached to the sliding assembly which in turn was mounted to a round, ¼ inch plate of aluminum. This plate was mounted to a second ¼ inch aluminum plate via two hex head screws.

The sliding assembly consisted of two rectangular pieces of steel. One of the steel rectangles fit into a channel machined in the other rectangle and could be slid back and forth. Ball bearings were incorporated between the first and second rectangular pieces of metal to provide smooth movement. One of the steel rectangles was attached to the upper platform, which enabled the second steel rectangle to slide back and forth relative to the platform. The upper reference electrode was then attached to the movable rectangle. Thin mica insulators were placed between the electrode and the steel rectangle to isolate the electrode electrically from the sliding assembly. The entire sliding assembly consisting of the two aluminum plates, sliding and fixed steel rectangles, and the reference electrode was then placed above the diffusion cell. Holes drilled in the aluminum plates, matching the pattern of the rods protruding up from the lower aluminum base, were used to align the sliding assembly directly above the diffusion cell. Allen key screws tapped into the upper plate held it in a fixed position above the cell. The two hex head screws could be turned forcing the aluminum plate containing the upper reference electrode down on top of the cell. In this position, the lower face of the upper reference electrode contacted the top of the diffusion cell. The pressure exerted on the cell by the upper reference electrode on the upper face of the diffusion cell could be varied by turning the two screws.

Two chromel–alumel thermocouples protruded down beside the diffusion cell and monitored the temperature near the cell. The absolute temperature of the working thermocouples were determined with respect to an ice reference thermocouple located in a dewer flask. The differences in potential between the working and reference thermocouples were displayed on a Keithly digital voltmeter.

A four foot length of flexible cable inside a cable guide was connected to the sliding assembly. Remote movement of the reference electrode was thus possible by moving the other end of the cable.

A small 2 mm hole was drilled through the upper molybdenum plate and threads were tapped into the hole from the side away from the cell. A small reservoir machined from stainless steel was constructed with a male connector which could be screwed into this upper reference electrode from above. A stainless steel hypodermic needle was fabricated with a threaded end which could also be screwed onto the reservoir. At the other end of the reservoir, male threads were machined. Attached to the reservoir, and extending upwards, was a stainless tube to which a vacuum or pressure line could be attached.

5.3.2.2. Furnace Well and Glove–Box

The diffusion cell was contained within a glove box complete with nitrogen, water, and oxygen removing capabilities. Photographs of the glove box and purifying equipment are shown in Figure 5–5. The glove box and purifiers were manufactured by the Vacuum Atmospheres Corporation (VAC) of Hawthorne, California. The glove box was a Dri–Lab model DL 002–D–P containing four work stations and a single vacuum/transfer chamber. Two furnace wells were installed in the bottom of the glove box. The dimensions

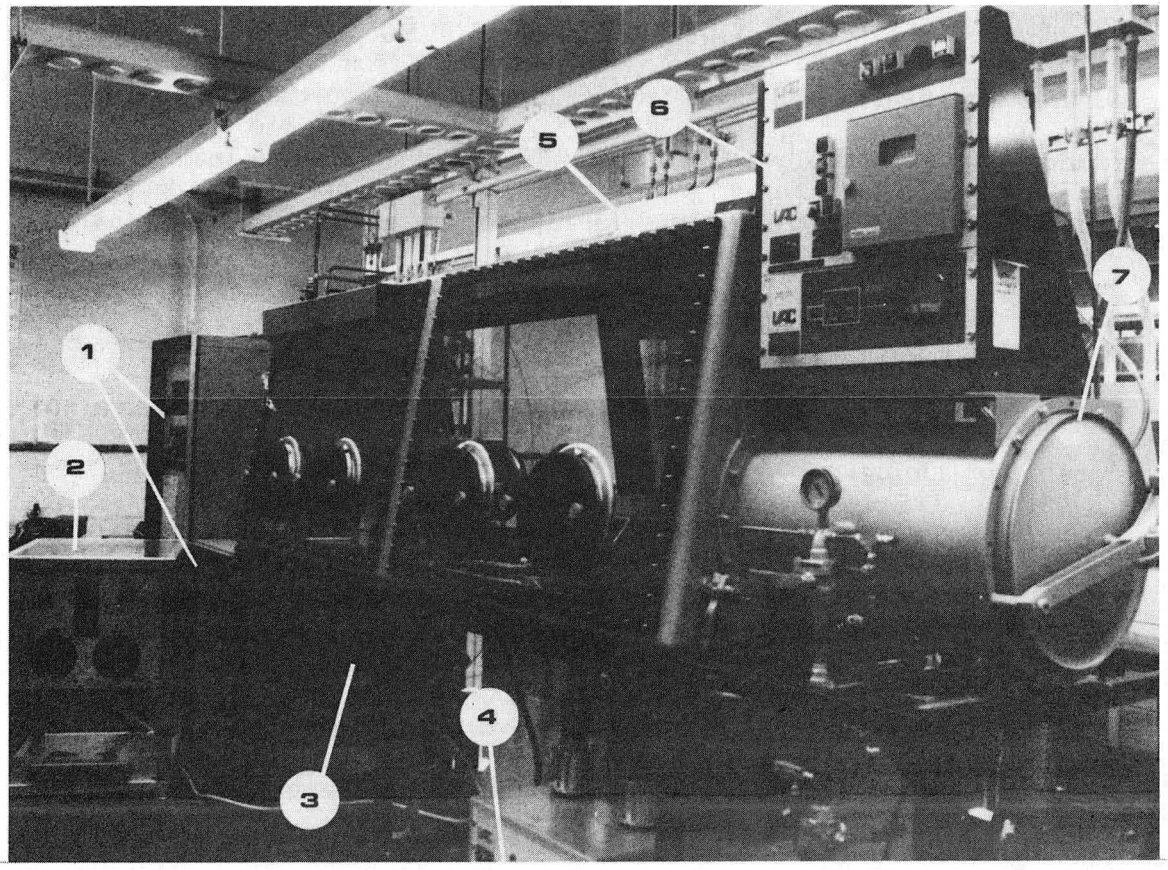

XBB 839-8335A

Figure 5-5 Photograph of glove box and purifying equipment showing: (1) nitrogen and oxygen purifying equipment, (2) furnace controllers, (3) furnace well and furnace, (4) glove box refrigeration unit, (5) glove box, (6) oxygen monitoring system, and (7) vacuum transfer chamber.

of these are given in Figure 5–6. A cooling coil was installed in the upper third of the furnace well to dissipate heat generated from the well.

The glove box was equipped with a Dri–train MO 40–2 dual bed inert gas purifier for the removal of water and oxygen. The purifiers contained 16 pounds of molecular sieve and 10 pounds of Ridox®, a dessicant. Each bed had enough capacity to operate for approximately three months before regeneration was required. Only a single bed operated at a time, the dual beds allowing the removal of oxygen even when the regeneration of one bed was necessary. Regeneration of the beds was performed by passing a gas stream containing 5% hydrogen and 95% helium through the beds. The oxygen was reduced to water by the hydrogen, while the water was removed when the temperature of the bed was increased by the hydrogen–oxygen reaction.

Nitrogen removal was performed by a Nitrain model Ni–20 single bed inert gas purifier. Ten pounds of titanium sponge operating at 1200 K removed the nitrogen on a batch basis. The bed required regeneration approximately every three months and was performed by increasing the temperature to 1500 K. For the time the bed was regenerating, no nitrogen removal occurred.

The inert gas within the glove box was grade A helium with a purity of 99.999%. This gas was continuously circulated through the purifiers by electric blowers. Because of small leaks in the box and the removal of gas lost by use of the transfer chamber, gas was constantly needed to replenish the supply in the box. The average residence time of gas in the box was about two weeks when work was being performed regularly.

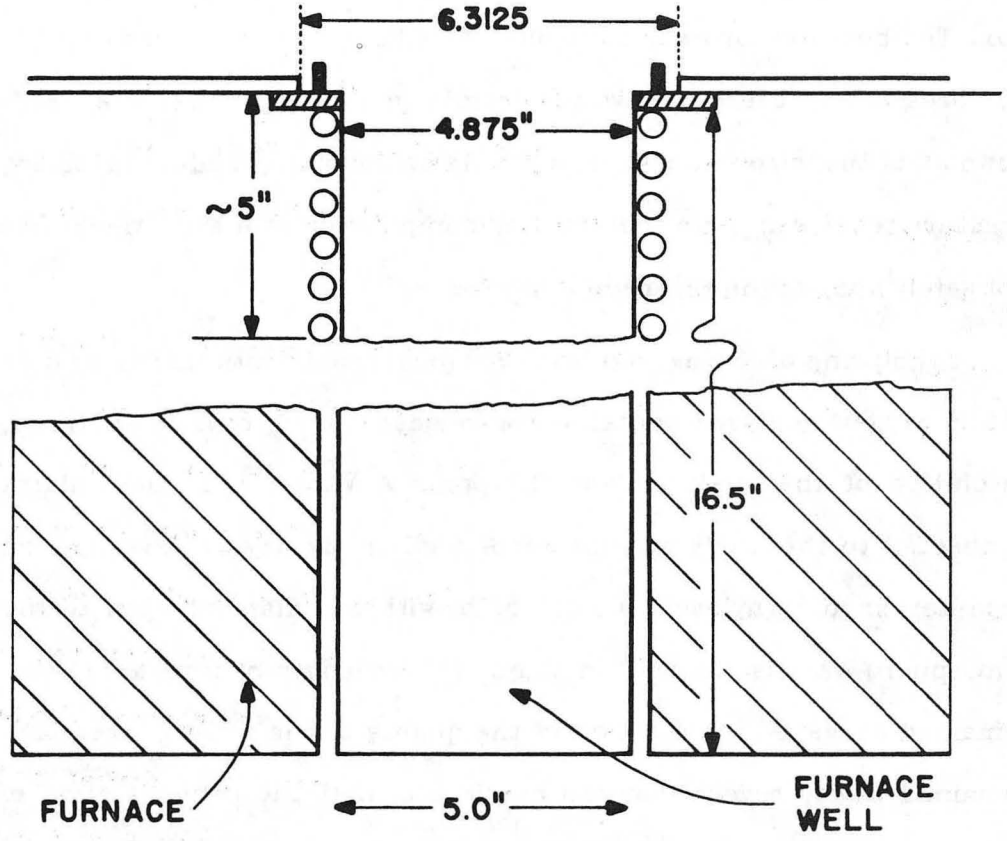

Figure 5–6 Diagram of furnace well.

The pressure of the inert gases in the box was kept at a pressure of two inches of water higher than the external, ambient pressure. This hindered the leakage of unwanted gases from the ambient atmosphere into the glove box. The box pressure was controlled by a Safe–Troll pressure regulator. If the pressure in the box deviated from a given range, the Safe–Troll shut down all of the circulation and purifying equipment. In addition, emergency pressure relief was performed by a silicon oil bubbler if the Safe–Troll could not safely control the variation in pressure.

Monotoring of the oxygen level was performed continuously by a VAC AO 316 H oxygen analyzer containing a Teledyne trace oxygen analyzer. The resolution of the analyzer was 0.1 ppm. A VAC A A–1 audio alarm was connected to the analyzer and warned when the oxygen level exceeded a predetermined high level. A light bulb, with the filament open to the box atmosphere was also located in the box. The length of time which the bulb remained lit, gave an indication of the quality of the atmosphere. The bulb remained lit for several months confirming that the concentration of the atmosphere was below the 0.1 ppm level of oxygen. Nitrogen and water monotoring was provided by batch mass spectroscopic analysis. This service was provided by on–site technicians. This was performed typically every three months.

The furnace well in the box were surrounded by Applied Test Systems, Split Type, #2961 furnaces. These operated on 230 VAC and contained three separate heating zones. Controlling the temperature of the furnaces were Panel Packer model number 61010 controllers manufactured by Research Incorporated. With these controllers, the furnaces could be operated in a direct mode or in a feedback loop where thermocouples located within the

furnaces monitored the temperature. In the direct mode, the heating rate to the furnaces was controlled while in the feedback mode the controllers maintained the temperature at a preselected value. The accuracy of the controllers was plus or minus 5 K from the specified set point with less than a 1 K variation during operation. To keep the inside of the glove box at a comfortable working temperature, a VAC Dri Kool DK 3E refrigeration unit was installed. The inside temperature of the box remained at 303 K plus or minus 5 K throughout all experiments.

5.3.2.3. Electronic Equipment

Equipment used to measure the potential difference between the two reference electrodes consisted of four different pieces of apparatus. These were two buffer amplifiers, a digital voltmeter, a printer, and a power supply. The electronic components and the interconnecting wiring are shown schematically in Figure 5–7. A photograph of this equipment is given in Figure 5–8.

Two Floyd Bell BA–1 buffer amplifiers connected in differential mode monitored the potential difference from the two molybdenum reference electrodes. The input impedance was greater than 10^{12} ohms, and the drift on the amplifiers was stated by the manufacturer not to exceed plus or minus 5 μV/month. The amplifiers each had their own separate internal battery–operated power so connection to an external AC source was not necessary. To prevent ground loops and to reduce noise, the inputs to the amplifiers were guarded by applying a potential in the shield equal to the potential being measured. The output from the amplifiers was connected to a Keithly 173A digital voltmeter. This digital voltmeter contained a digital interface which was connected to Keithly 750 printer. The readout from the

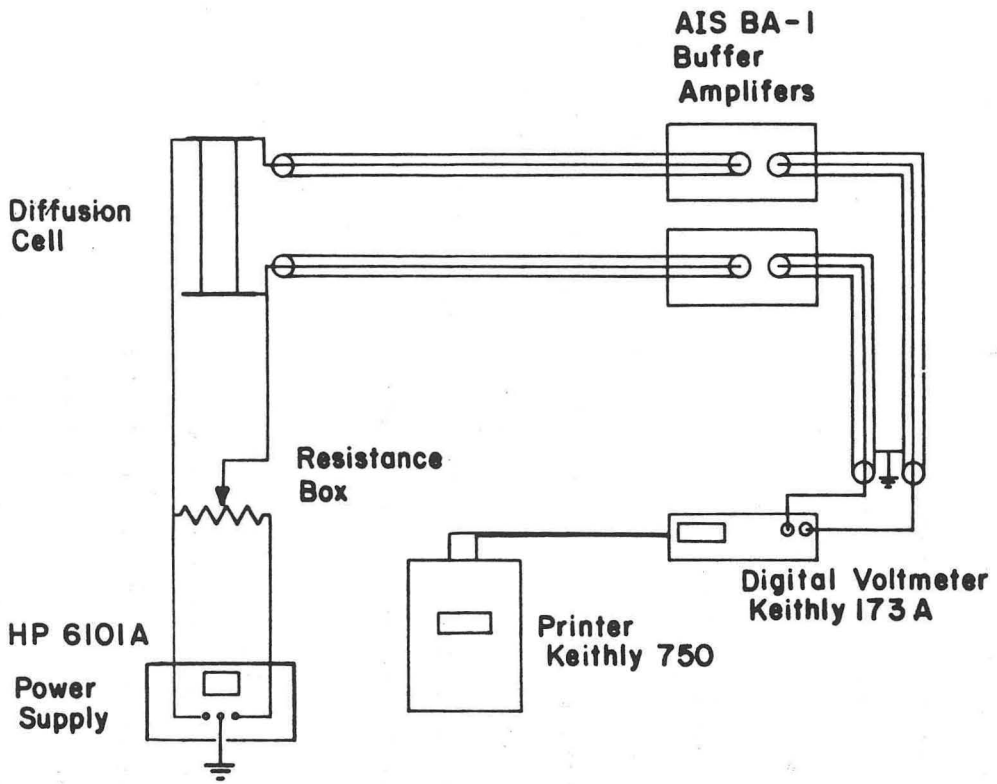

Figure 5–7 Wiring diagram showing electronic equipment.

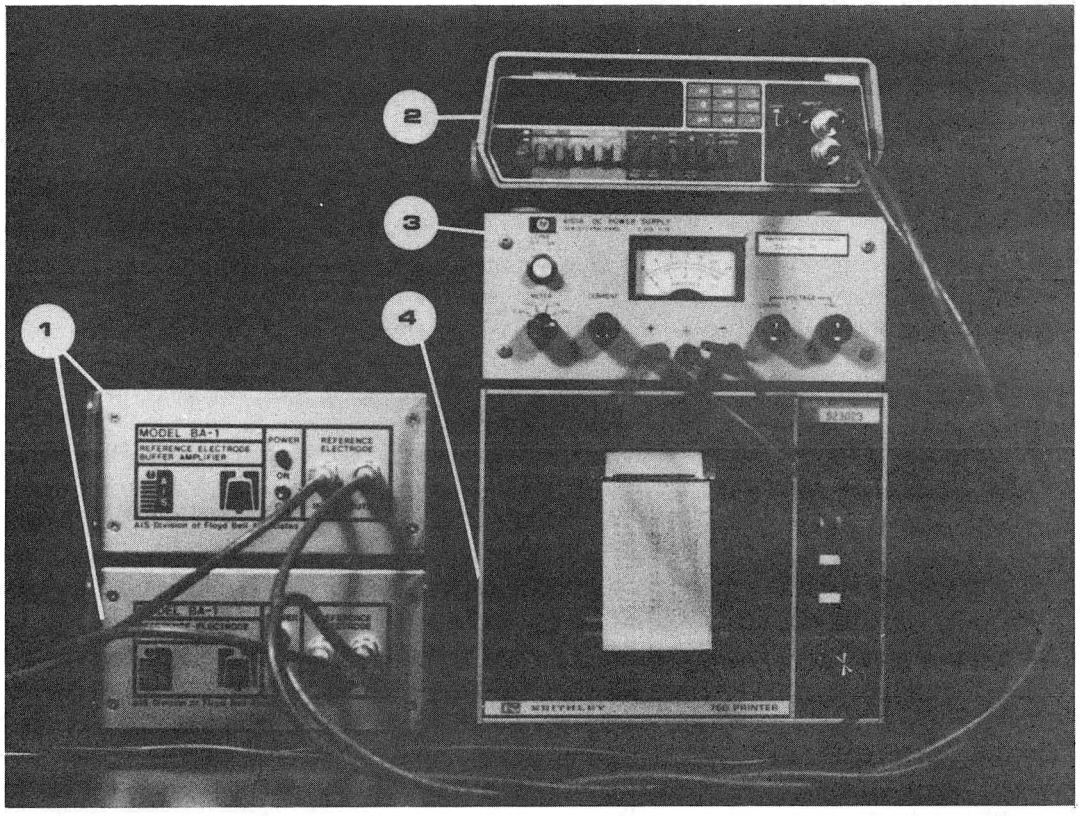

XBB 839-8331A

Figure 5-8 Photograph of electronic hardware showing: (1) buffer amplifiers, (2) digital voltmeter, (3) power supply, and (4) printer.

voltmeter, four and half digits of precision, could be recorded by the printer on a paper tape. The printing interval could be varied from less than every second to more than a week.

During the runs, the buffer amplifiers were placed inside the glove box in close proximity to the furnace well. Coaxial cable connected the buffer amplifiers to a junction box above the diffusion cell, external to the furnace well. Single conductor, high temperature Rockbestos–Micatemp® wire, obtained from the Cereske Electric Cable Company, connected the reference electrodes in the well to the junction box. This wire was rated to withstand temperatures in excess of 900 K. Coaxial cable also connected the buffer amplifiers to the voltmeter, which was located outside of the glove box.

A Hewlett–Packard 6101 A power supply was used when current was to be passed through the cell. Either the potential or current output of the supply could be adjusted to within less than one percent. Drift on the power supply averaged about 1 percent every three hours.

5.3.3. Chemicals

Sodium sulfide was purchased from the Noah Chemical Division of the Noah Industrial Corporation.* The rated purity was 99.99% as guaranteed by the manufacturer. A lot analysis performed by the manufacturer listed the levels of impurities shown in Table 3–1. The sodium sulfide was supplied ground to a uniform particle size of 100 mesh. Throughout the experiments, the unused sodium sulfide was stored inside two airtight jars inside the glove box.

---

*Noah Chemical Division, Noah Industrial Corporation, 87 Gazza Boulevard, Farmingdale, NY 11735

Table 3–1 Lot analysis for sodium sulfide, lot number 22719.

Element	Maximum Level Present, Percent
Ca	0.01
Cd	0.001
Fe	0.0002
K	0.01
Mg	0.0001
Mn	0.0001
Ni	0.0001

High grade purity sulfur was obtained from the Electronic Space Products Corporation.† The sulfur was guaranteed 99.999% pure. No lot analysis was available. Like the sodium sulfide, it too was stored in two airtight sealed jars.

Reagent grade sodium metal (lump) was obtained from the J. T. Baker Company.‡ A lot analysis performed by this company indicated levels of contamination shown in Table 3–2. The sodium metal was stored in a metal can which was suplied by the company. A slight oxidized film was present on the sodium during periods of nonuse.

5.3.4. Experimental Procedure

5.3.4.1. Preparation of Sodium Polysulfides

Sodium polysulfides were prepared by the procedure suggested by Rosén and Tegman[13] using sodium sulfide and sulfur. Briefly, stoichiometric

†Electronic Space Products Incorporated, 854 So. Robertson Blvd., Los Angeles, CA 90035.
‡J. T. Baker Chemical Company, Phillipsburg NJ 08865

Table 3–2 Lot analysis for sodium metal, lot number 14332.

Element	Maximum Level Present, Percent
Chloride	< 0.002
Nitrogen	< 0.002
Sulfate	
Iron	
Trace impurities in (ppm)	
Phosphates	< 3
Heavy Metals	< 5

amounts of sodium sulfide and sulfur were weighed on a Satorius Digital Balance to within 0.001 g. These were then placed in an open glass tube and placed inside a sealed stainless steel reservoir. The polysulfide was then formed by subjecting it to a series of heat treatments. First, the polysulfide was heated to 523 K for about 5 hours. The temperature was then increased to about 50 K above the melting point of the polysulfide and held for one hour. Finally, the temperature was reduced and returned to 523 K for another ten hours. When allowed to cool, solid of a uniform color was produced. The resulting polysulfide was then ground to a uniform powder in a small mortar with a pestle and placed in glass jars. Only about one gram of polysulfide was produced at one time.

5.3.4.2. Measurement of Diffusion Coefficients

The procedure for measuring the diffusion coefficient involved a number of complex steps. First, each end of the glass diffusion cell was coated with the high temperature vacuum grease. The cell was placed on

the bottom molybdenum electrode, and then the upper electrode was pressed down upon the upper face of the glass cell. The hole in the upper electrode was aligned with the hole in the glass cell. The hex screws were then tightened just enough to keep the cell securely pressed between the two electrodes. Even though the cell was pressed between the electrodes, the upper electrode was still free to slide when the external cable was pulled.

Next, a measured amount of the ground polysulfide powder was placed in the fill reservoir with the hypodermic needle screwed on the bottom. The long steel fill tube was then screwed onto the reservoir. The fill reservoir was then clamped above the upper electrode, with the needle extending down into the cell.

The clamped cell and reservoir were then placed in the furnace well with the flexible cable and the fill tube extending out of the well. Several convection shields, which were aluminum plates the same diameter as the furnace well were placed above the well at equally spaced intervals to reduce variations in temperature through the well.

The temperature in the furnace well was then increased to a point above the melting point of the polysulfide. After the temperature had increased, the hex screws were tightened further. The coefficient of thermal expansion of the glass and the aluminum were sufficiently different that two sequences were required. When the polysulfides in the reservoir had melted, pressure from a hypodermic syringe was applied to the fill tube protruding from the furnace well. This forced the polysulfides into the diffusion cell. The resistance between the two reference electrodes was monitored using an ohmmeter while the cell was being filled. When the resistance decreased

from the initially infinite value, the cell was filled with polysulfides. When all of the polysulfides filled the cell, the fill tube was removed, and the upper reference electrode was moved via the flexible cable. The cell then was completely closed and ready for the diffusion coefficient determination.

The initially required concentration gradient could be generated in one of two ways. First, the power supply could be used to generate electrochemically an excess concentration of polysulfide at one electrode, depleting the concentration at the other. A more direct way, if the first technique failed, was to fill the diffusion cell with polysulfide of two compositions. This technique was used in the original study performed by Newman and Chapman and in later work by Nisancioglu and Newman.[64]

5.3.5. Results

The results from the experiments were very disappointing, however. Several attempts were made to fill the cell, but it was not possible to form a leakproof seal between the reference electrodes and the glass cell. Electrical contact could only be established for a very short period, about five minutes. Post experiment examination revealed that the polysulfide could leak out of the cell through the small space between the glass and the metal. Also, contrary to the manufacturers specification, the vacuum grease did not seem to be stable at the temperature of 623 K at which the experiments were performed. Unfortunately, there was not enough time to continue the experiments further.

5.3.6. Future Work

At the present time, there are a number of unsolved problems which must be overcome before diffusion coefficients can be obtained. Primarily, the leakage in the cell must be stopped. The problems of glass–metal joints

which must remain leak free at 633 K are severe. In the experiments described above, vacuum grease was used as sealant. As described, this proved to be highly ineffective. The degradation of this material at the high temperatures cannot be avoided.

There are, however, a number of alternatives which might be tried. Other suggested materials are colloidal graphite and ceramic glues. Colloidal graphite is a very fine suspension of graphite particles. Since carbon has shown to be invulnerable to attack by molten polysulfides, this material might prove to a stable sealant. The small particles with a large surface area, though, would present a high surface area for reaction. Although, carbon is stable, the high surface area might be enough for a degradation reaction to occur to an appreciable extent.

Ceramic glues also can be suggested as sealants. These would be permanent, but this could be an advantage. Some require curing at high temperatures, but this should present no problem. The cell could be assembled cold and then heated to the curing temperature. Immediately after that, the experiments could be performed. Hopefully, the ceramic glues will be stable to the polysulfide.

Other significant problems which should be addressed are the mechanical stability of the apparatus, thermal convection within the cell, and noise that might be present in the potential measurement. The mechanical stability of the apparatus is paramount. The cell must remain vibration–free during the experiment. This is mentioned only because small vibrations of the furnace well were discovered. The source of these was found to be the gas purification equipment. These vibrations would cause problems later, if the experiments were to be continued.

Thermal convection within the cell and electrical noise do not seem to be insurmountable problems. The temperature variation in the furnace well was typically less than 1 K. The high viscosity of the melt, the small dimension of the cell, and small variation in temperature make thermal convection a problem which will probably not require attention. The small potential difference between the two electrodes might be more serious. The buffer amplifiers seemed to drift slightly with time. This problem could be overcome by zeroing the potential before each measurement. The convenience of automatic data collection with the present equipment would be lost, however.

5.4. Summary

In this chapter, the results of experiments to measure the diffusion coefficient of sodium polysulfide melts have been described. A number of unsolved problems exist which must be solved before results can be obtained. These are discussed and some possible solutions are suggested.

Chapter 6

Conclusions

We have investigated the transport properties for sodium polysulfide melts using two different transport models. A binary, macroscopic model has been formulated which defines the transport properties for a melt considering sodium cations and monosulfide anions in a neutral sulfur solvent. A more sophisticated and refined model considers the melt to be composed of several neutral polysulfide compounds. In both models, local equilibrium has been assumed to exist at all points.

For the three components defined in the binary model, three independent transport parameters define the processes occurring in the melt. These three transport parameters cannot be directly measured, but have been transformed into three measurable transport properties by inversion of the transport equations. The conductivity, transference number for sodium ions relative to sulfur solvent, and diffusion coefficient are the properties which have been defined. The values for each of these properties have been shown to be accessible from well defined experiments which have been described in detail.

From the three independent transport properties, the values for the three fundamental transport parameters have been calculated. Conductivity data was taken from the experiments of Cleaver and Davies[14] while transference numbers were calculated from open circuit potential measurements from Cleaver and Davies.[16] Values for diffusion coefficients were estimated. The resulting transport parameters were found to possess unpredictable behavior caused by the macroscopic assumptions of the

model

We then developed a more sophisticated model for the transport processes. This microscopic model was developed the interactions between sodium cations and polysulfide anions. For a melt composed of seven polysulfide anions and sodium cations, 28 fundamental transport parameters were defined and then related to equal number of microscopic transport properties. Because the transport of microscopic species could not be measured, it was necessary to transform the parameters appearing in the microscopic model to measurable melt properties. The conductivity, the transference number, and the diffusion coefficient in the binary model were chosen for this purpose. These three properties were defined in terms of the independent microscopic parameters and the concentrations of the individual microscopic ionic species.

The melt model of Tegman[17] was then used to predict the microscopic melt composition, open circuit potentials, and the thermodynamic activity coefficient factor. An empirical relationship for the 28 fundamental transport parameters was developed relating all of the 28 parameters to two new parameters. These were assumed to be dependent on temperature, but independent of the melt composition. The three measurable macroscopic transport properties were calculated for a set of values of the two parameters which were independent of melt composition. The melt conductivity and transference were predicted for the two temperatures of 573.15 and 633.15 K. Values of the diffusion coefficient were calculated and shown to lie within the ranges of conflicting experimental data.

A new technique to measure the diffusion coefficients in polysulfide melts has been described and some unsuccessful results were reported. The

method of restricted diffusion modified for opaque high temperature electrolytes has been investigated. Problems with the experiments were reported and suggestions for improvement have been given.

List of Symbols for Chapters One through Six

English Characters

a	height of diffusion cell, cm
a_i	activity of species i
A	constant defined by Equation (E–20)
A_n	constants defined by Equation (5–5)
B	constant defined by Equation (E–22)
c	concentration of electrolyte, mole/cm^3
c_i	concentration of species i, mole/cm^3
c_T	total solution concentration, mole/cm^3
C_p	heat capacity at constant pressure, J/mol–K
D	measured diffusion coefficient of electrolyte, cm^2/s
$\mathscr{D}$	diffusion coefficient of the electrolye, for a thermodynamic driving force, cm^2/s
$\mathscr{D}_{ij}$	diffusion coefficient for interaction of species i and j, cm^2/s
D	constant defined in Equation (3–47), gm/cm^3
E	constant defined in Equation (3–47), gm/cm^3-K
F	Faraday constant, 96,485 coulombs/equiv
H	enthalpy per mole, J/mol
G	free energy per mole, J/mol
i	current density, A/cm^2
k	Boltzmann constant, 1.3807 x 10^{-23} J/K
K_i	equilibrium constant for reaction i, atm$^{-(i-1)/2}$
K_{ij}	friction coefficient for interaction of species i and j, J–s/cm^5

L_{ij}^{N}	inverted transport coefficient with species N as the reference, $cm^5/J-s$
m	molality of electrolyte, mol/kg
M_i	molecular weight of species i, g/mol
M_e	molecular weight of electrolyte, g/mol
M_{ij}	modified friction coefficient, $J-s/cm^5$
n	number of electrons in reaction
n_i	particle fraction of species i
N	number of species present in solution
N_A	Avagadro's number, 6.023×10^{23} $(gm-mol)^{-1}$
$\mathbf{N}_i$	flux of species i, $mole/cm^2-s$
p	total pressure, atm
p	exponent defined in Equation (4–44)
p_i	partial pressure of component i, atm
q	exponent defined in Equations (4–45) and (4–46)
r_i	ionic radius, cm
R	universal gas constant, 8.314 J/mol–K
R_i	rate of homogeneous production of species i, mol/cm^3-s
s_i	stoichiometric coefficient species i in electrode reaction
S	entropy per mole, J/mol–K
t	time, sec
t_i^0	transference number of species i with respect to the solvent velocity
t_i^N	transference number of species i with respect to the velocity of species N
T	absolute temperature, K
U	equilibrium cell potential, V
$\mathbf{v}$	mass–averaged velocity, cm/s

$\mathbf{v}_i$	velocity of species i, cm/s
$\overline{V}_i$	molar volume of species i, cm^3/mol
x_e	mole fraction of electrolyte, $c_e/(c_e+c_o)$
x_i	mole fraction of component i
y	composition of sodium sulfide in Na_2S_y
z	charge number, equiv/mol

Greek Characters

α_1	constant defined in Equation (3–30) describing the open circuit cell potential of cell 1, V
α_2	constant defined in Equation (3–31) describing the open circuit cell potential of cell 2, V
β_1	constant defined in Equation (3–30) describing the open circuit cell potential of cell 1, V
β_2	constant defined in Equation (3–31) describing the open circuit cell potential of cell 2, V
ΔC_p^o	difference in standard state heat capacities for a reaction, J/mol–K
ΔG_i	change in free energy for reaction i, J/mol
ΔG_f^o	free energy of formation at the standard state, J/mol
ΔH_i	change in enthalpy for reaction i, J/mol
ΔH_f^o	enthalpy of formation at the the standard state, J/mol
ε_1	parameter defined in Equation (4–45), g cm^4/s
ε_2	parameter defined in Equation (4–46), g cm^4/s
γ_{+-}	mean molal activity coefficient of an electrolyte
κ	conductivity of fluid phase in bed, $(\Omega\text{–cm})^{-1}$
μ	dynamic viscosity, cp
μ_e	chemical potential of electrolyte, J/mol
μ_i	chemical potential of species i, J/mol

ν kinematic viscosity of fluid, cm^2/s

ν number of moles of ions into which a mole of electrolyte dissociates

ν_+, ν_- numbers of cations and anions into which a molecule of electrolyte dissociates

ρ density, g/cm^3

Φ electric potential, V

ω_i mass fraction of species i

ω_e mass fraction of electrolyte

Subscripts

a denoting the compound Na_2S_a

b denoting the compound Na_2S_b

i species number i

j species number j

k species number k

N species number N, Na^+ ions

o species o, neutral sulfur

Superscripts

o at the standard state

$*$ at the ideal gas state

Chapter 7

A Theoretical Comparison of Flow–Through and Flow–By Porous Electrodes at the Limiting Current; Introduction

Packed–bed porous electrodes have become increasingly attractive in the past several years for use in a number of industrially important processes. These electrodes have been suggested for such diverse applications as the removal of metal ions from dilute waste streams,[66] electro–organic synthesis,[67] and off–peak energy storage.[68]

Characteristic of all porous electrodes are the non–uniform distributions of potential and concentration throughout the electrode. Because of the coupled transport limitations and the non–uniform reaction rates within the electrode, changes in the concentrations of reacting species and the potential occur with time and position.

Even though the construction of a porous electrode may be irregular and the exact geometry of the pores unknown, continuous properties characteristic of the electrode can still be defined. These properties are obtained by averaging quantities over volume elements small compared to the length scale of the bulk variations but large with respect to the individual pore sizes. Since at least two phases are present, it is possible for the averaging process to be performed upon the same quantity, but within each phase. The resulting properties can then be assumed to be continuous in time and space and used within fundamental governing equations to predict the behavior of these electrodes.

The non-uniform distribution of properties within a porous electrode is illustrated in Figure 7–1. Here the variation of one averaged property, the potential, in two phases is shown. In this example, the potential varies in a monotonic and continuous manner in both phases, although for the matrix phase the variation is much smaller and the potential appears to be nearly constant. The variations of other properties also can be envisioned and plotted in the same way as in Figure 7–1. Examples might the be the concentration of reacting species, the current density, the reaction rate, and the electrode porosity, among others.

The maximum variation in solution phase potential is a quantity of great interest to the designer of porous electrodes. This quantity is denoted by the symbol $\Delta\Phi_2$ on Figure 7–1 and is the difference between the highest and lowest solution potentials within the electrode. For porous electrodes, it may be desirable to operate the reactor under conditions for which unwanted side reactions are minimized. To do so requires that the largest potential difference between the solution and matrix phases must be low enough so that side reactions do not occur to an appreciable extent. At the same time to insure a high processing rate, the lowest matrix-solution potential difference within the electrode must be sufficiently high to insure a limiting–current condition.

The maximum allowable variation in potential can be assessed experimentally from a limiting–current curve obtained from a rotating disk or other suitable electrode. Figure 7–2 illustrates limiting–current data obtained by Selman[69] from a rotating disk for the copper sulfate–sulfuric acid system. Point b on Figure 7–2 lies at the threshold of the limiting–current region, at potentials slightly lower than the end of the

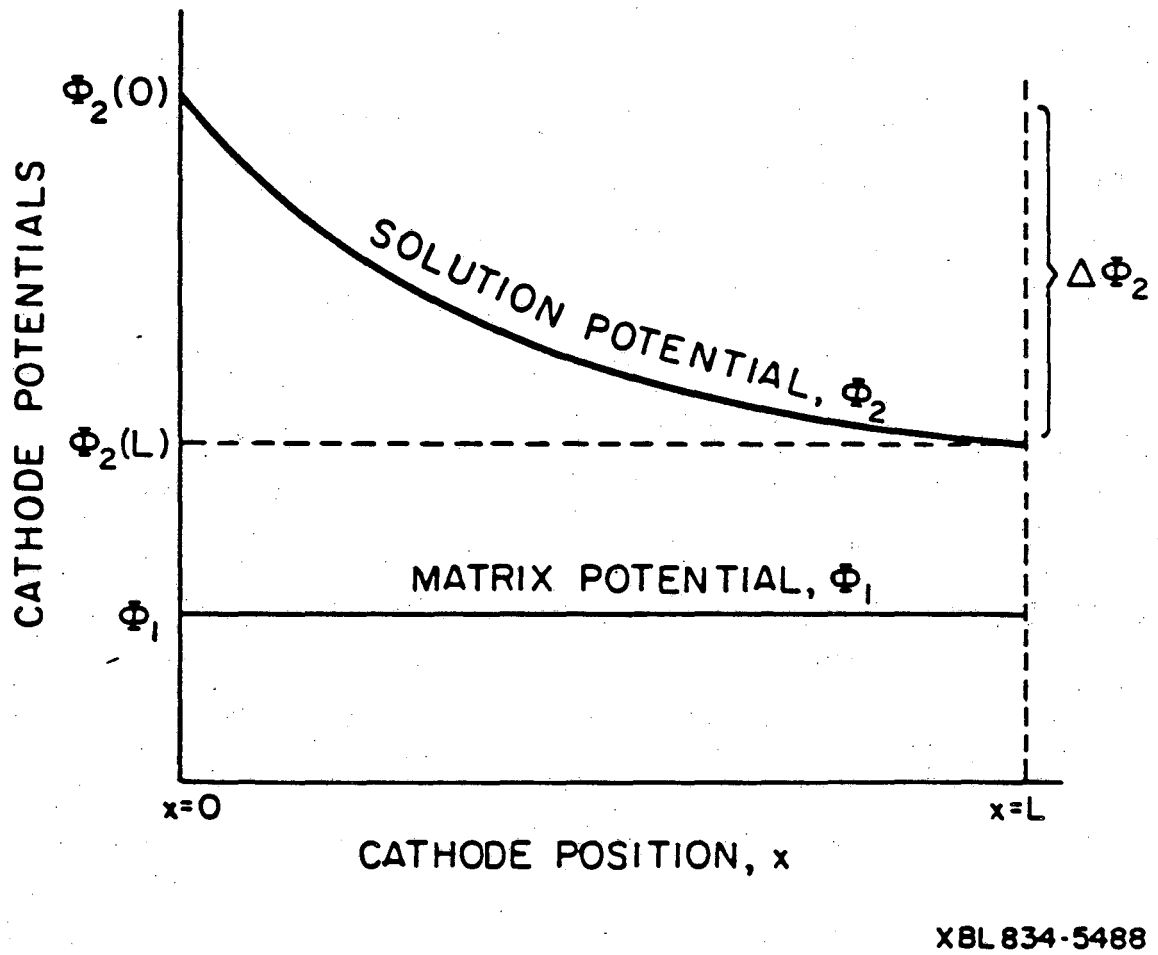

Figure 7-1. Solution-phase and matrix-phase potentials, as functions of position through a porous electrode.

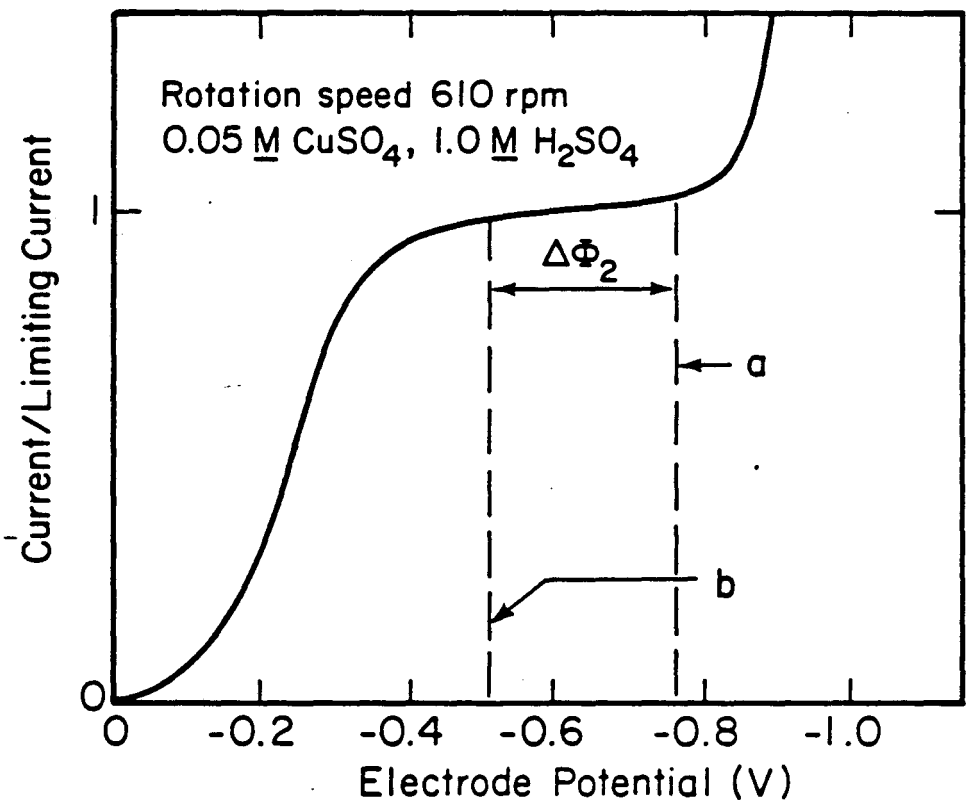

Figure 7–2. Current versus potential for the copper sulfate–sulfuric acid system obtained from a rotating disk electrode. The curve is reproduced from Selman.[69]

well–defined kinetic region. At the other end of the limiting–current region, point a lies just above the upturn in the current potential curve. Point a marks the onset of the side reaction region. To avoid operating in the kinetic or the side reaction region, the potential within the electrode must be held within the bounds given by points a and b. The difference in potential between these two points is the same potential difference which can be tolerated in the porous electrode. Using this figure as an example, the maximum potential difference which can be tolerated in an electrode can be seen to be approximately 0.2 V.

The maximum potential drop through a porous electrode is influenced by the transport of reactants and products through the electrode as well as the finite rates of the chemical or electrochemical reactions. The type of reactants, the physical properties of the solution, and the properties of the solid phase all affect the magnitude of the ohmic potential drop. Different potential drops would be observed if a one is processing a solution containing a high concentration of an excess supporting electrolyte, such as sulfuric acid, versus the same solution without the acid. Design constraints also affect the potential drop through the solution and must be considered in the design. For example, if the specified conversion of a reactant is changed, so will the ohmic potential drop, all other factors remaining the same. The potential drop through the electrode can also be influenced by more directly controllable variables. These operating variables may include such quantities as the flowrate of the reactant stream or perhaps the reactant concentration. The essence of this thesis thus deals with predicting the maximum potential drop for different physical properties, design constraints, and operating variables. The results will be useful to a designer. He will then be able to produce a porous electrode that will satisfy

the requirement of a given maximum ohmic potential drop and at the same time perform the required operations.

Porous electrodes may have stagnant fluids, as in lead acid battery plates or may involve flowing electrolytes. Redox energy storage cells are examples of this second kind. This thesis, however, deals only with the latter type. Two principal configurations for these porous flow electrodes have been developed: the flow–through configuration, where fluid flow and current are parallel; and the flow–by configuration, where the fluid flows perpendicularly to the current. Both configurations are illustrated in Figure 7–3; where the porous electrodes are represented by rectangles and the separators by dashed lines. For simplicity we choose to represent the counterelectrodes as planar electrodes; however, in general, the counterelectrodes can also be porous electrodes. The y direction in the figure denotes the direction of fluid flow.

Figure 7–3 a illustrates a flow–through electrode with an upstream counterelectrode. An upstream counterelectrode is favored over a downstream counterelectrode in the flow–through configuration, because it gives a lower ohmic potential drop, particularly at high conversions.[70] The variable L represents the length of the electrode in the y direction. For the flow–through configuration, the flow is divided as it enters and flows in different directions through the working electrode and counterelectrode. Both current and fluid flow parallel, along the y direction. The current, however, may flow in the same direction as the fluid flow or in the opposite direction, depending upon whether the porous electrode is an anode or cathode. Figure 7–3 a illustrates a porous electrode being operated as a cathode. In any case, the distinguishing feature of this configuration is the

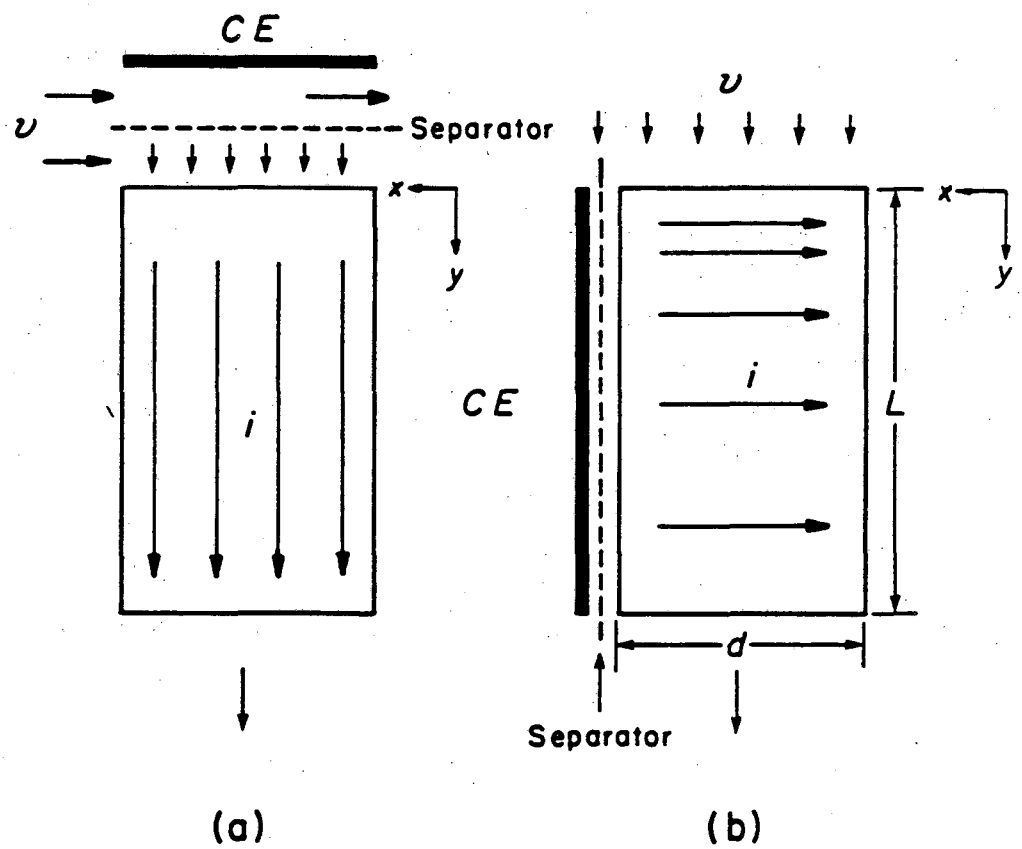

Figure 7–3. Porous electrode configurations, a) flow–through electrode, upstream counterelectrode, b) flow–by electrode.

parallel flow of fluid and current.

Figure 7–3 b illustrates a flow–by configuration. Again, we have designated the length of the electrode by the variable L. For this configuration the fluid flow is again divided, but here the flow to the working electrode and counterelectrode remains in the same direction. In this configuration, current generated within the porous electrode travels generally in the x direction, which is perpendicular to the direction of the fluid flow. Because the current and fluid flow are perpendicular, the width of the electrode is also important. Here, the variable d denotes the width of the electrode in the direction of current flow.

Bennion and Newman[66] developed a one–dimensional model for the flow–through electrode assuming its performance to be limited only by the transport of reactants from the bulk stream to the surface of the electrode. This limiting–current assumption considerably simplifies the analysis of porous electrodes. The limitations of the heterogeneous reaction occurring at the solution-matrix interface are ignored in this approximation. The limiting–current assumption implies a zero surface concentration of the reacting species at the matrix-solution interface. Consequently the concentration overpotential within the solution tends toward infinity. The actual operating cell potential therefore cannot be established from a limiting–current analysis.

One is not prevented from developing other more sophisticated models to describe the operation of porous flow electrodes. More realistic one–dimensional models for the flow–through electrode not restricted to the limiting–current assumption have subsequently been developed.[70,72] These models incorporate equilibrium constraints, kinetic limitations, and

parasitic side reactions in addition to the transport of reactants. However, because of the large number of parameters needed for such a model to describe the phenomena and the necessity for computer solution, the limiting–current assumption remains attractive. One may be content to sacrifice some predictive accuracy for simplicity in analysis. Hence, models employing the limiting–current assumption still find recent applications.[73,74]

Because the fluid and current travel in the same direction in the flow–through configuration, the analysis remains one–dimensional even in the general case. In the flow–by configuration, however, the general analysis is necessarily two–dimensional. The absence of a common space variable for the fluid and current flow requires that the analysis be formulated in terms of partial differential equations unless simplifications are made.

Alkire and Ng[75,76] simplified the analysis of the flow–by electrode by assuming current flow to travel directly perpendicular to the fluid flow. This assumption reduces the equation for the potential distribution from a partial differential equation to an ordinary differential equation. Recently, Fedkiw[73] has analyzed the special case of a flow–by electrode at the limiting current by including the two–dimensional nature of the current distribution and the effects of the finite electrode length. However, his analysis was specific, using only a single mass transfer correlation. He included only a single dependence of the mass–transfer coefficient on velocity.

Alkire and Ng,[75,76] Trainham and Newman,[68] and Fedkiw[73] have all considered the selection of the optimum electrode configuration for a given application. Trainham and Newman developed a method, applicable below the limiting current, to select the optimum configuration. They optimized

the design of a flow-through or flow-by electrode for the case where operating costs were dominated by the cost of electrical energy associated with the electrochemical reaction. Pumping costs were not included in their optimization. This assumption applies to systems processing feeds with high reactant concentrations, such as the redox flow energy storage system which they examined. Capital costs, included in their study, consisted of costs only for the electrochemical reactor. Costs for reactant storage such as external tanks and piping were excluded. Their reactor cost was subdivided into two categories: the cost for the bed material and the cost for the separator. From their optimization, Trainham and Newman were able to determine the optimum reactor configuration, dimensions, and feed flowrate which minimized the weighted sum of operating and capital costs. The flow-by configuration was found to be the most economical configuration under these conditions.

Alkire and Ng,[76] followed by Fedkiw,[73] considered the choice of the optimum configuration at the limiting current. Alkire and Ng maximized the volumetric current density to compare the two configurations. Fedkiw compared the maximum solution–phase potential drop for the flow–through configuration to the maximum solution–phase potential drop for the flow–by electrode. Equal electrode volumes and identical flow velocities were chosen as fixed quantities for these two comparisons. It will be shown in Chapter Nine that at the limiting current, the maximization of the volumetric current density or the minimization of the maximum ohmic potential drop lead to the same result.

In this thesis, we propose a limiting–form solution to the two–dimensional potential distribution. This solution shows that the

maximum solution–phase potential drop for the flow–by electrode is primarily dependent upon a dimensionless electrode width variable with only a secondary dependence upon the ratio of the electrode length to width. We then reexamine potential distribution derived by Fedkiw to determine the conditions under which the two–dimensional nature of the current distribution and the effects of the finite electrode should be included. This new solution, along with the expressions derived by Fedkiw and Alkire and Ng, is presented in a form that is not restricted to the single mass–transfer correlation presented by Fedkiw.

Using the potential distribution derived here, we then compare the flow-through and flow-by configurations using the maximum potential difference. These results are then compared to the results presented by Fedkiw.

The relevant design equations for flow–by porous electrodes operated at the limiting current are derived. Based on these design equations, the behavior of design variables is examined in relation to the cost–optimum design of a flow–by electrode at the limiting current. For dilute solutions of reactants, the optimal electrode configuration is predicted by minimizing the total cost of each configuration. Finally, the criteria giving the optimum electrode configuration for a specific application are examined and compared to the results of Alkire and Ng, Fedkiw, and Trainham and Newman.

Chapter 8

Potential Distribution

The starting point for the analysis will be the theoretical framework for porous electrodes developed by Bennion and Newman[66] and extended by Newman and Tiedemann.[77] The porous electrode is treated as a superposition of two continua, representing the fluid phase and the solid phase. The coordinate system and dimensions for the electrodes are given Figure 7–3. A single reaction of the form

$$\sum_i s_i M_i^{z_i} \rightarrow ne^- \tag{8–1}$$

will be assumed to occur within the electrode. Under these assumptions, the electrode reaction appears as a homogeneous source or sink term within the conservation of species equation. A solution with excess supporting electrolyte and a uniform solution conductivity will be assumed as well as a dilute solution of reacting species. Diffusion and dispersion will be neglected. Also, the velocity within the electrode is assumed to be plug–flow, one–dimensional in the y direction only. Under these conditions, at steady state, conservation of the reactant species for both the flow–through and flow–by electrode can be expressed as

$$v \frac{dc}{dy} = - ak_m c \ , \tag{8–2}$$

with the boundary condition

$$at \ y = 0, \ c = c_F \ . \tag{8–3}$$

Solution of Equation (8–2) subject the boundary condition of Equation (8–3) yields

$$c = c_F\, e^{-\alpha y}\,, \tag{8–4}$$

where

$$\alpha = \frac{ak_m}{v}\,. \tag{8–5}$$

The reciprocal of the parameter α can be thought of as a penetration length. The penetration length defines the distance where the reactant is depleted to 1/e of its inlet composition, or, as an order of magnitude, the length of the region where most of the reaction occurs within the electrode.

At the end of the bed ($y = L$), the concentration of the flowing stream will have reacted to the largest extent. Here the concentration of the reactant will be denoted as c_L. Equation (8–4) then gives at the end of the bed

$$c_L = c_F\, e^{-\alpha L}\,. \tag{8–6}$$

This may be rearranged for αL in terms of the inlet and outlet concentrations as

$$\alpha L = \ln \frac{c_F}{c_L}\,. \tag{8–7}$$

Equation (8–7) shows that the parameter αL specifies the natural logarithm of the conversion, or the ratio of the feed reactant concentration to the feed outlet concentration.

Now that the concentration distribution has been established, the solution to the potential distribution may proceed. For a uniform conductivity and negligible diffusion potential, Ohm's law governs the potential distribution within the fluid phase

$$i_2 = -\kappa \nabla \Phi_2\,. \tag{8–8}$$

Faraday's law relates the transfer current to the local rate of mass transfer within the electrode

$$j = \frac{nFak_m c}{s_R} . \qquad (8-9)$$

One must also employ the relationship

$$\nabla \cdot i_2 = j \qquad (8-10)$$

which defines the transfer current as the divergence of the total current. Substituting the concentration distribution obtained in Equation (8–4) into Equation (8–9) and using Equations (8–8) and (8–10), we obtain

$$\nabla^2 \Phi_2 = - \frac{nFak_m c_F}{s_R \kappa} e^{-ay} . \qquad (8-11)$$

In contrast to the solution for the concentration distribution, the solution to the potential distribution depends upon the electrode configuration.

Bennion and Newman[68] solved Equation (8–11) for a one–dimensional flow–through electrode. Alkire and Ng[75] solved this equation for the flow–by electrode assuming potential variation only in the direction perpendicular to fluid flow. This assumption reduces Equation (8–11) from a partial differential equation to an ordinary differential equation. Fedkiw[73] solved Equation (8–11) for two–dimensional current flow in a flow–by electrode of finite length.

Here, we propose to examine the limiting case of a flow–by electrode with an infinite aspect ratio. Thus our case will reflect the condition

$$R = \frac{L}{d} \to \infty . \qquad (8-12)$$

To solve Equation (8–11), one must specify an appropriate number of boundary conditions. For the semi–infinite rectangle, four such conditions are required. These conditions can be obtained from physical assumptions which one may obtain from the current flow. A good discussion of this point is given in the Appendix to Fedkiw.[73] Briefly, it is assumed that there will be no current density in the solution at the front of the bed ($y=0$) and along

one side wall ($x=0$). Also, far down the bed ($y \to \infty$), the current density will also approach zero. Finally, along the wall near the counterelectrode, the solution potential is assumed to be fixed, and equal to a constant. The boundary conditions appropriate to the assumptions above are

$$at \quad y = 0 , \quad \frac{\partial \Phi_2}{\partial y} = 0 , \tag{8-13}$$

$$as \quad y \to \infty , \quad \frac{\partial \Phi_2}{\partial y} \to 0 , \tag{8-14}$$

$$at \quad x = 0 , \quad \frac{\partial \Phi_2}{\partial x} = 0 , \tag{8-15}$$

and

$$at \quad x = d , \quad \Phi_2 = V . \tag{8-16}$$

The solution to Equation (8-11) subject to the boundary conditions in Equations (8-13) through (8-16) is given in detail in Appendix G. The final result is

$$\frac{\Phi_2 - V}{\frac{nFc_F v^2}{s_R \kappa a k_m}} = \left[\frac{\cos \alpha x}{\cos \alpha d} - 1 \right] e^{-\alpha y} + 2\alpha d \sum_{n=0}^{\infty} (-1)^n \left[\frac{1}{\lambda_n^2} - \frac{1}{\lambda_n^2 - (\alpha d)^2} \right] e^{-\lambda_n y / d} \cos \lambda_n x / d , \tag{8-17}$$

where

$$\lambda_n = \frac{(2n+1)\pi}{2} . \tag{8-18}$$

A more useful quantity than the potential distribution, from the standpoint of a designer, is the maximum potential drop. Chapter Seven discussed the importance of the maximum potential drop and its effects on the operation of the electrode. From these expressions for the potential distributions, the maximum potential difference can be obtained. For the

flow–by electrode configuration, the potential distribution indicates that the maximum solution phase potential drop occurs at the front of the electrode, $y=0$, between the two electrode boundaries, $x=0$ and $x=d$. This is the position where the greatest current is flowing. The maximum solution phase potential difference in dimensionless form for the semi–infinite electrode is

$$\frac{\Phi_2(x=0,y=0) - V}{\dfrac{nFc_F v^2}{s_R \kappa\, ak_m}} = \frac{\Delta\Phi_2}{\dfrac{nFc_F v^2}{s_R \kappa\, ak_m}} = \frac{\Delta\Phi_2}{\dfrac{\varepsilon nFc_F D_o}{s_R \kappa}} \frac{Sh}{Pe^2}$$

$$= \frac{1}{\cos \alpha d} - 1 + 2\alpha d \sum_{n=0}^{\infty} (-1)^n \left[\frac{1}{\lambda_n^2} - \frac{1}{\lambda_n^2 - (\alpha d)^2} \right] \quad (8\text{–}19)$$

This result can be compared to the results obtained by other investigators. The Alkire–Ng approximation for one–dimensional current flow gives for the maximum solution phase potential difference

$$\frac{\Phi_2(x=0,y=0) - V}{\dfrac{nFc_F v^2}{s_R \kappa\, ak_m}} = \frac{\Delta\Phi_2}{\dfrac{\varepsilon nFc_F D_o}{s_R \kappa}} \frac{Sh}{Pe^2} = \frac{1}{2}(\alpha d)^2 . \quad (8\text{–}20)$$

The solution obtained by Fedkiw, which includes the effects of the finite electrode length, is

$$\frac{\Phi_2(x=0,y=0) - V}{\dfrac{nFc_F v^2}{s_R \kappa\, ak_m}} = \frac{\Delta\Phi_2}{\dfrac{\varepsilon nFc_F D_o}{s_R \kappa}} \frac{Sh}{Pe^2} =$$

$$= 1 + 2\alpha d \sum_{n=0}^{\infty} \frac{(-1)^n}{\lambda_n} \left[\frac{1}{\tanh \lambda_n R} - \frac{e^{-aL}}{\sinh \lambda_n R} \right]$$

$$- \frac{2\alpha d}{R} \sum_{n=0}^{\infty} \frac{1}{1 + \delta_{n,0}} \frac{1}{\hat{\lambda}_n^2 + (\alpha d)^2} \frac{(-1)^n e^{-aL} - 1}{\cosh \hat{\lambda}_n} , \quad (8\text{–}21)$$

where

$$\lambda_n = \frac{(2n+1)}{2} , \quad (8\text{–}22)$$

$$\hat{\lambda}_n = \frac{n\pi}{R}, \tag{8-23}$$

and

$$\delta_{n,0} = \begin{cases} 1 & \text{if } n = 0 \\ 0 & \text{if } n \neq 0 \end{cases}. \tag{8-24}$$

This solution was obtained by Fedkiw in a way similar to the analysis presented here. The main difference is the boundary condition given by Equation (8–14), which for the finite electrode is modified to require the derivative of the solution potential to vanish at the finite electrode length

$$at\ y = L,\ \frac{\partial \Phi_2}{\partial y} = 0. \tag{8-25}$$

Examination of the infinite series in Equation (8–21) shows that it is poorly convergent for for large values of R combined with small values of αd. Equation (8–19), however, is much better behaved and gives more accurate results for the same number of terms in the series.

For the flow–through electrode, the maximum solution phase potential drop occurs between the front and the rear of the electrode, $y=0$ and $y=L$. From Bennion and Newman,[66] this is

$$\frac{\Phi_2(y=0) - \Phi_2(y=L)}{\dfrac{nFc_F v^2}{s_R \kappa a k_m}} = \frac{\Delta\Phi_2}{\dfrac{\varepsilon n F c_F D_0}{s_R \kappa}} \frac{Sh}{Pe^2} = 1 - e^{-\alpha L}(1 + \alpha L). \tag{8-26}$$

The above expressions for the maximum potential drops all contain the dimensionless group $s_R \kappa \Delta\Phi_2 / \varepsilon n F c_F D_0$. Each of the quantities contained within this group is a property of the packed bed, electrolyte, or electrode reaction. If the feed conditions and bed properties are known, then this dimensionless group can be thought of as a dimensionless maximum solution phase potential drop. Conversely, the reciprocal of this group can be thought of as a dimensionless concentration, if the maximum solution potential drop is specified. For now, we will assume that the feed properties

are all known, and that this group represents the dimensionless maximum potential drop through the electrode.

The dimensionless group $s_R \kappa \Delta\Phi_2 / \varepsilon n F c_F D_o$ can also be thought of as a measure of the ease in performing the desired reaction. Small values of this parameter are associated with solutions of high concentrations, low conductivities, and low maximum allowable solution potential drops. Reactions with solutions characterized by these low values are more difficult to process than operations where this parameter is large. When this parameter is small, one must flow the solution at slow velocities in the flow–through electrode configuration to achieve the desired conversion. At the other extreme, high values of the conductivity, high allowable solution potential drops, and low values of the reactant concentration assign a high value to this parameter. Reactions characterized by this condition are easier to perform.

A useful consequence of expressing the maximum potential differences in the non–dimensionalized forms of Equations (8–19) through (8–21) and Equation (8–26) above is the generality for determining the maximum allowable flow velocity. The expression for the potential drop for the flow–through electrode, Equation (8–26), indicates that the right side of the expression depends only upon the conversion of reactant. The left side, however, is a function of the maximum solution phase potential difference, the bed and fluid properties, and flow velocity. The maximum allowable flow velocity for a given conversion and maximum solution phase potential difference can be obtained on a log–log plot of Sherwood Number versus Péclet Number. At a fixed conversion, the maximum flow velocity can be found from the intersection of the Sherwood–Péclet Number relationship

and a straight line of slope two with intercept $\varepsilon nFc_F D_o / s_R \kappa \Delta\Phi_2 (1 - (1 + \alpha L) \cdot e^{-\alpha L})$. For very large conversions, or in the limit as αL approaches infinity, this intercept approaches a finite limit, $\varepsilon nFc_F D_o / s_R \kappa \Delta\Phi_2$. Figure 8–1 exemplifies a plot of the Sherwood Number versus the Péclet Number with several straight lines defined by Equation (8–26) intersecting this curve. The straight lines are for αL in Equation (8–26) equal to infinity. The relationship for the Sherwood Number to the Péclet Number has been taken from Fedkiw and Newman.[78] This graphical method is useful for visualizing the the way in which the operating variables can be obtained from the required design specifications. In addition, the graphical method allows this determination even if no analytic relationship between the Sherwood Number and the Péclet Number exists.

For the flow–by electrode configuration, the determination of the maximum flow velocity is more complex. Equations (8–19) through (8–21) show that k_m / v^2 and Sh / Pe^2 depend on αd as well as αL. One can still determine the maximum flow velocity by the same method outlined above for the flow–through electrode; however, now the intercept of the straight line intersecting the Sherwood–Péclet Number relationship will depend on a second variable, αd.

We now turn to the potential distribution for the flow–by electrode and the maximum potential difference defined by Equations (8–19) to (8–21). In Figure 8–2 we have plotted the dimensionless maximum potential drop times the ratio of the Sherwood Number to the square of the Péclet Number for a flow–by electrode versus αd as the independent variable. The ratio of the electrode length to width R, is used as a parameter. The semi–infinite electrode solution is denoted by $R \to \infty$. We have also included curves for

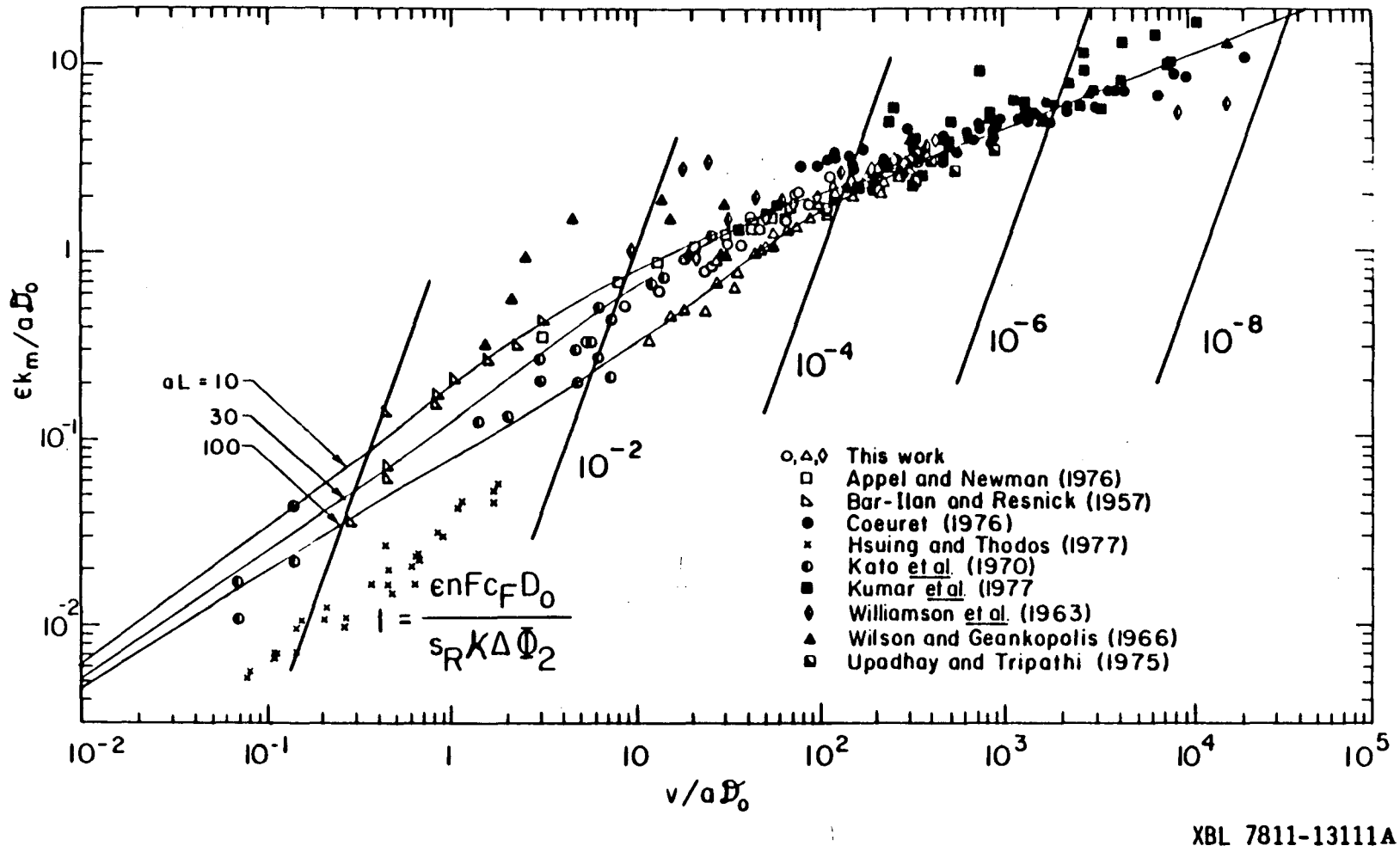

XBL 7811-13111A

Figure 8–1. Sherwood Number versus Péclet Number plot showing the intersection with Equation (8–26) ($aL = \infty$) for several values of $\epsilon n F c_F D_0 / s_R \kappa \Delta \Phi_2$. The graph is taken from Fedkiw and Newman.[78]

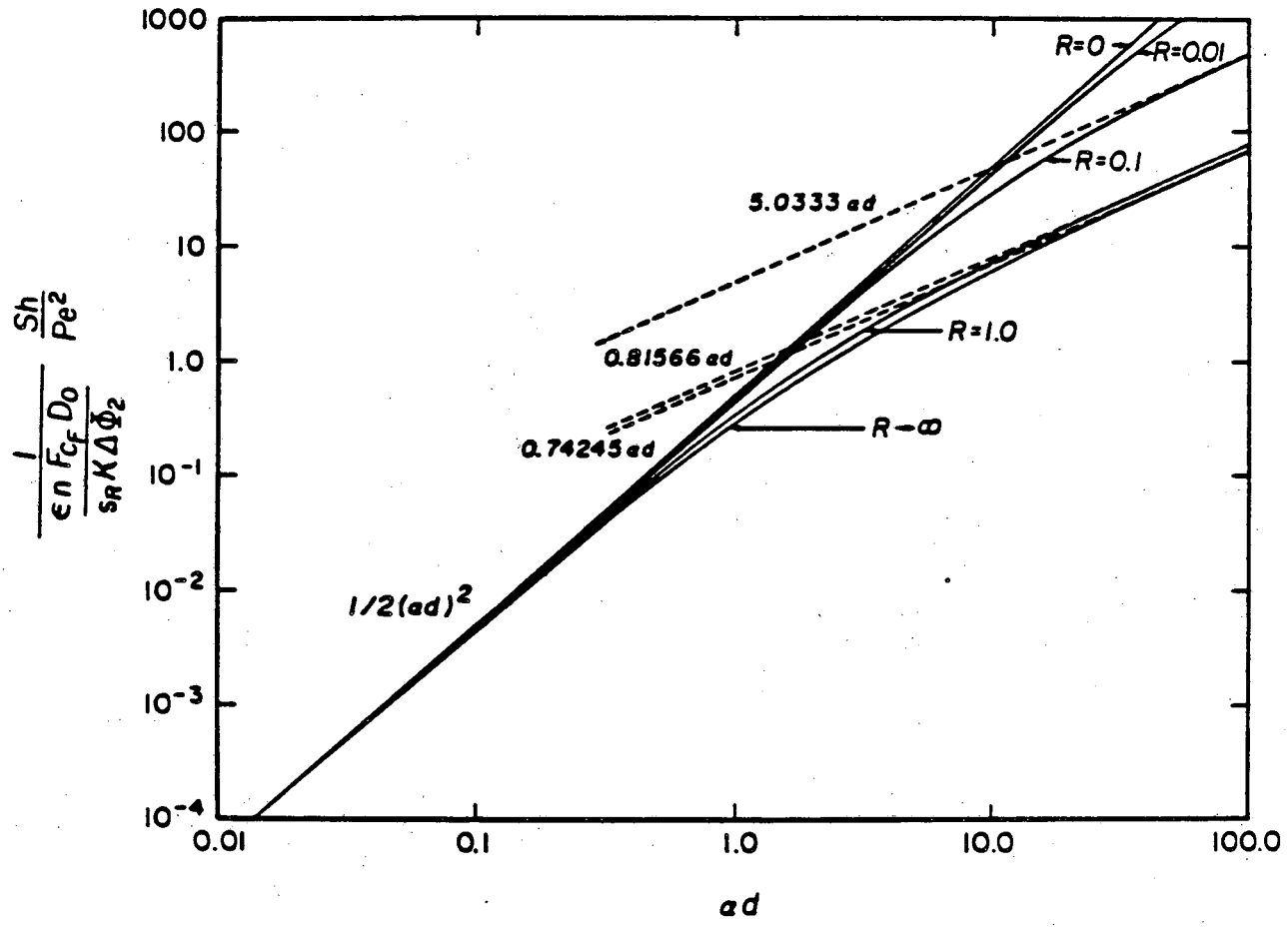

Figure 8–2. Dimensionless maximum potential drop times the ratio of the Sherwood to the square of the Péclet Number for the flow–by electrode of various aspect ratios R as a function of αd. Note $R = \alpha L / \alpha d$.

this same quantity for finite aspect ratio electrodes as derived by Fedkiw. In addition, the solution given by Alkire and Ng is shown. These curves are independent of any specific mass–transfer relationship. This figure clearly demonstrates five points.

(1) The dimensionless maximum potential drop times the ratio of the Sherwood Number to the square of the Péclet Number calculated by the finite–electrode solution, the semi–infinite–electrode solution, and the Alkire and Ng solution all approach the same limit as αd becomes small.

(2) The maximum dimensionless potential drop times the ratio of the Sherwood Number to the square of the Péclet Number approaches a limiting form for R becoming large. At large values of αd and large aspect ratios, this relationship becomes proportional to αd. In the limit of small αd, this relationship approaches a value given by $\frac{1}{2}(\alpha d)^2$.

(3) The maximum dimensionless solution phase potential drop times the ratio of Sherwood Number to the square of the Péclet Number for finite R asymptotically becomes proportional to αd at large values of αd. The value of this proportionality constant is determined by the magnitude of R.

(4) The effect of the finite electrode length is important only for values of R less than approximately one and then only at large values of αd.

(5) The Alkire and Ng one–dimensional solution is seen to reflect the limit as the aspect ratio of the flow–by electrode tends toward zero for all values of αd. This contrasts with earlier work which has assumed the Alkire and Ng solution results only as the aspect ratio R, goes to infinity.[73]

If the maximum dimensionless solution phase potential drop times the ratio of the Sherwood Number to the square of the Péclet Number for the flow–through electrode were plotted on this graph, the resulting curves would be horizontal straight lines. Equation (8–26) shows that for the flow–through electrode this quantity is not dependent upon the parameter αd. The positions of the lines are determined only by the conversion or the value of αL.

While Figure 8–2 is useful for understanding how the maximum potential drop varies with the aspect ratio R, seldom will this be useful for a designer. Most often, a designer will need to consider the variation in the maximum potential drop for a fixed conversion and not a fixed aspect ratio. Again, the parameter αL is an equivalent means of expressing the reactant conversion.

Figure 8–3 is a plot of the maximum potential drop times the ratio of the Sherwood Number to the square of the Péclet Number versus αd with αL as a parameter. The solution to the maximum potential drop for the semi–infinite electrode can be seen to be denoted by the curve marked $\alpha L \rightarrow \infty$. On this curve the value of R, which is the ratio of αL to αd, is also infinity. Finite values of αL are associated with the Fedkiw, finite electrode length solution.

Again, the significant features of this graph are the same as in Figure 8–2. At small values of αd, the semi–infinite solution, the finite length solution, and the Alkire and Ng solution all reduce to the same curve. For all values of αd, the Alkire and Ng solution is seen to be valid in the limit of zero conversions ($\alpha L = 0$). Finally, for complete conversions, the maximum potential drop times the ratio of the Sherwood to the square of the Péclet

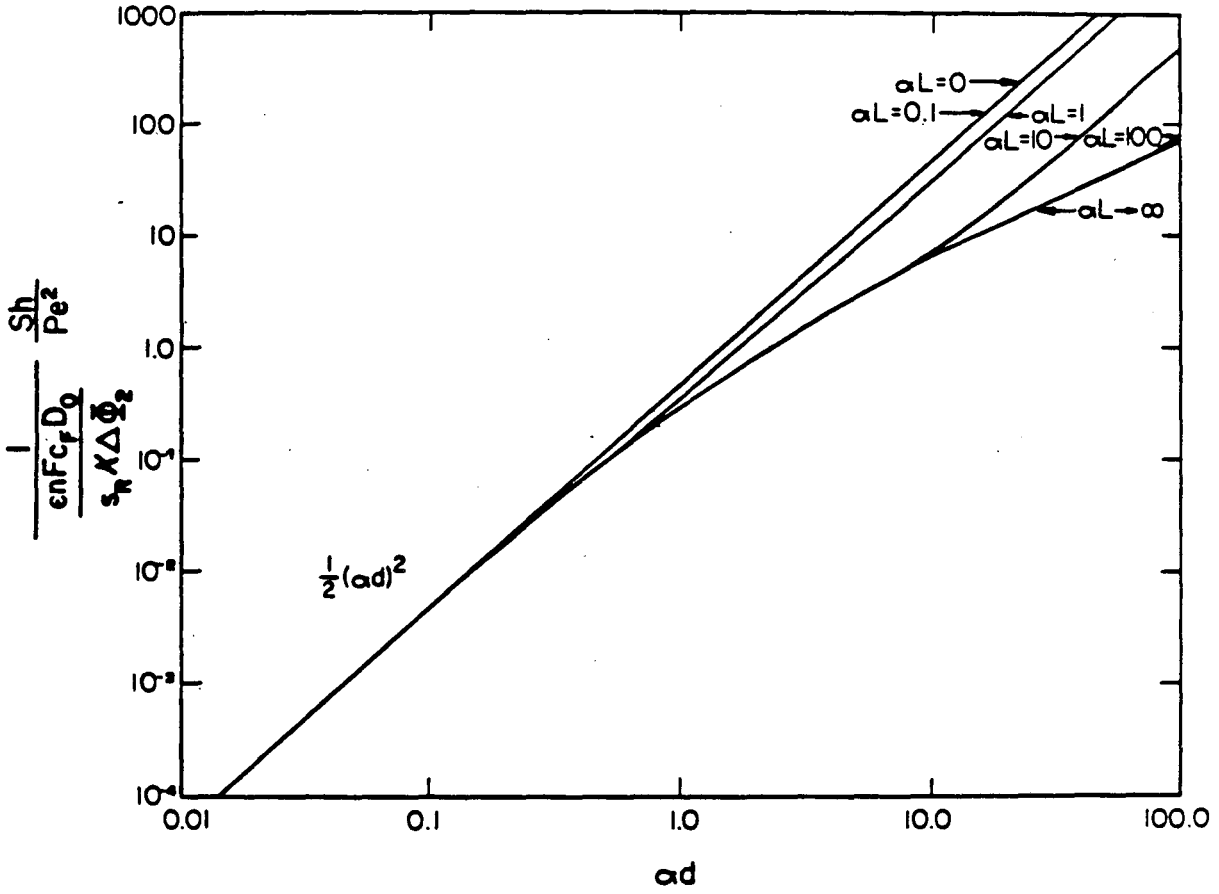

Figure 8–3. Dimensionless maximum potential drop times the ratio of the Sherwood to the square of the Péclet Number for the flow–by electrode at various reactant conversions αL as a function of αd.

Number approaches a limiting relationship. This relationship is the same relationship obtained for an electrode with an infinite aspect ratio .

To summarize, we have derived the potential distribution for a flow–by electrode of infinite aspect ratio. From this, we have obtained an expression for the maximum potential drop in this electrode. We have compared this to the results given by Alkire and Ng and Fedkiw and shown the conditions under which each of these approximations is valid. For a flow–through porous electrode, the maximum solution potential drop depends only upon the ratio of the electrode length and penetration depth αL. The expression for the maximum potential drop for infinitely long flow–by electrodes depends upon the dimensionless group αd. For finite length electrodes, the maximum potential drop depends on the variable αd as well as αL. All expressions for the maximum potential difference for flow–by electrodes, however, reduce to the simpler expression of Alkire and Ng in the limit of αd much less than one.

Chapter 9

Comparison of Flow-Through and Flow-By Porous Electrodes; Maximum Potential Drop

The choice of the optimum electrode configuration has been considered by Alkire and Ng, and Fedkiw using the maximum potential difference as a basis for comparison. Alkire and Ng assumed one dimensional current flow perpendicular to the fluid flow in calculating the potential drop of a flow–by porous electrode. To compare configurations, they then maximized the current density per unit volume for each configuration. Fedkiw, selected the configuration which, for equal electrode volumes and feed flowrates, gave the lower maximum potential drop. In this section we will show that each of these methods is equivalent and produces the same result.

The results of Alkire and Ng and Fedkiw can be reconciled by an order of magnitude analysis. This can be useful in determining the approximate conditions under which the flow–by configuration is superior to the flow–through configuration at the limiting current. Consider a flow–through and a flow–by electrode of equal dimensions and feed flow rates and with identical packings and feed compositions. Each reactor has a length L, width d, and height W. At the limiting current, the reactant flows through the electrode and reacts at a rate determined solely by the type of packing and the magnitude of the fluid flow. The distribution of the reaction and the total current will therefore be identical in the two reactors. For high conversions of reactant to product, most of the reactant will be depleted in a region very near the front of the electrode. The characteristic length of this region is the penetration depth, denoted by $1/\alpha$. Most of the

solution–side current in the flow–through electrode with an upstream counterelectrode, must travel an approximate distance $1/\alpha$, through an area of Wd. The majority of the solution–side current in the flow–by electrode, however, need only travel a distance comparable to the width of the electrode d, through an area of W/α. The superior electrode configuration is the configuration that yields a lower ohmic potential drop. The ohmic potential drop is the product of the total current times the length of travel divided by the cross sectional area to current flow. A comparison of the solution ohmic drop shows that the flow–by electrode configuration is preferred for high conversions if the approximate condition

$$\alpha d < 1 \qquad (9-1)$$

is satisfied. This result is identical to the result obtained by Alkire and Ng when they maximized the volumetric current density to compare configurations.

Now let us examine the optimum configuration for low conversions. At low conversions, the penetration length eventually becomes comparable to the electrode length. In this limit, the solution side current in the flow–through electrode now flows a distance L, rather than $1/\alpha$. Likewise in the flow–by electrode, the solution–side current flows through an area of WL. Equating the ohmic potential drop in the low–conversion limit results in the criterion that the flow–by configuration is favored for

$$\frac{L}{d} = R > 1 . \qquad (9-2)$$

Equation (9–1) shows that, at high conversions, the parameter αd is of primary importance in distinguishing the optimum electrode configuration and in determining the maximum potential drop in the flow–by configuration. At low conversions, Equation (9–2) shows that L/d can be

expected to be the parameter of primary importance in determining the optimum configuration.

As a first approximation, the point where the electrodes are equally competitive for a specified conversion can be found by equating the ratio of Sherwood to to the square of the Péclet Number divided by the parameter $\varepsilon n F c_F D_o / s_R \kappa \Delta\Phi_2$ for each configuration. Equating these expressions requires that the flow–through and flow–by have equal dimensions and flow–rates. In Figure 9–1 we have plotted the values of αd and R (as functions of αL) which give equal dimensionless maximum potential drops times the ratio of the Sherwood to the square of the Péclet Number for the flow–through electrode and for the flow–by electrode. We have also designated the regions where each type of configuration is preferred. Again, the variable αL directly represents the requirement of conversion that we have imposed on the design. The maximum dimensionless potential drop times the ratio of Sherwood to the square of the Péclet Number for the flow–through electrode has been calculated using Equation (8–26). We have included the three possibilities for evaluating the this quantity for the flow–by electrode. First, the flow–by electrode is assumed to be infinitely long, and Equation (8–19) is used. We can also assume that the one–dimensional potential variation of Alkire and Ng might be appropriate and use Equation (8–20). Finally, the effects of the finite electrode length also can be included. The relationship given by Fedkiw could also be used, Equation (8–21). For this finite electrode case, an additional constraint must be imposed since this function explicitly depends on the aspect ratio. The value of R is computed from

$$R = \frac{L}{d} = \frac{\alpha L}{\alpha d} . \qquad (9–3)$$

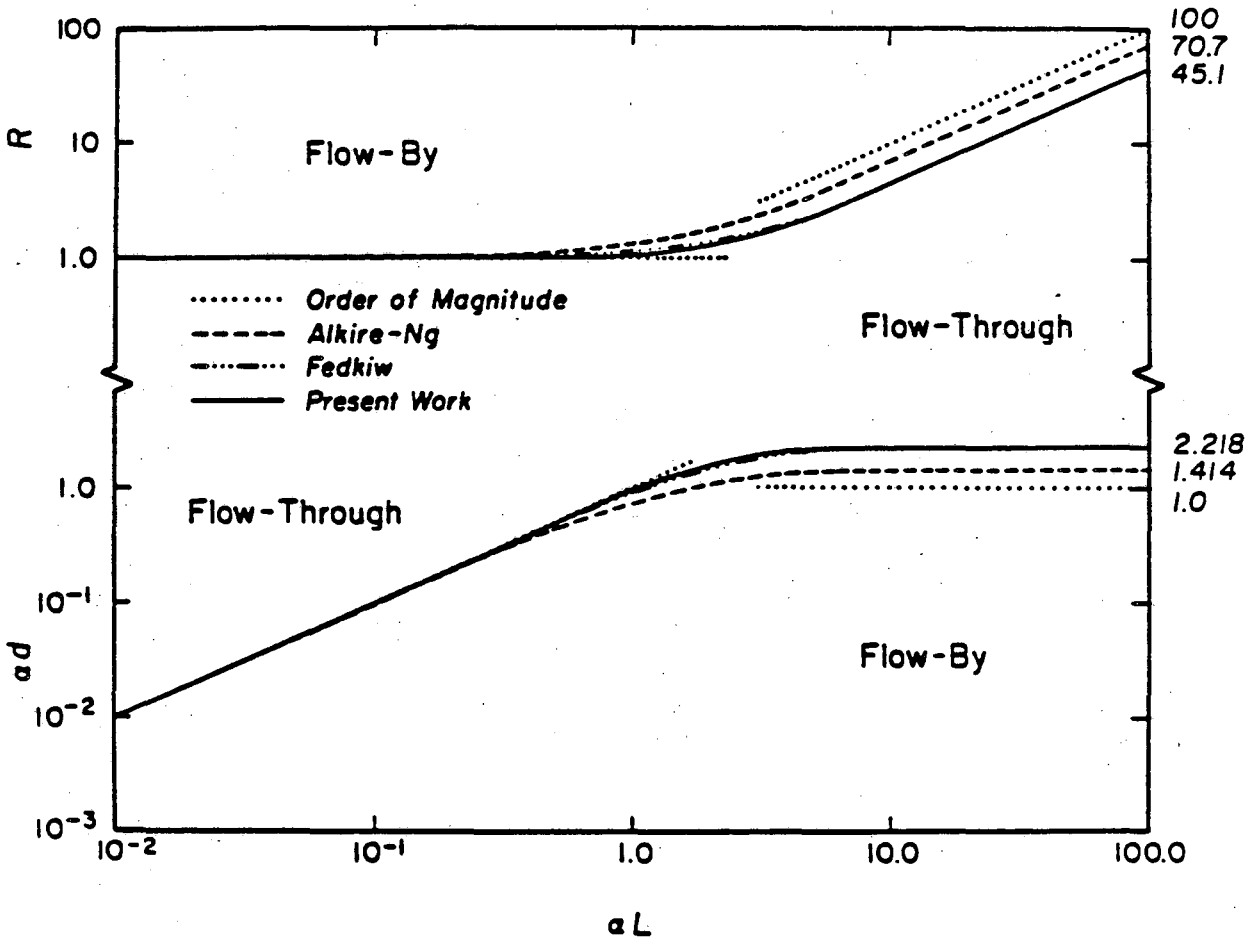

Figure 9–1. Values of αd and R for equal dimensionless potential drops times the ratio of the Sherwood Number to the square of the Péclet Number for the flow–through electrode and the flow–by electrode using: a) order of magnitude expressions, b) Alkire and Ng expression, c) semi–infinite electrode expression, d) Fedkiw expression. These two representations are equivalent since $R = \alpha L / \alpha d$.

Thus, the value of αd and the value of R is found for each value of αL such that the maximum dimensionless potential drops times the ratio of Sherwood to the square of the Péclet Number are equal. For comparison, we have also included the results of the order of magnitude analysis, which were derived earlier.

We emphasize here, that this comparison of the two electrode configurations does not require that we specify a mass–transfer coefficient relationship. This comparison does not depend upon the Sherwood–Péclet Number relationship. Fedkiw compared the two configurations in a similar way except that he introduced a specific Sherwood–Péclet Number relationship in his comparison. The comparison presented here is considered to be preferable because it is not restricted to a single correlation.

Figure 9–1 establishes several important points. At low values of αL and, consequently, low conversion, the aspect ratio and the value of αd for equal potential drops are independent of the flow–by potential drop relationship. The Alkire and Ng one–dimensional approximation, the semi–infinite electrode approximation, and the finite electrode relationship all predict the same geometry. In this low conversion range, αL less than one, the aspect ratio for equal potential drops is seen to approach one. The value of αd, given equal electrode cost, is seen to approach a limiting relationship of

$$\alpha d = \alpha L \,. \tag{9–4}$$

The conclusion to be made here is that a flow–by electrode is favored at low conversions if it can be constructed with an aspect ratio greater than one. Otherwise, a flow–through electrode would be a better choice. Equation

(9–4) is identical to Equation (9–2) obtained by the order of magnitude analysis in the introduction section.

At higher conversions, values of αL greater than about 2, the criterion that specifies the more economical configuration changes. In this region, the value of R delineating the optimum electrode configuration no longer is constant. Also, the one–dimensional Alkire and Ng approximation deviates from the two–dimensional solutions. Since the one–dimensional approximation over-predicts the potential drop, it results in a criterion giving a lower flow–by aspect ratio. The two–dimensional potential distributions are thus seen to affect the choice of electrode configurations only at high conversions. From Figure 9–1 we can see that at high conversion one would choose a flow–by electrode only if the resulting aspect ratio is greater than 0.45 times αL. According to Fedkiw,[73] the flow–by configuration was preferred over the flow–through configuration for

$$R \geq 5 . \qquad (9–5)$$

One can see, however, that this relationship holds only for values of αL near 10. In terms of αd, the flow–by electrode is superior at high conversions only if

$$\alpha d < 2.218 . \qquad (9–6)$$

Except for the factor of 2.218, Equation (9–6) is consistent with Equation (9–1) obtained by an order of magnitude estimate previously. This factor accounts for the variation of current across the flow–by electrode and the two–dimensional current flow which was not included in the earlier analysis.

Figure 9–1 also demonstrates another significant point. The curves for the optimum electrode configuration given by the finite length electrode or the semi–infinite electrode are very nearly the same. At high and low

conversions, the criterion becomes independent of whether one considers the finite electrode length. Only for a region of αL near one, does the effect of the finite electrode length on the criterion become noticeable. From Figure 8–1, one can see that only when the aspect ratio approaches one at high conversions does the effect of the finite electrode length on the potential drop become noticeable. But at large conversions, or large αL, it is impractical to construct a flow–by electrode with an aspect ratio near one. Consequently, considering the potential distribution in a flow–by electrode of finite length is not really important for practical flow–by designs when the maximum potential drop is used as a basis for comparison. The potential distribution for an electrode with an infinite aspect ratio gives results which are practically identical but in a less complicated expression. The potential distribution of Alkire and Ng, however, cannot be used to predict the optimum configuration accurately for all conversions. Therefore the semi–infinite electrode approximation retains the accuracy of the finite electrode expression, but reduces the complexity of calculations.

In this chapter, we have compared the flow–through and flow–by configurations using the maximum potential drop as a basis for comparison. The results of this work show that the criterion delineating the optimum electrode depend upon reactant conversion. Also, three expressions for the maximum flow–by potential drop have been compared. The semi–infinite electrode approximation embodies most of the accuracy of the Fedkiw expression, but retains some simplicity like the Alkire and Ng solution. The comparison presented in this section necessarily requires that the two configurations be compared when both electrodes have the same dimensions and equal feed flowrates. Also, it requires that one know these prior to the comparison. Chapters Ten and Eleven will present a method that relaxes

this restriction so that the flow–through and flow–by configurations can be compared under any conditions.

Chapter 10

Electrode Design

In the previous section we delineated the conditions under which the flow–by configuration was superior to the flow–through configuration by equating their maximum solution potential drops. This comparison implied equal electrode dimensions and feed flow rates.

In general, the optimal electrode configuration should not be determined solely from a comparison of the potential drop for each configuration, but it should be determined from cost considerations. The optimal electrode configuration should be found by minimizing the combined sum of operating and capital costs for each configuration and choosing the configuration which gives the resulting lower lifetime cost. In the previous section, by equating the maximum potential drops, we considered only those costs which were identical for each configuration. Since equal dimensions and feed flowrates were implied in the earlier analysis, only equal electrode costs arising from those factors were considered.

Now we address the question of how the cost–optimum electrode configuration and design can be determined for a given application. We consider fixed electrode costs which are directly related to the electrode volume and separator area, along with variable pumping costs. First, we discuss qualitatively the number of independent variables for each electrode configuration.

From Equation (8–26), for the flow–through electrode, one can see that the specification of the conversion or αL and the parameter

$\varepsilon nFc_P D_o / s_R \kappa \Delta\Phi_2$ specifies the required flow velocity if the relationship between the Sherwood and Péclet Number is known. Since the velocity is determined, the required electrode length can also be calculated from the parameter αL for specified bed properties. The required separator area per unit of volumetric flow can also be determined given this information. One therefore sees, that specifying the conversion and the parameter $\varepsilon nFc_P D_o / s_R \kappa \Delta\Phi_2$ is sufficient to determine completely the design of a flow–through electrode at the limiting current.

The analysis of the flow–by configuration is more complex, however. Equations (8–19) through (8–21) indicate that while the maximum allowable flow velocity may depend on αL, it also depends on a second variable αd. Consequently, it is not sufficient to specify only the conversion and the parameter $\varepsilon nFc_P D_o / s_R \kappa \Delta\Phi_2$ to determine the electrode dimensions. It is this added flexibility in the variable αd, which makes the flow–by configuration more versatile.

Let us derive the applicable design equations for a flow–through and a flow–by electrode operating at the limiting current considering variation in volumetric, pumping, and separator costs. We will assume a high current efficiency for each configuration one independent of all operating or design variables. The variation in the cost of electrical energy to provide the driving force for the electrochemical reaction will also be assumed to be negligible. This assumption will be most accurate if the solutions to be processed contain only dilute concentrations of reactants. Under this condition, the energy requirement to pump the feed through the electrode will far exceed the electrical energy needed to perform the reaction.

The given dimensions of the flow–by electrode are a width d, height W, and length L. It is not required for the flow–through electrode that its actual width and height be specified. These two quantities can be changed as matter of convenience in the design provided the required cross sectional area, or the product of the width and height is satisfied. Given the design conditions above, the cost–optimum dimensions of the flow–through and flow–by may not necessarily be the same. Consequently, the velocity of the fluid through each electrode also may be different. For the flow–through or the flow–by configuration, the volume of the electrode per quantity of feed can be expressed as

$$\frac{V_e}{Q} = \frac{L}{v}. \tag{10–1}$$

The required separator area for the flow–through electrode will be the cross sectional area perpendicular to the flow direction. In the flow–by design, the separator must be placed along one side wall parallel to the solution flow. The required separator area for the flow–by electrode is then the height of the electrode times the electrode length. In terms of the required separator area per volumetric quantity of feed, the flow–through electrode requires

$$\frac{A_s}{Q} = \frac{A_c}{A_c v} = \frac{1}{v} \tag{10–2}$$

area per volumetric flow. For the flow–by configuration, this quantity is given by

$$\frac{A_s}{Q} = \frac{WL}{Wdv} = \frac{L}{dv}. \tag{10–3}$$

Pumping losses are the product of the pressure difference through the bed times the volumetric flow. A relationship often used for the pressure drop in packed beds is the Ergun Equation.[79] In dimensionless form it is

$$\frac{\Delta \mathcal{P} \varepsilon^2}{\rho a^2 D_o^2} = \left(\frac{150}{36} Pe^2 Sc + \frac{1.75}{6} Pe^3 \right) \frac{\alpha L}{Sh} . \qquad (10-4)$$

The pressure drop is thus the work per unit of volumetric flow to move the fluid through the electrode. Equation (10–4) contains two terms representing the pressure drop in two flow regimes. In the low flow regime, the pressure drop is proportional to the velocity and viscosity. At higher flow rates, the pressure drop becomes independent of the viscosity but proportional to the square of the velocity.

It is also necessary to include the effect of mass transfer on the design of the porous electrode and the choice of the optimal configuration. For demonstration, a simplified Sherwood–Péclet number relationship of the form

$$Sh = A\, Pe^B \qquad (10-5)$$

will be used. This relationship is general, for most mass transfer data are correlated in this way. Rewriting Equations (10–1) through (10–4) in dimensionless form using Equation (10–5), we obtain for dimensionless electrode volume and pressure drop for the flow–through or flow–by configuration

$$\frac{V_e}{Q} \frac{a^2 D_o}{\varepsilon} = \frac{\alpha L}{A} \left(\frac{1}{A} \frac{Sh}{Pe^2} \right)^{\frac{B}{2-B}} . \qquad (10-6)$$

$$\frac{\Delta \mathcal{P} \varepsilon^2}{\rho a^2 D_o^2} = \frac{Pe^2}{Sh} \left(\frac{150}{36} Sc + \frac{1.75}{6} \left(A \frac{Pe^2}{Sh} \right)^{\frac{1}{2-B}} \right) \alpha L . \qquad (10-7)$$

The dimensionless separator area for the flow–through configuration is

$$\frac{A_s}{Q} a D_o = \left(\frac{1}{A} \frac{Sh}{Pe^2} \right)^{\frac{1}{2-B}} . \qquad (10-8)$$

and for the flow–by electrode is

$$\frac{A_s}{Q}\,\alpha D_o = \frac{\alpha L}{\alpha d}\left[\frac{1}{A}\,\frac{Sh}{Pe^2}\right]^{\frac{1}{2-B}} \qquad (10\text{–}9)$$

In Equations (10–6) through (10–9), the ratio of Sherwood Number to the square of the Péclet Number is evaluated using the relationships derived in the previous section. For the flow–through electrode, this function is given by Equation (8–26), while the for the flow–by electrode Equations (8–19) through (8–21) can be used.

Equations (10–6) through (10–9) indicate that the relationship between the required electrode volume, separator area, and pumping work per volumetric flow explicitly depend upon the mass–transfer relationship. For the flow–through configuration, these quantities also depend upon the ratio of the Sherwood Number to the square of the Péclet Number and on the conversion. Again, if the maximum solution potential drop, the conversion, and the bed and fluid properties are specified, then the ratio of the Sherwood to the square of the Péclet Number is also specified. Thus, the quantities in Equations (10–6) through (10–8) are determined uniquely under these conditions.. One can contrast this to the flow–by configuration. For this configuration, the ratio of the Sherwood Number to the square of the Péclet Number is also dependent upon the variable αd. Also Equation (10–9) shows an explicit dependence of the separator area per volumetric flow on αd. Thus the three dimensionless quantities require the additional specification of αd if they are to be calculated.

The actual operating and design variables of the electrodes can be related to the dimensionless quantities described before. The actual flow velocity and the length for the flow–through electrode can be determined from Equations (10–1) and (10–2) once the ratio of the Sherwood Number to the square of the Péclet Number is known. The flow velocity can be

determined from

$$v = \frac{Q}{A_s} \tag{10-10}$$

and the length can be found from

$$L = \frac{V_e}{Q} v \ . \tag{10-11}$$

If one also knows the value of αd, the actual operating and design variables of the flow-by electrode can also be determined. The superficial flow velocity v, for the flow-by electrode, can be calculated from

$$v = \frac{Q}{A_s} \frac{\alpha L}{\alpha d} \tag{10-12}$$

while the bed width d, can be calculated from

$$d = \frac{V_e}{Q} \frac{\alpha d}{\alpha L} v \ . \tag{10-13}$$

The required electrode length may then be found from

$$L = d \frac{\alpha L}{\alpha d} \ . \tag{10-14}$$

While these absolute variables are required to implement the design, the equivalent dimensionless variables formulated in the analysis are more useful. The dimensionless variables remain invariant during scale-up and predict the behavior of any system regardless of its absolute size. For this reason, only dimensionless variables will be used in the rest of this study.

One sees from these relationships for the flow-by configuration, that the variable αd is related indirectly to the superficial velocity of the fluid or the electrode width. The expressions for V_e / Q or A_s / Q are functions of the maximum dimensionless solution potential drop, which is dependent upon αd. We have chosen αd to be the independent variable because of its relevance in determining the potential drop. It is useful to examine the behavior of these relationships with variations in αd. In Figure 10-1 we

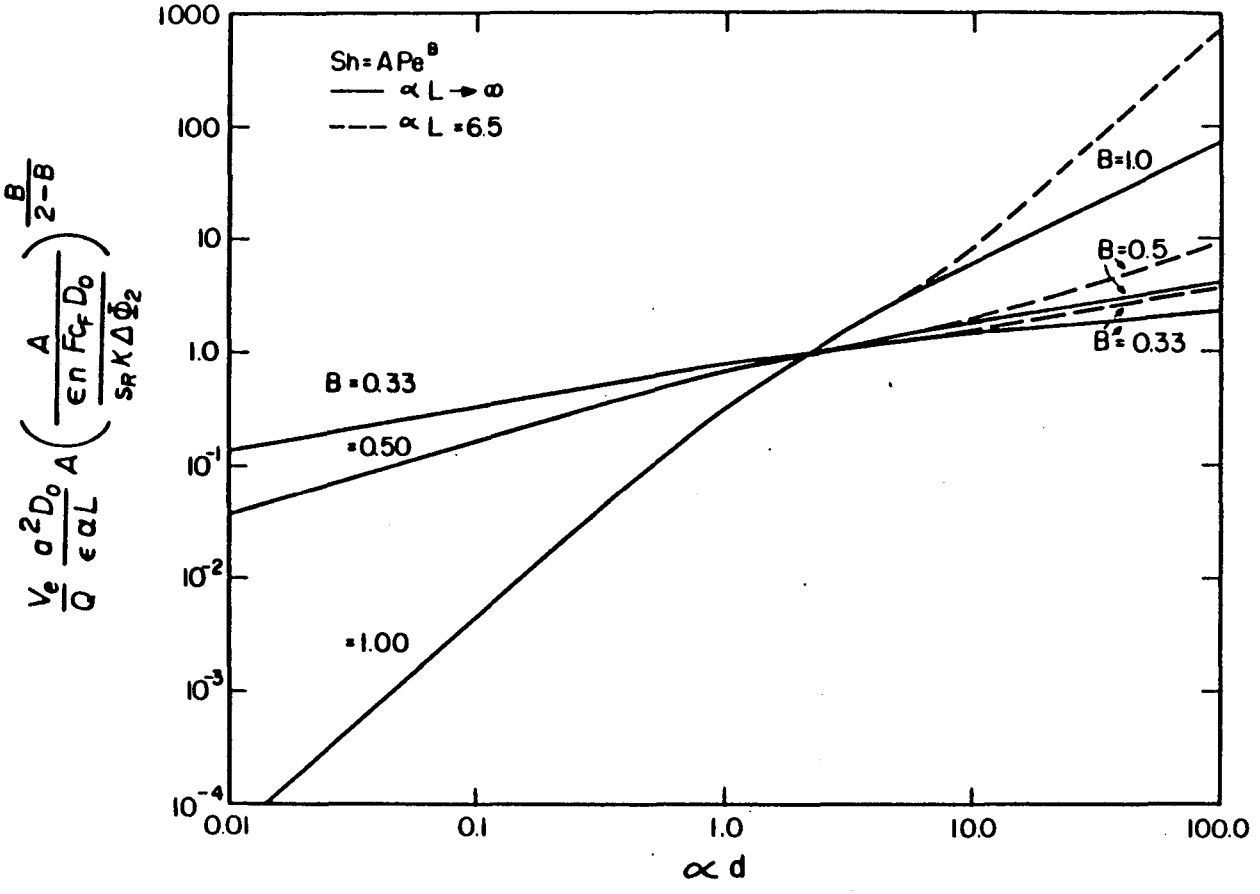

Figure 10–1. Variation in nondimensional flow–by electrode volume with αd for several values of the exponent B and for two conversions αL.

have plotted the variation of dimensionless V_e / Q with αd for the flow-by electrode with the exponent B as a parameter. For most mass-transfer correlations, the exponent B lies between 0.33 and 1.0, hence three values of B from 0.33 to 1.0 are shown. Two curves for two different conversions are also shown. The first is for αL equal 6.5, while the second is the limit for complete conversion. This figure shows that the required volume of electrode per volumetric quantity of feed monotonically increases with αd for the two conversions shown. In fact, the required volume to flowrate ratio is an increasing monotonic function for all values of αd given any conversion or αL. Reducing αd reduces the required volume of electrode for a set flow rate, conversion, and maximum solution potential drop.

In Figure 10-2, we have plotted the dimensionless separator area per volumetric flow rate of feed versus the variable αd. Again the exponent B is a parameter. Here, in contrast to the variation of the dimensionless electrode volume, the dimensionless separator area is not a monotonic function of αd for all values of the exponent B. Also, the general trend of the function depends upon the conversion. For finite values of αL, this function is seen to have a relative maximum near αd equal to one for values of the exponent less than one. As αL tends toward infinity, the relative maximum disappears and the curves for complete conversion show that an absolute maximum now occurs.

The dimensionless pressure drop given in Equation (10-7), unlike the relationships for the dimensionless electrode volume and separator area per volume of feed, can not easily be plotted in a general form. Instead, the general behavior of this relationship will be discussed. Equation (10-7) shows the pressure drop to be composed of two terms. The first term is

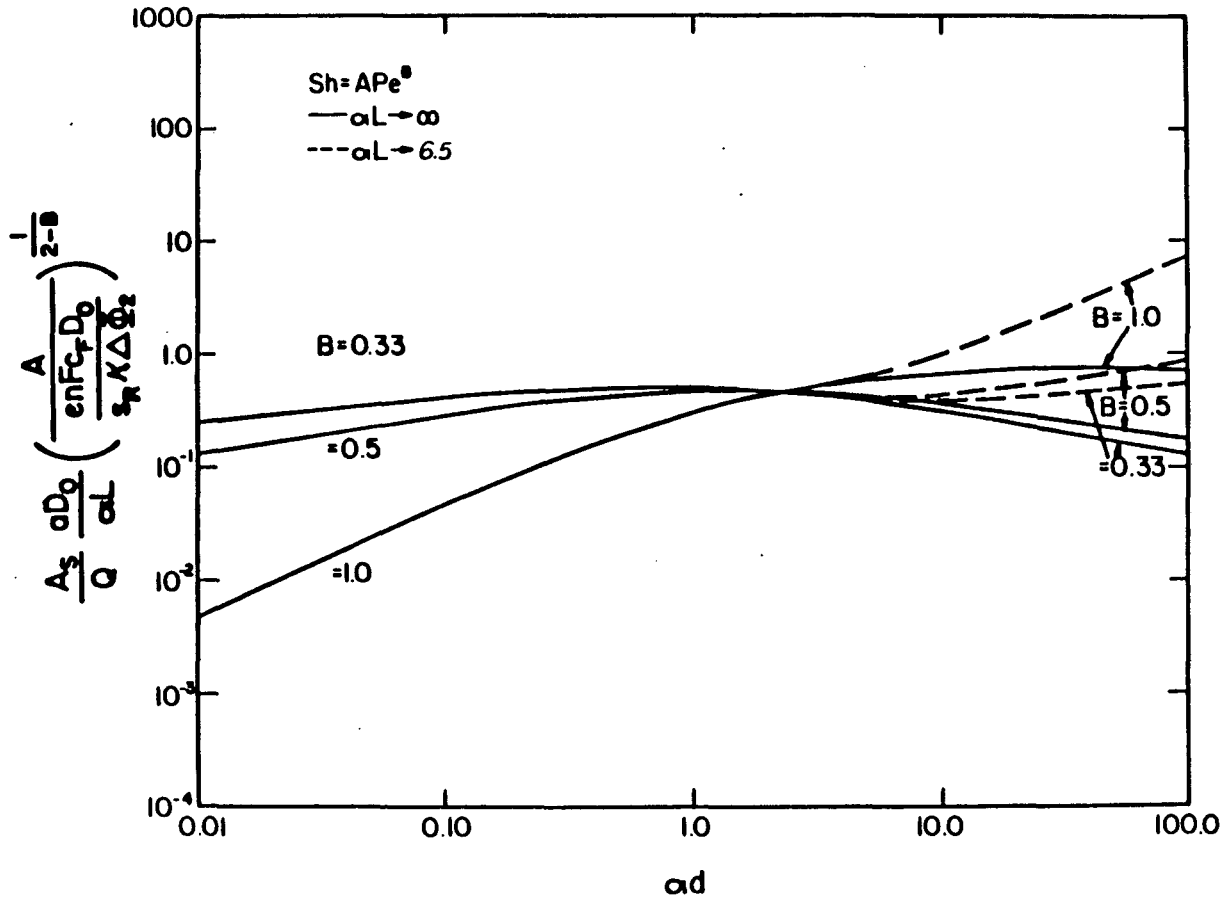

Figure 10–2. Variation in nondimensional flow–by separator area with αd for several values of the exponent B and for two conversions αL.

proportional to the Péclet Number squared over the Sherwood Number while the second term is proportional to this function to the $(3 - B)/(2 - B)$ power. For the flow-by electrode of infinite aspect ratio or at complete conversions, the dimensionless maximum potential drop is proportional the to square of αd at low αd and proportional to αd at large values of αd. The pressure drop is therefore seen to be made up of two terms, both of which increase as αd decreases. For less than complete conversions, the same behavior is observed. The pumping cost then, always increases as αd decreases.

In Figures 10-1 and 10-2, the dimensionless electrode volume and separator area for the flow-through electrode could also have been plotted on these graphs. Since the maximum solution phase potential drop is not dependent on αd, these quantities would be horizontal straight lines if plotted on these figures. The intercept of the horizontal lines with y axis would depend upon the chosen conversion, or the parameter αL, and the value of the exponent B. One sees, however, that while the separator area and the electrode volume are fixed quantities for the flow-through electrode, it is possible to reduce these quantities for the flow-by electrode by decreasing the value of αd.

From this analysis, we see that the optimal flow-by electrode design is constrained by pumping costs as αd is decreased. Volumetric electrode cost per volume of feed is seen to increase monotonically with αd. Separator costs per quantity of feed first increase with αd and then reach a maximum. If the conversion is complete, then the separator area per volumetric flow will then continue to decrease. For less than complete conversions, the dimensionless separator area begins to increase again at

high values of αd. The task now is to determine the optimum value of αd for the flow-by electrode, calculate the individual capital and operating costs for each configuration, and then compare the total costs.

Chapter 11

Electrode Cost Optimization

As we have mentioned in the Chapter Ten, the flow–by configuration allows one additional degree of freedom in the design of an electrode. One way of determining the value of αd is to minimize the combined capital cost and operating cost for the reactor. We consider a cost function consisting of the volumetric electrode cost and the area cost associated with the separator. Since we are also considering only dilute solutions with high flow rates, variable pumping costs will be included. A cost function given by

$$C_T = \left[C_V \frac{V_e}{Q} + C_S \frac{A_s}{Q} \right] r + C_P \Delta \mathcal{P} \qquad (11-1)$$

includes all of the factors given above. The total electrode cost per volumetric flow rate of feed C_T, is composed of these three costs. The factors C_V, C_S, and C_P represent the cost per volume of electrode, the cost per surface area of separator, and the cost of pumping power, respectively. The cost of the electrode may not scale linearly with size, and hence, these factors may be dependent upon the total quantity of feed processed. The factor r accounts for the time value of invested capital. It includes the effects of interest, taxes, and depreciation. The optimum value of αd may be found by minimizing the total cost given by Equation (11–1).

Let us now consider the design of a flow–through and flow–by electrode subject to some common design constraints. In this design we will specify the conversion of reactants to products. In addition, the maximum potential drop through the electrode will be constrained not to exceed a predetermined value. Presumably, this maximum allowable value would be

determined from other experiments as discussed in Chapter Seven. These specifications would be very common in practice, since the requirements for many processes entail a given conversion of reactants to products. The limit on the maximum potential drop is also realistic, since one would strive for an electrode with a high specificity for the desired product.

The optimization process will begin by rewriting Equation (11–1) in a dimensionless form. We choose to non-dimensionalize the Equation using the cost per unit volume as a common basis. If we rewrite Equation (11–1), substituting in expressions for the various cost relationships from Equations (10–6) through (10–9), this gives for the flow-through cost

$$\frac{C_{T,FT}a^2D_o}{C_V\varepsilon}\frac{1}{\tau} = \frac{\alpha L}{A}\left(\frac{1}{A}\frac{Sh}{Pe^2}\right)^{\frac{B}{2-B}} + \frac{C_S a}{C_V\varepsilon}\left(\frac{1}{A}\frac{Sh}{Pe^2}\right)^{\frac{1}{2-B}} + \frac{C_P\rho a^4 D_o^3}{C_V\varepsilon^3}\frac{1}{\tau}\frac{Pe^2}{Sh}\left(\frac{150}{36}Sc + \frac{1.75}{6}\left(A\frac{Pe^2}{Sh}\right)^{\frac{1}{2-B}}\right)\alpha L \quad (11\text{–}2)$$

The total cost for the flow-by electrode is

$$\frac{C_{T,FB}a^2D_o}{C_V\varepsilon}\frac{1}{\tau} = \frac{\alpha L}{A}\left(\frac{1}{A}\frac{Sh}{Pe^2}\right)^{\frac{B}{2-B}} + \frac{C_S a}{C_V\varepsilon}\frac{\alpha L}{\alpha d}\left(\frac{1}{A}\frac{Sh}{Pe^2}\right)^{\frac{1}{2-B}} + \frac{C_P\rho a^4 D_o^3}{C_V\varepsilon^3}\frac{1}{\tau}\frac{Pe^2}{Sh}\left(\frac{150}{36}Sc + \frac{1.75}{6}\left(A\frac{Pe^2}{Sh}\right)^{\frac{1}{2-B}}\right)\alpha L \quad (11\text{–}3)$$

The total electrode cost has been expressed for both configurations as functions of only the dimensionless ratio of the Sherwood to the square of the Péclet Number. The difference between Equations (11–2) and (11–3) is the factor of $\alpha L / \alpha d$ appearing in the separator cost term for the flow-by configuration. Also, the function Sh / Pe^2 depends upon the electrode configuration. For the flow-through electrode, this ratio depends only upon

the chosen conversion for a fixed maximum potential drop and feed concentration. In addition to these, this ratio also depends upon a second variable, αd, for the flow-by configuration.

One can observe an important restriction on the comparison of the two configurations based on the maximum potential difference. Equating the maximum dimensionless potential drops is identical to equating the electrode costs provided that the terms involving separator costs are not included. Thus, the earlier comparison is equivalent to a cost comparison which neglects separator costs.

Equations (11–2) and (11–3) above contain seven parameters characteristic of the bed properties, the mass transfer relationship, the materials cost, and the energy cost. As discussed before, the parameter αL can be thought of as a dimensionless conversion. The parameters A and B describe the mass transfer relationship between the Sherwood and Péclet Number. The parameter r reflects the time value of money and relates the outlay of capital cost in the present to the future saving in operating costs. The parameter Sc is the ratio of the diffusion coefficient to the kinematic viscosity, which is used for the pressure drop at low flowrates. Finally, the two parameters $C_S a / C_V \varepsilon$ and $C_P \rho a^4 D_o^3 / C_V \varepsilon^3$ are cost ratios for the cost of separator per unit area to cost of bed volume and the cost of pumping power to the cost of bed volume.

Even in this analysis, the number of parameters is large. To evaluate the effect of each of these parameters on the cost optimum designs would require an analysis beyond the scope of this work. To illustrate the optimization procedure, the values of several of these parameters will be fixed, and the dependence of the electrode optimum designs on them will

not be presented.

As an example, the values of these fixed parameters will be chosen to represent metal ion removal from an aqueous solution. Values for some the parameters have been taken from Bennion and Newman[66] for the removal of copper. While these parameters are specific to copper removal, they are used only to illustrate the principles discussed here. One may replace these values with others specific to the chosen systems. Table 11–1 presents the values of six parameters which have been fixed throughout the optimization.

The parameter αL has been set for a ratio of outlet concentration to inlet concentration of approximately 1.5 X 10^{-3}. The parameters A and B are taken from the data of Bennion and Newman,[66] as reduced by Trainham and Newman,[70] for the reduction of copper solutions. The factor r was calculated assuming a five year life on capital equipment using 12% interest compounded continuously. The fourth parameter in Table 11–1 expresses

Table 11–1 Values of selected parameters used in the optimization.

Parameter	Value
αL	6.5
A	0.07054
B	0.5454
$\frac{C_P \rho a^4 D_o^3}{C_V \varepsilon^3}$, yr^{-1}	5.0 X 10^{-13}
r, yr^{-1}	0.28429
Sc	1670

the ratio of pumping cost to volumetric bed cost. The magnitude for this parameter is best understood by translating it into absolute terms. As an example, take a reactor with specific surface area of 25 cm^{-1} and porosity of 0.3 with a fluid of density near 1 g/cm^3 and a diffusion coefficient of 6 X 10^{-6} cm^2/s. Then the cost of pumping power is about 5 X 10^{-5} \$/kJ for a bed costing 1 000 $\$/m^3$.

Now let us examine the behavior of Equation (11–2), which gives the total cost for the flow-through electrode configuration. Shown in Figure 11–1 is a plot of the total cost for a flow-through electrode versus the parameter $\varepsilon n F c_P D_e / s_R \kappa \Delta\Phi_2$. As described before, this parameter can be thought of as expressing the ease of separation. For a given reaction and fixed maximum ohmic potential drop, this parameter can also be thought of as dimensionless reactant concentration. Thus, Figure 11–1 shows the variation of total flow-through cost as a function of reactant concentration. The dimensionless total cost has been graphed with $C_S a / C_V \varepsilon$ as parameter which is a dimensionless separator area cost to electrode volume cost. Again, the magnitude of this parameter can best be understood in absolute terms. For the same conditions pertaining to the pumping cost to electrode volume cost ratio, a value of $C_S a / C_V \varepsilon = 1000$ implies a separator cost of 120 $\$/m^2$ for an electrode volume cost of 1 000 $\$/m^3$. Each curve on Figure 11–1 represents the total cost for a given separator area to electrode volume cost ratio.

Figure 11–1 is a "U" shaped curve typical of operating-capital cost trade-off behavior. The total cost is dominated by pumping costs at low values of $\varepsilon n F c_P D_e / s_R \kappa \Delta\Phi_2$. As values of the abscissa increase, the total electrode cost decreases, reaches a minimum, and then increases as the

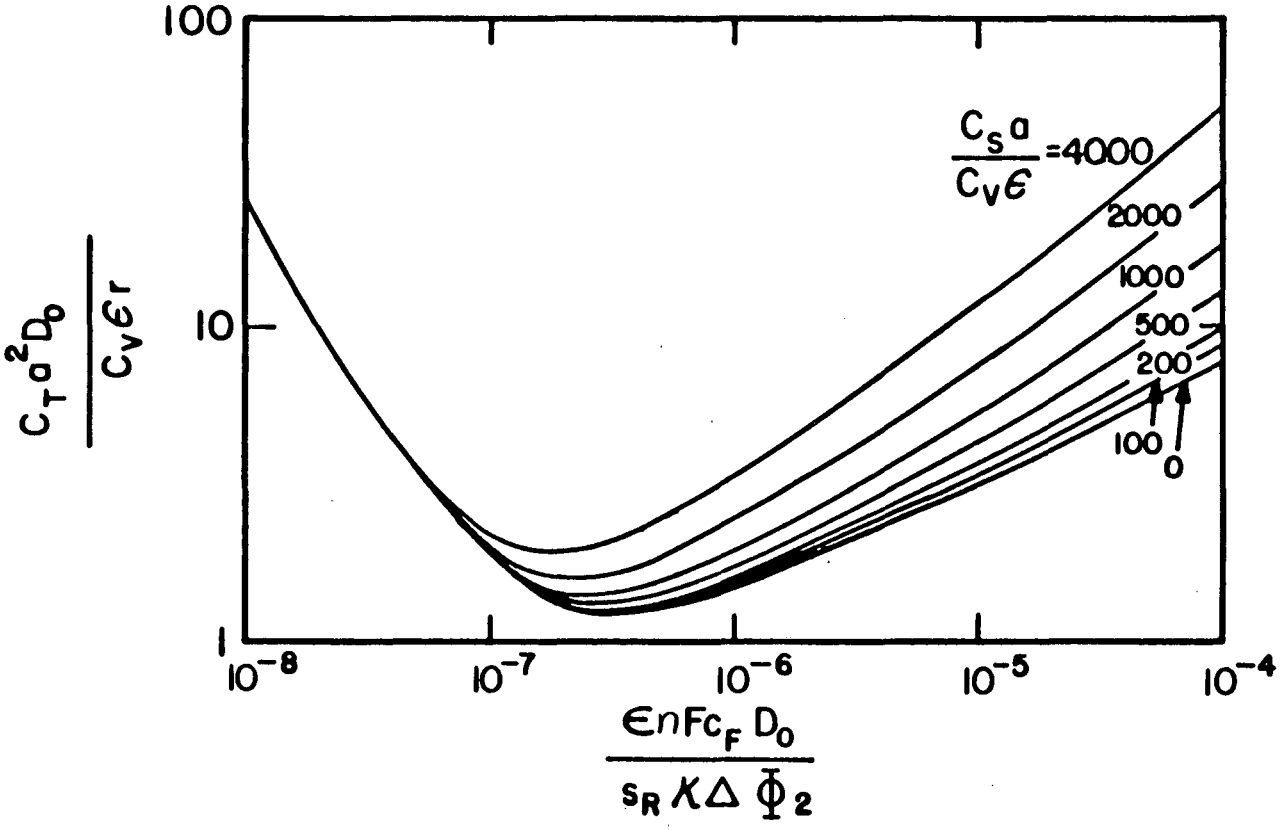

Figure 11–1. Total dimensionless flow–through electrode cost $C_T a^2 D_0 / C_V \varepsilon r$ versus the parameter $\varepsilon n F c_F D_0 / s_R \kappa \Delta \Phi_2$.

capital cost for the separator and electrode volume increases. At high values of $\varepsilon nFc_F D_o / s_R \kappa \Delta\Phi_2$ the total cost depends strongly upon the separator cost factor.

This curve demonstrates a very important point regarding the operation of a flow-through electrode. Up until now, we have assumed that the optimum conditions for the operation of the flow-through electrode will be at the ohmic limit. That is, the most economical operating condition for the flow-through electrode will be at conditions such that the maximum potential difference through the electrode will correspond to the maximum allowable potential drop. This is not always the case, however. Below a certain value of $\varepsilon nFc_F D_o / s_R \kappa \Delta\Phi_2$ one sees that it is most economical not to run the reactor at the ohmic limit. One should instead operate the reactor with a potential difference through the reactor which is lower than the maximum allowable difference, and correspondingly, at a flow rate lower than that determined from the ohmic limit. Physically, below a specific value of $\varepsilon nFc_F D_o / s_R \kappa \Delta\Phi_2$ one cannot economically run the reactor at ohmically limited conditions. To do so requires a flow rate so great that the pumping cost becomes greater than the gain obtained from the higher processing rate.

One can calculate the minimum cost and the value of $\varepsilon nFc_F D_o / s_R \kappa \Delta\Phi_2$ at this point by differentiating Equation (11–2) with respect to this variable and setting the resultant expression to zero. The resulting differentiated expression which must be solved is

$$\frac{d\left[\frac{C_{T,FT}a^2D_o}{C_V\varepsilon}\frac{1}{\tau}\right]}{d\left[\frac{\varepsilon nFc_FD_o}{s_R\kappa\Delta\Phi_2}\right]} = 0 = \left\{\alpha L\left[\frac{1}{A}\right]^{\frac{2}{2-B}}\frac{B}{(2-B)}\left[\frac{Sh}{Pe^2}\right]^{\frac{2B-2}{2-B}}\right.$$

$$+\frac{C_S a}{C_V\varepsilon}\left[\frac{1}{A}\right]^{\frac{1}{2-B}}\left[\frac{Sh}{Pe^2}\right]^{\frac{B-1}{2-B}} - \frac{C_P\rho a^4D_o^3}{C_V\varepsilon^3}\frac{Pe^2}{Sh}\left[\frac{150}{36}Sc\right.$$

$$\left.\left.+\frac{1.75}{6}\frac{(3-B)}{(2-B)}\left[\frac{1}{A}\frac{Pe^2}{Sh}\right]^{\frac{1}{2-B}}\right]\alpha L\right\}\cdot\frac{d\left[\frac{Sh}{Pe^2}\right]}{d\left[\frac{\varepsilon nFc_FD_o}{s_R\kappa\Delta\Phi_2}\right]} \quad (11\text{–}4)$$

The expression for the derivative of the Sherwood Number over the square of the Péclet Number with respect to $\varepsilon nFc_FD_o/s_R\kappa\Delta\Phi_2$ can be obtained from Equation (8–26). This is

$$\frac{d\left[\frac{Sh}{Pe^2}\right]}{d\left[\frac{\varepsilon nFc_FD_o}{s_R\kappa\Delta\Phi_2}\right]} = 1-(1+\alpha L)\cdot e^{-\alpha L}. \quad (11\text{–}5)$$

From Figure 11–1, one can also see that the value of $\varepsilon nFc_FD_o/s_R\kappa\Delta\Phi_2$ at the minimum depends upon the dimensionless ratio of separator cost to volumetric electrode cost. In Figure 11–2 we have solved for the value of $(\varepsilon nFc_FD_o/s_R\kappa\Delta\Phi_2)_{min}$ as a function of the separator area to volumetric electrode cost which gives the minimum electrode cost. We have also shown the dimensionless total cost for this minimum point as a function of this same variable. As expected, the lower the ratio of separator area to volumetric cost, the lower the minimum total electrode cost. Figure 11–2 also shows that as the ratio of the separator area to volumetric electrode cost is decreased the value $(\varepsilon nFc_FD_o/s_R\kappa\Delta\Phi_2)_{min}$ increases. Since the separator must be placed perpendicular to the flow direction, one may tolerate a smaller cross sectional area or higher flowrate and larger ohmic

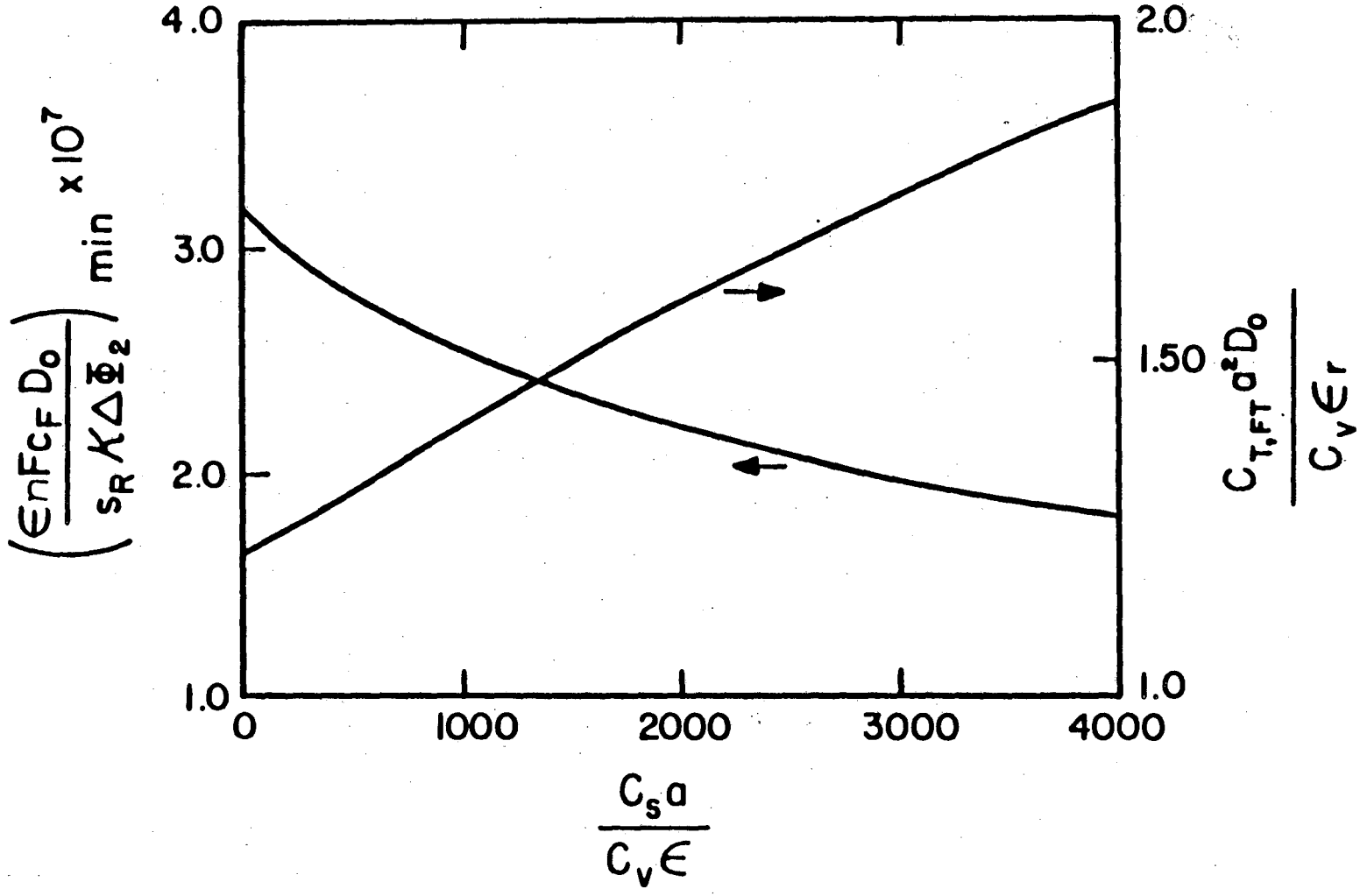

Figure 11–2. Variation in minimum dimensionless total flow–by electrode cost $C_T a^2 D_o / C_V \varepsilon r$ and $\varepsilon n F c_F D_o / s_R \kappa \Delta \Phi_2$ at the minimum cost versus dimensionless separator cost $C_S a / C_V \varepsilon$.

drop for a higher separator cost. Again, the value of $\varepsilon nFc_F D_o / s_R \kappa \Delta\Phi_2$ which gives the lowest flow–through cost is shown in Figure 11–2. It is only economical to run a flow–through electrode at ohmically limited conditions, provided $\varepsilon nFc_F D_o / s_R \kappa \Delta\Phi_2$ is greater than this minimum point.

We now turn to the optimization of the flow-by configuration. As discussed before, while the operating conditions for the flow-by electrode depend upon the parameter $\varepsilon nFc_F D_o / s_R \kappa \Delta\Phi_2$ at fixed conversion, they also depend upon the variable αd. Therefore, for each value of $\varepsilon nFc_F D_o / s_R \kappa \Delta\Phi_2$, one must also optimize the electrode cost over αd. At first, it would seem that the most economical flow–by design must be found by a more complicated process than the one used for the flow–through configuration. Both the value of $\varepsilon nFc_F D_o / s_R \kappa \Delta\Phi_2$ and αd can be varied which affect the total electrode cost. A simplification arises, however. The optimum flow–by electrode design always occurs for the reactor operating at the ohmic limit. That is, at the lowest possible value of $\varepsilon nFc_F D_o / s_R \kappa \Delta\Phi_2$. Therefore, the procedure reduces to a one–dimensional optimization over αd for a fixed $\varepsilon nFc_F D_o / s_R \kappa \Delta\Phi_2$. The minimum electrode cost for any value of $\varepsilon nFc_F D_o / s_R \kappa \Delta\Phi_2$, corresponding to the ohmic limit, is found by differentiating Equation (11–3) with respect to αd and setting this expression to zero. Performing this operation results in the following expression which must be solved

$$\frac{d\left[\frac{C_{T,FB}a^2D_o}{C_V\varepsilon}\frac{1}{r}\right]}{d(\alpha d)} = 0 = \left[\alpha L\left[\frac{1}{A}\right]^{\frac{2}{2-B}}\frac{B}{(2-B)}\left[\frac{Sh}{Pe^2}\right]^{\frac{2B-2}{2-B}}\cdot\frac{d\frac{Sh}{Pe^2}}{d\,\alpha d}\right.$$

$$+\frac{C_S a}{C_V\varepsilon}\frac{\alpha L}{(\alpha d)^2}\cdot\left[\alpha d\left[\frac{1}{A}\right]^{\frac{1}{2-B}}\frac{1}{(2-B)}\left[\frac{Sh}{Pe^2}\right]^{\frac{B-1}{2-B}}\cdot\frac{d\frac{Sh}{Pe^2}}{d\,\alpha d}\right.$$

$$\left.\left.-\left[\frac{1}{A}\frac{Sh}{Pe^2}\right]^{\frac{1}{2-B}}\right]-\frac{C_p\alpha L\rho a^2D_o^2}{\varepsilon^2}\left[\frac{Pe^2}{Sh}\right]^2\left[\frac{150}{36}Sc\right.\right.$$

$$\left.\left.+\frac{1.75}{6}\frac{(3-B)}{(2-B)}\left[A\frac{Pe^2}{Sh}\right]^{\frac{1}{2-B}}\right]\frac{d\left[\frac{Sh}{Pe^2}\right]}{d(\alpha d)}\right. \qquad (11\text{–}6)$$

The expression for the derivative of the ratio of the Sherwood Number to the square of the Péclet Number depends upon the expression chosen for the potential distribution. If the semi–infinite electrode approximation is chosen, then this derivative can be obtained by differentiating Equation (8–19). The resulting expression is

$$\frac{d\left[\frac{Sh}{Pe^2}\right]}{d(\alpha d)} = \frac{\varepsilon nFc_F D_o}{s_R\,\kappa\,\Delta\Phi_2}\left[\frac{\sin\alpha d}{\cos^2\alpha d}+2\sum_{n=0}^{\infty}\left[\frac{1}{\lambda_n^2}-\frac{1}{\lambda_n^2-(\alpha d)^2}\right]\right.$$

$$\left.-4(\alpha d)^2\sum_{n=0}^{\infty}\frac{(-1)^n}{(\lambda_n^2-(\alpha d)^2)^2}\right]. \qquad (11\text{–}7)$$

For the finite length electrode, this derivative is obtained from Equation (8–21)

$$\frac{d\,\frac{Sh}{Pe^2}}{d\,\alpha d} = \frac{\varepsilon n F c_F D_o}{s_R\,\kappa\,\Delta\Phi_2}\left\{2\sum_{n=0}^{\infty}\frac{(-1)^n}{\lambda_n^2}\left[\frac{1}{\tanh\lambda_n R}-\frac{e^{-\alpha L}}{\sinh\lambda_n R}\right]\right.$$

$$+\,2\sum_{n=0}^{\infty}\frac{(-1)^n}{\lambda_n}R\left[\frac{1}{\sinh^2\lambda_n R}-\frac{e^{-\alpha L}}{\sinh\lambda_n R}\,\frac{1}{\tanh\lambda_n R}\right]$$

$$\left.+\,\frac{2}{R}\sum_{n=0}^{\infty}\frac{\hat{\lambda}_n\tanh\hat{\lambda}_n}{\cosh\hat{\lambda}_n}\,\frac{(-1)^n\,e^{-\alpha L}-1}{(\alpha d)^2+\hat{\lambda}_n^2}\,\frac{1}{(1+\delta_{n,0})}\right\}. \qquad (11\text{–}8)$$

It is appropriate to discuss the relevance of Equations (11–7) and (11–8) in comparison to Figure 8–2. Equations (11–7) and (11–8) are related to the slopes of the curves appearing on this figure. They differ only by a factor of $\varepsilon n F c_F D_o / s_R \kappa \Delta\Phi_2$.

We have numerically solved for the optimum value of αd giving the lowest flow-by cost. Equations (11–6) and (11–7) have been used to calculate minimum cost for a semi–infinite flow–by electrode while Equations (11–6) and (11–8) have been used for the finite electrode. In each case, the independent variable is chosen to be $\varepsilon n F c_F D_o / s_R \kappa \Delta\Phi_2$. In Figure 11–3, we have plotted the minimum total flow-by electrode cost as a function of $\varepsilon n F c_F D_o / s_R \kappa \Delta\Phi_2$. Again, we have used the dimensionless separator cost to volumetric cost ratio as a parameter. Two expressions for the ratio of the Sherwood to the Péclet Number and its derivative have been used. This figure shows that the cost of the flow-by electrode depends strongly upon the ratio of separator to volume cost at high values of $\varepsilon n F c_F D_o / s_R \kappa \Delta\Phi_2$, but becomes constant at lower values of this parameter. Unlike the flow-through configuration, there is no minimum point in the cost

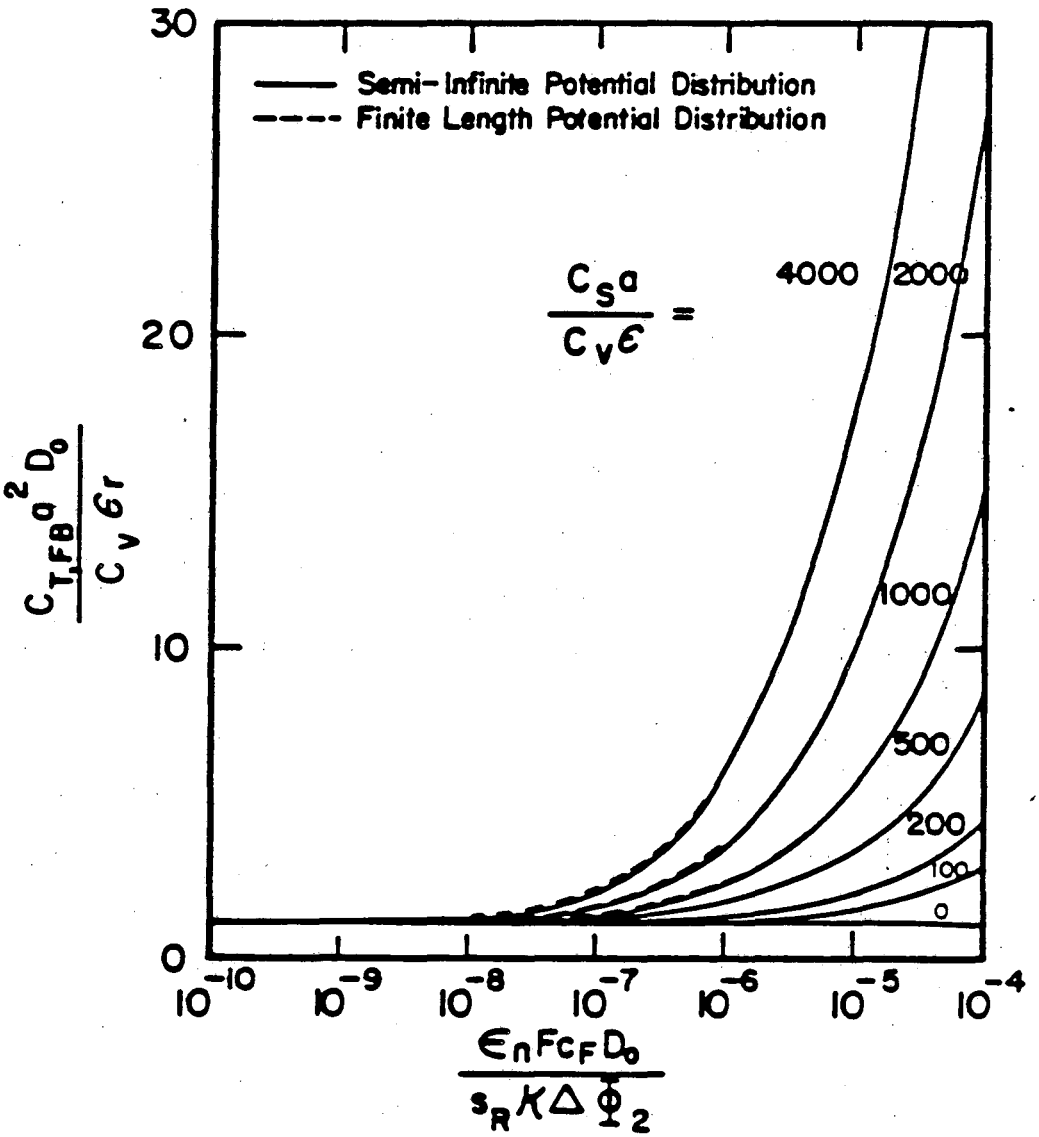

Figure 11–3. Minimum total dimensionless total flow–by electrode cost $C_T a^2 D_0 / C_V \epsilon r$ versus $\epsilon n F c_F D_0 / s_R \kappa \Delta \Phi_2$ given various values of the dimensionless separator cost $C_S a / C_V \epsilon$ for a) semi–infinite electrode, b) finite length electrode.

curve. This substantiates the assertion that the optimum operating conditions always occur at the ohmic limit. One may also see that the minimum cost of the flow–by electrode depends very little upon the assumption made for the electrode geometry, whether it is infinitely long or not.

The optimum value of αd for the minimum flow-by total cost is plotted in Figure 11–4 and 11–5. Figure 11–4 is the optimum αd calculated using the semi–infinite electrode approximation while Figure 11–5 is for a finite length electrode. Again $C_S a / C_V \varepsilon$ is parameter in these curves. These curves show that the optimum value of αd depends upon the approximation for the flow–by electrode geometry at small values of $\varepsilon n F c_F D_o / s_R \kappa \Delta\Phi_2$. At large values of $\varepsilon n F c_F D_o / s_R \kappa \Delta\Phi_2$, the resulting value of αd is the same when calculated from the two expressions. From Figure 11–4 or 11–5 in this region, the value of αd becomes small compared to the assumed value for αL. Thus, the length to width ratio becomes very large. This is exactly the condition where the semi–infinite potential expression is most accurate and hence the two expressions become equivalent. Again, however, the resulting total cost is very insensitive to this choice for any value of $\varepsilon n F c_F D_o / s_R \kappa \Delta\Phi_2$.

From the optimizations presented for each configuration we may now make a comparison to identify the more cost effective configuration. The ratio of the total flow-through cost to the flow-by cost has been plotted versus the value of the separation parameter $\varepsilon n F c_F D_o / s_R \kappa \Delta\Phi_2$ in Figure 11–6. At very low values of $\varepsilon n F c_F D_o / s_R \kappa \Delta\Phi_2$, the optimum flow-by configuration has the lower total cost. In an intermediate region, the flow-through electrode becomes more cost effective. Finally, in the last region, the flow-by electrode configuration again becomes the lower–cost

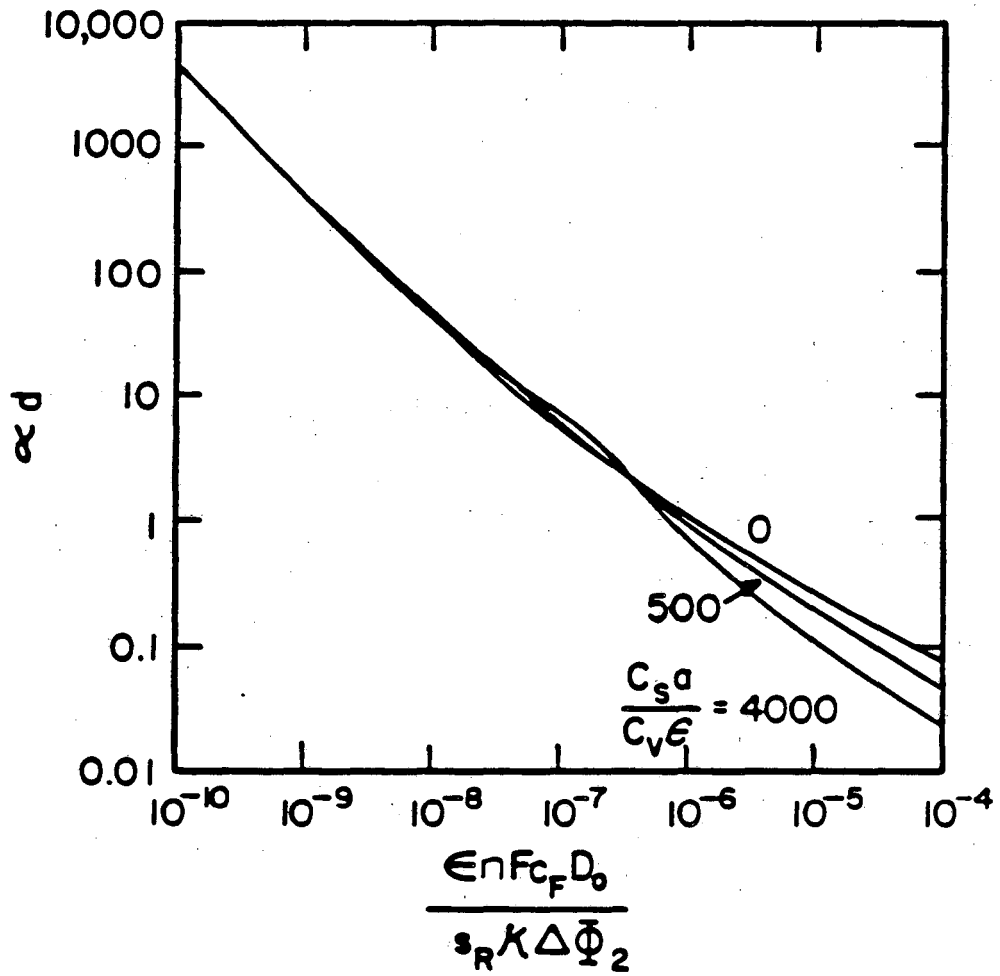

Figure 11–4. Optimum value of αd versus $\epsilon n F c_F D_0 / s_R \kappa \Delta \Phi_2$ for the semi–infinite flow–by electrode. The quantity $C_S a / C_V \epsilon$ is a parameter.

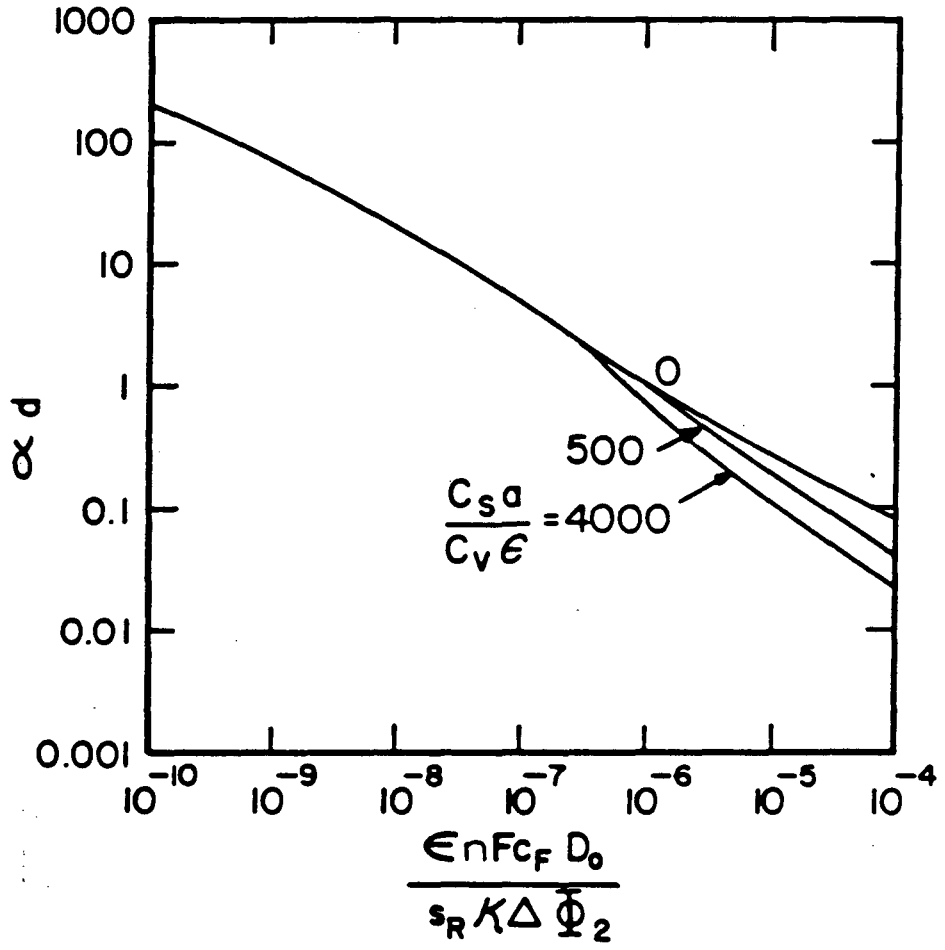

Figure 11–5. Optimum value of αd versus $\varepsilon n F c_F D_o / s_R \kappa \Delta \Phi_2$ for the finite length flow–by electrode. The quantity $C_S a / C_V \varepsilon$ is a parameter.

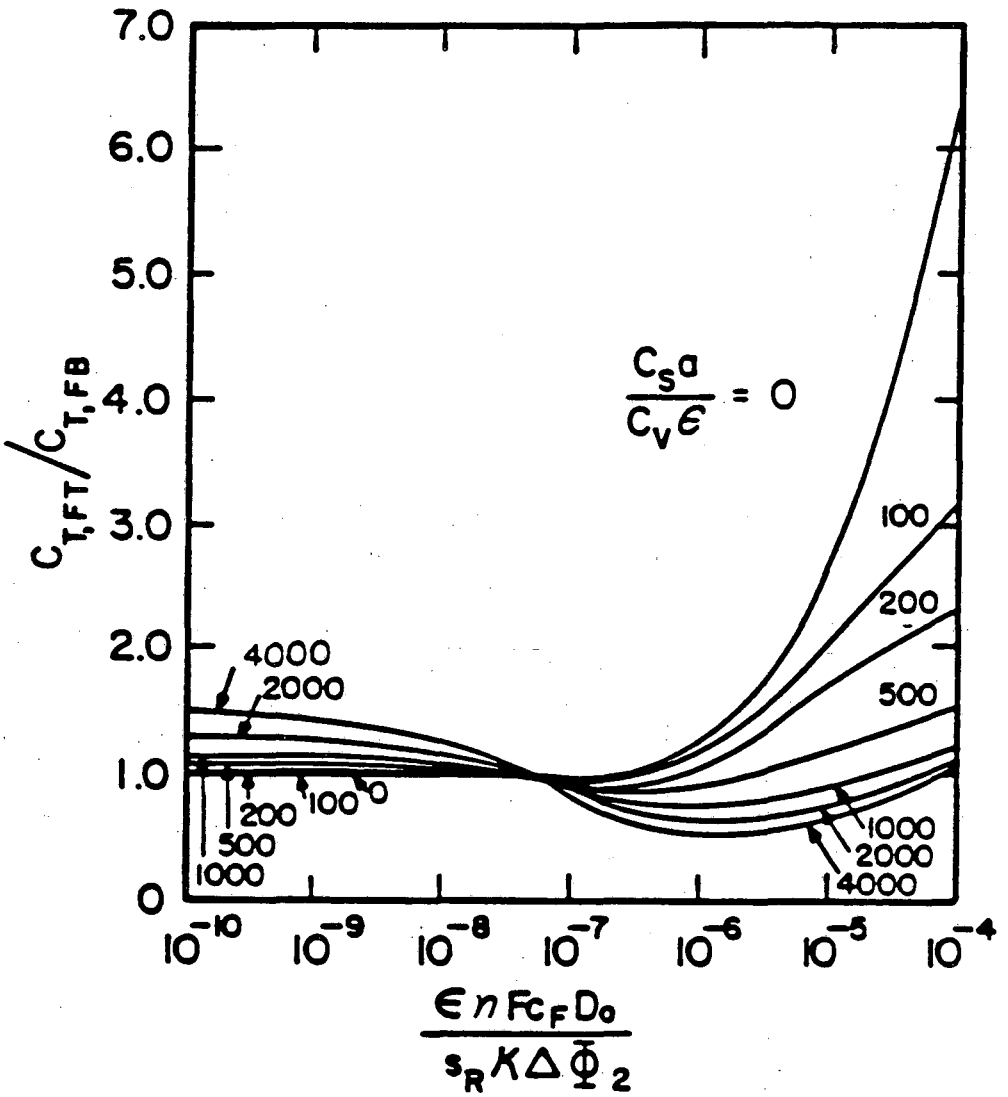

Figure 11–6. Ratio of the total flow–through electrode cost to the total flow–by electrode as a function of $\varepsilon n F c_F D_o / s_R \kappa \Delta \Phi_2$ for various dimensionless separator costs $C_S a / C_V \varepsilon$.

configuration.

The behavior of this curve can be explained from the analysis presented here and the results of Chapter Ten. At very low values of $\varepsilon nFc_F D_o / s_R \kappa \Delta\Phi_2$, the flow–through configuration is constrained by the high cost of pumping. To offset this disadvantage, the optimum flow–through electrode requires a large flow cross section or separator area to balance the pumping cost. The optimum flow cross section becomes so large, and consequently the flow velocity so small, that the flow–through electrode cannot be run at the ohmic limit. This constrains the design of this configuration. In contrast, the low feed concentration is an advantage for the flow–by configuration. The extra variable αd allows he flow–by configuration to operate at the ohmic limit regardless of the value of $\varepsilon nFc_F D_o / s_R \kappa \Delta\Phi_2$. In this region the optimum value of αd becomes very large, much greater than the value of αL Very high values of αd combined with the low value of $\varepsilon nFc_F D_o / s_R \kappa \Delta\Phi_2$ give the flow–by configuration a lower separator cost. While Figure 10–2 shows that the separator area increases as αd becomes large, the decreasing value of $\varepsilon nFc_F D_o / s_R \kappa \Delta\Phi_2$ offsets this increase.

In the intermediate region, the flow–through electrode is preferred primarily because it has a lower separator cost than the flow–by configuration. In this region the optimum αd is near one. Figure 10–2 shows that in this region the separator cost reaches a relative maximum. When combined with the values of $\varepsilon nFc_F D_o / s_R \kappa \Delta\Phi_2$, the separator cost is greater for the flow–by configuration than for the flow–through configuration.

In the last region, the flow–by electrode again becomes the lower–cost configuration. In this region, the lower volume and separator costs give the

flow–by configuration an advantage. Again, Figure 10–2 and 10–3 show that the separator cost and the volumetric cost for the flow–by electrode decrease relative to the flow–through cost for small as αd.

Figure 11–4 or 11–5 also is useful for determining the aspect ratio R of the cost–optimum flow–by electrode. Since the value of αL has been fixed in the optimization, the aspect ratio can be determined from the ratio of αL to αd. The curve in Figure 11–4 or 11–5 shows that while at high values of $\varepsilon n F c_P D_o / s_R \kappa \Delta\Phi_2$ the optimum value of αd depends upon the approximation made for the electrode length, in general the aspect ratio increases as $\varepsilon n F c_P D_o / s_R \kappa \Delta\Phi_2$ increases. Thus narrow flow–by electrodes are preferred for feeds with high concentrations. As the concentration of the reactant decreases, the optimum flow–by design requires a progressively wider and shorter electrode.

From a practical point of view, the flow-through electrode may be cheaper to construct because it may be possible to eliminate the separator from the design. In the flow-through configuration, the fluid streams enter the cell, immediately separate, and flow in different directions. If no separator is present, then the two streams can mix if the products of the two electrodes can diffuse against the fluid flow. In the flow-by configuration, however, the products need only diffuse perpendicularly to the fluid flow. Thus it appears likely that a barrier impermeable to fluid flow is needed more in this design if separate anolyte and catholyte streams are desired. This reason makes the flow–by configuration much more dependent on a separator for a high separation efficiency. Natural convection may also be an important consideration in both design if sufficiently large density gradients are produced. If this occurs, then mixing of the two streams will

be much more likely to occur. Separators may then be required for each design. The flow–through configuration, then, may not have an appreciable advantage.

Figures 11–7, 11–8, and 11–9 compare the cost of a flow-by electrode with a separator to the cost of a flow-through electrode without a separator. Each figure presented gives a different separator cost for the flow-by configuration. While the elimination of the separator may reduce the cost based on superficial area, it may not totally eliminate such a cost. We therefore have plotted several curves representative of a low flow-through separator cost relative to the cost for the separator in the flow-by configuration. These curves show that, at higher values of the parameter $\varepsilon nFc_P D_o / s_R \kappa \Delta\Phi_2$, the reduced flow-through separator cost makes the flow-through configuration much more attractive. At lower values of this parameter, however, the flow-by electrode still remains cheaper. The flow-by electrode retains this superiority despite its higher separator cost per unit area.

These results are generally in agreement with the work of Trainham and Newman.[68] Their comparison was much more specific and considered the case where the electrical energy to provide the faradaic reaction dominated operating costs. In addition, their study included operation of the electrodes below the limiting current. While the differences between these two studies are apparent, the general trends predicted by the two models are very similar. Both models predict a distinct advantage for the flow–by configuration for processes with high feed concentrations. Also, each study predicts that long, narrow flow–by electrodes are preferred for these conditions. Thus, one may conclude that the flow–by electrode is generally

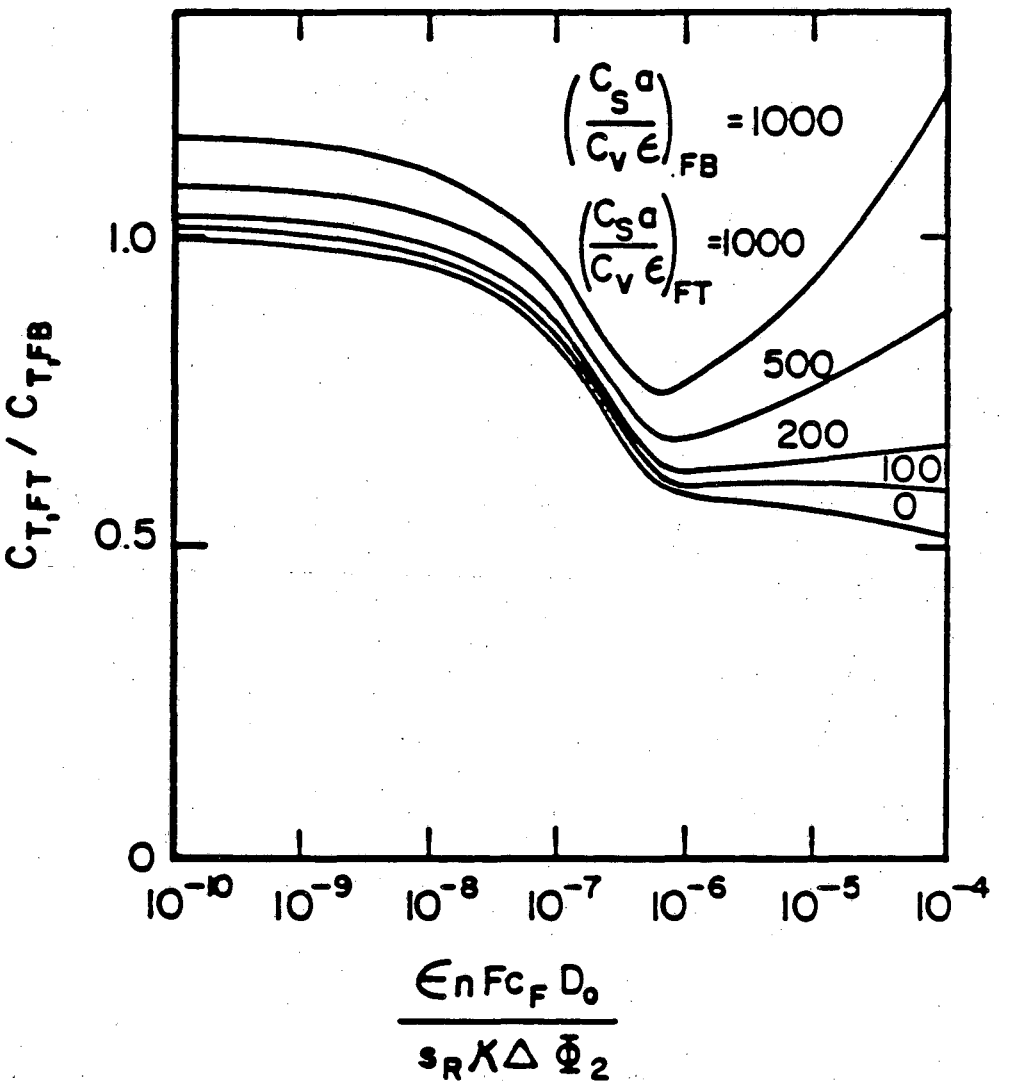

Figure 11–7. Ratio of total flow–through electrode cost to total flow–by electrode cost as a function of $\epsilon n F c_F D_o / s_R \kappa \Delta \Phi_2$. Dimensionless flow–by separator cost is equal to 1000. Dimensionless flow–through separator cost is a parameter.

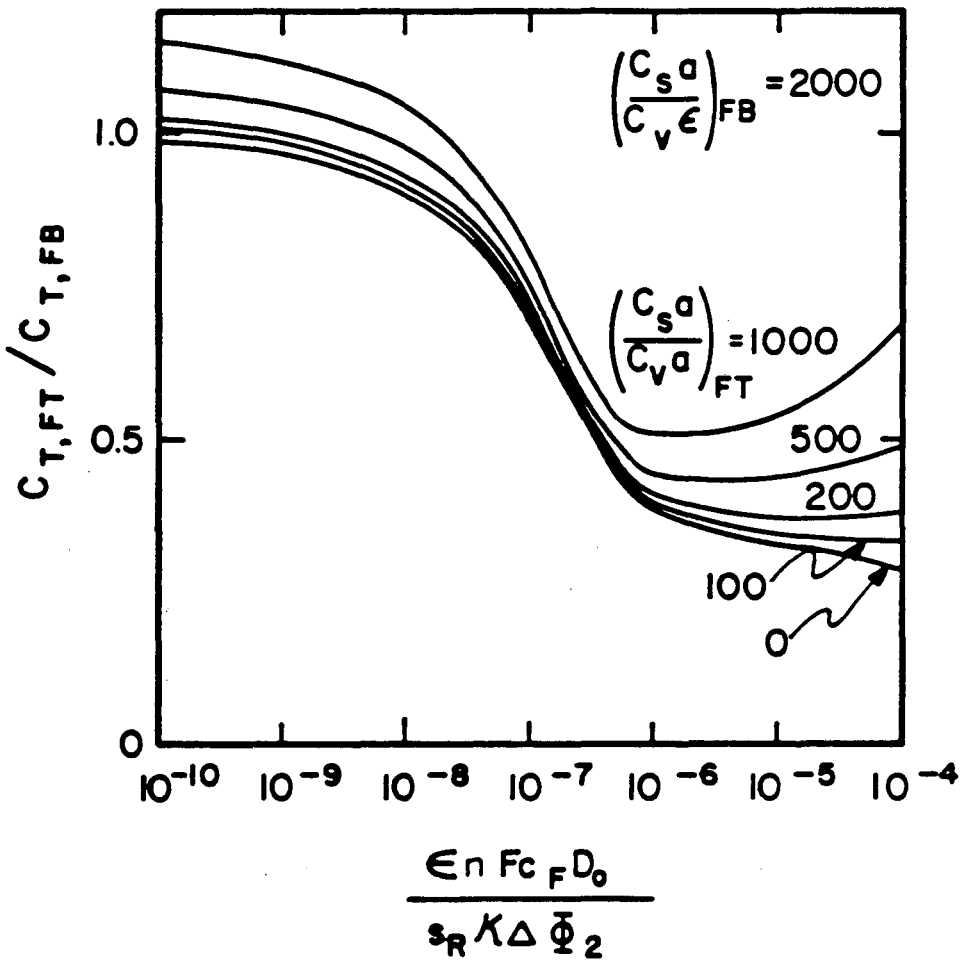

Figure 11–8. Ratio of total flow–through electrode cost to total flow–by electrode cost as a function of $\varepsilon n F c_F D_0 / s_R \kappa \Delta \Phi_2$. Dimensionless flow–by separator cost is equal to 2000. Dimensionless flow–through separator cost is a parameter.

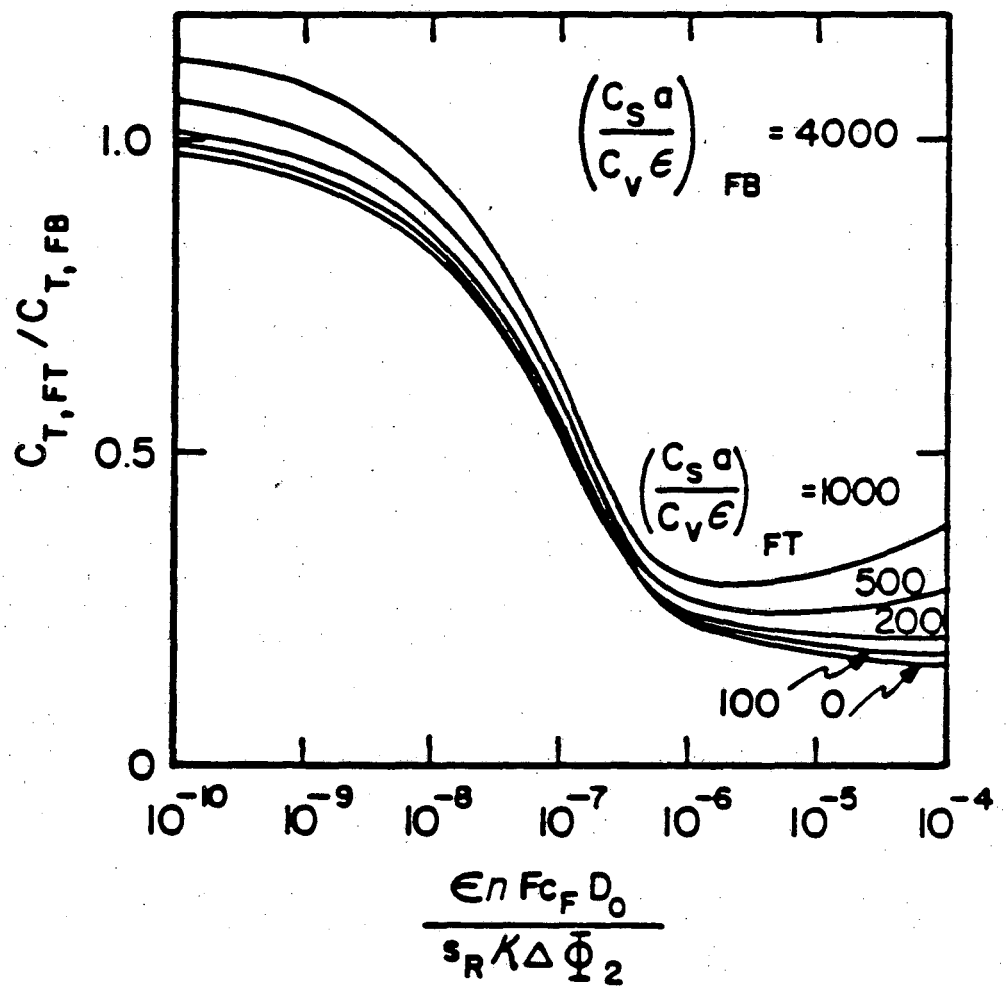

Figure 11–9. Ratio of total flow–through electrode cost to total flow–by electrode cost as a function of $\epsilon n F c_F D_0 / s_R \kappa \Delta \Phi_2$. Dimensionless flow–by separator cost is equal to 4000. Dimensionless flow–through separator cost is a parameter.

superior for processes with high feed concentrations. The flow–through electrode, however, is useful for processing lower feed concentrations and can be less expensive than the flow–by configuration under these conditions.

One may wonder how the economic optimization presented here is related to the comparison of the two configurations based on their maximum potential drops. Again, the ohmic drop comparison required electrodes with the same dimensions and flow–rates. Also, the cost of the separator was not included in this optimization. The results of Chapter Nine showed that the optimum configuration could be distinguished using only the variable αd or R for a given conversion. From this chapter, one can see that considering the cost of the separator considerably alters the results of the comparison. The results presented here show that the choice of the optimum electrode depends upon the conversion, as well as the feed conditions and the cost of the separator. An equivalent relationship delineating the optimum configuration involving only αd cannot be produced.

The flow–through and flow–by configurations have been compared in this chapter by comparing the minimized sum of operating and capital costs. Capital costs consisting of volumetric electrode cost and separator area cost have been included. The cost for pumping energy is the only operating cost considered in the optimization. The cost of electrical energy needed to provide the faradaic reaction has been neglected. This assumption is justified provided the solutions contain only dilute concentrations of reactants where such a cost is secondary. The results of the optimization show that neither the flow–by nor the flow–through configuration is

preferred for all operating conditions.

Chapter 12

Summary

In this thesis, we have examined the flow–through and flow–by electrodes to determine the preferred configuration. We have shown, that there are several different ways to compare these two configurations. Figures 12–1 and 12–2 illustrate the procedure developed for these comparisons and summarize all of this work.

The comparison starts in the upper right hand corner. As given information, the conversion αL and the separation factor or dimensionless concentration $\varepsilon n F c_F D_0 / s_R \kappa \Delta\Phi_2$ have been assumed. These two quantities were always assumed to be known whenever the two configurations were compared. One progresses through the flow–chart from top to bottom, branching at the diamond shaped decision points. Needed calculations are represented by the rectangles. These figures also refer to key equations and figures presented in previous chapters. The result of the comparison is the configuration which has the lower cost satisfying the constraints on the design.

In Chapter Nine, the two electrode configurations were compared on the basis of the lower maximum potential drop. If the electrode with the lower total cost was to be found by this comparison, two restrictive conditions were required. First, equal electrode dimensions and feed flowrates were assumed for each configuration. Second, no costs based on the separator area could be included in the comparison. If these two conditions were satisfied, then Figure 9–1 could be used to determine the less expensive configuration.

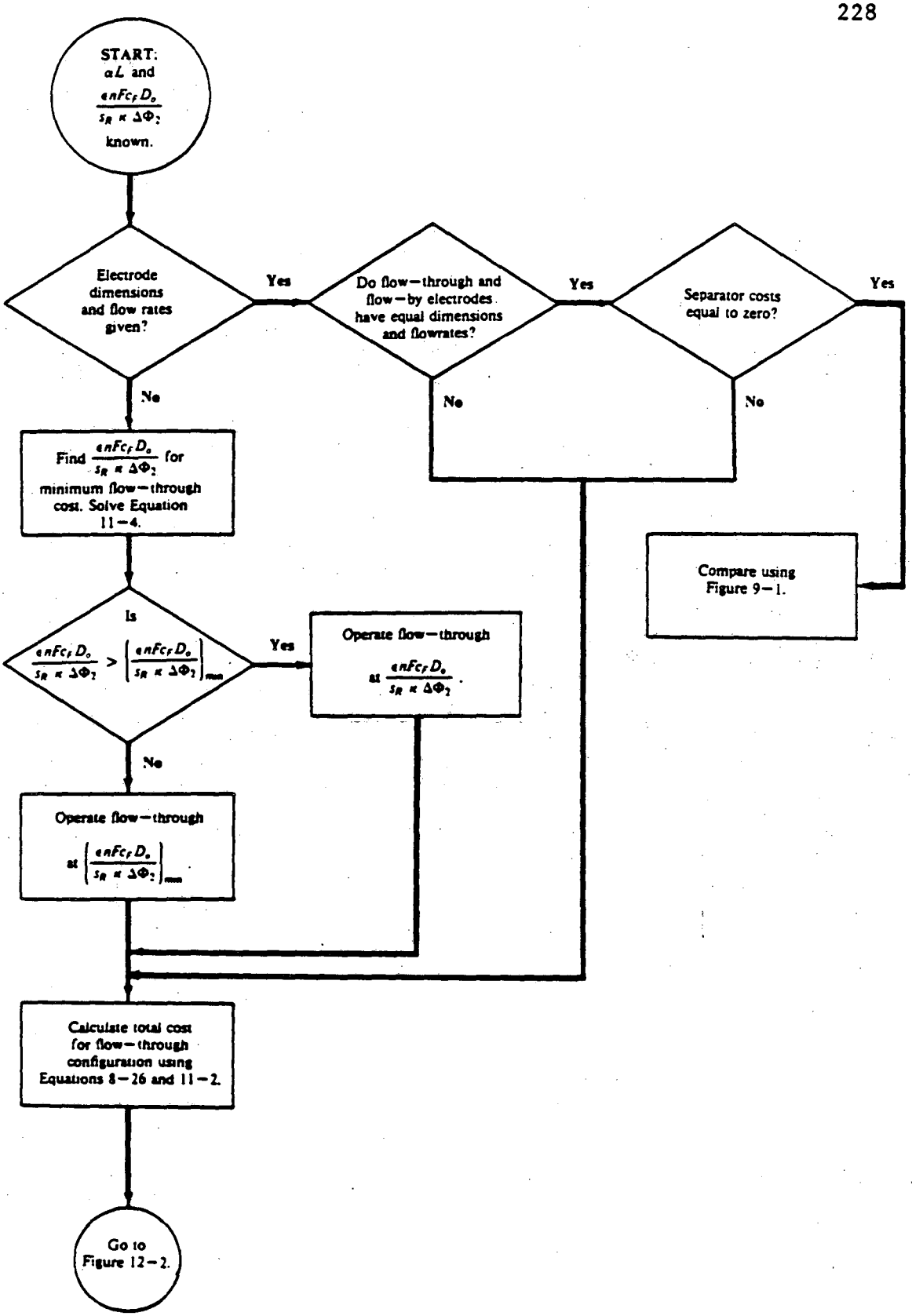

Figure 12-1 Flowchart for cost comparison of flow-through and flow-by configurations, part A.

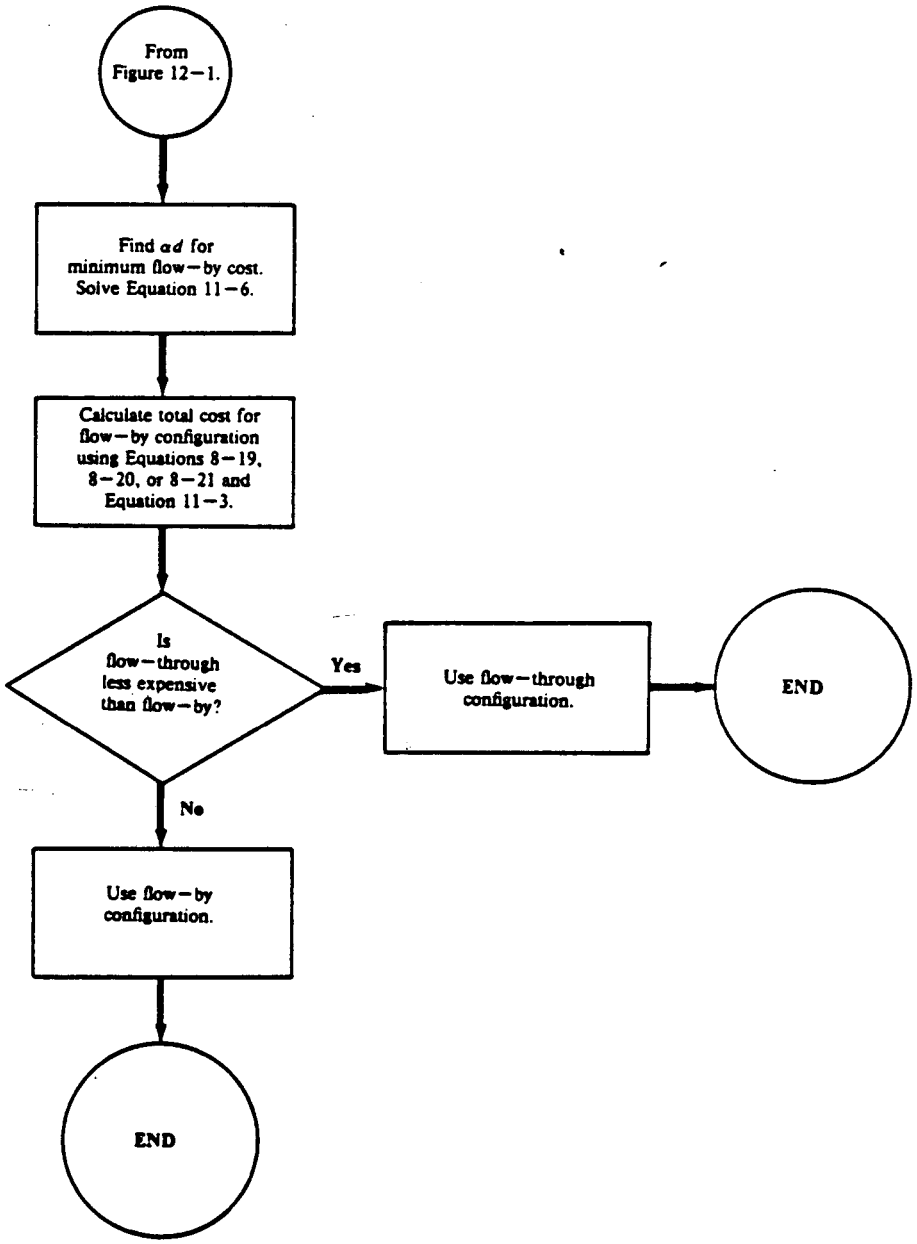

Figure 12−2 Flowchart for cost comparison of flow−through and flow−by configurations, part B.

The somewhat unrealistic assumptions in the above comparison were then relaxed. Chapter Ten developed the general cost equations applicable to each configuration. The restriction of no costs dependent upon the separator area was removed. Provided one still knew the dimensions of each electrode, the given cost factors, and the feed flowrates, the less expensive electrode configuration could now be found.

Finally, Chapter Eleven presented the most general comparison. Here, the least expensive possible flow–through electrode was compared to the least expensive flow–by electrode. The two electrodes were optimized using an objective function consisting of volumetric electrode capital costs, separator capital costs, and pumping operating costs. The optimum operating conditions for the flow–by and the flow–through configuration were then found. An example considered the optimization of the two configurations for single conversion. Equal volumetric cost factors and pumping cost factors were assumed. However, the separator cost factor was parametrized, and the influence of the separator cost was examined.

Chapter 13

Conclusions

The two–dimensional potential distribution for a flow–by porous electrode of infinite length to width ratio operating at the limiting current has been derived. It is shown that the maximum solution phase potential drop depends primarily on the ratio of the electrode width and the penetration depth, αd. The potential drop for practical flow–by designs depends only weakly upon the length to width ratio. This result has been compared to the potential drop for a finite length electrode given by Fedkiw and the one–dimensional potential drop of Alkire and Ng.

The flow–through and flow–by electrode configurations have been compared at the limiting current using the maximum solution phase potential difference as a basis for comparison. This comparison is independent of any specific mass–transfer coefficient correlation. Criteria delineating the optimum electrode configuration have been given which depend upon the reactant conversion. At low conversion a flow–by electrode is favorable providing that it can be constructed with a length to width ratio greater than one. At high conversions, however, a flow–by electrode is favorable if the ratio of the electrode width and penetration depth is less than 2.218.

A method for determining the cost optimum design of flow–through or flow–by porous electrodes also has been developed. Optimization of these two configurations was performed for fixed values of the conversion and fixed dimensionless maximum potential drop. Each electrode was optimized with respect to the sum of operating costs and capital costs. Capital costs

consisted of a volumetric electrode cost and a separator cost while pumping was the only operating cost considered. Results from this optimization for equal flow–through and flow–by separator costs show that the the optimum electrode configuration depends upon the the dimensionless group $\varepsilon nFc_F D_o / s_R \kappa \Delta\Phi_2$ and the dimensionless separator cost. For very low and high values of the parameter $\varepsilon nFc_F D_o / s_R \kappa \Delta\Phi_2$, the flow–by electrode is preferred. The flow–through electrode is preferred for an intermediate range of this parameter. A flow–through electrode without a separator has been compared to a flow–by electrode with a separator. The flow–through configuration becomes preferable for a greater range of $\varepsilon nFc_F D_o / s_R \kappa \Delta\Phi_2$ and separator cost, but the flow–by electrode still is preferred under many conditions.

List of Symbols for Chapters Seven through Thirteen

English Characters

a	specific interfacial surface area, cm^2/cm^3
A	constant in Sherwood number relationship, Equation (10–5)
A_c	cross sectional area to flow for flow-through electrode, cm^2
A_s	surface area of separator in flow-through or flow-by electrode, cm^2
B	exponent in Sherwood number relationship, Equation (10–5)
c	pore averaged concentration, mol/cm^3
C_P	pumping cost factor, \$/J
C_S	separator cost factor, $\$/cm^2$
C_T	total electrode cost per volume of feed, $\$/cm^3$
C_V	volumetric electrode cost factor, $\$/cm^3$
d	flow–by electrode bed width perpendicular to fluid–flow direction, cm
D_o	free stream diffusion coefficient of reacting species, cm^2/s
F	Faraday constant, 96,485 coulombs/equiv
G	constant equal to $nFak_m c_F / s_R \kappa$, V/cm^2
i_2	superficial current density for electrolyte phase, A/cm^2
j	transfer current density, A/cm^3
k_m	mass transfer coefficient, cm/s
L	bed depth in direction of fluid flow, cm
M	arbitrary species
n	number of electrons transferred in reaction

Q	volumetric flow rate of feed, cm^3/s
Pe	Péclet number, v / aD_e
r	factor accounting for interest, depreciation, and taxes on capital equipment, s^{-1}
R	bed aspect ratio, L / d
Sc	Schmidt Number, ν / D_e
Sh	Sherwood number, $\varepsilon k_m / aD_e$
s_R	stoichiometric coefficient of reactant
v	superficial fluid velocity, cm/s
V	reference potential of flow–by electrode at $y = d$, V
V_e	volume of flow-through or flow-by electrode, cm^3
z	charge number, equiv/mol

Greek Characters

α	reciprocal of penetration length, ak_m / v, cm^{-1}
$\Delta\mathcal{P}$	dynamic pressure drop across electrode, Pa
$\Delta\Phi_2$	maximum allowable solution potential drop, V
ε	bed porosity or void fraction
κ	conductivity of fluid phase in bed, $(\Omega\text{–cm})^{-1}$
λ	dimensionless eigenvalue defined in Equation (7–18)
$\hat{\lambda}$	dimensionless eigenvalue defined in Equation (7–23)
Φ_2	solution potential, V
ρ	fluid density, g/cm^3
ν	kinematic viscosity of fluid, cm^2/s

Subscripts

i	species number
n	eigenvalue number
F	feed condition
FB	for the flow–by configuration
FT	for the flow–through configuration
L	exit condition
min	at the minimum cost

Superscripts

A	solution to Equation (G–10)
B	solution to Equation (G–19)

References

(1) Erik Rosén, "Calculation for the Gasification of Spent Cooking Liquors," *Svensk. Kem. Tidskr.*, **76**, 195-198 (1964).

(2) Richard W. Garner and William B. White, "Growth of Cinnabar (HgS) from Sodium Sulfide–Sulfur Fluxes," *J. Cryst. Growth*, **7**, 343–347 (1970).

(3) Elton J. Cairns, "Secondary Batteries–New Batteries: High Temperature," in *Comprehensive Treatise in Electrochemistry*, J. O'M. Bockris *et al.*, eds., Plenum Press, New York, 341–368 (1981).

(4) Charles Tobias and others, *Assessment of Research Needs for Advanced Battery Systems*, Report of the Committee on Battery Materials Technology to the National Materials Advisory Board, Commission on Engineering Technical Systems, National Research Council, NMAB-390, National Academy Press, Washington, D.C. (1982).

(5) Elton J. Cairns and Earl Heitbrink, "Electrochemical Power for Transportation," in *Comprehensive Treatise of Electrochemistry*, J. O'M Bockris *et al.*, eds., Plenum Press, New York, 421-498 (1981).

(6) Lynn S. Marcoux and Eddie T. Seo, "Sodium–Sulfur Batteries," in *New Uses of Sulfur*, James R. West, ed., ACS Press, Washington, 216-225 (1975).

(7) Nirmal K. Gupta and Ragnar P. Tischer, "Thermodynamic and Physical Properties of Molten Sodium Polysulfides from Open–Circuit Voltage Measurements," *J. Electrochem. Soc.*, **119**, 1033-1037 (1972).

(8) J. T. Kummer and N. Weber, *Proc. Power Sources Conf.*, **21**, 37 (1967).

(9) J. T. Kummer and N. Weber, "A sodium–sulfur secondary battery," presented at SAE Automotive Engineering Conference, Detroit, Michigan, Preprint No. 670179, January 9-13, 1967.

(10) Ford Sodium Sulfur Battery, EVEM–1 Bench Test Review, July 18–19, 1983.

(11) Lutgard C. De Jonghe, "Transport Number Gradients and Solid Electrolyte Degradation," *J. Electrochem Soc.*, **129**, 752–755 (1982).

(12) George Brauer, *Handbook of Preparative Inorganic Chemistry*, Second Edition, Vol. 1, Academic Press, New York, 350–367, (1963–1965).

(13) Erik Rosén and Ragnar Tegman, "A Preparative and X–Ray Powder Diffraction Study of the Polysulfides Na_2S_2, Na_2S_4, Na_2S_5," *Acta Chem. Scand.*, **25**, 3329–3336 (1971).

(14) B. Cleaver, A. J. Davies, and M. D. Hames, "Properties of Fused Polysulfides–I. The Electrical Conductivity of Fused Sodium and Potassium Polysulfides," *Electrochim. Acta*, **18**, 719–726 (1973).

(15) B. Cleaver, and A. J. Davies, "Properties of Fused Polysulfides–II. The Density, Surface Tension and Viscosity of Fused Sodium Polysulfides," *ibid.*, **18**, 727–732 (1973).

(16) B. Cleaver, and A. J. Davies, "Properties of Fused Polysulfides–III. *EMF* Measurements on the Sodium–Sulfur Cell, and Sulfur Activities and Constitution in Fused Sodium Polysulfides," *ibid.*, **18**, 733-739 (1973).

(17) Ragnar Tegman, "Thermodynamic Studies of High Temperature Equilibria," *Chemica Scripta*, **9**, 158–166 (1976).

(18) A. Rule and J. S. Thomas, *J. Chem. Soc.*, 1063 (1917).

(19) T. G. Pearson and P. L. Robinson, "The Polysulfides of the Alkali Metals. Part I. Sodium(i).," *J. Chem Soc.*, 1473–1497 (1930).

(20) Djong–Gie Oei, "The Sodium–Sulfur System. I. Differential Thermal Analysis," *Inorganic Chemistry*, **12**, 435–437 (1973).

(21) Erik Rosén and Ragnar Tegman, "Solid, Liquid, and Gas Phase Equilibria in the System Sodium Monosulfide–Sodium Polysulfide–Sulfur," *Chemica Scripta*, **2**, 221–225 (1972).

(22) K. Freidlich, *Metall. Erz*, **88** (1914).

(23) T. Yoshida and K. Nakajima, "Behavior of S_x^{2-} Species in Molten Sodium Polysulfide," *J. Electrochem. Soc.*, **128**, 1–6 (1981).

(24) Ragnar P. Tischer and Frank A. Ludwig, "The Sulfur Electrode in Nonaqueous Media," in *Advances in Electrochemistry and Electrochemical Engineering*, Vol. 10, Heinz Gerischer and Charles Tobias, eds., John Wiley and Sons, New York, 391–482 (1977).

(25) R. D. Armstrong, T. Dickenson, and M. Reid, "Rotating Disc Studies of the Vitreous Carbon–Sodium Polysulfide Interface," *Electrochim. Acta*, **20**, 709–714 (1975).

(26) K. D. South, J. L. Sudworth, and G. Gibson, "Electrode Processes in Sodium Polysulfide Melts," *J. Electrochem. Soc.*, **119**, 554–558 (1972).

(27) J. Divisek *et al.*, "Mass Transport Phenomena in the Molten Sulfur–Sodium Polysulfide System," *ibid.*, **127**, 357–363 (1980).

(28) L. Nanis and I. Klein, "Transient Mass Transfer at the Rotating Disk," *ibid.*, **119**, 1683–1687 (1972).

(29) R. D. Armstrong, T. Dickenson, and M. Reid, "Alternating Current Impedance Measurements of the Vitreous Carbon/Sodium Polysulfide

Interphase at 350°C," *Electrochim. Acta*, **21**, 935–942 (1976).

(30) Djong–Gie Oei, "The Sodium–Sulfur System. II. Polysulfides of Sodium," *Inorg. Chem.*, **12**, 438–441 (1973).

(31) G. J. Janz *et al.*, "Raman Studies of Sulfur–Containing Anions in Inorganic Polysulfides. Sodium Polysulfides," *ibid.*, **15**, 1759–1763 (1976).

(32) F. G. Bodewig and James A. Plambeck, "Electrochemical Behavior of Sulfide in Fused LiCl–KCl Eutectic," *J. Electrochem. Soc.* **116**, 607–611 (1969).

(33) B. Cleaver, A. J. Davies, and D. J. Schiffrin, "Properties of Fused Polysulfides V. Voltametric Studies on Sulfur and Polysulfides in Fused KSCN and LiCl–KCl Eutectic," *Electrochim. Acta*, **18**, 747–776 (1973).

(34) B. Cleaver and A. J. Davies, "Properties of Fused Polysulfides IV. Cryoscopic Studies on Solutions of Alkali Metal Polysulfides in Potassium Thyocyanate," *ibid.*, **18**, 741–745 (1973).

(35) J. G. Gibson, "The distribution of potential and electrochemical reaction rate in molten polysulfide electrodes," *J. Appl. Electrochem.*, **4**, 125–134 (1974).

(36) J. Euler and W. Nonnenmacher, "Stromverteilung in porösen Electroden," *Electrochim. Acta*, **2**, 268–286 (1960).

(37) M. P. J. Brennan, "An Equivalent Circuit Method For the Sulfur Electrode Modelling," *ibid.*, **24**, 473–476 (1979).

(38) M. W. Breiter and B. Dunn, "Potential distribution model for rechargeable sulfur electrodes in sodium sulfur cells," *J. Appl. Electrochem.*, **9**, 291–299 (1979).

(39) Y. K. Kao and P. C. Wayner, Jr., "The Effect of Nonuniform Concentration on the Distribution and Reaction Rate in Molten Polysulfide Electrodes," *J. Electrochem. Soc.*, **124**, 632–638 (1976).

(40) Y. K. Kao and P. C. Wayner, Jr., "The Transient Response of the Sulfur/Polysulfide Electrode Based on a Varying Concentration Model," *ibid.*, **124**, 230–236 (1977).

(41) Richard Pollard and John Newman, "Mathematical Modeling of the Lithium–Aluminum, Iron Sulfide Battery I. Galvanostatic Discharge Behavior," *ibid.*, **128**, 491–502 (1981).

(42) Richard Pollard and John Newman, "Mathematical Modeling of the Lithium–Aluminum, Iron Sulfide Battery II., The Influence of Relaxation Time on the Charging Characteristics," *ibid.*, **128**, 503–507 (1981).

(43) John Newman, Douglas Bennion, and Charles Tobias, "Mass Transfer in Concentrated Binary Electrolytes," *Berichte der Bunsengesellschaft für physikalische Chemie*, **68**, 608–612 (1965). [For corrections see *ibid.*, **70**, 493 (1966).]

(44) John Newman, *Electrochemical Systems*, Prentice Hall, Englewood Cliffs, 239–253 and 266–275 (1973).

(45) J. O. Hirschfelder, C. F. Curtis, and R. B. Bird, *Molecular Theory of Gasses and Liquids*, John Wiley and Sons Inc., New York, 714 (1954)

(46) John Newman, private communication, May 1982.

(47) G. J. Janz *et al.*, "Raman Studies of Sulfur–Containing Anions in Inorganic Polysulfides. Barium Trisulfide," *Inorg. Chem.*, **15**, 1751–1754 (1976).

(48) G. J. Janz *et al.*, "Raman Studies of Sulfur–Containing Anions in Inorganic Polysulfides. Potassium Polysulfides," *ibid.*, **15**, 1755–1758 (1976).

(49) *JANAF Thermochemical Tables*, D. R. Stull, H. Prophet, eds., Second Edition, NSRDS–NBS 37, (1971).

(50) Richard Pollard and John Newman, "Transport Equations for a Mixture of Two Binary Molten Salts in a Porous Electrode," *J. Electrochem. Soc.*, **126**, 1713–1717 (1979).

(51) Peter N. Pintauro, *Mass Transfer of Electrolytes in Membranes*, Dissertation, University of California, Los Angeles (1980).

(52) R. B. Bird, W. E. Stewart, and E. N. Lightfoot, *Transport Phenomena*, John Wiley and Sons Inc., New York, p. 510 (1960).

(53) S. Gladstone, K. J. Laidler, H. Eyring, *Theory of Rate Processes*, McGraw–Hill, New York, Chapter IX (1941).

(54) J. C. M. Li and P. Chang, "Self Diffusion Coefficient and Viscosity in Liquids," *J. Chem. Phys.*, **23**, 518–520 (1955).

(55) C. R. Wilke and P. Chang, "Correlations of Diffusion Coefficients in Dilute Solutions," *AIChE J.*, **1**, 264 (1955).

(56) B. Levich, "The Theory of Concentration Polarization," *Acta Physiochimica U.R.S.S.*, **17**, 257–307 (1942).

(57) H. A. Laitinen and I. M. Kolthoff, "A Study of Diffusion Processes by Electrolysis with Microelectrodes," *J. Amer. Chem. Soc.*, **61**, 3344 (1939).

(58) John Newman and Thomas W. Chapman, "Restricted Diffusion in Binary Solutions," *AIChE J.*, **19**, 343–348 (1973).

(59) L. Nanis, M. Litt, and J. Chen, "An Improved Model for Capillary Diffusion with no External Stirring," *J. Electrochem. Soc.*, **12**, 509–512 (1973).

(60) John Newman, *Electrochemical Systems*, Prentice Hall, Englewood Cliffs, 272–274 (1973).

(61) John Newman, private communication, December, 1981.

(62) H. S. Harned and D. M. French, "A Conductance Method for the Determination of the Diffusion Coefficients of Electrolytes," *Annals New York Acad. Sci.*, **46**, 267 (1945).

(63) R. A. Robinson and R. H. Stokes, *Electrolyte Solutions*, Butterworths, London, Revised Second Edition, 253–283 (1965).

(64) Kemal Nisancioglu and John Newman, "Diffusion in Nitric Acid Solutions," *AIChE Journal*, **19**, 797–801 (1973).

(65) John Newman, *Chemical Engineering 256 Advanced Transport Class Notes*, Department of Chemical Engineering, University of California, Berkeley, California, Chapter 11.

(66) Douglas Bennion and John Newman, "Electrochemical removal of copper ions from very dilute solutions," *J. Appl. Electrochem.*, **2**, 113–122 (1972).

(67) J. L. Fitzjohn, "Electro–organic Synthesis," *Chemical Engineering Progress*, 71, 85–91 (1975).

(68) James A. Trainham and John Newman, "A Comparison Between Flow–Through and Flow–By Porous Electrodes For Redox Energy Storage," *Electrochim. Acta*, **26**, 455–469 (1981).

(69) Jan Robert Selman, *Measurement and Interpretation of Limiting Currents*, Dissertation, No. UCRL–20557, University of California,

Berkeley (June 1971).

(70) James A. Trainham and John Newman, "The Effect of Electrode Placement and Finite Matrix Conductivity on the Performance of Flow–Through Porous Electrodes," *J. Electrochem. Soc.*, **125**, 58–68 (1978).

(71) Richard Alkire and Brian Gracon, "Flow–Through Porous Electrodes," *ibid*, **122**, 1594–1601 (1975).

(72) James A. Trainham and John Newman, "A Flow–Through Porous Electrode Model: Applications to Metal–Jon Removal from Dilute Streams," *ibid*, **124**, 1528–1539 (1977).

(73) Peter Fedkiw, "Ohmic Potential Drop in Flow–Through and Flow–By Porous Electrodes," *ibid*, **128**, 831–838 (1980).

(74) R. Pollard, and J. A. Trainham, "Analysis of The Flow-Through Porous Trielectrode Reactor, *ibid*, **130**, 1531–1535 (1983).

(75) Richard Alkire and Patrick Ng, "Two–Dimensional Current Distribution Within a Packed–Bed Electrochemical Flow Reactor," *ibid*, **121**, 95–103 (1974).

(76) Richard Alkire and Patrick Ng, "Studies on Flow–By Porous Electrodes Having Perpendicular Directions of Current and Electrolyte Flow," *ibid*, **124**, 1220–1227 (1977).

(77) John Newman and William Tiedemann, "Flow-through Porous Electrodes," *Advances in Electrochemistry and Electrochemical Engineering*, Vol. 11, Heinz Gerischer and Charles Tobias, eds., Wiley Interscience, New York, 353–438 (1978).

(78) Peter S. Fedkiw and John Newman, "Mass–Transfer Coefficients in Packed Beds at Very Low Reynolds Numbers," *Int. J. Heat Mass Transfer*, **25**, 935-943 (1982).

(79) R. Byron Bird, Warren E. Stewart, and Edwin N. Lightfoot, *Transport Phenomena*, John Wiley, New York, 200 (1960).

(80) John Newman, *Electrochemical Systems*, Prentice Hall, Englewood Cliffs, 43 (1973).

Appendix A

Binary Composition Conventions

For a polysulfide melt composed of nonstoichiometric amounts of sodium and sulfur, the composition of the melt can be described by a number of conventions. We consider the melt here to be pseudo–binary compound composed of three distinct species. The melt can be described by considering anions, cations, and a neutral solvent, or two anions and a common cation. We examine each of these models individually and compare concentrations based on each of these microscopic melt models.

First we will consider the melt to be composed of a Na_2S in a neutral sulfur solvent. Thus, we will include monosulfide anions, sodium cations, and neutral sulfur solvent to be present within the melt. We begin by establishing a common basis to compare each convention. This is defined to be the mole fraction of the undissociated Na_2S electrolyte in a neutral sulfur solvent x_e. The variable x_e is defined to be the moles of Na_2S divided by moles of Na_2S plus moles of free neutral sulfur. For a melt composition denoted by the non–stoichiometric formula Na_2S_y, the variable y is related to the mole fraction of Na_2S by

$$y = \frac{1}{x_e}, \tag{A–1}$$

or

$$x_e = \frac{1}{y}. \tag{A–2}$$

One could also use the particle fraction of sulfur computed on the basis of a dissociated electrolyte and a melt containing monosulfide ions, sodium ions, and sulfur solvent. Using this convention, the particle fraction of

sulfur, both ions and atoms is

$$n_S = \frac{1}{1 + 2x_e} . \tag{A-3}$$

The mass fraction can also be used to describe the composition of the melt. Commonly used to describe the composition of the melt is the mass fraction of sulfur, both ions and molecules ω_S where the other component is sodium. It is related to the mole fraction of Na_2S by

$$\omega_S = \frac{1}{2x_e M_{Na}/ M_S + 1} \tag{A-4}$$

and

$$x_e = \frac{1}{2} \frac{(1 - \omega_S)}{\omega_S} \frac{M_S}{M_{Na}} . \tag{A-5}$$

Next we will consider the melt to be composed of two anionic species $S_a^=$ and $S_b^=$ and sodium cations Na^+. Thus we can identify two neutral compounds Na_2S_a and Na_2S_b. The mole fraction of the compound Na_2S_a which is defined as moles of electrolyte A per total moles of electrolyte A and B is

$$x_a = \frac{1}{(a - b)} \left[\frac{1}{x_e} - b \right] . \tag{A-6}$$

and

$$x_e = \frac{1}{(a - b)x_a + b} . \tag{A-7}$$

Here the mole fraction of Na_2S_b can be determined from

$$x_a + x_b = 1 . \tag{A-8}$$

Finally, the mass fraction of the electrolytes Na_2S_a and Na_2S_b can also be used. These are defined analogously to the mole fractions of the two electrolytes. That is, mass of one electrolyte to per total mass of melt. The mass fraction of Na_2S_a is terms of the mole fraction of Na_2S_a is

$$\omega_a = \frac{2M_{Na}/M_S + a}{(a - b) + \dfrac{b + 2M_{Na}/M_S}{x_a}} \qquad \text{(A–9)}$$

and

$$x_a = b + \frac{2M_{Na}/M_S}{\dfrac{2M_{Na}/M_S + a)}{\omega_a} + (b - a)} . \qquad \text{(A–10)}$$

These manipulations are performed by the FORTRAN subroutine CONVRT which will interconvert between any of the given composition variables.

Appendix B

Calculation of Transference Numbers for Sodium Polysulfide Melts

Consider the following electrochemical cell from Cleaver and Davies[18]

$$C \mid \quad Na_2S_y \mid \quad \mid Na_2S_{y'} \mid \quad S\,(l) \quad \mid C$$

and rewrite it equivalently as

$$\begin{array}{ccccccc} & \alpha & & \beta & & \gamma & \delta & \alpha' \\ C \mid & Na_2S + (y-1)\,S\,(l) \mid & & \mid Na_2S + (y'-1)\,S\,(l) & & \mid S(l) & \mid C\,. \end{array}$$

Here three components have been defined: Na^+, $S^=$, and S. The potential of this cell is given as

$$FU_2 = -F(\Phi^{\alpha} - \Phi^{\alpha'}) = \mu_{e^-}^{\alpha} - \mu_{e^-}^{\alpha'}\,. \tag{B–1}$$

If equilibrium between phases α and β, and γ and δ are assumed, then

$$\mu_{S^=}^{\beta} = \mu_S^{\beta} + 2\mu_{e^-}^{\alpha}\,, \tag{B–2}$$

and

$$\mu_{S^=}^{\gamma} = \mu_S^{\gamma} + 2\mu_{e^-}^{\alpha'}\,, \tag{B–3}$$

and if the sulfur in phase δ is assumed to be pure

$$\mu_S^{\gamma} = \mu_S^{\delta} = \mu_S^{o}\,. \tag{B–4}$$

Combining Equations (B–1) through (B–4) thus gives for the potential of the cell

$$FU_2 = \mu_{e^-}^{\alpha} - \mu_{e^-}^{\alpha'} = \frac{1}{2}\left(\mu_{S^=}^{\beta} - \mu_{S^=}^{\gamma}\right) + \frac{1}{2}\left(\mu_S^{\gamma} - \mu_S^{\beta}\right). \tag{B–5}$$

Now Equation (16–3) from Newman[80] is

$$\frac{1}{z_n}\nabla\mu_n = -\frac{F}{\kappa}\,i - \sum_i \frac{t_i^o}{z_i}\left(\nabla\mu_i - \frac{z_i}{z_n}\nabla\mu_n\right). \tag{B–6}$$

Here we will let species n be $S^=$ and transference numbers will be taken relative to neutral sulfur, S. Also we will take i to be zero. This equation combined with the Gibbs–Duhem Equation which requires

$$x_e d\mu_e + (1 - x_e) d\mu_o = 0 , \qquad \text{(B–7)}$$

results in

$$\frac{1}{2} \nabla\mu_{S^=} = - t^o_{Na^+} \cdot \frac{1 - x_e}{x_e} \nabla\mu_o . \qquad \text{(B–8)}$$

The mole fraction of Na_2S has been represented by the variable x_e and the activity of sulfur by μ_o. Integration of Equation (B–8) from the composition in phase γ to the composition in phase β gives

$$\frac{1}{2} \int_\gamma^\beta \nabla\mu_{S^=} = \frac{1}{2} (\mu^\beta_{S^=} - \mu^\gamma_{S^=}) = - \frac{1}{2} \int_\gamma^\beta t^o_{Na^+} \frac{1 - x_e}{x_e} \nabla\mu_o . \qquad \text{(B–9)}$$

This gives for the potential of the cell from Equation (B–5)

$$FU_2 = - \frac{1}{2} \int_\gamma^\beta \left[t^o_{Na^+} \frac{1 - x_e}{x_e} + 1 \right] d\mu_o . \qquad \text{(B–10)}$$

If the the activity of sulfur is defined to be

$$\mu_S = \mu_o = \mu^o_o + RT \ln a_o , \qquad \text{(B–11)}$$

and the activity of sulfur in phase δ and γ is assumed to be equal to that of pure sulfur which is one,

$$U_2 = - \frac{RT}{2F} \int_1^\beta \left[t^o_{Na^+} \frac{1 - x_e}{x_e} + 1 \right] d(ln\ a_o) . \qquad \text{(B–12)}$$

Finally, Equation (B–12) can be differentiated to give

$$dU_2 = - \frac{RT}{2F} \left[t^o_{Na^+} \frac{1 - x_e}{x_e} + 1 \right] d(ln\ a_o) . \qquad \text{(B–13)}$$

The activity of sulfur can be obtained from the equilibrium potential of the following cell

Na (l) | β–alumina | Na_2S_y (l) | C

with cell potential denoted by U_1. Rewrite it as

$$\begin{array}{ccccc} \alpha & \beta & \gamma & \delta & \alpha' \\ C \mid & Na\ (l) & \mid \beta\text{–alumina} \mid & Na_2S + (y-1)\,S(l) & \mid C\,. \end{array}$$

The following reactions will be assumed to occur

$$Na \rightarrow Na^+ + e^- \qquad \text{(B–14)}$$

$$S^= \rightarrow S + 2\,e^- \qquad \text{(B–15)}$$

at the anode and cathode respectively. These two reactions can be combined to yield the overall cell reaction of

$$2\,Na + S \rightarrow Na_2S\,. \qquad \text{(B–16)}$$

Equilibria among the various phases gives

$$\mu^{\beta}_{Na} = \mu^{\gamma}_{Na^+} + \mu^{\alpha}_{e^-}\,, \qquad \text{(B–17)}$$

and

$$\mu^{\delta}_{S^=} = 2\,\mu^{\alpha'}_{e^-} + \mu^{\delta}_{S}\,. \qquad \text{(B–18)}$$

The cell potential can be expressed as

$$FU_1 = \mu^{\alpha}_{e^-} - \mu^{\alpha'}_{e^-} = \mu^{\beta}_{Na} - \mu^{\gamma}_{Na^+} - \frac{1}{2}\,\mu^{\delta}_{S^=} + \frac{1}{2}\,\mu^{\delta}_{S}\,. \qquad \text{(B–19)}$$

Assuming sodium metal in phase β to be pure and assuming sodium ions are equilibrated between the γ and δ phases gives

$$\mu^{\beta}_{Na} = \mu^{o}_{Na}\,, \qquad \text{(B–20)}$$

and

$$\mu^{\gamma}_{Na^+} = \mu^{\delta}_{Na^+}\,. \qquad \text{(B–21)}$$

The potential of the cell is thus

$$FU_1 = \mu^{\beta}_{Na} + \frac{1}{2}\,\mu^{\delta}_{S} - \frac{1}{2}\,\mu^{\delta}_{e}\,. \qquad \text{(B–22)}$$

When one takes the differential of Equation (B–22) and applies the Gibbs–Duhem equation Equation (B–7) this yields

$$F dU_1 = \frac{1}{2} \frac{1}{x_s} d\mu_o \,. \tag{B-23}$$

For the same definition of sulfur activity given in Equation (B-11), Equation (B-22) is

$$dU_1 = \frac{RT}{2F} \frac{1}{x_s} d(ln\ a_o) \,, \tag{B-24}$$

or

$$d(ln\ a_o) = \frac{2F}{RT} x_s\ dU_1 \tag{B-25}$$

Using Equation (B-25) gives for the differential of potential of cell two

$$dU_2 = - \left[t^o_{Na^+} \frac{1 - x_s}{x_s} + 1 \right] x_s\ dU_1 \,. \tag{B-26}$$

The transference number of sodium ions relative to neutral sulfur is thus

$$t^o_{Na^+} = \frac{- \frac{dU_2}{dx_s} \frac{dx_s}{dU_1} - x_s}{1 - x_s} \,. \tag{B-27}$$

The two derivatives of cell potential with electrolyte mole fraction can be obtained from the slope of cell potential data versus composition.

Appendix C

Entropy Production

From Newman[65], binary interaction coefficients must obey the following two inequalities

$$\frac{c_i}{\mathscr{D}_{ij}} + \frac{c_k}{\mathscr{D}_{ik}} \geq 0 , \tag{C-1}$$

and

$$\frac{c_j}{c_i \mathscr{D}_{jk} + c_k \mathscr{D}_{ij}} + \frac{c_i}{\mathscr{D}_{ik}} \geq 0 , \tag{C-2}$$

where species i, j, and k are arbitrary. Now choose

$$i \rightarrow + , \tag{C-3}$$

$$j \rightarrow o , \tag{C-4}$$

and

$$k \rightarrow - , \tag{C-5}$$

then

$$c_i = c_+ = \nu_+ c , \tag{C-6}$$

$$c_j = c_o = c_T - \nu c , \tag{C-7}$$

and,

$$c_k = c_- = \nu_- c , \tag{C-8}$$

where c is the concentration of electrolyte.

Criterion number one given by Equation (C-1) requires

$$\frac{\nu_+ c (c_T - \nu c)}{\mathscr{D}_{o+}} + \frac{\nu_- c (c_T - \nu c)}{\mathscr{D}_{o-}} \geq 0 , \tag{C-9}$$

while criterion number two given by Equation (C-2) gives

$$\frac{(c_T - \nu c)}{\nu_+ c \mathscr{I}_{o-} + \nu_- c \mathscr{D}_{+o}} + \frac{\nu_+ c}{\mathscr{D}_{+-}} \geq 0 . \tag{C-10}$$

The expressions for $\mathscr{D}_{o+}$, $\mathscr{D}_{o-}$, and $\mathscr{I}_{+-}$ are found in Newman[44]

$$\mathscr{D}_{o+} = \frac{-z_-}{z_+ - z_-} \frac{\mathscr{D}}{1 - t_+^o}, \tag{C-11}$$

$$\mathscr{D}_{o-} = \frac{z_+}{z_+ - z_-} \frac{\mathscr{D}}{t_+^o}, \tag{C-12}$$

and,

$$\frac{1}{\mathscr{D}_{+-}} = -\frac{z_+ z_- c_T F^2}{RT\kappa} - \frac{z_+ - z_-}{z_+ \nu_+} \frac{c_o t_+^o t_-^o}{c\,\mathscr{D}}. \tag{C-13}$$

Using these definitions in Equations (C-9) and (C-10) one obtains a restriction upon the diffusion coefficient as

$$\mathscr{D} \geq 0, \tag{C-14}$$

and a restriction upon the conductivity as

$$\kappa \geq 0. \tag{C-15}$$

Therefore, the second law is satisfied for combinations of the $\mathscr{D}_{ij}$ parameters if they are calculated from a diffusion coefficient and a conductivity which are both greater than zero.

Appendix D

Multicomponent Melt Phase Compositions

From Tegman,[17] the composition of sodium polysulfide melts can be calculated from equilibria among the monosulfide ion and each polysulfide ion in the melt. Consider the following general reaction between the single sulfide ion with gaseous sulfur dimer to form a polysulfide ion

$$\frac{i-1}{2} S_2(g) + S^{=} \rightarrow S_i^{=} . \qquad \text{(D-1)}$$

At equilibrium

$$c_i = K_i \, c_1 \, p_{S_2}^{\frac{i-1}{2}} . \qquad \text{(D-2)}$$

Here the variable p_{S_2} represents the partial pressure of dimer sulfur vapor and c_1 and c_i the concentrations of monosulfide ion and arbitrary polysulfide ion with formula $S_i^{=}$ respectively. Equation (D-2) can be rewritten in terms of the particle fraction of sulfur species

$$n_i = K_i \, n_1 \, p_{S_2}^{\frac{i-1}{2}} , \qquad \text{(D-3)}$$

where

$$n_i = \frac{c_i}{\sum_{j=1}^{N-1} c_j} . \qquad \text{(D-4)}$$

The parameter N denotes the number of total species, hence the number of anionic polysulfide species is given by $N-1$. The equilibrium coefficients can be determined from the free energy change for each reaction. The free energy change is assumed to be expressed as

$$\Delta G_i^{\circ} = \Delta H_i^{\circ} - T \, \Delta S_i^{\circ} \qquad \text{(D-5)}$$

where ΔH_i° and ΔS_i° are independent of temperature and pressure. The standard state for each reaction is taken to be ideal dimer sulfur vapor at

one atmosphere. Using the definition

$$\Delta G_i^o = - RT \ln K_i \qquad \text{(D–6)}$$

results in

$$K_i = \exp\left[- \frac{\Delta H_i^o}{RT} + \frac{\Delta S_i^o}{R} \right] \qquad \text{(D–7)}$$

Values of ΔH_i^o and ΔS_i^o for several polysulfide ions are given in Table D–1.[17]

Table D–1 Values of ΔH_i^o and ΔS_i^o for several polysulfide ions taken from Tegman[17]

i in $S_i^=$	ΔH_i^o, kJ/mol			ΔS_i^o, J/mol K		
2	-68.52	±	7.3	-37.65	±	6.3
3	-135.08	±	6.1	-85.00	±	5.9
4	-204.04	±	6.3	-155.54	±	6.0
5	-267.22	±	8.7	-228.69	±	12.4
6	-333.24	±	11.9	-312.07	±	24.0
8	-417.14	±	6.3	-392.60	±	6.2

A material balance for the melt composed of $N-1$ polysulfide ions requires

$$\sum_{i=1}^{N-1} n_i = 1 , \qquad \text{(D–8)}$$

and

$$\sum_{i=1}^{N-1} i \, n_i = y , \qquad \text{(D–9)}$$

where y denotes the composition of the melt with an overall formula of Na_2S_y. Using Equations (D–3) and (D–8) gives for the particle fraction of monosulfide ion as

$$n_1 = \frac{1}{1 + \sum_{i=2}^{N-1} K_i p_{S_2}^{\frac{(i-1)}{2}}} \quad \text{(D-10)}$$

Substitution of Equation (D-10) into (D-9) gives for the overall melt composition

$$y = \frac{1 + \sum_{i=2}^{N-1} i\, K_i\, p_{S_2}^{\frac{(i-1)}{2}}}{1 + \sum_{i=2}^{N-1} K_i p_{S_2}^{\frac{(i-1)}{2}}} \quad \text{(D-11)}$$

One must solve Equation (D-11) by trial and error for the partial pressure of sulfur vapor for a given overall melt composition. The monosulfide ion particle fraction can then be determined from Equation (D-10). Finally, the particle fraction for each species can then be determined from Equation (D-3) once the monosulfide ion particle fraction is known.

These equations are programmed into the subroutines COMP and PLYSLFD which will calculate the melt composition for any temperature and overall sulfur melt composition. The iteration is performed using subroutine SECANT.

Appendix E

Multi–Anion Transport Equations and Properties

Table (E–1) defines the convention used to represent ionic species in the melt.

Table (E-1) Ions in Multicomponent Model.

Ions	Species Number
$S^{=}$	1
$S_2^{=}$	2
$S_3^{=}$	3
.	.
.	.
.	.
$S_j^{=}$	j
.	.
.	.
.	.
$S_{N-1}^{=}$	N-1
Na^{+}	N

At constant temperature and pressure

$$c_j \nabla \mu_j = \sum_{k=1}^{N-1} M_{jk} \, (\mathbf{v}_k - \mathbf{v}_N) \,, \qquad \text{(E–1)}$$

where

$$M_{jk} = K_{jk} \quad j \neq k \qquad \text{(E–2)}$$

$$M_{jk} = K_{jk} - \sum_{i=1}^{N-1} K_{ji} \quad j = k \,. \qquad \text{(E–3)}$$

Inversion of the above equations for velocity differences in terms of

gradients of electrochemical potential gives

$$(\nabla_k - \nabla_N) = -\sum_{j=1}^{N-1} L_{kj}^N c_j \nabla\mu_j \,, \tag{E-4}$$

where

$$\mathbf{L}^N = -(\mathbf{M})^{-1} \,. \tag{E-5}$$

The definition of the current density is

$$\mathbf{i} = F\sum_{k=1}^{N} z_k c_k v_k = F\sum_{k=1}^{N-1} z_k c_k (\nabla_k - \nabla_N) \,. \tag{E-6}$$

Using the expression for the velocity differences in terms of the gradients of the electrochemical potentials gives for the current density

$$\mathbf{i} = -F\sum_{k=1}^{N-1} z_k c_k \sum_{j=1}^{N-1} L_{kj}^N c_j \nabla\mu_j \,. \tag{E-7}$$

For a solution of uniform composition, any electrochemical potential for any ion reduces to

$$\nabla\mu_j = z_j F \nabla\Phi \,. \tag{E-8}$$

Therefore in a solution of uniform composition, the current density is

$$\mathbf{i} = -F^2 \sum_{k=1}^{N-1} z_k c_k \sum_{j=1}^{N-1} L_{kj}^N c_j z_j \nabla\Phi \,. \tag{E-9}$$

Ohm's Law also governs the flow of current under these conditions

$$\mathbf{i} = -\kappa \nabla\Phi \,, \tag{E-10}$$

and one can therefore identify the conductivity as

$$\kappa = F^2 \sum_{k=1}^{N-1}\sum_{j=1}^{N-1} z_k c_k z_j c_j L_{kj}^N \,. \tag{E-11}$$

Although L_{kj}^N's depend upon the reference frame chosen, the conductivity is invariant with respect to the choice of the reference frame.

Now we will derive the binary melt transference number for sodium ions relative to neutral sulfur and the binary diffusion coefficient for a melt consisting of an arbitrary number of polysulfide species. Again, the definition for the current density in the melt is

$$\mathbf{i} = -F\sum_{k=1}^{N-1} z_k c_k \sum_{j=1}^{N-1} L_{kj}^{N} c_j \nabla\mu_j \,. \qquad \text{(E-12)}$$

The gradients of electrochemical potential for each ionic species can be obtained by considering the following general chemical reaction

$$S_j^{=} \rightarrow S^{=} + (j-1)S \,. \qquad \text{(E-13)}$$

Expressing the equality of the electrochemical potential for reactants and products in terms of the electrochemical potential for species in the anion–cation–solvent model gives

$$\nabla\mu_j = \nabla\mu_- + (j-1)\nabla\mu_o \,. \qquad \text{(E-14)}$$

The Gibbs–Duhem Equation for the melt in the anion–cation–solvent model requires

$$c_o\nabla\mu_o + c\,\nabla\mu_e = 0 \,, \qquad \text{(E-15)}$$

while the definition for the electrochemical potential of the electrolyte is

$$\nabla\mu_e = \nu_+\nabla\mu_+ + \nu_-\nabla\mu_- \,. \qquad \text{(E-16)}$$

Equations (E–14), (E–15), and (E–16) give the gradient of electrochemical potential of species j as

$$\nabla\mu_j = \left[\frac{1}{\nu_-} - (j-1)\,\frac{c}{c_o}\right]\nabla\mu_e - \frac{\nu_+}{\nu_-}\nabla\mu_+ \,. \qquad \text{(E-17)}$$

The expression for the current density given by Equation (E–12) is then

$$\mathbf{i} = -F\sum_{k=1}^{N-1} z_k c_k \sum_{j=1}^{N-1} L_{kj}^{N} c_j \left[\frac{1}{\nu_-}\nabla\mu_e - (j-1)\,\frac{c}{c_o}\nabla\mu_e - \frac{\nu_+}{\nu_-}\nabla\mu_+\right]. \qquad \text{(E-18)}$$

Equation (E–18) can then be rearranged to obtain the gradient of electrochemical potential of sodium ions in terms of the gradient of the chemical potential of the electrolyte and the current density. This expression can then be substituted into Equation (E–17) to give

$$\nabla\mu_j = \left[\frac{B}{A} - (j-1)\right]\frac{c}{c_o}\nabla\mu_e + \frac{\mathbf{i}}{A} \qquad \text{(E-19)}$$

where A and B are given by

$$A = -F\sum_{k=1}^{N-1} z_k c_k \sum_{j=1}^{N-1} L_{kj}^{N} c_j \qquad \text{(E-20)}$$

and

$$B = -F\sum_{k=1}^{N-1} z_k c_k \sum_{j=1}^{N-1} L_{kj}^{N} c_j (j-1) . \qquad \text{(E-21)}$$

The flux of each ionic species can be written as

$$\mathbf{N}_k = c_k \mathbf{v}_k = -c_k \sum_{j=1}^{N-1} L_{kj}^{N} c_j \nabla\mu_j + c_k \mathbf{v}_N \qquad \text{(E-22)}$$

or using the Equation (E-19) this becomes

$$\mathbf{N}_k = c_k \mathbf{v} = -c_k \sum_{j=1}^{N-1} L_{kj}^{N} c_j \left[\left[\frac{B}{A} - (j-1)\right]\frac{c}{c_o}\nabla\mu_o + \frac{\mathbf{i}}{A}\right] + c_k \mathbf{v}_N . \qquad \text{(E-23)}$$

Independent of the reference frame of model, the flux of sodium and sulfur must be identical. Equal sulfur fluxes require

$$\sum_{k=1}^{N-1} k\, \mathbf{N}_k = \mathbf{N}_o + \mathbf{N}_- , \qquad \text{(E-24)}$$

while the condition of equal sodium fluxes gives

$$\mathbf{N}_N = \mathbf{N}_+ . \qquad \text{(E-25)}$$

Equations (E-24) and (E-25) also account for conservation charge. If each side of each equation were multiplied by the charge number of the ions, equal currents would be defined on both sides of each equation. Definitions for the fluxes in each system require for equal sulfur fluxes

$$\sum_{k=1}^{N-1} k c_k \left[-\sum_{j=1}^{N-1} L_{kj}^{N} c_j \left[\left[\frac{B}{A} - (j-1)\right]\frac{c}{c_o}\nabla\mu_o + \frac{\mathbf{i}}{A}\right] + \mathbf{v}_N\right]$$

$$= c_o \mathbf{v}_o - \frac{\nu_- \mathscr{D}}{\nu RT}\frac{c_T}{c_o} c\, \nabla\mu_o + \frac{\mathbf{i} t_-^o}{z_- F} + c_- \mathbf{v}_o . \qquad \text{(E-26)}$$

while for equal sodium fluxes we have

$$c_N \mathbf{v}_N = -\frac{\nu_+ \mathscr{D}}{\nu RT}\frac{c_T}{c_o} c\, \nabla\mu_o + \frac{\mathbf{i} t_+^o}{z_+ F} + c_+ \mathbf{v}_o . \qquad \text{(E-27)}$$

Eliminating the velocity of species N in Equation (E-26) using Equation (E-27) gives

$$\left[\nu_- - \nu_+ \sum_{k=1}^{N-1} k c_k\right] \frac{\mathscr{D}}{\nu RT} \frac{c_T}{c_o} c \nabla\mu_e - \sum_{k=1}^{N-1} k c_k \sum_{j=1}^{N-1} L_{kj}^N c_j \left[\frac{B}{A} - (j-1)\right] \frac{c}{c_o} \nabla\mu_e$$

$$+ \frac{i t_+^o}{z_+ F} \sum_{k=1}^{N-1} k \frac{c_k}{c_N} - \frac{i t_-^o}{z_- F} - \frac{i}{A} \sum_{k=1}^{N-1} k c_k \sum_{j=1}^{N-1} L_{kj}^N c_j$$

$$+ \sum_{k=1}^{N-1} k \frac{c_k c_+}{c_N} \nabla_o - c_o \nabla_o - c_- \nabla_o = 0 . \qquad \text{(E–28)}$$

In a solution of uniform composition with no current flow, Equation (E–28) reduces to

$$c_- \nabla_o + c_o \nabla_o - \frac{c_+}{c_N} \sum_{k=1}^{N-1} k c_k \nabla_o = 0 . \qquad \text{(E–29)}$$

Definitions for the concentrations in the two models require

$$c_+ = c_N \qquad \text{(E–30)}$$

and

$$c_o + c_- = \sum_{k=1}^{N-1} k c_k . \qquad \text{(E–31)}$$

Thus one sees that Equation (E–29) is identically zero, and the convective terms make no contribution to Equation (E–28).

In a solution of uniform composition, the migration term is

$$\frac{i t_+^o}{z_+ F} \frac{1}{c_N} \sum_{k=1}^{N-1} k c_k - \frac{i t_-^o}{z_- F} - \frac{i}{A} \sum_{k=1}^{N-1} k c_k \sum_{j=1}^{N-1} L_{kj}^N c_j = 0 . \qquad \text{(E–32)}$$

Solving Equation (E–32) along with the definition of A gives for the transference number of sodium ions relative to sulfur solvent as

$$t_+^o = \frac{\frac{1}{z_-} - \frac{\sum_{k=1}^{N-1} k c_k \sum_{j=1}^{N-1} L_{kj}^N c_j}{\sum_{k=1}^{N-1} z_k c_k \sum_{j=1}^{N-1} L_{kj}^N c_j}}{\frac{1}{z_-} + \frac{1}{z_+} \sum_{k=1}^{N-1} k \frac{c_k}{c_N}} \qquad \text{(E–33)}$$

One may also distinguish the transference numbers of the individual anionic species in two ways. If the migration contributions to the flux of

species k in Equation (E–23) can assumed to be in a form given by

$$\frac{i t_k^N}{z_k F} = - \frac{i}{A} c_k \sum_{j=1}^{N-1} L_{kj}^N c_j \, . \tag{E–34}$$

then

$$t_k^N = \frac{c_k z_k \sum_{j=1}^{N-1} L_{kj}^N c_j}{\sum_{k=1}^{N-1} z_k c_k \sum_{j=1}^{N-1} L_{kj}^N c_j} \tag{E–35}$$

with the definition

$$t_N^N = 0 \, . \tag{E–36}$$

It can be seen from Equation (E–35) above that

$$\sum_{k=1}^{N-1} t_k^N = 1 \, . \tag{E–37}$$

The transference numbers for each species can also be determined if one again considers a solution of uniform composition. The velocity of any species relative to species N will then be given by

$$c_k (v_k - v_N) = \frac{i t_k^N}{z_k F} \, . \tag{E–38}$$

Again in a solution of uniform composition, Ohm's Law given in Equation (E–10) governs the current flow. Using this definition along with Equations (E–9) and (E–38) gives the transference number of species j relative to species N as

$$t_k^N = - \frac{1}{\kappa} F^2 z_k c_k \sum_{k=1}^{N-1} L_{jk}^N c_k z_k \, . \tag{E–39}$$

Equation (E–39) reduces to the previously derived expression, Equation (E–35), provided the charge numbers of all species included within the summation in Equation (E–39) are equal. This requirement is fulfilled, since all of the anionic species have equal charges.

Using Equation (E–33) and Equation (E–35), the transference number of sodium ions relative to sulfur solvent in terms of the anion transference numbers relative to sodium ions is

$$t_+^o = \frac{\dfrac{1}{z_-} - \sum_{k=1}^{N-1} k \dfrac{t_k^N}{z_k}}{\dfrac{1}{z_-} + \dfrac{1}{z_+} \sum_{k=1}^{N-1} k \dfrac{c_k}{c_N}} . \qquad \text{(E–40)}$$

One can simplify this expression by noting again that the charges of all anionic species are the same and using the definition in Equation (E–31) This gives

$$t_+^o = \frac{\sum_{k=1}^{N-1} k\ t_k^c - 1}{y - 1} . \qquad \text{(E–41)}$$

Finally, the diffusion coefficient in the binary anion-cation-solvent model also can be determined from Equation (E–28). In a solution where no current is flowing, only the diffusive terms remain, and Equation (E–28) becomes

$$\frac{\mathscr{D}}{\nu RT} \frac{c_T}{c_o} c \left[\frac{\nu_+}{c_N} \sum_{k=1}^{N-1} k c_k - \nu_- \right] \nabla \mu_e + \sum_{k=1}^{N-1} k c_k \sum_{j=1}^{N-1} L_{kj}^N c_j \left[\frac{B}{A} - (j-1) \right] \frac{c}{c_o} \nabla \mu_e = 0 . \qquad \text{(E–42)}$$

Solving for the diffusion coefficient gives

$$\mathscr{D} = - \frac{\nu RT}{c_T} \frac{\sum_{k=1}^{N-1} k c_k \sum_{j=1}^{N-1} L_{kj}^N c_j \left[\dfrac{B}{A} - (j-1) \right]}{\left[\dfrac{\nu_+}{c_N} \sum_{k=1}^{N-1} k c_k - \nu_- \right]} . \qquad \text{(E–43)}$$

Again, after some substitution, Equation (E–43) can be simplified, and the diffusion coefficient in the binary system can be expressed as

$$\mathscr{D} = \frac{3RT}{c} \frac{\sum_{k=1}^{N-1} k c_k \sum_{j=1}^{N-1} L_{kj}^{N} c_j \left[\frac{B}{A} - (j-1)\right]}{(y+2)(y-1)}. \qquad \text{(E-44)}$$

where

$$\frac{A}{B} = \frac{\sum_{k=1}^{N-1} c_k \sum_{j=1}^{N-1} L_{kj}^{N} c_j}{\sum_{k=1}^{N-1} c_k \sum_{j=1}^{N-1} L_{kj}^{N} c_j (j-1)}. \qquad \text{(E-45)}$$

Appendix F

Computer Programs for Sodium Polysulfide Melts

This section presents a listing of the two computer programs used in the determination of the transport properties of sodium–sulfur melts. Two programs have been used: COMPOS and SSTP.

Program COMPOS calculates the equilibrium microscopic melt composition using the model developed by Tegman.[17] It also determines the open–circuit cell potential for a sodium sulfur cell and the activity coefficient factor. The subroutines and their purpose in COMPOS are listed in Table F–1.

Table F–1 Subroutines and Purpose in Program COMPOS

Subroutine	Purpose
PLYSFD	Calculates the equilibrium constants, material balances, and the variation in the particle fraction of monosulfide ion with electrolyte mole fraction on a sodium polysulfide melt using the model of Tegman.[17]
SECANT	Performs an iteration on a one–dimensional function using a *regula–falsi* technique.

Program COMPOS calculates the particle of polysulfide anions in the melt, the open circuit potential, and the activity coefficient factor. Needed inputs are the melt temperature and standard differences in chemical potentials for molten sodium metal, liquid sodium sulfide, and ideal sulfur vapor. A program listing and sample output follows.

```
      PROGRAM COMPOS(INPUT,OUTPUT,TAPE5=INPUT,TAPE6=OUTPUT)
C
C     ..................................................
C
C     PROGRAM COMPOS
C
C     PURPOSE CALCULATE THE MICROSCOPIC COMPOSITION, THE CELL
C             POTENTIAL, AND THE VARIATION OF THE ACTIVITY
C             WITH COMPOSITION FOR A POLYSULFIDE MELT OF A GIVEN
C             COMPOSTION USING THE MODEL PROPOSED BY TEGMAN.
C             THIS PROGRAM FIRST CALCULATES THE PARTICLE FRACTIONS
C             OF THE VARIOUS POLYSULFIDE IONS.
C             SECOND ,IT DETERMINES THE OPEN CIRCUIT POTENTIAL
C             OF A CELL FORMED BY A SULFUR ELECTRODE WITH A
C             SINGLE PHASE OF GIVEN COMPOSITION COMBINED WITH
C             A LIQUID SODIUM ELECTRODE.
C             FINALLY, IT DETERMINES THE DERIVATIVE OF THE LOGARITHM
C             OF THE ACTIVITY COEFFICENT WITH RESPECT TO THE
C             LOGARITHM OF THE MOLALITY OF SODIUM SULFIDE.
C
C     SUBROUTINES REQUIRED
C
C             PLYSFD
C             SECANT
C
C     REVISED 8-6-83
C     ..................................................
C
      REAL LGPS2,LGPS21,LGPS22,MU0
      EXTERNAL PLYSFD
      DIMENSION DELTAG(8),IN(8),X(8)
      COMMON/FIRST/ DELTAG,DXSDXE,IN,XE,X,TEMP
      DATA IN/1,1,1,1,1,1,0,1/
      DATA R,F/8.3143,96485.0/
C
C     PROGRAM CONDITIONS FOLLOW
C
      XESTRT=0.20
      DXE=0.005
      XSAT=0.1920
      NINT=32
      TEMP=633.15
      DELTAG0=42.817
C
C     WRITE OUT TEMPERATURE
C
      WRITE(6,100) TEMP
C
C     CALCULATE STANDARD CHEMICAL POTENTIAL
C
      MU0=4.184*1000.0*DELTAG0
```

```
C
C       FOR EACH COMPOSITION, CALCULATE COMPOSITIONS, CELL
C       POTENTIAL, AND DLGDLM
C
        DO 20 K=1,NINT
        IF(K.EQ.1) XE=XSAT
        IF(K.EQ.2) XE=XESTRT
C
C       ITERATIVELY SOLVE MATERIAL BALANCES
C
C       STARTING GUESSES FOLLOW
C
        LGPS21=-1.0
        LGPS22=-5.0
        CALL SECANT(PLYSFD,LGPS21,YFUNC,LGPS22,1.0E-06,IERR,20)
C
C       FIRST TIME PRINT OUT DELTA G'S
C
        IF(K.NE.1) GO TO 10
        DO 5 I=2,8
        IF(IN(I).EQ.0) GO TO 5
        WRITE(6,101) I,DELTAG(I)
5       CONTINUE
        WRITE(6,102)
C
C       CALCULATE POTENTIAL ETC.
10      RTLNA=0.5*R*TEMP*ALOG(X(4)/X(2)/X(2))
        POT=(MU0+0.5*DELTAG(4)-DELTAG(2)+RTLNA)/F
        DLGDLM=XE*(1.0-XE)/3.0/X(1)*DXSDXE
C
C       WRITE THEM OUT
C
        WRITE(6,103) XE,X(1),X(2),X(3),X(4),X(5),X(6),X(8),POT,DLGDLM
        XE=XE+DXE
20      CONTINUE
C
C       FORMAT STATEMENTS FOLLOW
C
100     FORMAT(* *,//* *,*TEMPERATURE = *,F7.2,*K*//
     1         * *,*DELTAG VALUES*/)
101     FORMAT(* *,*DELTAG(*,I1,*) = *,1PE15.8)
102     FORMAT(* *,//,* *,5X,*XE*,8X,*X(1)*,7X,*X(2)*,7X,*X(3)*,7X,
     1 *X(4)*,7X,*X(5)*,7X,*X(6)*,7X,*X(8)*,7X,*U1*,5X,*1+DLGDLM*/)
103     FORMAT(* *,10(F8.5,3X))
        END

        SUBROUTINE PLYSFD (LGPS2,DIFF)
C
C       ..........................................................
C
C       SUBROUTINE PLYSFD
```

```
C
C       PURPOSE TO CALCULATE THE MATERIAL BALANCES FOR A POLYSULFIDE
C               MELT.
C
C       USAGE   CALL PLYSFD(LGPS2,DIFF)
C
C       DESCRIPTION OF PARAMETERS
C
C               LGPS2   THE COMMON LOGRITHM OF THE SULFUR VAPOR
C                       PRESSURE. THIS PARAMETER IS THE INDEPENDENT
C                       VARIABLE INPUT INTO THE MATERIAL BALANCES.
C
C               DIFF    THE DIFFERENCE BETWEEN THE CALCULATE
C                       MOLE FRACTION OF ELECTROLYTE AND THE
C                       GIVEN MOLE FRACTION OF ELECTROLYTE.
C
C
C       SUBROUTINES REQUIRED
C
C               NONE
C
C       REFERENCES
C
C               RAGNAR TEGMAN, THERMODYNAMIC STUDIES OF HIGH
C               TEMPERATURE EQULIBRIA, CHEMICA SCRIPTA, 1976,
C               9, 158-166.
C
C       REVISED 8-6-83
C       ..............................................................
C
        REAL K,LGPS2,NUMER
        COMMON/FIRST/ DELTAG,DXSDXE,IN,XE,X,TEMP
        DIMENSION DELTAH(8),DELTAS(8),DELTAG(8),IN(8),K(8),X(8)
C
C       DATA OF TEGMAN FOLLOWS
C
        DATA DELTAH, DELTAS/
     1  0.0,-68.52,-135.08,-204.04,-267.22,-333.24,0.0,-417.14,
     2  0.0,-37.65, -85.00,-155.64,-228.69,-312.07,0.0,-392.60/
C
C       INITIALIZE SOME CONSTANTS
C
        DATA R/8.314/
        DATA N/8/
        DELTAG(1)=0.0
        NUMER=1.0
        DENOM=1.0
        PS2=10.0**(LGPS2)
        DSUM1=0.0
        DSUM2=0.0
C
```

```
C       FOR EACH COMPONENT IN THE MELT, CLACULATE DELTA G'S
C       AND RELATIVE COMPOSITIONS
C
        DO 10 I=2,N
        X(I)=0.0
C
C       CALCULATE DELTA G VALUES
C
        IF(IN(I).EQ.0) GO TO 10
        DELTAG(I)=DELTAH(I)*1000.0-TEMP*DELTAS(I)
C
C       NOW CALCULATE K'S
C
        K(I)=EXP(-DELTAG(I)/R/TEMP)
        X(I)=K(I)*PS2**(FLOAT(I-1)/2.0)
        NUMER=NUMER+X(I)
        DENOM=DENOM+FLOAT(I)*X(I)
        DSUM1=DSUM1+X(I)*FLOAT(I-1)/PS2
        DSUM2=DSUM2+FLOAT(I*(I-1))*X(I)/PS2
10      CONTINUE
C
C       DETERMINE MONOSULFIDE ION COMPOSITION
C
        XCALC=NUMER/DENOM
        X(1)=1.0/NUMER
C
C       DETERMINE HIGHER POLYSULFIDE COMPOSITIONS
C
        DO 20 I=2,N
        IF (IN(I).EQ.0) GO TO 20
        X(I)=X(I)*X(1)
20      CONTINUE
C
C       CALCULATE DERIVATIVE OF MONOSULFIDE ION PARTICLE FRACTION
C       WITH RESPECT TO TOTAL SODIUM SULFIDE MOLE FRACTION.
C
        DXSDXE=X(1)/XE/(XE*DSUM2/DSUM1-1)
C
C       CALCULATE DIFFERENCE BETWEEN GIVEN SODIUM SULFIDE
C       MOLE FRACTION AND CALCULATED MOLE FRACTION.
C
        DIFF=XCALC-XE
        RETURN
        END

        SUBROUTINE SECANT(FCNY,X1,Y,X2,TOL,IERR,NITER)
C
C       ..................................................
C
C       SUBROUTINE SECANT
C
```

```
C       PURPOSE PERFORM AN ITERATION USING THE SECANT METHOD ON
C               A ONE-DIMENSIONAL FUNCTION.
C
C       USAGE   CALL SECANT(FCNY,X1,Y1,X2,TOL,IERR,NITER)
C
C       DESCRIPTION OF PARAMETRS
C
C               FCNY    NAME OF SUBROUTINE CONTAINING THE EXPRESSION
C                       OF THE FUNCTION TO BE ITERATED UPON.
C               X1      FIRST GUESS FOR INDEPENDENT VARIABLE.
C                       FINAL VALUE OF INDEPENDENT VARIABLE
C                       IS RETURNED HERE.
C               Y       FINAL VALUE OF DEPENDENT VARIABLE IS
C                       RETURNED HERE. DEPENDENT
C                       VARIABLE IS ITERATED TO ZERO.
C               X2      SECOND GUESS FOR INDEPENDENT VARIABLE.
C               TOL     ITERATION TOLERANCE EXPRESSED AS A
C                       FRACTION CHANGE OF THE INDEPENDENT
C                       VARIABLE.
C               IERR    ERROR FLAG.
C                       = 1     IF NUMBER OF SPECIFIED ITERATIONS
C                               ARE EXCEEDED.
C               NITER   NUMBER OF ITERATIONS. IERR IS ASSIGNED A
C                       VALUE OF ONE IF THE NUMBER OF
C                       ITERATIONS EXCEEDS THIS PARAMETER.
C
C       SUBROUTINES REQUIRED
C
C               FCNY    SUBROUTINE TO EVALUATE THE INDEPENDENT
C                       VARIABLE FOR A GIVEN VALUE OF THE
C                       DEPENDENT VARIABLE.
C
C       REVISED 1-29-83
C       ..................................................................
C
        DIMENSION DELTAG(8),IN(8),X(8)
        COMMON/FIRST/ DELTAG,DXSDXE,IN,XE,X,TEMP
        N=1
C
C       EVALUATE FUNCTION FOR INITIAL GUESSES
C
        CALL FCNY(X1,Y1)
        CALL FCNY(X2,Y2)

C
C       COMPUTE NEW VALUE FROM PREVIOUS GUESSES
C
1       X3=X2-(X2-X1)/(Y2-Y1)*Y2
        CALL FCNY(X3,Y3)
C
C       DETERMINE IF ITERATION TOLERANCE HAS BEEN MET
```

```
C
      IF(ABS((X3-X2)/X3).LT.TOL) GO TO 2
C
C     DETERMINE IF SPECIFIED NUMBER OF ITERATIONS
C           HAS BEEN EXCEEDED
C
      IF(N.GT.NITER) GO TO 3
C
C     IF NOT TRY AGAIN !
C
      X1=X2
      Y1=Y2
      X2=X3
      Y2=Y3
      N=N+1
      GO TO 1
C
C     SUCCESS ! RETURN VALUES
C
2     X1=X3
      Y=Y3
      RETURN
C
C     RETURN AN ERROR
C
3     IERR=1
      RETURN
      END
```

Sample Output for Program COMPOS

TEMPERATURE = 633.15K

DELTAG VALUES

DELTAG(2) = -4.46819025E+04
DELTAG(3) = -8.12622500E+04
DELTAG(4) = -1.05496534E+05
DELTAG(5) = -1.22424927E+05
DELTAG(6) = -1.35652880E+05
DELTAG(8) = -1.68565310E+05

XE	X(1)	X(2)	X(3)	X(4)	X(5)	X(6)	X(8)	UI	1+DLGDLM
.19200	.00001	.00153	.06825	.29258	.31307	.16586	.15872	2.09345	2.77111
.20000	.00001	.00210	.08483	.32792	.31639	.15114	.11760	2.07905	2.81314
.20500	.00001	.00256	.09659	.34919	.31509	.14077	.09579	2.07002	2.86977
.21000	.00002	.00311	.10959	.36962	.31115	.12969	.07681	2.06090	2.94717
.21500	.00002	.00379	.12400	.38900	.30459	.11809	.06051	2.05160	3.04262
.22000	.00003	.00461	.13997	.40703	.29543	.10617	.04675	2.04209	3.15228
.22500	.00004	.00563	.15767	.42338	.28376	.09416	.03535	2.03232	3.27086
.23000	.00006	.00688	.17722	.43763	.26975	.08232	.02614	2.02228	3.39155
.23500	.00008	.00842	.19867	.44936	.25368	.07091	.01889	2.01197	3.50656
.24000	.00010	.01031	.22202	.45812	.23594	.06016	.01334	2.00142	3.60814
.24500	.00014	.01263	.24716	.46356	.21701	.05030	.00921	1.99069	3.69002
.25000	.00019	.01544	.27385	.46540	.19742	.04146	.00624	1.97982	3.74847
.25500	.00025	.01882	.30179	.46354	.17772	.03373	.00414	1.96889	3.78270
.26000	.00034	.02286	.33058	.45801	.15839	.02712	.00271	1.95797	3.79436
.26500	.00046	.02762	.35978	.44898	.13985	.02157	.00175	1.94710	3.78655
.27000	.00061	.03319	.38895	.43675	.12241	.01699	.00112	1.93634	3.76279
.27500	.00081	.03962	.41761	.42170	.10629	.01326	.00070	1.92571	3.72631
.28000	.00106	.04700	.44532	.40429	.09161	.01028	.00044	1.91525	3.67963
.28500	.00139	.05537	.47166	.38497	.07843	.00791	.00027	1.90497	3.62451
.29000	.00181	.06478	.49624	.36422	.06673	.00605	.00017	1.89489	3.56198
.29500	.00234	.07526	.51871	.34252	.05646	.00461	.00010	1.88503	3.49258
.30000	.00300	.08683	.53877	.32031	.04753	.00349	.00006	1.87540	3.41648
.30500	.00382	.09947	.55620	.29799	.03985	.00264	.00004	1.86602	3.33376
.31000	.00481	.11315	.57082	.27592	.03329	.00199	.00002	1.85689	3.24453
.31500	.00602	.12780	.58253	.25441	.02773	.00150	.00001	1.84803	3.14909
.32000	.00746	.14334	.59130	.23371	.02306	.00113	.00001	1.83945	3.04798
.32500	.00916	.15965	.59717	.21402	.01915	.00085	.00001	1.83117	2.94199
.33000	.01115	.17659	.60025	.19548	.01589	.00064	.00000	1.82320	2.83219
.33500	.01345	.19403	.60068	.17817	.01319	.00048	.00000	1.81553	2.71981
.34000	.01608	.21181	.59866	.16212	.01096	.00037	.00000	1.80817	2.60614
.34500	.01906	.22976	.59444	.14735	.00912	.00028	.00000	1.80113	2.49248
.35000	.02239	.24774	.58824	.13382	.00760	.00021	.00000	1.79439	2.38004

Program SSTP calculates the values of ε_1 and ε_2 which best fit the experimental data of conductivity and transference number. Program SSTP also calculates the melt viscosity and density. Conductivities, densities, and viscosities have been calculated using the data of Cleaver and Davies.[14-16] The subroutines in program SSTP are listed in Table F–2.

Table F–2 Subroutines in Program SSTP

Subroutine	Purpose
COMP	Determines the equilibrium constants for the microscopic reactions and calculates material balances on the melt. This is very similar to subroutine PLYSFD except that the variation of the monosulfide ion with mole fraction of sodium sulfide is not calculated.
SECANT	Performs an iteration on a one–dimensional function using a *regula–falsi* iteration scheme.
MATINV	Inverts a matrix or solves a set of linear equations by a Gauss–Jordan reduction method. Subroutine MATINV was written by John Newman.
FUNDER	Sets up the equations and computes the derivatives for a two–dimensional Newton–Raphson iteration.
FUNCT	Sets up the matrix for the calculation of binary transport properties from the fundamental $\mathscr{D}_{ij}$ parameters.
PROPRT	Calculates the physical and transport properties of sodium–sulfur melts using the data of Cleaver and Davies.[14,16]
CUBSPL	Calculate a cubic spline through a given set of data points.
CURVE	Interpolate a set of points. If the set of points contains more than three points, use a cubic spline. If there are less than three points, use a Legendre polynomial.
CONVRT	Convert the composition of sodium polysulfides from one compositional variable to another.

A program listing and sample output follows.

```
C
C       ..................................................
C
C       PROGRAM SSTP (SODIUM-SULFUR TRANSPORT PROPERTIES)
C
C       PURPOSE CALCULATE THE BINARY TRANSPORT PROPERTIES FOR SODIUM
C               POLYSULFIDE MELTS FROM A MICROSCOPIC MODEL.
C
C       SUBROUTINES REQUIRED
C
C               COMP    CALCULATES MATERIAL BALANCES ON A POLYSULFIDE
C                       MELT. THIS SUBROUTINE IS NEARLY IDENTICAL
C                       SUBROUTINE PLYSFD IN PROGRAM COMPOS.
C
C               SECANT  PERFORMS A SECANT ITERATION ON A
C                       ONE-DIMENSIONAL FUNCTION.
C
C               MATINV  INVERTS A MATRIX OR SOLVES THE SYSTEM
C                       OF EQUATIONS BX = D.
C                       MATINV WAS WRITTEN BY JOHN NEWMAN.
C
C               FUNDER  CALCULATES THE FUNCTION AND NUMERICALLY
C                       EVALUATES THE DERIVATIVES FOR A TWO-
C                       DIMENSIONAL NEWTON-RAPHSON ITERATION.
C
C               FUNCT   CALCULATES THE MELT TRANSFERENCE NUMBER,
C                       CONDUCTIVITY, AND DIFFUSION COEFFICIENT
C                       BY INVERSION OF THE TRANSPORT COEFFICIENT
C                       MATRIX.
C
C               PROPRT  COMPUTES THE TRANSPORT AND PHYSICAL PROPERTIES
C                       FOR SODIUM POLYSULFIDE MELTS AT SEVERAL SPECIFIC
C                       COMPOSITIONS AS A FUNCTION OF TEMPERATURE
C                       THIS SUBROUTINE UTILIZES THE EXPERIMENTAL DATA
C                       OF CLEAVER AND DAVIES AND CAN RETURN
C                       VALUES OF THE DENSITY, CONDUCTIVITY, VISCOSITY,
C                       AND SURFACE TENSION.
C
C               CUBSPL  CALCULATES A CUBIC SPLINE THROUGH N DATA
C                       POINTS. CUBSPL IS USED TO DETERMINE MELT
C                       PROPERTIES AT INTERMEDIATE COMPOSITIONS NOT
C                       GIVEN BY PROPRT.
C
C               CURVE   USED IN CONJUNCTION WITH CUBSPL TO INTERPOLATE
C                       BETWEEN DATA POINTS TO CALCULATE PROPERTY
C                       AT DESIRED COMPOSITION.
C
C               CONVRT  CONVERTS THE COMPOSITION OF SODIUM POLYSULFIDE
C                       MELTS FROM ONE COMPOSITIONAL VARIABLE TO
C                       ANOTHER. CONVRT IS USED TO CONVERT THE
C                       EXPERIMENTAL DATA FROM CLEAVER AND DAVIES WHICH
```

```
C                       IS GIVEN IN MASS FRACTION OF SULFUR TO
C                       MOLE FRACTION OF SODIUM SULFIDE WHICH IS
C                       THE COMPOSITION CONVENTION USED IN THE PROGRAM.
C                       SSTP.
C
C       REVISED 10-7-83
C       ..........................................................
C


        PROGRAM SSTP(INPUT,OUTPUT,TAPE5=INPUT,TAPE6=OUTPUT)
        EXTERNAL COMP
        REAL LGPS2,LGPS21,LGPS22
        REAL KAPPA,MNA,MU,MWAV,MNA2S,MWOD,MS,MSMNA,MWSUM
        DIMENSION DELTA(8)
        DIMENSION PARAM(2),PARAM0(2),YO(2),DX(2),DYDX(2,2)
        DIMENSION DELTAG(8),X(8),IN(8)
        DIMENSION XD(10),YD(10),XK(10),YK(10),XV(10),YV(10),AA(10,4),
     1 SD(10),SK(10),SV(10)
        COMMON/FIRST/ DELTAG,IN,XE
        COMMON/THIRD/ C,DELTA,F,MSMNA,N,RBRA0,Y
        COMMON/FOURTH/ R,TEMP,X
        COMMON/FIFTH/ POWER2,SCRPTD
C
C       DATA STATEMENTS FOLLOW
C
        DATA R,F/8.314,9.6485E4/
        DATA DELTA/1.0,2.0,3.0,4.0,5.0,6.0,8.0,0.0/
        DATA IN/6*1,0,1/
        DATA DX/1.0E-08,1.0E-08/
        DATA MNA,MNA2S,MS/22.98977,78.03934,32.06/
        DATA IDSIZE,IKSIZE,IVSIZE/3*1/
C
C       INITIALIZE PARAMETERS
C
        POWER1=1.5
        POWER2=3.0
        A=5.9060
        B=44.58998
        DELTAG(1)=0.0
        NITER1=20
        NITER2=20
        N=8
        RBRA0=(B/2.0/A)**(1.0/3.0)
        TCOEF=0.9721
        TEMP=633.15
        TOL1=1.0E-06
        TOL2=1.0E-04
        PARAM0(1)=1.0E-04
        PARAM0(2)=1.0E-04
C
```

```
C       PRINT OUT TEMPERATURE AND POWER ON DIJ'S
C
        WRITE(6,5) TEMP,POWER2
5       FORMAT(*1*,////* *,*TEMPERATURE = *,F8.2,* K*/
     1 * *,*POWER2 = *,F10.5//)
C
C       PRINT OUT HEADING
C
        WRITE(6,6)
6       FORMAT(* *,*NITER*,4X,*XE*,8X,*KAPPA*,6X,*MU*,8X,*TOPLUS*,3X,
     1 *EXP DENS*,3X,*CALC DENS*,6X,*SCRIPTD*,7X,*4PIE1NA/3MUV1*,
     2 4X,*4PIE2NA/3MUV1*/)
C
C       STARTING MELT COMPOSITION FOLLOWS.
C
        XE=0.21
C
C       GET EXPERIMENTAL PROPERTIES
C
C       FIRST GET DENSITY
C
        CALL PROPRT(TEMP,XD,YD,10,IDSIZE,1)
        IF(IDSIZE.EQ.0) GO TO 5000
        DO 10 J=1,IDSIZE
        XIN=XD(J)
10      CALL CONVRT(XIN,XD(J),5,1)
        IF(IDSIZE.LE.3) GO TO  20
        CALL CUBSPL(XD,YD,SD,AA,10,IDSIZE,1)
C
C       NEXT GET CONDUCTIVITY DATA.
C
20      CALL PROPRT(TEMP,XK,YK,10,IKSIZE,4)
        IF(IKSIZE.EQ.0) GO TO 5000
        DO 30 J=1,IKSIZE
        XIN=XK(J)
30      CALL CONVRT(XIN,XK(J),5,1)
        IF(IKSIZE.LE.3) GO TO 40
        CALL CUBSPL(XK,YK,SK,AA,10,IKSIZE,1)
C
C       NEXT GET VISCOSITY DATA.
C
40      CALL PROPRT(TEMP,XV,YV,10,IVSIZE,2)
        IF(IVSIZE.EQ.0) GO TO 5000
        DO 50 J=1,IVSIZE
        XIN=XV(J)
50      CALL CONVRT(XIN,XV(J),5,1)
        IF(IVSIZE.LE.3) GO TO 60
        CALL CUBSPL(XV,YV,SV,AA,10,IVSIZE,1)
C
C       CALCULATE EPSILONS FOR EACH MELT COMPOSITION
C
```

```
60      DO 2000 NNN=1,12
C
C       STARTING ITERATION GUESSES HERE
C
        PARAM(1)=PARAM0(1)
        PARAM(2)=PARAM0(2)
C
C       CALCULATE SOME OTHER IMPORTANT QUANTITIES
C
        Y=1.0/XE
        MWAV=(1-XE)*MS+XE*MNA2S
        MSMNA=MS/MNA
C
C       DETERMINE MICROSCOPIC COMPOSITION
C
        LGPS21=-1.0
        LGPS22=-5.0
        CALL SECANT(COMP,LGPS21,YFUNC,LGPS22,TOL1,IERR,NITER1)
        IF(IERR.EQ.1) GO TO 1101
        X(7)=X(8)
        X(8)=2.0
C
C       CALCULATE THEORETICAL DENSITY FROM EMPIRICAL
C       MOLAR VOLUME FIT
C
        XWEIGHT=0.0
        DO 70 I=1,N-1
        XWEIGHT=XWEIGHT+X(I)*DELTA(I)**POWER1
70      CONTINUE
        MWOD=A*XWEIGHT+B
        MWSUM=MS*Y+2.0*MNA
        DENSTY=MWSUM/MWOD
        C=DENSTY*XE/MWAV
C
C       NOW GET EXPERIMENTAL DENSITY,
C
        CALL CURVE(TRUDEN,XE,XD,YD,SD,IDSIZE,IDERR)
        IF(IDERR.EQ.1) GO TO 1000
C
C       CONDUCTIVITY,
C
        CALL CURVE(KAPPA,XE,XK,YK,SK,IKSIZE,IKERR)
        IF(IKERR.EQ.1) GO TO 1000
C
C       AND VISCOSITY.
C
        CALL CURVE(MU,XE,XV,YV,SV,IVSIZE,IVERR)
        IF(IVERR.EQ.1) GO TO 1000
C
C       DETERMINE EXPERIMENTAL TRANSFERENCE NUMBER
C
```

```
      TOPLUS=(TCOEF-XE)/(1.0-XE)
C
C     NOW LETS ITERATE THE THEORETICAL EXPRESSION
C     FOR CONDUCTIVITY AND TRANSFERENCE NUMBER
C     TO FIND VALUES OF PARAM
C
      NCOUNT=1
80    CALL FUNDER(PARAM,YO,DX,DYDX)
      YO(2)=-YO(2)+1.0-TOPLUS
      YO(1)=-YO(1)+KAPPA
      CALL MATINV(2,1,DET,DYDX,YO)
C
C     DAMPEN CHANGES IN DEPENDENT VARIABLES IF
C     TOO LARGE
C
      IF(ABS(YO(1)/PARAM(1)).GT.2.0) YO(1)=SIGN(2.0*PARAM(1),YO(1))
      IF(ABS(YO(2)/PARAM(2)).GT.2.0) YO(2)=SIGN(2.0*PARAM(2),YO(2))
      PARAM(1)=PARAM(1)+YO(1)
      PARAM(2)=PARAM(2)+YO(2)
C
C     ITERATION TOLERANCE COMPUTED HERE
C
      DIFF=(ABS(YO(1))+ABS(YO(2)))/(ABS(PARAM(1))+ABS(PARAM(2)))
      NCOUNT=NCOUNT+1
      IF(NCOUNT.GT.NITER2) GO TO 1100
      IF(DIFF.GT.TOL2) GO TO 80
C
C     WRITE OUT RESULTS
C
      WRITE(6,100) NCOUNT,XE,KAPPA,MU,TOPLUS,TRUDEN,DENSTY,SCRPTD,
     1 PARAM(1),PARAM(2)
100   FORMAT(* *I2,3X,6(F8.6,3X),3(1PE14.7,3X))
      GO TO 1200
C
C     ERRORS PROCESSED HERE
C
1000  WRITE(6,1001) XE
1001  FORMAT(* *,
     1 *++++++++++ *,
     2 *NO PROPERTY AT A COMPOSITION OF XE = *,F6.4,
     3 * ++++++++++*/)
      GO TO 1200
1100  IERR=2
1101  WRITE(6,1102) IERR
1102  FORMAT(* *,
     1 *++++++++++ *,
     2 *TOO MANY ITERATIONS REQUIRED IERR = *,I1,
     3 * ++++++++++*)
1200  XE=XE+0.01
2000  CONTINUE
      STOP
```

```
5000     WRITE(6,5001) TEMP
5001     FORMAT(* *,
     1 *++++++++++ *,
     2 *NO PROPERTY AT A TEMPERATURE OF = *,F6.2,
     3 * ++++++++++*)
         STOP
         END

         SUBROUTINE COMP(LGPS2,DIFF)
C
C        ..........................................................
C
C        SUBROUTINE COMP
C
C        PURPOSE TO CALCULATE THE MATERIAL BALANCES FOR A POLYSULFIDE
C                MELT.
C
C        USAGE   CALL COMP(LGPS2,DIFF)
C
C        DESCRIPTION OF PARAMETERS
C
C                LGPS2   THE COMMON LOGARITHM OF THE SULFUR VAPOR
C                        PRESSURE. THIS PARAMETER IS THE INDEPENDENT
C                        VARIABLE INPUT INTO THE MATERIAL BALANCES.
C
C                DIFF    THE DIFFERENCE BETWEEN THE CALCULATED MOLE
C                        FRACTION OF ELECTROLYTE AND THE GIVEN
C                        MOLE FRACTION OF ELECTROLYTE.
C
C        SUBROUTINES REQUIRED
C
C                NONE
C
C        REFERENCE
C
C                RAGNAR TEGMAN, THERMODYNAMIC STUDIES OF HIGH
C                TEMPERATURE EQULIBRIA, CHEMICA SCRIPTA, 1976,
C                9, 158-166.
C
C        REVISED 8-24-83
C        ..........................................................
C
         REAL K,LGPS2,NUMER
         COMMON/FIRST/ DELTAG,IN,XE
         COMMON/FOURTH/R,TEMP,X
         DIMENSION DELTAH(8),DELTAS(8),DELTAG(8),IN(8),K(8),X(8)
C
C        DATA OF TEGMAN FOLLOWS
C
         DATA DELTAH, DELTAS/
     1   0.0,-68.52,-135.08,-204.04,-267.22,-333.24,0.0,-417.14,
```

```
     2  0.0,-37.65, -85.00,-155.64,-228.69,-312.07,0.0,-392.60/
C
C       INITIALIZE SOME CONSTANTS
C
        DATA N/8/
        NUMER=1.0
        DENOM=1.0
        PS2=10.0**(LGPS2)
C
C       FOR EACH COMPONENT IN THE MELT, CALCULATE DELTA G'S
C       AND RELATIVE COMPOSITIONS
C
        DO 10 I=2,N
C
C       CALCULATE DELTA G VALUES
C
        DELTAG(I)=DELTAH(I)*1000.0-TEMP*DELTAS(I)
        IF(IN(I).EQ.0) GO TO 10
C
C       NOW CALCULATE K'S
C
        K(I)=EXP(-DELTAG(I)/R/TEMP)
        X(I)=K(I)*PS2**(FLOAT(I-1)/2.0)
        NUMER=NUMER+X(I)
        DENOM=DENOM+FLOAT(I)*X(I)
10      CONTINUE
C
C       DETERMINE MONOSULFIDE ION COMPOSITION
C
        XCALC=NUMER/DENOM
        X(1)=1.0/NUMER
C
C       DETERMINE HIGHER POLYSULFIDE COMPOSITIONS
C
        DO 20 I=2,N
        IF (IN(I).EQ.0) GO TO 20
        X(I)=X(I)*X(1)
20      CONTINUE
C
C       RETURN COMPOSITION VALUES
C
        DIFF=XCALC-XE
        RETURN
        END

        SUBROUTINE SECANT(FCNY,X1,Y,X2,TOL,IERR,NITER)
C
C       ..................................................
C
C       SUBROUTINE SECANT
C
```

```
C       PURPOSE PERFORM AN ITERATION USING THE SECANT METHOD ON
C               A ONE-DIMENSIONAL FUNCTION.
C
C       USAGE   CALL SECANT(X1,Y1,X2,TOL,IERR,NITER)
C
C       DESCRIPTION OF PARAMETERS
C
C               X1      FIRST GUESS FOR INDEPENDENT VARIABLE.
C                               FINAL VALUE OF INDEPENDENT VARIABLE
C                               IS RETURNED HERE.
C               Y       FINAL VALUE OF DEPENDENT VARIABLE IS
C                               RETURNED HERE. DEPENDENT
C                               VARIABLE IS ITERATED TO ZERO.
C               X2      SECOND GUESS FOR INDEPENDENT VARIABLE.
C               TOL     ITERATION TOLERANCE EXPRESSED AS A
C                               FRACTION CHANGE OF THE INDEPENDENT
C                               VARIABLE.
C               IERR    ERROR FLAG.
C                       = 1     IF NUMBER OF SPECIFIED ITERATIONS
C                               ARE EXCEEDED.
C               NITER   NUMBER OF ITERATIONS. IERR IS ASSIGNED A
C                               VALUE OF ONE IF THE NUMBER OF
C                               ITERATIONS EXCEEDS THIS PARAMETER.
C
C       SUBROUTINES REQUIRED
C
C               FCNY    SUBROUTINE TO EVALUATE THE INDEPENDENT
C                               VARIABLE FOR A GIVEN VALUE OF THE
C                               DEPENDENT VARIABLE.
C
C       REVISED 1-29-83
C       ..................................................................
C
        DIMENSION DELTAG(8),IN(8),X(8)
        COMMON/FIRST/ DELTAG,IN,XE
        COMMON/FOURTH/ R,TEMP,X
        N=1
C
C       EVALUATE FUNCTION FOR INITIAL GUESSES
C
        CALL FCNY(X1,Y1)
        CALL FCNY(X2,Y2)

C
C       COMPUTE NEW VALUE FROM PREVIOUS GUESSES
C
1       X3=X2-(X2-X1)/(Y2-Y1)*Y2
        CALL FCNY(X3,Y3)
C
C       DETERMINE IF ITERATION TOLERANCE HAS BEEN MET
C
```

```
      IF(ABS((X3-X2)/X3).LT.TOL) GO TO 2
C
C     DETERMINE IF SPECIFIED NUMBER OF ITERATIONS
C           HAS BEEN EXCEEDED
C
      IF(N.GT.NITER) GO TO 3
C
C     IF NOT TRY AGAIN !
C
      X1=X2
      Y1=Y2
      X2=X3
      Y2=Y3
      N=N+1
      GO TO 1
C
C     SUCCESS ! RETURN VALUES
C
2     X1=X3
      Y=Y3
      RETURN
C
C     RETURN AN ERROR
C
3     IERR=1
      RETURN
      END

      SUBROUTINE MATINV(N,M,DETERM,B,D)
C
C     PROGRAM WRITTEN BY J. NEWMAN
C
C     COMMENTS HAVE BEEN OMITTED TO SAVE SPACE
C
      DIMENSION ID(7),B(N,N),D(N,M)
      DETERM=1.0
      DO 1 I=1,N
1     ID(I)=0
      DO 18 NN=1,N
      BMAX=1.1
      DO 6 I=1,N
      IF(ID(I).NE.0) GOTO 6
      BNEXT=0.0
      BTRY=0.0
      DO 5 J=1,N
      IF(ID(J).NE.0) GOTO 5
      IF(ABS(B(I,J)).LE.BNEXT) GOTO 5
      BNEXT=ABS(B(I,J))
      IF(BNEXT.LE.BTRY) GOTO 5
      BNEXT=BTRY
      BTRY=ABS(B(I,J))
```

```
      JC=J
5     CONTINUE
      IF(BNEXT.GE.BMAX*BTRY) GOTO 6
      BMAX=BNEXT/BTRY
      IROW=I
      JCOL=JC
6     CONTINUE
      IF(ID(JC).EQ.0) GOTO 8
      DETERM=0.0
      RETURN
8     ID(JCOL)=1
      IF(JCOL.EQ.IROW) GOTO 12
      DO 10 J=1,N
      SAVE=B(IROW,J)
      B(IROW,J)=B(JCOL,J)
10    B(JCOL,J)=SAVE
      DO 11 K=1,M
      SAVE=D(IROW,K)
      D(IROW,K)=D(JCOL,K)
11    D(JCOL,K)=SAVE
12    F=1.0/B(JCOL,JCOL)
      DO 13 J=1,N
13    B(JCOL,J)=B(JCOL,J)*F
      DO 14 K=1,M
14    D(JCOL,K)=D(JCOL,K)*F
      DO 18 I=1,N
      IF(I.EQ.JCOL) GO TO 18
      F=B(I,JCOL)
      DO 16 J=1,N
16    B(I,J)=B(I,J)-F*B(JCOL,J)
      DO 17 K=1,M
17    D(I,K)=D(I,K)-F*D(JCOL,K)
18    CONTINUE
      RETURN
      END

      SUBROUTINE FUNDER(XO,YO,DX,DYDX)
C
C     .................................................
C
C     SUBROUTINE FUNDER
C
C     PURPOSE CALCULATE THE VALUES OF THE FUNCTION AND
C             NUMERICALLY EVALUATE DERIVATIVES FOR A
C             TWO-DIMENSIONAL NEWTON-RAPHSON ITERATION.
C
C     USAGE CALL FUNDER(XO,YO,DX,DYDX)
C
C     DESCRIPTION OF PARAMETERS
C
C             XO      A VECTOR CONTAINING THE VALUES OF THE TWO
```

```
C                       INDEPENDENT VARIABLES.
C
C               YO      A VECTOR CONTAINING THE VALUES OF THE
C                       DEPENDENT VARIABLE AT THE CORRESPONDING
C                       VALUES OF THE INDEPENDENT VARIABLE IN XO.
C
C               DX      A VECTOR CONTAINING THE HALF INTERVAL OVER
C                       WHICH THE DERIVATIVES ARE NUMERICALLY
C                       EVALUATED. A CENTRAL DIFFERENCE APPROXIMATION
C                       FOR THE DERIVATIVE IS USED WITH A TOTAL
C                       INTERVAL DIFFERENCE OF 2*DX.
C
C               DYDX    A MATRIX CONTAINING THE DERIVATIVES OF
C                       THE TWO INDEPENDENT VARIABLES WITH RESPECT
C                       INDEPENDENT VARIABLES.
C
C       SUBROUTINES REQUIRED
C
C               FUNCT   EVALUATES THE INDEPENDENT VARIABLES FOR ANY
C                       VALUES OF THE TWO DEPENDENT VARIABLES.
C
C       REVISED 8-24-83
C       ..........................................................
C
        COMMON/THIRD/ C,DELTA,F,MSMNA,NCOMP,RBRAO,Y
        COMMON/FOURTH/ R,TEMP,X
        COMMON/FIFTH/POWER2, SCRPTD
        REAL MSMNA
        DIMENSION DELTA(8),X(8)
        DIMENSION XX(2),DX(2),DYDX(2,2),XO(2),YO(2),YY(3),YMAT(2,2)
C
C       FIRST SET UP THE GIVEN VALUES OF THE DEPENDENT VARIABLE INTO
C       ANOTHER REGISTER
C
        DO 1 M=1,2
        XX(M)=XO(M)
1       CONTINUE
C
C       NOW GET THE VALUES OF THE INDEPENDENT VARIABLES
C       AT THE GIVEN VALUES OF THE DEPENDENT VARIABLES
C
        CALL FUNCT(XX,YY)
        DO 2 M=1,2
        YO(M)=YY(M)
2       CONTINUE
C
C       NOW NUMERICALLY CALCULATE THE DERIVATIVES USING A
C       CENTRAL DIFFERENCE APPROXIMATION
C
        DO 7 J=1,2
C
```

```
C       FIND THE VALUES OF THE DEPENDENT VARIABLES
C
        DO 3 M=1,2
        XX(M)=XO(M)
3       CONTINUE
        XX(J)=XX(J)-DX(J)
C
C       NOW GET THE VALUES OF THE INDEPENDENT VARIABLES
C
        DO 5 K=1,2
        CALL FUNCT(XX,YY)
        DO 4 N=1,2
        YMAT(N,K)=YY(N)
4       CONTINUE
C
C       INCREMENT INDEPENDENT VARIABLE
C
        XX(J)=XX(J)+2.0*DX(J)
5       CONTINUE
C
C       CALCULATE THE DERIVATIVES
C
        DO 6 N=1,2
        DYDX(N,J)=(YMAT(N,2)-YMAT(N,1))/2.0/DX(J)
6       CONTINUE
7       CONTINUE
C
C       NOW RETURN
C
        RETURN
        END

        SUBROUTINE FUNCT(PARAM,YFUNC)
C
C       ..........................................................
C
C       SUBROUTINE FUNCT
C
C       PURPOSE CALCULATE THE MELT TRANSFERENCE NUMBER, CONDUCTIVITY,
C               AND DIFFUSION COEFFICIENT FOR THE POLYSULFIDE
C               MELT BY INVERSION OF THE TRANSPORT MATRIX.
C
C       USAGE   CALL SUBROUTINE FUNCT(PARAM,YFUNC)
C
C       DESCRIPTION OF PARAMETERS
C
C               PARAM   VECTOR OF INDEPENDENT PARAMETERS
C
C               YFUNC   VECTOR RETURNING CALCULATED TRANSFERENCE
C                       NUMBER AND DIFFUSION COEFFICIENT.
C
```

```
C       SUBROUTINES REQUIRED
C
C               NONE
C
C       REVISED 8-24-83
C
C       ..........................................................
C
        REAL KAPPA,MSMNA,L,M,KK
        COMMON/THIRD/ C,DELTA,F,MSMNA,N,RBRAO,Y
        COMMON/FOURTH/ R,TEMP,X
        COMMON/FIFTH/ POWER2,SCRPTD
        DIMENSION D(8,8),L(7,7),M(7,7),KK(8,8),TC(8)
        DIMENSION DELTA(8),X(8)
        DIMENSION YFUNC(2),PARAM(2)
        DATA M,L,KK/162*0.0/
C
C       CALCULATE D MATRIX
C
        DO 1 I=1,N-1
        DO 2 J=I,N-1
        IF(I.EQ.J) GO TO 2
        TOP=1.0
        BOT=(SQRT(DELTA(I))+SQRT(DELTA(J)))**POWER2
        D(I,J)=PARAM(1)*(TOP/BOT)
        D(J,I)=D(I,J)
2       CONTINUE
        RI=1.0/(RBRAO+SQRT(DELTA(I)))**POWER2
        D(I,N)=RI*PARAM(2)
        D(N,I)=D(I,N)
1       CONTINUE
C
C       CALCULATE K MATRIX
C
        RTC=C*R*TEMP
        RTC3=RTC/3.0
        DO 3 I=1,N-1
        DO 3 J=I+1,N
        IF (I.EQ.J) GO TO 3
        KK(I,J)=RTC3*X(I)*X(J)/D(I,J)
        KK(J,I)=KK(I,J)
3       CONTINUE

C
C       SET UP M MATRIX
C
        DO 6 I=1,N-1
        DO 6 J=I,N-1
        M(I,J)=KK(I,J)
        IF(I.NE.J) GO TO 5
        DO 4 K=1,N
```

```
      M(I,J)=M(I,J)-KK(I,K)
4     CONTINUE
      IF(I.EQ.J) GO TO 6
5     M(J,I)=M(I,J)
6     CONTINUE
C
C     SET UP THE IDENTITY MATRIX IN THE L MATRIX
C
      DO 10 I=1,N-1
      L(I,I)=1.0
10    CONTINUE
C
C     NOW INVERT M MATRIX
C
      CALL MATINV(N-1,N-1,DETERM,M,L)
C
C     CALCULATE TRANSFERENCE NUMBERS,
C     DIFFUSION COEFFICIENTS, AND
C     CONDUCTIVITY
C
      APR=0.0
      BPR=0.0
      SUM4=0.0
      DO 200 K=1,N-1
      SUM1=0.0
      SUM2=0.0
      DO 100 J=1,N-1
      TERM=L(K,J)*X(J)
      SUM1=SUM1+TERM
      SUM2=SUM2+TERM*(DELTA(J)-1.0)
100   CONTINUE
      TC(K)=X(K)*SUM1
      APR=APR+TC(K)
      BPR=BPR+SUM2*X(K)
      SUM4=SUM4+DELTA(K)*X(K)*SUM2
200   CONTINUE
      SUM3=0.0
      DO 300 K=1,N-1
      TC(K)=TC(K)/APR
      SUM3=SUM3+TC(K)*DELTA(K)
300   CONTINUE
      TOPLUS=(SUM3-1.0)/(Y-1.0)
      SCRPTD=3.0*RTC/(Y+2.0)/(Y-1.0)*(BPR*SUM3-SUM4)
      KAPPA=-4.0*F*F*C*C*APR
      YFUNC(2)=1.0-TOPLUS
      YFUNC(1)=KAPPA
      RETURN
      END

      SUBROUTINE PROPRT(TEMP,WS,PROP,N,ISIZE,IPROP)
C     ..................................................
```

```
C
C       PROGRAM PROPRT
C
C       PURPOSE COMPUTE TRANSPORT AND PHYSICAL PROPERTIES FOR
C               SODIUM POLYSULFIDE MELTS AT SPECIFIC COMPOSITIONS
C               AS A FUNCTION OF TEMPERATURE. SUBROUTINE PROPRT
C               CALCULATES ALL OF THE COMPOSITIONAL DATA FOR
C               A GIVEN PROPERTY AT A SELECTED TEMPERATURE.
C
C       USAGE CALL PROPRT(TEMP,WS,PROP,N,ISIZE,IPROP)
C
C       PARAMETERS
C                        TEMP    TEMPERATURE
C                        WS      WEIGHT PERCENT SULFUR
C                        PROP    PHYSICAL OR TRANSPORT PROPERTY
C                        N       SIZE OF ARRAY PROP AND X
C                        ISIZE   NUMBER OF COMPOSITIONS
C                        IPROP   VARIABLE INDICATING DESIRED
C                                TRANSPORT PROPERTY
C
C                                = 1     DENSITY
C                                = 2     VISCOSITY
C                                = 3     SURFACE TENSION
C                                = 4     CONDUCTIVITY
C
C       SUBROUTINES REQUIRED
C               NONE
C
C       REFERENCES
C               B. CLEAVER, A.J. DAVIES, AND M.D. HAMES,
C               'PROPERTIES OF FUSED POLYSULFIDES - I. II., III.'
C               ELECTROCHEMICA ACTA, 18, 1973, PP. 719 - 739.
C
C       REVISED 1-20-83
C       ..................................................
C
        REAL KCOEF
        DIMENSION ILNGTH(6),ICODE(6),
     1  PCOEF(5,5),ECOEF(8,6),GCOEF(10,5),
     2  KCOEF(7,6),PROP(N),WS(N)
        DATA ((PCOEF(I,J),J=1,5),I=1,5),
     2       ((ECOEF(I,J),J=1,6),I=1,8),
     3       ((GCOEF(I,J),J=1,5),I=1,10),
     4       ((KCOEF(I,J),J=1,6),I=1,7)/
C
C         DENSITY COEFFICIENTS FOLLOW.
C
     1  6.76E-01,5.90E02,6.83E02,1.887E00,-5.65E-04,
C
C       NEXT DATA STATEMENT IS CHANGED
C       DOES NOT REFLECT CLEVER AND DAVIES DATA EXACTLY
```

```
C       LINE SHOULD CORRECTLY READ AS FOLLOWS
C
C     2  6.97E-01,5.76E02,6.89E02,1.901E00,-7.96E-04,
C
     2  6.97E-01,5.73E02,6.89E02,1.901E00,-7.96E-04,
     3  7.20E-01,5.63E02,6.69E02,1.926E00,-5.47E-04,
     4  7.54E-01,5.71E02,6.80E02,1.869E00,-6.66E-04,
     5  7.70E-01,5.73E02,6.83E02,1.876E00,-7.16E-04,
C
C         VISCOSITY COEFFICIENTS FOLLOW.
C
     1  6.84E-01,5.77E02,6.53E02,5.647E-01,8.428E03,3.32E02,
     2  7.00E-01,5.89E02,6.47E02,3.344E-01,1.124E04,2.88E02,
     3  7.17E-01,5.58E02,6.46E02,6.351E-01,7.915E03,3.42E02,
     4  7.31E-01,5.33E02,6.52E02,4.055E-01,9.283E03,3.26E02,
     5  7.40E-01,5.87E02,6.41E02,4.079E-01,9.333E03,3.28E02,
     6  7.51E-01,5.72E02,6.75E02,8.021E-01,6.020E03,3.90E02,
     7  7.68E-01,5.57E02,6.54E02,4.733E-01,8.181E03,3.56E02,
     8  7.85E-01,6.20E02,6.48E02,1.717E+00,3.125E03,4.65E02,
C
C         SURFACE TENSION COEFFICIENTS FOLLOW.
C
     1  6.77E-01,5.83E02,6.91E02,1.738E02,-6.00E-02,
     2  6.85E-01,5.88E02,6.73E02,1.653E02,-1.19E-01,
     3  6.97E-01,5.86E02,6.71E02,1.526E02,-6.50E-02,
     4  7.15E-01,5.89E02,6.77E02,1.416E02,-3.40E-02,
     5  7.24E-01,5.39E02,6.76E02,1.320E02,-3.60E-02,
     6  7.40E-01,5.56E02,6.41E02,1.282E02,-5.80E-02,
     7  7.51E-01,6.02E02,6.76E02,1.278E02,-6.70E-02,
     8  7.63E-01,5.62E02,6.71E02,1.272E02,-7.10E-02,
     9  7.68E-01,6.25E02,6.88E02,1.280E02,-9.10E-02,
     *  7.84E-01,6.16E02,6.61E02,1.153E02,-3.90E-02,
C
C         CONDUCTIVITY COEFFICIENTS FOLLOW.
C
     1  6.00E-01,7.28E02,8.40E02,5.478E00,3.079E03,4.99E02,
     2  6.61E-01,6.42E02,6.98E02,3.836E00,2.478E03,4.58E02,
     3  6.75E-01,5.82E02,6.93E02,7.033E00,5.693E03,3.29E02,
     4  7.01E-01,4.58E02,6.94E02,7.048E00,5.854E03,3.30E02,
     5  7.23E-01,4.28E02,6.94E02,7.056E00,6.436E03,3.25E02,
     6  7.48E-01,4.56E02,6.71E02,6.279E00,6.163E03,3.41E02,
     7  7.78E-01,4.77E02,6.81E02,5.815E00,6.329E03,3.44E02/
C
C
C
      DATA ILNGTH/5,8,10,7/
      DATA R/8.314/
      ISIZE=1
      DO 100 I=1,ILNGTH(IPROP)
      GO TO (10,20,30,40), IPROP
C
```

```
C       DENSITY CALCULATED HERE
C
10      IF(TEMP.LT.PCOEF(I,2)) GO TO 100
        IF(TEMP.GT.PCOEF(I,3)) GO TO 100
        PROP(ISIZE)=PCOEF(I,4)+PCOEF(I,5)*(TEMP-600.)
        WS(ISIZE)=PCOEF(I,1)
        GO TO 50
C
C       VISCOSITY HERE
C
20      IF(TEMP.LT.ECOEF(I,2)) GO TO 100
        IF(TEMP.GT.ECOEF(I,3)) GO TO 100
        PROP(ISIZE)=ECOEF(I,4)*EXP(ECOEF(I,5)/(R*(TEMP-ECOEF(I,6))))
        WS(ISIZE)=ECOEF(I,1)
        GO TO 50
C
C       SURFACE TENSION HERE
C
30      IF(TEMP.LT.GCOEF(I,2)) GO TO 100
        IF(TEMP.GT.GCOEF(I,3)) GO TO 100
        PROP(ISIZE)=GCOEF(I,4)+GCOEF(I,5)*(TEMP-600.)
        WS(ISIZE)=GCOEF(I,1)
        GO TO 50
C
C       CONDUCTIVITY HERE
C
40      IF(TEMP.LT.KCOEF(I,2)) GO TO 100
        IF(TEMP.GT.KCOEF(I,3)) GO TO 100
        PROP(ISIZE)=KCOEF(I,4)*EXP(-KCOEF(I,5)/(R*(TEMP-KCOEF(I,6))))
        WS(ISIZE)=KCOEF(I,1)
50      CONTINUE
        ISIZE=ISIZE+1
100     CONTINUE
        ISIZE=ISIZE-1
        RETURN
        END

        SUBROUTINE CUBSPL(X,Y,S,A,N,NPTS,IEND)
C
C       ..................................................
C
C       SUBROUTINE CUBSPL
C
C       PURPOSE COMPUTE A CUBIC SPLINE FOR N DATA POINTS.
C
C       USAGE   CALL CUBSPL(X,Y,S,A,N,NPTS,IEND)
C
C       DESCRIPTION OF PARAMETERS
C
C               X       ARRAY OF INDEPENDENT VARIABLE
C               Y       ARRAY OF DEPENDENT VARIABLE
```

```
C               N       SIZE OF ARRAYS
C               NPTS    NUMBER OF POINTS
C               IEND    TYPE OF END CONDITION TO BE USED.
C
C                       =1      LINEAR ENDS; S(1)=S(N)=0
C                       =2      PARABOLIC ENDS S(1)=S(2), S(N)=S(N-1)
C                       =3      CUBIC ENDS; S(1), S(N) ARE EXTRAPOLATED
C
C       REMARKS PROGRAM SETS UP AND SOLVES TRIDIAGONAL MATRIX.
C               PROGRAM RETURNS VALUES OF SECOND DERIVATIVE
C               AT EACH END POINT.
C
C       SUBROUTINES AND SUBPROGRAMS REQUIRED
C               NONE
C
C       METHOD  TRIDIAGONAL MATRIX EVALUATION IS USED.
C               REFERENCES: CURTIS GERALD, 'APPLIED NUMERICAL
C               ANALYSIS', SECOND EDITION, ADDISON AND WESTLEY,
C               1978, CHAPTER 10, SECTION 3, PP. 474-482.
C
C       REVISED 12-12-82
C       ..........................................................
C
        DIMENSION X(N),Y(N),S(N),A(N,4)
C
C       COMPUTE FOR N-2 ROWS.
C
        NM2=NPTS-2
        NM1=NPTS-1
        DX1=X(2)-X(1)
        DY1=(Y(2)-Y(1))/DX1*6.0
        DO 10 I=1,NM2
        DX2=X(I+2)-X(I+1)
        DY2=(Y(I+2)-Y(I+1))/DX2*6.0
        A(I,1)=DX1
        A(I,2)=2.0*(DX1+DX2)
        A(I,3)=DX2
        A(I,4)=DY2-DY1
        DX1=DX2
        DY1=DY2
10      CONTINUE
C
C       ADJUST FIRST AND LAST ROWS APPROPRIATE TO END CONDITION.
C
        GO TO (20,50,80), IEND
C
C       FOR IEND = 1, NO CHANGE IS NEEDED.
C
20      GO TO 100
C
C       FOR IEND = 2, S(1)=S(2), S(N-1)=S(N), PARABOLIC ENDS.
```

```
C
50      A(1,2)=A(1,2)+X(2)-X(1)
        A(NM2,2)=A(NM2,2)+X(NPTS)-X(NM1)
        GO TO 100
C
C       FOR IEND = 3, CUBIC ENDS, S(1) AND S(N) ARE EXTRAPOLATED.
C
80      DX1=X(2)-X(1)
        DX2=X(3)-X(2)
        A(1,2)=(DX1+DX2)*(DX1+2.0*DX2)/DX2
        A(1,3)=(DX2*DX2-DX1*DX1)/DX2
        DXN2=X(NM1)-X(NM2)
        DXN1=X(NPTS)-X(NM1)
        A(NM2,1)=(DXN2*DXN2-DXN1*DXN1)/DXN2
        A(NM2,2)=(DXN1+DXN2)*(DXN1+2.*DXN2)/DXN2
C
C       NOW SOLVE TRIDIAGONAL SYSTEM.
C
C       FIRST REDUCE ROWS.
C
100     DO 110 I=2,NM2
        A(I,2)=A(I,2)-A(I,1)/A(I-1,2)*A(I-1,3)
        A(I,4)=A(I,4)-A(I,1)/A(I-1,2)*A(I-1,4)
110     CONTINUE
C
C       NOW BACK SUBSTITUTE
C
        A(NM2,4)=A(NM2,4)/A(NM2,2)
        DO 120 I=2,NM2
        J=NM1-I
        A(J,4)=(A(J,4)-A(J,3)*A(J+1,4))/A(J,2)
120     CONTINUE
C
C       TABULATE S VECTOR
C
        DO 130 I=1,NM2
        S(I+1)=A(I,4)
130     CONTINUE
C
C       SUBSTITUTE END CONDITIONS
C
        GO TO (150,160,170), IEND
C
C       FOR LINEAR ENDS, S(1)=0, S(N)=0
C
150     S(1)=0.
        S(NPTS)=0.
        RETURN
C
C       FOR PARABOLIC ENDS, S(1)=S(2), S(N)=S(N-1)
C
```

```
160     S(1)=S(2)
        S(NPTS)=S(NPTS-1)
        RETURN
C
C       FOR CUBIC ENDS, EXTRAPOLATE.
C
170     S(1)=((DX1+DX2)*S(2)+DX1*S(3))/DX2
        S(NPTS)=((DXN2+DXN1)*S(NM1)-DXN1*S(NM2))/DXN2
        RETURN
        END
        SUBROUTINE CURVE(Y1,X1,X,Y,S,ISIZE,IERR)
C
C       ..........................................................
C
C       SUBROUTINE CURVE
C
C       PURPOSE INTERPOLATE BETWEEN AN ARBITRARY SET OF POINTS.
C               IF THE SET OF POINTS CONTAINS MORE THAN
C               THREE POINTS, CURVE USES THE VALUES OF SECOND
C               DERIVATIVES AT EACH POINT TO DETERMINE A CUBIC
C               SPLINE THROUGH THE POINTS. IF THREE OR LESS POINTS
C               ARE GIVEN, CURVE USES A LEGENDRE INTERPOLATING
C               POLYNOMINAL TO DETERMINE VALUES AT INTERMEDIATE
C               POINTS.
C
C       USAGE   CALL CURVE(Y1,X1,X,Y,S,ISIZE,IERR)
C
C       DESCRIPTION OF PARAMETERS
C
C               Y1      INTERPOLATED VALUE OF DEPENDENT VARIABLE
C                       REQUIRED AT X1.
C               X1      VALUE OF INDEPENDENT VARIABLE.
C               X       ARRAY OF INDEPENDENT VARIABLE VALUES.
C               Y       ARRAY OF DEPENDENT VARIABLE VALUES
C                       CORRESPONDING TO POINTS IN ARRAY X.
C               S       ARRAY OF SECOND DERIVATIVE VALUES
C                       CORRESPONDING TO POINTS IN ARRAY X.
C               ISIZE   NUMBER OF POINTS IN ARRAYS X,Y AND S.
C               IERR    ERROR FLAG
C                       =1      IF REQUIRED POINT TO BE
C                               INTERPOLATED LIES OUTSIDE THE
C                               RANGE OF VALUES IN ARRAY X.
C
C       REMARKS VALUES IN ARRAY X MUST BE ARRANGED IN DECREASING
C               ORDER. VALUES FOR SECOND DERIVATIVES CAN BE
C               OBTAINED FROM SUBROUTINE CUBSPL.
C
C       REVISED 1-29-83
C       ..........................................................
C
        DIMENSION X(10),Y(10),S(10)
```

```
      IERR=0
      DO 1 J=1,ISIZE-1
      IF(X1.LT.X(J+1)) GO TO 1
      IF(X1.GT.X(J)) GO TO 1
      GO TO 2
1     CONTINUE
      IERR=1
      RETURN
C
C     IF MORE THAN THREE POINTS USE CUBIC SPLINE
C
2     IF(ISIZE.LE.3) GO TO 3
      DXJ=X(J+1)-X(J)
      DYJ=Y(J+1)-Y(J)
      DSJ=S(J+1)-S(J)
      A1=DSJ/6.0/DXJ
      A2=S(J)/2.0
      A3=DYJ/DXJ-(2.0*S(J)+S(J+1))*DXJ/6.0
      A4=Y(J)
      DX=X1-X(J)
      Y1=((A1*DX+A2)*DX+A3)*DX+A4
      RETURN
C
C     IF THREE POINTS OR LESS USE LEGENDRE POLYNOMIAL
C
3     Y1=0.0
      DO 4 I=1,ISIZE
      HOLD=1.0
      DO 5 J=1, ISIZE
      IF(I.EQ.J) GO TO 5
      HOLD=HOLD*(X1-X(J))/(X(I)-X(J))
5     CONTINUE
      Y1=Y1+HOLD*Y(I)
4     CONTINUE
      END

      SUBROUTINE CONVRT(XIN,XOUT,IXIN,IXOUT)
C
C     ..............................................................
C
C     SUBROUTINE CONVRT
C
C     PURPOSE CONVERT THE COMPOSITION OF SODIUM POLYSULFIDE
C             FROM ONE COMPOSITIONAL VARIABLE TO ANOTHER.
C             ALLOWABLE VARIABLES ARE
C
C                     MOLE FRACTION SODIUM SULFIDE
C                     MOLE FRACTION SULFUR
C                     Y IN NA(2)S(Y)
C                     MASS FRACTION SODIUM SULFIDE
C                     MASS FRACTION SULFUR
```

```
C
C       USAGE   CALL CONVRT(XIN,XOUT,IXIN,IXOUT)
C
C       DESCRIPTION OF PARAMETERS
C
C               XIN     INPUT COMPOSITION VARIABLE
C               XOUT    OUTPUT COMPOSITION VARIABLE
C               IXIN    INPUT COMPOSITION  VARIABLE CODE
C                       DETERMINES TYPE OF INPUT COMPOSITION VARIABLE
C
C                       =1      COMPOSITION IN MOLE FRACTION SODIUM
C                                       SULFIDE
C                       =2      COMPOSITION IN MOLE FRACTION SULFUR
C                       =3      COMPOSITION IN NA(2)S(X)
C                       =4      COMPOSITION IN MASS FRACTION SODIUM
C                                       SULFIDE
C                       =5      COMPOSITION IN MASS FRACTION SULFUR
C
C               IXOUT   OUTPUT COMPOSITION VARIABLE CODE
C                       DETERMINES TYPE OF OUTPUT COMPOSITION VARIABLE
C
C                       =1      COMPOSITION IN MOLE FRACTION SODIUM
C                                       SULFIDE
C                       =2      COMPOSITION IN MOLE FRACTION SULFUR
C                       =3      COMPOSITION IN NA(2)S(X)
C                       =4      COMPOSITION IN MASS FRACTION SODIUM
C                                       SULFIDE
C                       =5      COMPOSITION IN MASS FRACTION SULFUR
C
C       REMARKS PROGRAM FIRST TAKES INPUT COMPOSITION AND CONVERTS
C               IT TO MASS FRACTION OF SULFUR. THEN THE OUTPUT
C               COMPOSITION IS COMPUTED FROM THE MASS FRACTION
C               OF SULFUR.
C
C       REVISED 1-30-83
C       ..........................................................
C
C
        RMW=22.98977/32.06
        IF (IXIN.EQ.IXOUT) GO TO 110
        GO TO (10,20,30,40,50), IXIN
C
C       MOLE FRACTION SODIUM SULFIDE TO MASS FRACTION SULFUR
C
10      XOUT=1.0/(1.0+2.0*RMW*XIN)
        GO TO 55
C
C       MOLE FRACTION SULFUR TO MASS FRACTION SULFUR
C
20      XOUT=1.0/(1.0+RMW*(1.0-XIN)/XIN)
        GO TO 55
```

```
C
C       X IN NA(2)S(X) TO MASS FRACTION SULFUR
C
30      XOUT=1.0/(1.0+2.0*RMW/XIN)
        GO TO 55
C
C       MASS FRACTION SODIUM SULFIDE TO MASS FRACTION SULFUR
C
40      XOUT=XIN/(2.0*RMW+1.0)+(1.0-XIN)
        GO TO 55
C
C       MASS FRACTION SULFUR TO MASS FRACTION SULFUR
C
50      XOUT=XIN
55      GO TO (60,70,80,90,100), IXOUT
C
C       MASS FRACTION SULFUR TO MOLE FRACTION SODIUM SULFIDE
C
60      XOUT=(1.0-XOUT)/2.0/XOUT/RMW
        RETURN
C
C       MASS FRACTION SULFUR TO MOLE FRACTION SULFUR
C
70      XOUT=1.0/(1.0+(1.0-XOUT)/XOUT/RMW)
        RETURN
C
C       MASS FRACTION SULFUR TO X IN NA(2)S(X)
C
80      XOUT=2.0*RMW*XOUT/(1.0-XOUT)
        RETURN
C
C       MASS FRACTION SULFUR TO MASS FRACTION SODIUM SULFIDE
C
90      XOUT=(1.0+1.0/2.0/RMW)*(1.0-XOUT)
100     RETURN
C
C       MASS FRACTION SULFUR TO MASS FRACTION SULFUR
C
110     XOUT=XIN
        RETURN
        END
```

Sample Output for Program SSTP

TEMPERATURE = 633.15 K
POWER2 = 3.00000

NITER	XE	KAPPA	MU	TOPLUS	EXP DENS	CALC DENS	SCRIPTD	4PIE1NA/3MUV1	4PIE2NA/3MUV1
5	.210000	.443306	16.49896	.964684	1.851059	1.847236	5.5725906E-07	1.8400366E-04	2.2971109E-04
5	.220000	.465608	16.05445	.964231	1.845884	1.858264	5.6658035E-07	2.1308857E-04	2.2223057E-04
5	.230000	.486746	15.74387	.963766	1.848753	1.867299	5.7550735E-07	2.4966713E-04	2.1512016E-04
6	.240000	.506273	16.12326	.963289	1.862294	1.874239	5.8348153E-07	2.8728933E-04	2.0821354E-04
6	.250000	.526028	15.81848	.962800	1.880946	1.879175	5.9246791E-07	3.1729431E-04	2.0223615E-04
6	.260000	.550084	15.39426	.962297	1.898210	1.882364	6.0677991E-07	3.3525272E-04	1.9851363E-04
6	.270000	.582561	16.22135	.961781	1.907587	1.884112	6.3055738E-07	3.4256081E-04	1.9806504E-04
6	.280000	.623313	16.96809	.961250	1.904154	1.884676	6.6322396E-07	3.4023977E-04	2.0031362E-04
6	.290000	.664693	17.02000	.960704	1.891936	1.884230	6.9646342E-07	3.2505718E-04	2.0251821E-04
6	.300000	.698322	16.77246	.960143	1.878116	1.882889	7.2172121E-07	2.9537001E-04	2.0227115E-04
5	.310000	.719701	16.55735	.959565	1.869348	1.880732	7.3478274E-07	2.5478601E-04	1.9868842E-04
5	.320000	.731671	16.39042	.958971	1.866618	1.877826	7.3902322E-07	2.1130727E-04	1.9297754E-04

Appendix G

Derivation of Potential Distribution for a Semi–Infinite Flow–By Electrode at the Limiting Current

The governing equation for the potential distribution at the limiting current is

$$\nabla^2 \Phi_2 = - \frac{nFak_m c_F}{s_R \kappa} e^{- \frac{ak_m}{\upsilon} y} \tag{G–1}$$

with the boundary conditions

$$at\ y = 0,\ \frac{\partial \Phi_2}{\partial y} = 0, \tag{G–2}$$

$$as\ y \to \infty,\ \frac{\partial \Phi_2}{\partial y} \to 0, \tag{G–3}$$

$$at\ x = 0,\ \frac{\partial \Phi_2}{\partial x} = 0, \tag{G–4}$$

and

$$at\ x = d,\ \Phi_2 = V\ . \tag{G–5}$$

For simplicity, rewrite Equation (G–1) as

$$\nabla^2 \Phi_2 = - Ge^{- ay}\ , \tag{G–6}$$

where

$$G = \frac{nFak_m c_F}{s_R \kappa}\ , \tag{G–7}$$

and

$$\alpha = \frac{ak_m}{\upsilon}\ . \tag{G–8}$$

By superposition, let

$$\Phi_2 = - \frac{G}{\alpha^2} e^{- ay} + \Phi_2^A + \Phi_2^B + V\ . \tag{G–9}$$

Here, Φ_2 has been decomposed into a sum of a particular solution and three

homogeneous solutions. The last term in Equation (G–9) is the third homogeneous solution, which has been solved by inspection.

The particular solution to Equation (G–1) above satisfies the differential equation; however, it introduces a nonhomogeneous boundary condition which extends from y=0 to infinity along $x=d$. First, this must be removed. Let Φ_2^A be the solution to

$$\nabla^2\Phi_2^A = 0\,, \tag{G–10}$$

with the boundary conditions

$$as\ y \to \infty,\ \frac{\partial\Phi_2^A}{\partial y} = 0, \tag{G–11}$$

$$at\ x = 0,\ \frac{\partial\Phi_2^A}{\partial x} = 0, \tag{G–12}$$

$$at\ x = d,\ \Phi_2^A = \frac{G}{\alpha^2}\,e^{-\alpha y}\,. \tag{G–13}$$

Because the dimensions of the electrode extend to infinity in the y direction, there are no eigenvalues determined in the y direction. Therefore the nonhomogeneity along $x = d$ must be transformed to a boundary extending in the x direction. In order to remove this non–homogeneous boundary condition, one is not at liberty to prescribe four boundary conditions upon Φ_2^A, but only three. Solution of Equation (G–10) by separation of variables subject to the three boundary conditions of Equations (G–11) through (G–13) gives

$$\Phi_2^A = \frac{G}{\alpha^2\cos\alpha d}\,e^{-\alpha y}\cos\alpha x\,. \tag{G–14}$$

Because we have specified only three boundary conditions in the solution to Φ_2^A, we must now evaluate the effect of this solution upon the fourth boundary. Using the original boundary conditions combined with the values of the particular and two homogeneous solutions at the boundaries

now gives the boundary conditions for Φ_2^B as

$$at\ y=0,\ \frac{\partial \Phi_2^B}{\partial y} = \frac{G}{\alpha}\left[\frac{\cos \alpha x}{\cos \alpha d} - 1\right], \tag{G-15}$$

$$as\ y \to \infty,\ \frac{\partial \Phi_2^B}{\partial y} = 0\ , \tag{G-16}$$

$$at\ x = 0,\ \frac{\partial \Phi_2^B}{\partial x} = 0\ , \tag{G-17}$$

and

$$at\ x = d,\ \Phi_2^B = 0\ . \tag{G-18}$$

The homogeneous solution Φ_2^B must satisfy

$$\nabla^2 \Phi_2^B = 0\ . \tag{G-19}$$

Again, solution by separation of variables gives

$$\Phi_2^B = \sum_{n=0}^{\infty} C_n e^{-\lambda_n y/d} \cos \lambda_n x/d\ , \tag{G-20}$$

where

$$\lambda_n = \frac{(2n+1)\pi}{2}\ . \tag{G-21}$$

The constants in Equation (G-20) are evaluated using the boundary condition at $y = 0$, Equation (G-15). Differentiating Equation (G-20) with respect to y and applying Equation (G-15) yields

$$\frac{\partial \Phi_2^B}{\partial y} = -\sum_{n=0}^{\infty} \frac{C_n \lambda_n}{d} e^{-\lambda_n y/d} \cos\left(\lambda_n x/d\right) = \frac{G}{\alpha}\left[\frac{\cos \alpha x}{\cos \alpha d} - 1\right]. \tag{G-22}$$

The constants C_n are determined by Fourier's Theorem which requires

$$\int_0^d \frac{C_n \lambda_n}{d} \cos^2\left(\lambda_n x/d\right) dx = -\frac{G}{\alpha}\int_0^d \left[\frac{\cos \alpha x}{\cos \alpha d} - 1\right]\cos\left(\lambda_n x/d\right) dx \tag{G-23}$$

The expression on the left of Equation (G-23) can be integrated, and for all values of λ_n it becomes

$$\int_0^d \frac{C_n \lambda_n}{d} \cos^2\left(\lambda_n x/d\right) dx = \frac{1}{2} C_n \lambda_n\ . \tag{G-24}$$

To evaluate the integral on the right of Equation (G-23), we must distinguish

to cases:

$$Case\ 1 \quad \lambda_n^2 = (\alpha d)^2 , \tag{G-25}$$

and

$$Case\ 2 \quad \lambda_n^2 \neq (\alpha d)^2 . \tag{G-26}$$

For case 1

$$\frac{1}{2} C_n \lambda_n = - \frac{G}{\alpha} \int_0^d \left[\frac{\cos \alpha x}{\cos \alpha d} - 1 \right] \cos (\lambda_n x / d)\, dx , \tag{G-27}$$

$$= \frac{Gd(-1)^n}{\lambda_n \alpha} - \frac{1}{2} \frac{Gd}{\alpha \cos \alpha d} , \tag{G-28}$$

or

$$C_n = \frac{2G(-1)^n}{\alpha^3 d} - \frac{G}{\alpha^2 \cos \alpha d} . \tag{G-29}$$

For case 2

$$\frac{1}{2} C_n \lambda_n d = - \frac{G}{\alpha} \int_0^d \left[\frac{\cos \alpha x}{\cos \alpha d} - 1 \right] \cos (\lambda_n x / d)\, dx , \tag{G-30}$$

$$= \frac{Gd(-1)^n}{\alpha \lambda_n} - \frac{Gd}{\alpha \cos \alpha d} \left[\frac{\sin (\lambda_n - \alpha d)}{2(\lambda_n - \alpha d)} + \frac{\sin (\lambda_n + \alpha d)}{2(\lambda_n + \alpha d)} \right] , \tag{G-31}$$

or

$$C_n = \frac{2Gd(-1)^n}{\alpha \lambda_n^2} - \frac{2Gd}{\alpha \lambda_n \cos \alpha d} \left[\frac{\sin (\lambda_n - \alpha d)}{2(\lambda_n - \alpha d)} + \frac{\sin (\lambda_n + \alpha d)}{2(\lambda_n + \alpha d)} \right] , \tag{G-32}$$

$$= \frac{2G(-1)^n d}{\alpha \lambda_n^2} - \frac{2G(-1)^n}{\alpha(\lambda_n^2 - (\alpha d)^2)} . \tag{G-33}$$

For the case of $\lambda_n \neq \alpha d$, the potential distribution then becomes

$$\frac{\Phi_2 - V}{\frac{nFc_P v^2}{s_P \kappa \alpha k_m}} = e^{-\alpha y} \left[\frac{\cos \alpha x}{\cos \alpha d} - 1 \right]$$

$$+ 2\alpha d (-1)^n \sum_{n=0}^{\infty} \left[\frac{1}{\lambda_n^2} - \frac{1}{\lambda_n^2 - (\alpha d)^2} \right] e^{-\lambda_n y / d} \cos \lambda_n x / d . \tag{G-34}$$

The maximum potential difference occurs within the flow-by electrode between the points $x=0, y=0$ and $x=d, y=0$. From Equation (G-34) above

this is

$$\frac{\Phi_2(x=0,y=0)-V}{\dfrac{nFc_F v^2}{s_R\,\kappa\,ak_m}} = \frac{\Delta\Phi_2}{\dfrac{nFc_F v^2}{s_R\,\kappa\,ak_m}} = \frac{\Delta\Phi_2}{\dfrac{\varepsilon nFc_F D_o}{s_R\,\kappa}}\,\frac{Sh}{Pe^2}$$

$$= \frac{1}{\cos\alpha d} - 1 + 2\alpha d\sum_{n=0}^{\infty}(-1)^n\left[\frac{1}{\lambda_n^2} - \frac{1}{\lambda_n^2-(\alpha d)^2}\right] \quad \text{(G–35)}$$

If αd is an eigenvalue of the system, then the term in the summations appearing in Equations (G–34) and (G–35) corresponding to this eigenvalue should be replaced with the appropriate constant calculated in Equation (G–29). In this case the potential distribution is

$$\frac{\Phi_2 - V}{\dfrac{nFc_F v^2}{s_R\,\kappa\,ak_m}} = -e^{-\alpha y}$$

$$+ 2\alpha d\sum_{n=0}^{\infty}(-1)^n\left[\frac{1}{\lambda_n^2} - \frac{1}{\lambda_n^2-\alpha d^2}\right]e^{-\lambda_n y/d}\cos\lambda_n x/d \qquad n \neq \frac{\alpha d}{\pi} - \frac{1}{2}$$

$$+ \frac{2(-1)^n}{\alpha d}\,e^{-\alpha y}\cos\alpha x \qquad n = \frac{\alpha d}{\pi} - \frac{1}{2} \quad \text{(G–36)}$$

Likewise, the maximum potential difference is

$$\frac{\Phi_2(x=0,y=0)-V}{\dfrac{nFc_F v^2}{s_R\,\kappa\,ak_m}} = \frac{\Delta\Phi_2}{\dfrac{nFc_F v^2}{s_R\,\kappa\,ak_m}} = \frac{\Delta\Phi_2}{\dfrac{\varepsilon nFc_F D_o}{s_R\,\kappa}}\,\frac{Sh}{Pe^2}$$

$$= -1$$

$$+ 2\alpha d\sum_{n=0}^{\infty}(-1)^n\left[\frac{1}{\lambda_n^2} - \frac{1}{\lambda_n^2-(\alpha d)^2}\right] \qquad n \neq \frac{\alpha d}{\pi} - \frac{1}{2}$$

$$+ \frac{2(-1)^n}{\alpha d} \qquad n = \frac{\alpha d}{\pi} - \frac{1}{2} \quad \text{(G–37)}$$

Appendix H

Computer Programs For Porous Electrodes

This section presents a listing of the computer programs used in the comparison of flow-through and flow-by porous electrodes at the limiting current. The programs and their purpose are summarized in Table H–1.

Table (H–1) Computer Programs and Their Purpose

Program Name	Purpose
OPTCON	Main program to determine cost optimum flow-through and flow-by designs.
COST	Calculate the total cost for the flow-through or flow-by configurations.
FCNY1	Calculate the derivative of the total flow-through cost with respect to $\varepsilon n F c_F D_0 / s_R \kappa \Delta\Phi_2$.
FCNY2	Calculate the derivative of total flow-by electrode cost with respect to αd.
POTFB	Calculate the maximum potential drop for a flow-by electrode of finite length at the limiting current.
POTFT	Calculate the maximum potential drop for a flow-through electrode at the limiting current.
POTINF	Calculate the maximum potential drop for a flow-by electrode of infinite length at the limiting current.
DERIV1	Calculate the derivative of the ratio of the Sherwood Number to the square of the Péclet Number Number for a flow-by electrode of infinite length at the limiting current.
DERIV2	Calculate the derivative of the ratio of the Sherwood Number to the square of the Péclet Number Number for a flow-by electrode of finite length at the limiting current.

SECANT	Perform a *regula-falsi* or secant iteration on a one dimensional function.

Program OPTCON was written to compare the cost of the optimum flow-through electrode to the optimum flow-by electrode. For a given value of the parameter $\varepsilon nFc_F D_o / s_R \kappa \Delta\Phi_2$ (CFOKAP) this program will calculate the following:

(1) The value of $\varepsilon nFc_F D_o / s_R \kappa \Delta\Phi_2$ yielding the minimum flow-through electrode cost.

(2) The cost of this flow-through electrode.

(3) The cost of the flow-through electrode at the chosen value of $\varepsilon nFc_F D_o / s_R \kappa \Delta\Phi_2$.

(4) The value of αd giving the lowest flow-by electrode cost at the chosen value of $\varepsilon nFc_F D_o / s_R \kappa \Delta\Phi_2$.

(5) The cost of this flow-by electrode.

(6) The ratio of the cost of the cheaper flow-through electrode to the cost of the flow-by electrode. If the value of $\varepsilon nFc_F D_o / s_R \kappa \Delta\Phi_2$ yielding the minimum electrode is larger than the chosen value of $\varepsilon nFc_F D_o / s_R \kappa \Delta\Phi_2$ then the minimum flow-through cost is used. Otherwise the cost for the electrode computed at the chosen value of $\varepsilon nFc_F D_o / s_R \kappa \Delta\Phi_2$ is used.

Subroutines DERIV1 and POTINF can be used interchangeably with subroutines DERIV2 and POTFB. DERIV1 and POTINF are used for a semi-infinite electrode while DERIV2 and POTFB are for a finite length electrode. One must change the calling statement for POTFB and POTINF.

A sample output follows the computer programs.

```
      PROGRAM OPTCON(INPUT,OUTPUT,TAPE5=INPUT,TAPE6=OUTPUT)
C
C     ..................................................
C
C     PROGRAM OPTCON
C
C     PURPOSE
C             DETERMINE THE COST-OPTIMUM POROUS ELECTRODE AT THE
C             LIMITING CURRENT. PROGRAM WILL COMPARE THE MOST
C             ECONOMICAL FLOW-THROUGH OR FLOW-BY  ELECTRODE
C             CONSIDERING COSTS BASED ON THE VOLUME OF THE
C             ELECTRODE, SEPARATOR AREA, AND PUMPING POWER.
C
C     SUBROUTINES REQUIRED
C             COST    CALCULATES ELECTRODE COST
C             FCNY1   DERIVATIVE OF FLOW-THROUGH COST
C             FCNY2   DERIVATIVE OF FLOW-BY COST
C
C                     FCNY2 REQUIRES
C
C                             POTFB   POTENTIAL DROP FOR FLOW-BY
C                                     ELECTRODE
C                             DERIV2  DERIVATIVE OF THE RATIO OF THE
C                                     SHERWOOD TO THE SQUARE OF THE
C                                     PECLET NUMBER WITH RESPECT TO
C                                     ALPHAD
C
C
C             POTFT   POTENTIAL DROP FOR FLOW-THROUGH ELECTRODE
C             POTFB   POTENTIAL DROP FOR FLOW-BY ELECTRODE
C             SECANT  SECANT ITERATION ROUTINE
C
C     REVISED 7-11-83
C     ..................................................
C
      EXTERNAL FCNY1,FCNY2
      COMMON/MAIN/ ALPHAL,A,B,CFOKAP,CSCV,CPCV,SMALLR,
     1 NTERMS,FBPOT,FTPOT,SC,R
      DIMENSION CT(2),CSCV(2),CPCV(2)
      DATA CSCV,CPCV/1000.0,1000.0,5.0E-13,5.0E-13/
C
C     INITIALIZE IMPORTANT CONSTANTS
C
C
C     PARAMETERS FOR BENNION AND NEWMAN CORRELATION FOLLOW
C
      A=0.07054
      B=0.5454
C
C     GUESSES FOR FLOW-THROUGH ITERATION FOLLOW
C
```

```
      CFOKP1=1.0E-7
      CFOKP2=2.0E-7
C
C     OTHER PARAMETERS FOLLOW
C
      IERR=0
      NITER=40
      NTERMS=500
      SMALLR=0.28429
      SC=1670
      TOL=1.0E-06
C
C     VALUES OF THE THREE ELECTRODE OPERATING PARAMETERS FOLLOW
C
      ALPHAL=6.5
      GAMMA=10.0
      CFOKAP=1.0E-7
C
C     PRINT OUT IMPORTANT PARAMETERS
C
      WRITE(6,100) A,B,ALPHAL,SMALLR,SC,CSCV(1),CPCV(1),
     1 CSCV(2),CPCV(2)
C
C     FIND MINIMUM FLOW-THROUGH COST
C
      WRITE(6,101)
      CALL POTFT(ALPHAL,FTPOT)
      X1=ALOG10(CFOKP1)
      X2=ALOG10(CFOKP2)
      CALL SECANT(FCNY1,X1,Y1,X2,TOL,IERR,NITER)
      IF(IERR.EQ.1) GO TO 1000
      CFKPMN=10.0**X1
      SHPEMN=FTPOT*CFKPMN
      CALL COST(SHPEMN,1,GAMMA,CVT,CST,CPT,CTMN)
      WRITE(6,102) CFKPMN
      WRITE(6,104) FTPOT,SHPEMN
      WRITE(6,105) CVT,CST,CPT
      WRITE(6,106) CTMN
C
C     NOW CALCULATE BEST FLOW-BY CASE
C     AND COMPARE IT TO FLOW-THROUGH CASE
C
      DO 40 J=1,2
      IF(J.EQ.2) GO TO 10
      WRITE(6,103)
      POT=FTPOT
      GO TO 20
C
C     FOR FLOW-BY CONFIGURATION FIND OPTIMUM GAMMA
C
10    WRITE(6,107)
```

```
      GAMMA1=GAMMA
      GAMMA2=GAMMA/1.5
      CALL SECANT(FCNY2,GAMMA1,Y1,GAMMA2,TOL,IERR,NITER)
      IF(IERR.EQ.1) GO TO 1000
      GAMMA=GAMMA1
      WRITE(6,108) GAMMA
      POT=FBPOT
C
C     DETERMINE FLOW-THROUGH COST
C     DETERMINE FLOW-BY COST AT OPTIMUM GAMMA
C
20    SHOPE2=POT*CFOKAP
      CALL COST(SHOPE2,J,GAMMA,CVT,CST,CPT,CT(J))
      WRITE(6,102) CFOKAP
      WRITE(6,104) POT,SHOPE2
      WRITE(6,105) CVT,CST,CPT
      WRITE(6,106) CT(J)
40    CONTINUE
C
C     CALCULATE RATIO OF  FLOW-THROUGH COST TO FLOW-BY COST
C
      CTR=CT(1)
C
C     WARNING MESSAGE PRINTED
C
      IF(ALPHAL/GAMMA.LT.5.0) WRITE(6,110)
C
C     COMPARE CHEAPER FLOW-THROUGH COST IF
C     CFOKAP IS LESS THAN CFKPMN
C
      IF(CFOKAP.GT.CFKPMN) GO TO 50
      CTR=CTMN
      WRITE(6,109)
50    RTC1=CTR/CT(2)
      WRITE(6,111) RTC1
      STOP
C
C     FORMAT STATEMENTS FOLLOW
C
100   FORMAT(* */*VALUES OF PARAMETERS USED IN THE OPTIMIZATION*/
     1          /* *,*A = *,F10.6
     2          /* *,*B = *,F10.6
     3          /* *,*ALPHAL = *,F10.4,
     4          /* *,*SMALLR = *,F10.6,
     5          /* *,*SC = *,F6.2//
     6          /* *,20X,*CSCV*,11X,*CPCV*/
     7          /*FLOW-THROUGH*,5X,F10.2,5X,1PE10.3
     8          /*FLOW-BY*,10X,0PF10.2,5X,1PE10.3//)
101   FORMAT(* */* *,*OPTIMUM FLOW-THROUGH DESIGN*/)
102   FORMAT(* */* *,*CFOKAP = *,1PE12.5/)
103   FORMAT(* *//* *,*FLOW-THROUGH CONFIGURATION*)
```

```
104     FORMAT(* *,*DELTA PHI = *,1PE12.5,5X,*SH/PE2 = *,1PE12.5/)
105     FORMAT(* *,*CV = *,1PE12.5,5X,*CS = *,1PE12.5,5X,
    1             *CP = *,1PE12.5/)
106     FORMAT(* *,*CT = *,1PE12.5)
107     FORMAT(* *//* *,*FLOW-BY CONFIGURATION*//)
108     FORMAT(* */* *,*OPTIMUM ALPHAD = *,1PE12.5)
109     FORMAT(* *,*MINIMUM FLOW-THROUGH COST USED FOR COMPARISON*)
110     FORMAT(* *,///* *,
    1 *WARNING; SEMI-INFINITE FLOW-BY RESULTS NOT VALID,*,
    2 * R < 5*)
111     FORMAT(* */* *,*RATIO OF FLOW-THROUGH TO FLOW-BY COST = *,
    1 F10.6)
C
C       ERROR PROCESSED HERE
C
1000    WRITE(6,115) NITER
115     FORMAT(* *,/*NO CONVERGENCE AFTER*,1X,I3,1X,*ITERATIONS*/)
        STOP
        END

        SUBROUTINE COST(SHOPE2,ITYPE,GAMMA,CVT,CST,CPT,CT)
C
C       ..........................................................
C
C       SUBROUTINE COST
C
C       PURPOSE CALCULATE THE TOTAL WEIGHTED SUM OF OPERATING AND
C               CAPITAL COSTS FOR A FLOW-THROUGH AND FLOW-BY
C               ELECTRODE AT THE LIMITING CURRENT.
C
C       USAGE   CALL COST(SHOPE2,ITYPE,GAMMA,CVT,CST,CPT,CT)
C
C       DESCRIPTION OF PARAMETERS
C
C               SHOPE2  THE SHERWOOD NUMBER DIVIDED BY THE
C                       SQUARE OF THE PECLET NUMBER
C               ITYPE   TYPE OF ELECTRODE CONFIGURATION
C
C                       =1      FLOW-THROUGH CONFIGURATION
C                       =2      FLOW-BY CONFIGURATION
C
C               GAMMA   THE QUANTITY ALPHA*D (ONLY USED FOR
C                       THE FLOW-BY CONFIGURATION)
C
C               CVT     VOLUMETRIC CAPITAL COST
C               CST     SEPARATOR CAPITAL COST
C               CPT     PUMPING OPERATING COST
C               CT      TOTAL COST ; WEIGHTED SUM OF
C                       VOLUMETRIC, SEPARATOR, AND PUMPING
C                       COSTS.
C
```

```
C       SUBROUTINES REQUIRED
C
C               NONE
C
C       REVISED 8-18-1983
C       ..........................................................
C
        COMMON/MAIN/ ALPHAL,A,B,CFOKAP,CSCV,CPCV,SMALLR,
     1 NTERMS,FBPOT,FTPOT,SC,R
        DIMENSION CSCV(2),CPCV(2)
C
C       COMPUTE VOLUMETRIC ELECTRODE COST
C
        CVT=ALPHAL/A*(SHOPE2/A)**(B/(2.0-B))
C
C       NOW CALCULATE SEPARATOR COST
C
C       FLOW-THROUGH ELECTRODE CALCULATED HERE
C
        FACTOR=1.0
C
C       FLOW-BY ELECTRODE HERE
C
        IF(ITYPE.EQ.2) FACTOR=ALPHAL/GAMMA
        PE=(SHOPE2/A)**(-1.0/(2.0-B))
        ASOQ=FACTOR/PE
        CST=CSCV(ITYPE)*ASOQ
C
C       CALCULATE PUMPING COST
C
        DELTAP=ALPHAL/SHOPE2*(150.0/36.0*SC+1.75/6.0*PE)
        CPT=CPCV(ITYPE)*DELTAP
C
C       FINALLY CALCULATE TOTAL COST
C
        CT=CVT+CST+CPT/SMALLR
        RETURN
        END

        SUBROUTINE FCNY1(X,DCTDCF)
C
C       ..........................................................
C
C       SUBROUTINE FCNY1
C
C       PURPOSE CALCULATE THE DERIVATIVE OF THE TOTAL COST FOR
C               FLOW-THROUGH ELECTRODE WITH RESPECT TO THE
C               PARAMETER CFOKAP AT THE LIMITING CURRENT
C
C       USAGE   CALL FCNY1(X,DCTDCF)
C
```

```
C       DESCRIPTION OF PARAMETERS
C
C               X       NATURAL LOGARITHM OF THE VARIABLE CFOKAP
C               DCTDCF  DERIVATIVE OF TOTAL COST WITH RESPECT
C                       TO THE VARIABLE CFOKAP
C
C
C       SUBROUTINES REQUIRED
C
C               NONE
C
C
C       REVISED 8-18-83
C       ..........................................................
C
        COMMON/MAIN/ ALPHAL,A,B,CFOKAP,CSCV,CPCV,SMALLR,
     1 NTERMS,FBPOT,FTPOT,SC,R
        DIMENSION CSCV(2),CPCV(2)
        CFKPMN=10.0**X
C
C       CALCULATE SHERWOOD NUMBER OVER THE PECLET NUMBER SQUARED
C
        SHOPE2=CFKPMN*FTPOT
C
C       CALCULATE DERIVATIVE OF VOLUMETRIC COST
C
        DCVT=ALPHAL*B/(2.0-B)/A**(2.0/(2.0-B))*
     1 SHOPE2**((2.0*B-2.0)/(2.0-B))
C
C       CALCULATE DERIVATIVE OF SEPARATOR COST
C
        DCST=CSCV(1)/(2.0-B)/A**(1.0/(2.0-B))*SHOPE2**((B-1.0)/(2.0-B))
C
C       CALCULATE DERIVATIVE OF PUMPING COST
C
        DCPT=-CPCV(1)*ALPHAL/SHOPE2*(150.0/36.0*SC/SHOPE2+
     1  1.75/6.0*A**(1.0/(2.0-B))*(3.0-B)/(2.0-B)/SHOPE2**
     2  ((3.0-B)/(2.0-B)))
C
C       CALCULATE DERIVATIVE OF TOTAL WEIGHTED COST
C
        DCTDCF=(DCVT+DCST+DCPT/SMALLR)*FTPOT
        RETURN
        END

        SUBROUTINE FCNY2(GAMMA,DCTDGM)
C
C       ..........................................................
C
C       SUBROUTINE FCNY2
C
```

```
C       PURPOSE CALCULATE THE DERIVATIVE OF THE TOTAL COST FOR
C               FLOW-BY ELECTRODE WITH RESPECT TO THE VARIABLE
C               GAMMA AT THE LIMITING CURRENT
C
C       USAGE   CALL FCNY2(GAMMA,DCTDCF)
C
C       DESCRIPTION OF PARAMETERS
C
C               GAMMA   THE QUANTITY ALPHA*D
C               DCTDCF  DERIVATIVE OF TOTAL COST WITH RESPECT
C                       TO THE VARIABLE GAMMA
C
C
C       SUBROUTINES REQUIRED
C
C               DERIV2  CALCULATES THE DERIVATIVE OF THE SHERWOOD
C                       NUMBER DIVIDED BY THE PECLET NUMBER SQUARED
C                       FOR A FLOW-BY ELECTRODE OF FINITE LENGTH
C
C               POTFB   CALCULATES THE POTENTIAL DISTRIBUTION FOR A
C                       FLOW-BY ELECTRODE OF FINITE LENGTH
C
C
C       REVISED 8-18-83
C       ..........................................................
C
      COMMON/MAIN/ ALPHAL,A,B,CFOKAP,CSCV,CPCV,SMALLR,
     1 NTERMS,FBPOT,FTPOT,SC,R
      DIMENSION CSCV(2),CPCV(2)
C
C     CALCULATE ASPECT RATIO
C
      R=ALPHAL/GAMMA
C
C     NOW GO GET THE DERIVATIVE OF THE SHERWOOD OVER THE PECLET
C     NUMBER SQUARED WITH RESPECT TO THE VARIABLE GAMMA
C
      CALL DERIV2(GAMMA,DSHDGM)
C
C     GO GET THE MAXIMUM MAXIMUM POTENTIAL DROP FOR THE FLOW-BY
C     ELECTRODE OF FINITE LENGTH
C
      CALL POTFB(GAMMA,R,NTERMS,FBPOT,TOL)
      SHOPE2=CFOKAP*FBPOT
C
C     CALCULATE THE DERIVATIVE OF VOLUMETRIC COST WITH GAMMA
C
      DCVT=ALPHAL*(1.0/A)**(2.0/(2.0-B))*B/(2.0-B)*SHOPE2**
     1 ((2.0*B-2.0)/(2.0-B))*DSHDGM
C
C     CALCULATE THE DERIVATIVE OF SEPARATOR COST WITH GAMMA
```

```
C
      DCST=CSCV(2)*ALPHAL/GAMMA/GAMMA*(1.0/A)**(1.0/(2.0-B))*
     1 (GAMMA/(2.0-B)*SHOPE2**((B-1.0)/(2.0-B))*DSHDGM-
     2 SHOPE2**(1.0/(2.0-B)))
C
C       CALCULATE THE DERIVATIVE OF PUMPING COST WITH GAMMA
C
      DCPT=-CPCV(2)*DSHDGM*ALPHAL*(150.0/36.0*SC/SHOPE2**2+
     1 1.75/6.0*A**((1.0)/(2.0-B))*(3.0-B)/(2.0-B)/SHOPE2**
     2 ((5.0-2.0*B)/(2.0-B)))
C
C       FINALLY CALCULATE THE DERIVATIVE OF THE TOTAL COST
C       WITH GAMMA
C
      DCTDGM=(DCVT+DCST+DCPT/SMALLR)
      RETURN
      END

      SUBROUTINE DERIV2(GAMMA,DSHDGM)
C
C       ..............................................................
C
C       SUBROUTINE DERIV2
C
C       PURPOSE CALCULATE THE DERIVATIVE OF THE SHERWOOD NUMBER OVER
C               THE SQUARE OF THE PECLET NUMBER WITH RESPECT THE
C               VARIABLE GAMMA FOR A FLOW-BY ELECTRODE OF FINITE
C               LENGTH
C
C       USAGE   CALL DERIV2(GAMMA,DSHDGM)
C
C       DESCRIPTION OF PARAMETERS
C
C               GAMMA   THE QUANTITY ALPHA*D
C               DSHDGM  THE VALUE OF THE DERIVATIVE OF THE SHERWOOD
C                       NUMBER OVER THE PECLET NUMBER SQUARED WITH
C                       RESPECT THE VARIABLE GAMMA
C
C       SUBROUTINES REQUIRED
C
C               NONE
C
C       REVISED 8-16-83
C
C       ..............................................................
C
      COMMON/MAIN/ ALPHAL,A,B,CFOKAP,CSCV,CPCV,SMALLR,
     1 NTERMS,FBPOT,FTPOT,SC,R
      DIMENSION CSCV(2),CPCV(2)
      REAL LAMBDA,LAMHAT,MS1N
      PI=3.14159265358979
```

```
C
C       INITIALIZE SUMS
C
        SUM1=0.0
        SUM2=0.0
        SUM3=0.0
        SUM4=0.0
        SUM5=0.0
        SUM6=0.0
        DELTA=0.5
        EXPAL=EXP(-ALPHAL)
C
C       NOW CALCULATE SUMS TERM BY TERM
C
C       SPECIAL CASE FOR THE FIRST TERM
C
        DO 10 I=1,NTERMS
        SINHAR=0.0
        COSHLM=0.0
C
C       CALCULATE EIGENVALUES
C
        LAMBDA=(2.0*FLOAT(I-1)+1.0)*PI/2.0
        LAMHAT=FLOAT(I-1)*PI/R
        MS1N=(-1.0)**(I-1)
        FACTOR=MS1N/LAMBDA/LAMBDA
        ARG=LAMBDA*R
        TANHAR=1.0/TANH(ARG)
C
C       SPECIAL CASE FOR LARGE EIGENVALUES
C
        IF(ARG.GT.650.0) GO TO 5
        SINHAR=1.0/SINH(ARG)
5       TERM1=TANHAR*FACTOR
        TERM2=SINHAR*FACTOR
        TERM3=SINHAR*SINHAR*ARG*FACTOR
        TERM4=TANHAR*SINHAR*ARG*FACTOR
        GMMNLM=1.0/(GAMMA*GAMMA+LAMHAT*LAMHAT)
C
C       SPECIAL CASE FOR LARGE EIGENVALUES
C
        IF(LAMHAT.GT.650.0) GO TO 6
        COSHLM=1.0/COSH(LAMHAT)
6       TERM5=LAMHAT*TANH(LAMHAT)*COSHLM*GMMNLM*DELTA
        TERM6=TERM5*MS1N
C
C       ADD TERMS TO SUMS
C
        SUM1=SUM1+TERM1
        SUM2=SUM2+TERM2
        SUM3=SUM3+TERM3
```

```
      SUM4=SUM4+TERM4
      SUM5=SUM5+TERM5
      SUM6=SUM6+TERM6
      DELTA=1.0
10    CONTINUE
C
C     NOW CALCULATE DERIVATIVE
C
      DSHDGM=2.0*CFOKAP*(SUM1+SUM3-SUM5/R+
     1 EXPAL*(SUM6/R-SUM2-SUM4))
      RETURN
      END

      SUBROUTINE POTFB(GAMMA,R,NTERMS,POT,TOL)
C     ..................................................
C
C     SUBROUTINE POTFB
C
C     PURPOSE CALCULATE THE MAXIMUM SOLUTION PHASE POTENTIAL DROP
C             FOR A FLOW-BY ELECTRODE OF FINITE ASPECT RATIO AT THE
C             LIMITING CURRENT.
C
C     USAGE   CALL POTFB(GAMMA,R,NTERMS,POT,TOL)
C
C     DESCRIPTION OF PARAMETERS
C
C             GAMMA   THE QUANTITY ALPHA*D
C             R       ELECTRODE ASPECT RATIO
C             NTERMS  NUMBER OF TERMS IN SUM
C             POT     RESULTING MAXIMUM POTENTIAL DROP
C             TOL     TOLERANCE IN POTENTIAL, EXPRESSED AS A
C                     FRACTIONAL CHANGE TO THE SUM FROM THE
C                     LAST TERM OF THE SERIES
C
C     SUBROUTINES REQUIRED
C
C             NONE
C
C     REMARKS PROGRAM CALCULATES MAXIMUM POTENTIAL DROP USING
C             AN INFINITE SERIES. ASSUMED BOUNDARY CONDITIONS
C             ARE ZERO FLUXES AT THE INLET, OUTLET AND ONE SIDE
C             OF THE ELECTRODE AND A CONSTANT POTENTIAL ALONG THE
C             OTHER SIDE OF THE ELECTRODE.
C
C     REFERENCE
C
C             FEDKIW, PETER, "OHMIC POTENTIAL DROP IN FLOW-THROUGH
C             AND FLOW-BY POROUS ELECTRODES", J. ELECTROCHEM. SOC.,
C             128, PP. 831-838, 1981.
C
C     REVISED 7-18-83
```

```
C     ..............................................................
C
      REAL LAMBDA,LAMHAT,MNS1N
      PI=3.14159265358979
C
C     INITIALIZE SUMS
C
      SUM1=0.0
      SUM2=0.0
      SUM3=0.0
      SUM4=0.0
      DELTA=0.5
C
C     DETERMINE POTENTIAL DROP TERM BY TERM
C
      DO 3 I=1,NTERMS
C
C     INITIALIZE TERMS
C
      TERM2=0.0
      TERM3=0.0
      TERM4=0.0
C
C     CALCULATE EIGENVALUES
C
      LAMBDA=(2.0*FLOAT(I-1)+1.0)*PI/2.0
      LAMHAT=FLOAT(I-1)*PI/R
      MNS1N=(-1.0)**(I-1)
      FACTOR=MNS1N/LAMBDA/LAMBDA
      TERM1=1.0/TANH(LAMBDA*R)
C
C     SPECIAL CASE FOR LARGE EIGENVALUES
C
      IF(R*LAMBDA.GT.650.0) GO TO 1
      TERM2=1.0/SINH(R*LAMBDA)
C
C     SPECIAL CASE FOR LARGE EIGENVALUES
C
1     IF(LAMHAT.GT.650.0) GO TO 2
      TERM3=DELTA/(LAMHAT*LAMHAT+GAMMA*GAMMA)/COSH(LAMHAT)
      TERM4=MNS1N*TERM3
C
C     ADD TERMS TO SUMS
C
2     SUM1=SUM1+FACTOR*TERM1
      SUM2=SUM2+FACTOR*TERM2
      SUM3=SUM3+TERM3
      SUM4=SUM4+TERM4
      DELTA=1.0
3     CONTINUE
C
```

```
C       CALCULATE POTENTIAL DROP FROM SUMS
C
        POT=2.0*GAMMA*(SUM1-EXP(-GAMMA*R)*(SUM2+1.0/R*SUM4)+1.0/R*
     1      SUM3)-1.0
C
C       CALCULATE TOLERANCE
C
        TOL=2.0*GAMMA*(FACTOR*TERM1-EXP(-GAMMA*R)*
     1      (TERM1*TERM2+1.0/R*TERM4)+1.0/R*TERM3)/(POT+1.0)
        RETURN
        END

        SUBROUTINE POTFT(ALPHAL,POT)
C
C       .....................................................
C
C       SUBROUTINE POTFT
C
C       PURPOSE CALCULATE THE MAXIMUM SOLUTION PHASE POTENTIAL DROP
C               FOR A FLOW-THROUGH ELECTRODE AT THE LIMITING CURRENT.
C
C       USAGE   CALL POTFT(ALPHAL,POT)
C
C       DESCRIPTION OF PARAMETERS
C
C               ALPHAL  THE QUANTITY ALPHA*L
C               POT     RESULTING MAXIMUM POTENTIAL DROP
C
C       SUBROUTINE REQUIRED
C
C               NONE
C
C       REMARKS PROGRAM CALCULATES MAXIMUM POTENTIAL DROP
C               FOR A FLOW-THROUGH ELECTRODE. BOUNDARY CONDITIONS
C               USED ARE A FIXED UPSTREAM POTENTIAL AND ZERO
C               FLUX DOWNSTREAM AT THE END OF THE BED. THE CASE
C               FOR ALPHAL GREATER THAN 700 IS TREATED AS A SPECIAL
C               CASE.
C
C       REVISED 6-25-83
C       .....................................................
C
        THETA=0.0
C
C       SPECIAL CASE FOR LARGE ALPHAL
C
        IF(ALPHAL.GT.700.0) GO TO 1
        THETA=EXP(-ALPHAL)
1       POT=1.0-(1.0+ALPHAL)*THETA
        RETURN
        END
```

```
      SUBROUTINE SECANT(FCNY,X1,Y,X2,TOL,IERR,NITER)
C
C     ..................................................
C
C     SUBROUTINE SECANT
C
C     PURPOSE PERFORM AN ITERATION USING THE SECANT METHOD ON
C             A ONE-DIMENSIONAL FUNCTION.
C
C     USAGE   CALL SECANT(FCNY,X1,Y1,X2,TOL,IERR,NITER)
C
C     DESCRIPTION OF PARAMETERS
C
C             FCNY    FUNCTION TO BE ITERATED UPON.
C             X1      FIRST GUESS FOR INDEPENDENT VARIABLE.
C                       FINAL VALUE OF INDEPENDENT VARIABLE
C                       IS RETURNED HERE.
C             Y       FINAL VALUE OF DEPENDENT VARIABLE IS
C                       RETURNED HERE. DEPENDENT
C                       VARIABLE IS ITERATED TO ZERO.
C             X2      SECOND GUESS FOR INDEPENDENT VARIABLE.
C             TOL     ITERATION TOLERANCE EXPRESSED AS A
C                       FRACTION CHANGE OF THE INDEPENDENT
C                       VARIABLE.
C             IERR    ERROR FLAG.
C                     = 1     IF NUMBER OF SPECIFIED ITERATIONS
C                       ARE EXCEEDED.
C
C             NITER   NUMBER OF ITERATIONS. IERR IS ASSIGNED A
C                       VALUE OF ONE IF THE NUMBER OF
C                       ITERATIONS EXCEEDS THIS PARAMETER.
C
C     SUBROUTINES REQUIRED
C
C             FCNY    SUBROUTINE TO EVALUATE THE INDEPENDENT
C                       VARIABLE FOR A GIVEN VALUE OF THE
C                       DEPENDENT VARIABLE.
C
C     REVISED 7-11-83
C     ..................................................
C
      COMMON/MAIN/ ALPHAL,A,B,CFOKAP,CSCV,CPCV,SMALLR,
     1 NTERMS,FBPOT,FTPOT,SC,R
      DIMENSION CSCV(2),CPCV(2)
      N=1
C
C     EVALUATE FUNCTION FOR INITIAL GUESSES
C
      CALL FCNY(X1,Y1)
      CALL FCNY(X2,Y2)
C
```

```
C       COMPUTE NEW VALUE FROM PREVIOUS GUESSES
C
1       XCHG=(X2-X1)/(Y2-Y1)*Y2
        X3=X2-XCHG
C
C       LIMIT MAXIMUM CHANGE IN ITERATED VARIABLE
C
        IF(ABS(XCHG).GT.ABS(0.5*X2)) X3=X2*(1.0-SIGN(0.5,XCHG))
        CALL FCNY(X3,Y3)
C
C       DETERMINE IF ITERATION TOLERANCE HAS BEEN MET
C
        IF(ABS((X3-X2)/X3).LT.TOL) GO TO 2
C
C       DETERMINE IF SPECIFIED NUMBER OF ITERATIONS
C               HAS BEEN EXCEEDED
C
        IF(N.GT.NITER) GO TO 3
C
C       IF NOT TRY AGAIN !
C
        X1=X2
        X2=X3
        Y1=Y2
        Y2=Y3
        N=N+1
        GO TO 1
C
C       SUCCESS ! RETURN VALUES
C
2       X1=X3
        Y=Y3
        WRITE(6,101) N
101     FORMAT(* *,I4,* ITERATIONS WERE REQUIRED*)
        RETURN
C
C       RETURN AN ERROR
C
3       IERR=1
        RETURN
        END


        SUBROUTINE DERIV1(GAMMA,DSHDGM)
C
C       ..........................................................
C
C       SUBROUTINE DERIV1
C
C       PURPOSE CALCULATE THE DERIVATIVE OF THE SHERWOOD NUMBER OVER
C               THE SQUARE OF THE PECLET NUMBER WITH RESPECT THE
```

```
C               VARIABLE GAMMA FOR A FLOW-BY ELECTRODE OF INFINITE
C               LENGTH
C
C       USAGE   CALL DERIV1(GAMMA,DSHDGM)
C
C       DESCRIPTION OF PARAMETERS
C
C               GAMMA   THE QUANTITY ALPHA*D
C               DSHDGM  THE VALUE OF THE DERIVATIVE OF THE SHERWOOD
C                       NUMBER OVER THE PECLET NUMBER SQUARED WITH
C                       RESPECT THE VARIABLE GAMMA
C
C       SUBROUTINES REQUIRED
C
C               NONE
C
C       REVISED 8-23-83
C
C       ..................................................................
C
        COMMON/MAIN/ ALPHAL,A,B,CFOKAP,CSCV,CPCV,SMALLR,
     1 NTERMS,FBPOT,FTPOT,SC
        DIMENSION CSCV(2),CPCV(2)
        REAL LAMBDA,MS1N
        PI=3.14159265358979
C
C       DETERMINE OPTIMUM STARTING TERM FOR SUMS
C
        ISTART=IFIX((2.0*GAMMA/PI-1.0-NTERMS)/2.0)
        IF(ISTART.LT.1) ISTART=1
        ISTOP=ISTART+NTERMS
C
C       INITIALIZE SUMS
C
        SUM1=0.0
        SUM2=0.0
        SUM3=0.0
C
C       CALCULATE SUMS TERM BY TERM
C
        DO 10 I=ISTART,ISTOP
        LAMBDA=(2.0*FLOAT(I-1)+1.0)*PI/2.0
        MS1N=(-1.0)**(I-1)
        DENOM=LAMBDA*LAMBDA-GAMMA*GAMMA
        TERM2=MS1N/DENOM
        TERM3=MS1N/DENOM/DENOM
        SUM2=SUM2+TERM2
        SUM3=SUM3+TERM3
10      CONTINUE
C
C       ASYMPTOTIC LIMIT FOR GAMMA GOING TO INFINITY FOLLOWS
```

```
C
      SUM1=0.91596559417722*4.0/PI/PI
C
C     FINALLY CALCULATE DERIVATIVE
C
      DSHDGM=CFOKAP*(SIN(GAMMA)/(COS(GAMMA)**2)+
     1 2.0*(SUM1-SUM2)-4.0*GAMMA*GAMMA*SUM3)
      RETURN
      END

      SUBROUTINE POTINF(GAMMA,NTERMS,POT,TOL)
C
C     .....................................................
C
C     SUBROUTINE POTINF
C
C     PURPOSE CALCULATE THE MAXIMUM SOLUTION PHASE POTENTIAL DROP
C             FOR A FLOW-BY ELECTRODE OF INFINITE ASPECT RATIO AT
C             THE LIMITING CURRENT.
C
C     USAGE   CALL POTINF(GAMMA,NTERMS,FLBYPT,TOL)
C
C     DESCRIPTION OF PARAMETERS
C
C             GAMMA   THE QUANTITY ALPHA*D
C             NTERMS  NUMBER OF TERMS IN SERIES
C             POT     RESULTING MAXIMUM POTENTIAL DROP
C             TOL     TOLERANCE IN POTENTIAL EXPRESSED AS A
C                     FRACTIONAL CHANGE IN THE SUM FROM THE LAST
C                     TERM IN THE SERIES
C
C     SUBROUTINE REQUIRED
C
C             NONE
C
C     REMARKS PROGRAM CALCULATES MAXIMUM POTENTIAL DROP IN THE
C             LIMIT OF AN INFINITELY LONG ELECTRODE. BOUNDARY
C             CONDITIONS USED ARE ZERO FLUXES AT THE INLET,
C             OUTLET AND ONE SIDE WALL OF THE ELECTRODE WITH
C             A CONSTANT POTENTIAL CONDITION ALONG THE OTHER
C             SIDE WALL.
C
C
C     REVISED 8-23-83
C     .....................................................
C
      REAL LAMBDA,MNS1N
      PI=3.14159265358979
C
C     CALCULATE OPTIMUM STARTING TERM
C
```

```
      ISTART=IFIX((2.0*GAMMA/PI-1.0-NTERMS)/2.0)
      IF(ISTART.LT.1) ISTART=1
      ISTOP=ISTART+NTERMS
C
C     SUM POTENTIAL TERM BY TERM
C
      SUM=0.0
      DO 10 I=ISTART,ISTOP
      LAMBDA=(2.0*FLOAT(I-1)+1.0)*PI/2.0
      MNS1N=(-1.0)**(I-1)
      TERM=MNS1N/(LAMBDA*LAMBDA-GAMMA*GAMMA)
      SUM=SUM-TERM
10    CONTINUE
C
C     CALCULATE POTENTIAL DROP
C
      SUM=SUM+0.91596559417722*4.0/PI/PI
      POT=2.0*GAMMA*SUM+1.0/COS(GAMMA)-1.0
C
C     CALCULATE TOLERANCE
C
      TOL=2.0*GAMMA*TERM
      RETURN
      END
```

Sample Output for Program OPTCON

VALUES OF PARAMETERS USED IN THE OPTIMIZATION

A = .070540
B = .545400
ALPHAL = 6.5000
SMALLR = .284290
SC = 1670.0

	CSCV	CPCV
FLOW-THROUGH	1000.00	5.000E-13
FLOW-BY	1000.00	5.000E-13

OPTIMUM FLOW-THROUGH DESIGN

6 ITERATIONS WERE REQUIRED

CFOKAP = 2.55770E-07

DELTA PHI = 9.88724E-01 SH/PE2 = 2.52886E-07

CV = 8.36936E-01 CS = 1.80448E-01 CP = 1.10199E-01

CT = 1.40501E+00

FLOW-THROUGH CONFIGURATION

CFOKAP = 1.00000E-07

DELTA PHI = 9.88724E-01 SH/PE2 = 9.88724E-08

CV = 5.88531E-01 CS = 9.46162E-02 CP = 3.30053E-01

CT = 1.84412E+00

FLOW-BY CONFIGURATION

7 ITERATIONS WERE REQUIRED

OPTIMUM ALPHAD = 5.12539E+00

CFOKAP = 1.00000E-07

DELTA PHI = 3.15881E+00 SH/PE2 = 3.15881E-07

CV = 9.09728E-01 CS = 2.66654E-01 CP = 8.58641E-02

CT = 1.47841E+00

WARNING; SEMI-INFINITE FLOW-BY RESULTS NOT VALID, R < 5
MINIMUM FLOW-THROUGH COST USED FOR COMPARISON

RATIO OF FLOW-THROUGH TO FLOW-BY COST = .950352

TECHNICAL INFORMATION DEPARTMENT
LAWRENCE BERKELEY LABORATORY
UNIVERSITY OF CALIFORNIA
BERKELEY, CALIFORNIA 94720